2018

Mechanisms Of RAD51D-Dependent Repair Of DNA And Telomere Damage Induced By Interstrand Crosslinking Agents And Thiopurines

Nicole M. Reilly
University of South Carolina

MECHANISMS OF RAD51D-DEPENDENT REPAIR OF DNA AND TELOMERE DAMAGE INDUCED BY INTERSTRAND CROSSLINKING AGENTS AND THIOPURINES

by

Nicole M. Reilly

Bachelor of Science
Appalachian State University, 2012

Submitted in Partial Fulfillment of the Requirements

for the Degree of Doctor of Philosophy in

Pharmaceutical Sciences

College of Pharmacy

University of South Carolina

2018

Accepted by:

Douglas L. Pittman, Major Professor

Michael D. Wyatt, Chair, Examining Committee

Kim E. Creek, Committee Member

Danyelle M. Townsend, Committee Member

Lydia E. Matesic, Committee Member

Cheryl L. Addy, Vice Provost and Dean of the Graduate School

DEDICATION

This work is dedicated to my grandmother, Colleen Winifred O'Dougherty Melville, for her eternal love that guided and protected me through this journey.

ACKNOWLEDGEMENTS

Firstly, I would like to thank my advisor, Dr. Douglas L. Pittman, for his limitless support and enthusiasm that were instrumental to my success. The experience and knowledge that I gained by working alongside him is invaluable to me, and I will always be grateful. I also thank Dr. Michael D. Wyatt for acting as a second mentor to me and for giving me the opportunity to work on the 6-thioguanine project. I am thankful to my committee, Drs. Kim E. Creek, Danyelle M. Townsend, and Lydia E. Matesic, for their guidance. I am especially grateful to my colleagues: Ms. Latarsha L. Porcher, Mr. Michael G. Marone, Ms. Erin L. Anderson, Ms. Deborah O. Adedokun, Ms. Claire L. Chabot, and Ms. Morgan Ingerson for their technical assistance and friendship. I am also very appreciative of the support of other faculty members in the Department of Drug Discovery and Biomedical Sciences: Dr. Phillip J. Buckhaults for his assistance on the RNA Seq portion of my gene expression project and for recommending me to Dr. Alberto Bardelli as a post-doctoral research fellow, Dr. Diego Altomare, for his collaborative efforts on the microarray aspect of my gene expression project, and Dr. Jill R. Turner and Dr. Jason A. Stewart for technical assistance.

I would like to thank my family – Pamela, Carl, Chris, and Kaitlin – for their love, support, and patience as I worked to complete this goal, and to my fellow graduate students – Anusha, Katie, Pamela, Sara, Tim – for their support and friendship.

Finally, to Murphy Cameron and Spud Bear, for the love and snuggles that kept me going for the past five years. *E ora qualcosa di completamente diverso...*

ABSTRACT

Mutations in homologous recombination (HR) genes increase genomic instability, an enabling characteristic of cancer. However, the status of these same genes can also determine chemotherapy outcomes. RAD51D is a breast and ovarian cancer susceptibility gene that is an important component of HR. Mammalian cells defective for RAD51D have extensive chromosomal aberrations and are more sensitive to the interstrand crosslink-inducing agent mitomycin C (MMC) and the thiopurine 6-thioguanine (6TG). Previously, the RNF138 E3 ubiquitin ligase was identified to promote RAD51D ubiquitination, and loss of RNF138 also increased cellular sensitivity to MMC. Ubiquitination assays were used to show that a 3-ubiquitin modification occurs along the RAD51D wild-type protein. To identify potential sites of ubiquitination, amino acid substitutions were generated at all thirteen lysine residues along RAD51D. Arginine substitutions at K235 (K235R) and K298 (K298R) were found to confer cellular sensitivity to MMC. In addition, protein stability of K235R and K298R were 2 to 3-fold higher as compared with wild-type RAD51D.

RAD51D is also known to contribute to telomere maintenance, although its precise function at the telomeres remains unclear. In this dissertation, I investigated the activity of RAD51D at telomeres and the contribution of RAD51D to protect against 6TG-induced telomere damage. As measured by γ-H2AX induction and foci formation, the extent of γ-H2AX telomere localization following 6TG treatment was higher in *Rad51d*-deficient cells than in *Rad51d*-proficient cells. In the final portion of this

dissertation, *Rad51d*-deficient cells were used as a model for genome unstable mammalian cells to identify genetic compromises that support cell proliferation. Gene expression profiles of *Rad51d*-proficient and -deficient primary mouse embryonic fibroblasts were analyzed by microarray and RNA Seq. In both analyses, the highest proportion of genes were associated with cellular growth and proliferation. In summary, the data presented in this dissertation identified potential regulatory sites along RAD51D that mediate its function during ICL repair, elucidated the role of RAD51D in maintaining telomere integrity in the presence of thiopurine-induced DNA damage, and revealed genetic compromises in *Rad51d*-deficient cells that promote cell proliferation.

TABLE OF CONTENTS

Dedication iii

Acknowledgements iv

Abstract v

List of Tables ix

List of Figures x

List of Abbreviations xii

Chapter 1: Introduction 1

Chapter 2: Literature 5

Chapter 3: RNF138 zinc finger motifs mediate its interaction with RAD51D 42

Chapter 4: RAD51D lysine residues 235 and 298 are required for DNA interstrand crosslink repair 54

Chapter 5: Thiopurine-induced telomeric damage in *Rad51d*-deficient mammalian cells 88

Chapter 6: Genome-wide identification and expression analysis of gene differences between *Rad51d*-proficient and -deficient primary mouse embryonic fibroblasts 110

Chapter 7: Discussion 143

References 160

Appendix A: Genes with differential expression in the absence of *Rad51d* identified by microarray 182

Appendix B: Genes with differential expression in the absence of *Rad51d* identified by RNA Seq 200

Appendix C: RAD51D and RNF138 expression constructs 219

Appendix D: Permission to reprint data in Chapter 3.....224

Appendix E: Permission to reprint data in Chapter 5 226

LIST OF TABLES

Table 2.1 Risk factor mutant alleles of RAD51 genes..... 29

Table 4.1 Primer sequences used for *MmRad51d* cDNA site-directed Mutagenesis 76

Table 5.1 Cytological analysis of MEFs treated with 6TG 104

Table 6.1 Genes associated with "cellular growth and proliferation" identified by microarray 128

Table 6.2 Genes associated with "cell cycle progression" identified by microarray.....130

Table 6.3 Genes associated with "cellular growth and proliferation" identified by RNA Seq 131

Table 6.4 Chromosome fusions identified in the RNA Seq samples by TopHat-Fusion.....134

Table 6.5 Genes identified by both microarray and RNA Seq 135

Table 6.6 Genes associated with "cellular growth and proliferation" identified by both microarray and RNA Seq.....138

Table 6.7 Genes associated with "cell cycle progression" identified by both microarray and RNA Seq.....139

Table A.1. Genes identified by microarray.....183

Table B.1. Genes identified by RNA Seq 201

Table C.1. Prokaryotic expression constructs.....220

Table C.2. Eukaryotic expression constructs 221

Table C.3. Yeast expression constructs 222

.

Table C.4. Fluorescent expression constructs.....223

LIST OF FIGURES

Figure 2.1 Overview of consequences of DNA damage....6

Figure 2.2 DNA break induced by ionizing radiation....8

Figure 2.3 Platinum compounds binding to guanine nucleotides....9

Figure 2.4 Metabolism of 6TG into cytotoxic nucleotides....10

Figure 2.5 Model of homologous recombination-mediated double strand break repair....15

Figure 2.6 Key proteins in multiple pathways that repair DNA interstrand crosslinks....17

Figure 2.7 Structure of RAD51 and its paralogs indicating known domains....22

Figure 2.8 Ubiquitin modification of target proteins....31

Figure 2.9 Model of the SUMOylation cascade....35

Figure 2.10 Post-translational modifications along RAD51 and its paralogs....38

Figure 3.1 Predicted structure of RNF138....51

Figure 3.2 Summary of *Mus musculus Rnf138* splice variants....52

Figure 3.3 RAD51D is ubiquitinated in the absence of over-expressed RNF138 and in the presence of MG132....53

Figure 4.1 Alignment between *Homo sapiens* RAD51D (328 amino acids) and *Mus musculus* (C56BL/6) RAD51D (329 amino acids)....77

Figure 4.2 Conserved lysine residues along *Mus musculus* RAD51 family members....78

Figure 4.3 Complementation analysis of RAD51D lysine to arginine substitution Alleles....79

Figure 4.4 Intracellular localization of RAD51D variants....80

Figure 4.5 Yeast-two-hybrid protein interaction analysis between RAD51D variants and RAD51C, XRCC2, and RNF138 81

Figure 4.6 Stability of RAD51D variants 82

Figure 4.7 Ubiquitination of RAD51D variants 83

Figure 4.8 Recruitment of FANCD2, Ku86, and RAD51 to MMC-induced DNA Damage 84

Figure 4.9 Measurement of HR by reconstitution of GFP fluorescence in HeLa DRGFP cells 85

Figure 4.10 Proposed model of RAD51D ubiquitination during interstrand crosslink repair 87

Figure 5.1 Induction of γ-H2AX following treatment with 6TG 105

Figure 5.2 Co-localization of γ-H2AX with telomeres following treatment with 6TG 106

Figure 5.3 6TG induced chromosome fusions in *Rad51d*-deficeint immortalized MEFs 107

Figure 5.4 6TG treatment induces increased multinucleation in *Rad51d*-deficient and *Mlh1*-proficient MEFs 108

Figure 5.5 6TG treatment does not affect telomere distribution across nuclei within multinucleated cells 109

Figure 6.1 *Rad51d* expression and RNA quality assessment 140

Figure 6.2 Biological functions as identified by Ingenuity Pathway Analysis (IPA) in microarray data 141

Figure 6.3 Biological functions as identified by IPA of RNA Seq data set 142

Figure 7.1 Proposed RAD51 paralog complexes that function in response to DNA interstrand crosslinks and double strand breaks 147

Figure 7.2 Stability of RAD51D protein variants 150

Figure 7.3 Proposed model of RAD51D ubiquitination during DNA inter-strand crosslink repair 158

LIST OF ABBREVIATIONS

6TG 6-thioguanine

Bp ..... Base pair

DSB ..... Double strand break

dsDNA ..... Double stranded DNA

ICL ..... DNA interstrand crosslink

E1 ..... Ubiquitin activating enzyme

E2 ..... Ubiquitin conjugating enzyme

E3 ..... Ubiquitin ligating enzyme

FA ..... Fanconi Anemia

HECT ..... Homologous to the E6AP carboxyl terminus

HR ..... Homologous recombination

IR ..... Ionizing radiation

kDA ..... Kilodalton

MEF ..... Mouse embryonic fibroblast

MMR ..... Mismatch repair

MMC ..... Mitomycin C

NER ..... Nucleotide excision repair

NHEJ ..... Non-homologous end joining

ONPG ..... Ortho-nitrophenyl-β-galactosidase

PTM ..... Post-translational modification

RING ..... Really interesting new gene

SDM.....Site-directed mutagenesis

SSB ..... Single strand break

ssDNA..... single stranded DNA

SUMO ..... Small ubiquitin-like modifier

UIM..... Ubiquitin interacting motif

Y2H..... Yeast-two-hybrid

ZF.....Zinc finger

CHAPTER 1

INTRODUCTION

Six identifiable biological characteristics of tumor development termed the "hallmarks of cancer" were classified by Hanahan and Weinberg (Hanahan and Weinberg 2000). In addition to these features, cancer cells acquire 'enabling characteristics' that contribute to carcinogenesis. In 2011, 'genome instability' was recognized as an enabling characteristic, and Hanahan and Weinberg argued that tumor growth can often be attributed to acquisition of mutations that promote cell proliferation and inhibit cell death (Hanahan and Weinberg 2011). The idea that genome instability contributes to cancer development was actually first proposed in 1914 by Theodor Boveri (Boveri 2008), and studies throughout the 21st century strongly support this theory. Boveri's observations that abnormal chromosomal arrangements are passed to sea urchin off-spring lead to the hypothesis that tumor development was a cellular problem and that cancer is, in fact, a genetic disease (Boveri 2008; Hansford and Huntsman 2014). Similarly, the observation that cancer is a mutation-driven disease led to the "Mutator Phenotype Hypothesis." First described by Lawrence Loeb, this hypothesis states that "mutations occur randomly throughout the genome, and among these would be mutations in genes that guarantee the fidelity of DNA replication… and repair" (Loeb, Springgate, and Battula 1974). Together, these ideas have led to the current belief that "defects in genome maintenance are… instrumental for tumor progression" (Hanahan and Weinberg 2011). The data

presented in this dissertation offer insights into how the RAD51D DNA repair protein contributes towards maintaining genomic integrity.

Chapter 2 provides an overview of literature discussing types of DNA damage that are recognized and repaired by the homologous recombination (HR) proteins, that specifically includes double strand breaks (DSBs), interstrand crosslinks (ICLs), and thiopurine-induced base pair mismatches. The RAD51 family of proteins – RAD51, RAD51B, RAD51C, RAD51D, XRCC2, and XRCC3 – are described, and their activity during HR-mediated repair is discussed. Post-translational modifications (PTMs) regulate DNA repair pathways. Ubiquitination and SUMOylation are described, and the function of these PTMs during DNA repair is highlighted. Finally, PTMs that occur along RAD51 proteins are discussed. Experiments in subsequent chapters focus on the RAD51D HR protein.

Chapter 3 presents work that was published in the research article entitled "RNF138 interacts with RAD51D and is required for DNA interstrand crosslink repair and maintaining chromosome integrity" in *DNA Repair* in April 2016 (Yard et al. 2016). The data in this paper demonstrated that RAD51D directly interacts with the E3 ubiquitin ligase RNF138, and that this interaction is mediated by the regions encoded by exon 5 and exon 7 along RNF138. RNF138 ubiquitinates RAD51D, and data presented in this Chapter also demonstrate that this modification occurs along RAD51D and not the RAD51C protein.

Chapter 4 presents work that identified two lysine residues along RAD51D – K235 and K298 – that are critical for ICL repair. In this study, single point mutations were generated in lysine codons along the *MmRad51d* gene to introduce arginine at those

locations. Substitution of two lysines – K235R and K298R –conferred cellular sensitivity to mitomycin C (MMC). Yeast-two-hybrid analysis demonstrated that these residues are not required for RAD51D interaction with RAD51C, XRCC2, or RNF138. A lysine-null mutant (K0) was 3 times more stable than wild-type RAD51D, and stability of K235R and K298R was increased 2- and 3-fold, respectively, compared with wild-type. *In vivo* ubiquitination assays detected a band corresponding to 3 ubiquitin molecules was present in wild-type, but not K0 samples, suggesting loss of a short ubiquitin chain along the protein in the absence of lysine residues. Furthermore, homology-directed repair assays suggest that neither K235 nor K298 is required for repair of *Sce*I induced DSBs.

Chapter 5 presents data that were published in the research article entitled "Thiopurine-induced mitotic catastrophe in *Rad51d*-deficient mammalian cells" in *Environmental and Molecular Mutagenesis* in September 2017 (Wyatt et al. 2017). The focus of this work was RAD51D function in response to 6-thioguanine (6TG)-induced base pair mismatches. In *Rad51d*-deficient cells, there was increased co-localization of telomere probes with γ-H2AX foci compared to *Rad51d*-proficient cells, which further increased upon treatment with 6TG. Chromosome fusions following 6TG treatment were detected, and telomere positive staining was observed at fusion points. These findings demonstrate that RAD51D provides a protective role against the telomeric DNA damage and chromosomal instability caused by thiopurine treatment.

Rad51d-deficient cells have extensive chromosomal aberrations, such as fusions, translocations, and telomere defects, that are often observed in ovarian cancer cells. For this reason, *Rad51d*-deficient mouse embryonic fibroblasts (MEFs) can be used as a model for genomic unstable ovarian cancers. In Chapter 6, gene expression profiles of

Rad51d$^{+/+}$*Trp53*$^{-/-}$ (*Rad51d*-proficient) and *Rad51d*$^{-/-}$*Trp53*$^{-/-}$ (*Rad51d*-deficient) primary MEF cell lines were assessed by microarray and RNA Seq analyses. Six hundred eighteen genes with differential expression between the *Rad51d*-proficient and -deficient cell lines were identified by microarray. Twenty-one of the identified genes are associated with cell cycle progression, and included: *Id1*, *Id2*, and *Cdkn1a(p21)*. RNA Seq analysis identified 928 genes that were differentially expressed. In addition, five gene fusions were identified in the *Rad51d*-proficient cell lines, and one of these fusions was also present in the *Rad51d*-deficient samples. Comparison between the two data sets identified 111 genes that were differentially expressed between *Rad51d*-proficient and -deficient cell lines. Together these data provide insight into gene expression compromises that support cell division in a chromosomal unstable cell line.

In Chapter 7, a model of RAD51D ubiquitination during interstrand crosslink repair is proposed, and I hypothesize that ubiquitination at K235 and K298 is required for RAD51 recruitment to DSBs. Follow-up experiments to better elucidate the role of K235 and K298 for RAD51D function are proposed, and I predict that these residues will also be necessary for cellular resistance to 6TG. Finally, mass spectrometry analysis should be performed to identify specific PTMs that occur along the RAD51D protein.

CHAPTER 2

LITERATURE

Accurate repair of DNA damage is essential for maintaining genomic integrity, and accumulation of mutations is one of the early steps that lead to cancer development. Boveri's observations that abnormal chromosomal arrangements were passed to sea urchin off-spring and Loeb's "Mutator Hypothesis" support the idea that "defects in genome maintenance are… instrumental for tumor progression" (Hanahan and Weinberg 2011; Loeb, Springgate, and Battula 1974; Boveri 2008). Mutations in several key DNA damage response genes, including BRCA1, BRCA2, and the RAD51 family of proteins, are associated with increased cancer risk (Prakash et al. 2015). In addition to protecting the cell from genomic insult, RAD51 and its paralogs – RAD51B, RAD51C, RAD51D, XRCC2, and XRCC3 – function during the homologous recombination pathway that recognizes and repairs DNA double strand breaks. These lesions can be directly introduced through exogenous agents, such as ionizing radiation, or through the repair of other forms of damage, such as cisplatin-induced DNA interstrand crosslinks and thiopurine-induced base pair mismatches (Figure 2.1) (Karran 2006; Suchankova et al. 2012).

The following sections of this introduction will describe three types of DNA damage – DNA double strand breaks, DNA interstrand crosslinks, and thiopurine-induced base pair mismatches – that affect both strands of the DNA double helix. I will focus on the RAD51 family of proteins and discuss current knowledge regarding the

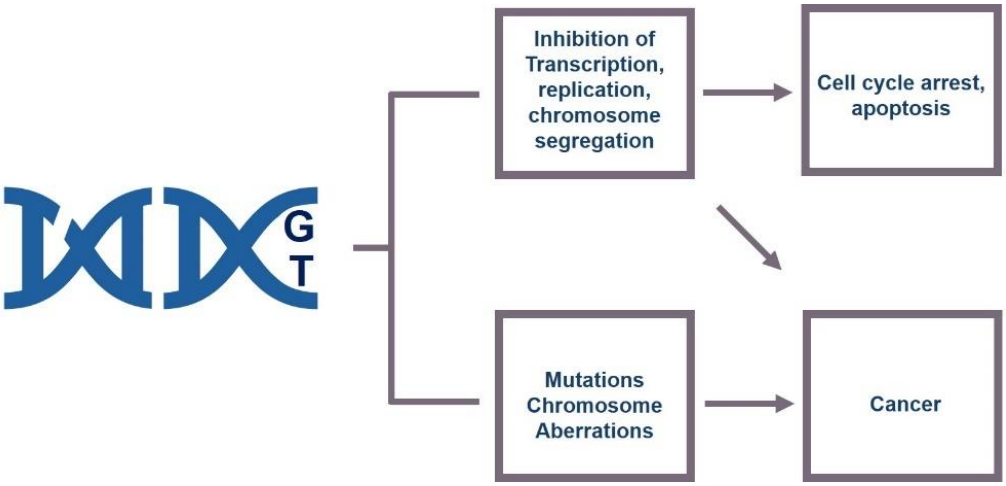

Figure 2.1. Overview of the cellular consequences of DNA damage. Single strand breaks (represented on the left), double strand breaks (represented in the middle), and base pair mismatches (represented on the right) left unrepaired or incorrectly repaired lead to cell cycle arrest, apoptosis, or cancer.

function of these proteins during homologous recombination-mediated DNA repair. In the second section, post-translational modifications, particularly ubiquitination, that regulate proteins during DNA damage response will be discussed. Finally, the focus of the last portion of this chapter will be post-translational modifications along the RAD51 paralogs.

Types of DNA Damage

For this section, I will describe three types of DNA damaging agents – ionizing radiation, interstrand crosslinking agents, and thiopurine nucleotide analogs – that lead to double strand breaks repaired by the RAD51 family of proteins. If left unrepaired or if repaired incorrectly, this damage can result in gene deletions, or chromosome translocations and fusions. These types of agents were utilized for experiments investigating the function of RAD51D in Chapters 4 and 5 of this dissertation.

Ionizing radiation induced damage

Genotoxic damage induced by ionizing radiation (IR), including β-, x-, and γ-rays, is a result of high-energy particles entering the cell and directly impacting the DNA. This radiative energy can induce a break in one or both strands of double stranded DNA (dsDNA) (Boudaiffa et al. 2000). The strand break is caused by electron attachment to a DNA component, such as the phosphate group, that initiates a resonance anion state, and produces repulsive energy along the nearby atomic bonds. The repulsive energy results in bond rupture and produces fragments along the DNA strand (Figure 2.2). Typically, electron attachment results in single strand breaks (SSBs), but observations of two strand breaks occurring locally within 10 bases of each other (Hieda 1994) suggests that the fragments produced by the bond rupture also react with DNA components on complementary strands, leading to an energy transfer that induces a second bond break and produces a DNA double strand break (DSB) (Boudaiffa et al. 2000). Although primary electrons from the IR source are a prominent cause of damage, DSBs can occur at lower energy levels, suggesting that these lesions are generated by secondary electrons in addition to the primary radiation source (Boudaiffa et al. 2000).

DNA interstrand crosslinks

Interstrand crosslinks (ICLs) occur when two complementary DNA strands become covalently linked. This type of damage is induced by endogenous reactive aldehydes or by exogenous chemicals, most commonly platinum-based chemotherapy drugs. Cisplatin is a chemotherapeutic agent used to treat breast, cervical, and ovarian cancers (Dasari and Tchounwou 2014). This chemical induces ICLs by binding the N7 of guanine nucleotides

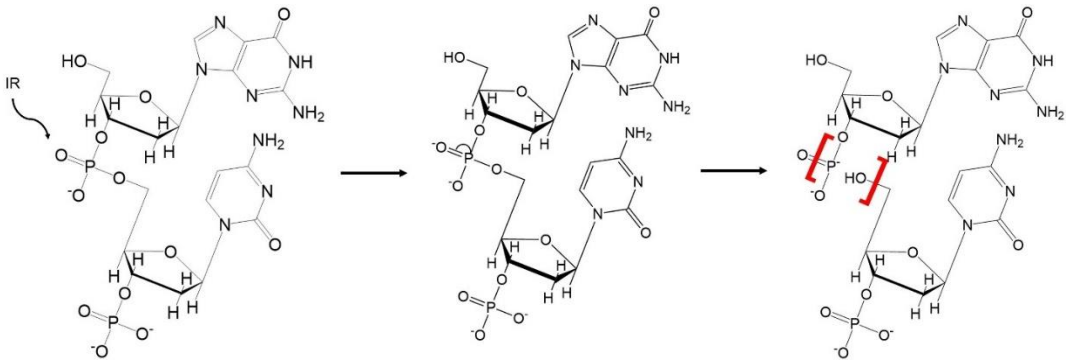

Figure 2.2. DNA damage break induced by ionizing radiation (IR). An IR source emits an energy particle (represented by the black arrow) that interacts with the phosphate group. The electron is absorbed by one of the atoms in the group, which initiates resonance and electron transfer to the phosphorous atom. The additional electron increases the energy state of the phosphorous atom and leads to hybridization into the d orbital. The higher energy state induced by hybridization generates a repulsive energy in the group and leads to one of the atomic bonds breaking and the DNA becoming fractured (red bracket).

at 5′ -GC-3′ sequences and 5′ -CG-3′ sequences (Figure 2.3) (Zou, Van Houten, and Farrell 1994). Cisplatin-induced ICLs that occur at 5′ -CG-3′ sequences can distort the DNA helix, shifting the platinum residue into the minor groove and bending the DNA strand so that the cytosine nucleotide sticks out of the plane of the helix (Malinge, Giraud-Panis, and Leng 1999; Huang et al. 1995). Distortions induced by the crosslink increases flexibility of the DNA structure, allowing for more thermodynamically favorable binding of the damaged DNA in the active site of repair enzymes (Lando et al. 2014). Cisplatin-induced crosslinks that occur at 5′ -GC-3′ sequences do not induce helical distortion (Wu et al. 2007), and have a structural conformation resembling native DNA. Nevertheless, repair proteins still recognize these lesions.

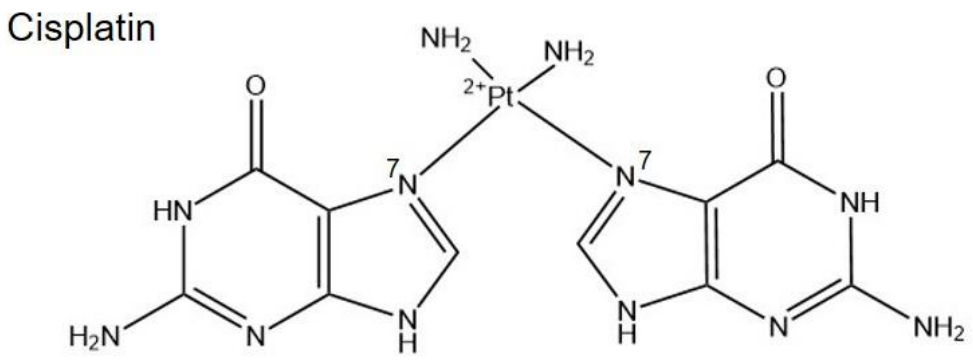

Figure 2.3 Platinum compounds binding guanine nucleotides. Cisplatin binds the N7 position on two guanine nucleotides in the same DNA strand.

Thiopurine-induced DNA mismatches

Thiopurines, including 6-thioguanine (6TG), are a class of purine analogs used for the treatment of cancer, particularly childhood leukemias (Munshi, Lubin, and Bertino 2014). First reported in 1954, 6TG is a guanine analog with a thiol group attached at the C6 in place of a carbonyl (Figure 2.4A) (Hitchings and Elion 1954). Thiopurines are pro-drugs metabolized to cytotoxic thioguanine nucleotides by hypoxanthine-guanine phosphoribosyl transferase (HGPRT) (Munshi, Lubin, and Bertino 2014; Coulthard and Hogarth 2005). During the metabolism of 6TG, HGPRT catalyzes the addition of 5-phosphoribosyl-1-pyrophosphate to the N9 residue of the 6TG molecule producing 6-thioguanosine monophosphate. Subsequent phosphorylation and reduction by nucleotide kinases and reductases result in the production of 6-thioguanine triphosphate (Figure 2.4B), which can be incorporated into DNA during replication.

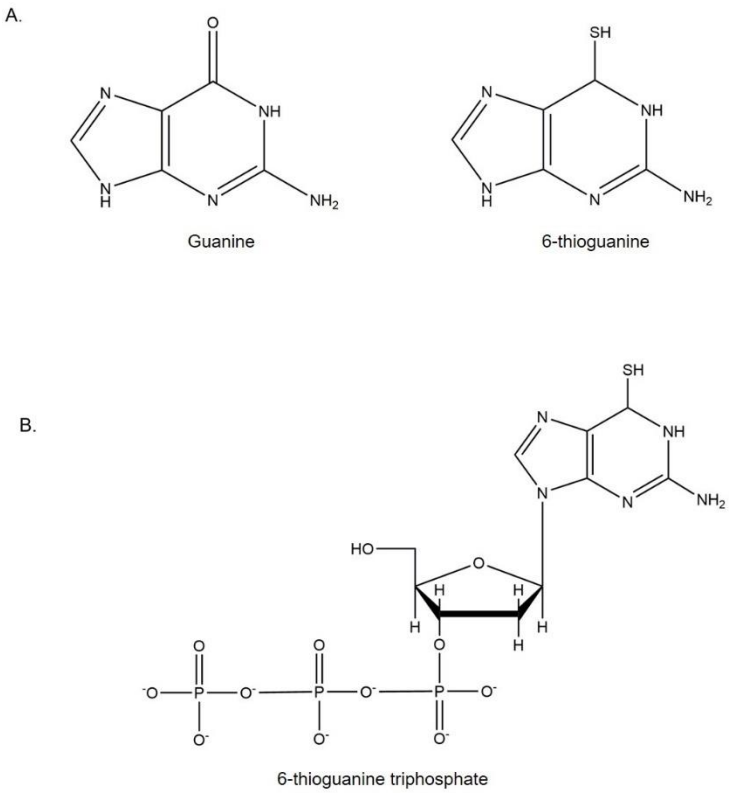

Figure 2.4. Metabolism of 6TG into cytotoxic nucleotides. (A) Chemical structure of guanine and 6-thioguanine. (B) Chemical structure of 6-thioguanine triphosphate (6TGTP).

The Michaelis-Menten constant (K_m) of 6TG incorporation into DNA is similar to that of guanine, therefore, polymerases are as likely to add a 6TG molecule to the DNA strand instead of guanine. Elongation of DNA containing 6TG is not inhibited by the analog, and is not recognized as a mismatch during initial incorporation (Karran and Attard 2008). Chemically, 6TG nucleotides are more reactive than canonical nucleotides, and are methylated *in situ* to produce methyl-6TG. During subsequent rounds of replication, the methyl-6TG resembles an adenine nucleotide and there is approximately equal probability of either a cytosine or thymine being added opposite to 6TG during replication in the daughter DNA strand, leading to a base pair mismatch (Rappaport 1993). DNA duplexes containing 6TG:thymine base pairs exhibit a slight helical

distortion (Bohon and de los Santos 2005, 2003) that shifts the thymine into the major groove of the DNA duplex and the 6TG into the minor groove (Bohon and de los Santos 2005; Somerville et al. 2003). Interestingly, thermodynamic analysis demonstrates that 6TG:thymine base pairs are more stable than 6TG:cytosine pairs (Bohon and de los Santos 2005), and suggest that the minor distortion does not destabilize the DNA helix.

In the event of a 6TG:thymine base pair, this lesion is recognized as a mismatch by mismatch repair (MMR) proteins, which initiate removal of the newly added thymine molecule during replication (Yuan and Wang 2008; Singh et al. 1996). The "futile cycle" model proposes that 6TG remains in the template strand, and additional mismatches are likely to occur in subsequent rounds of replication. Repetitive addition and removal of nucleotides opposite the 6TG base prolongs activation of the MMR proteins, ultimately leading to a DNA double strand break (Iyer et al. 2006; Li 2008, 1999).

DNA double strand break repair by homologous recombination proteins

DNA double strand breaks (DSBs) induced by ionizing radiation (IR) are recognized and resolved by proteins in the homologous recombination (HR) (Figure 2.5) and the non-homologous end-joining pathways. The damage is first recognized by poly(ADP-ribose) polymerase 1 (PARP1), a protein that scans the genome and detects DSB lesions (Ciccia and Elledge 2010). PARP1 marks the damage site by attaching ADP-ribose molecules to chromatin-bound proteins surrounding the break (Haince et al. 2008; Kim, Zhang, and Kraus 2005). The ADP-ribose units are essential for recruitment of meiotic recombination 11 (MRE11), RAD50, and Nijmegen Breakage Syndrome (NBS1) proteins, which form the MRN complex. MRN binding triggers recruitment of the ataxia

telangiectasia mutated (ATM) kinase that phosphorylates downstream repair proteins. One ATM substrate is C-terminal binding protein interacting protein 1 (CtIP), an exonuclease that acts in conjunction with the MRN complex to excise DNA and produce single strand DNA (ssDNA) surrounding the break (Dodson et al. 2010; Huen, Sy, and Chen 2010; You and Bailis 2010; Haince et al. 2008). Following MRN/CtIP-mediated nucleotide excision, the single strand binding protein replication protein A (RPA) stabilizes the newly produced ssDNA overhangs (Marechal and Zou 2015). Concurrently, additional substrates of ATM, including histone H2A and MDC1, are modified by a phosphate group. Phosphorylation of histone H2A at Ser139 (γ-H2AX) by ATM marks the DSB damage (Mah, El-Osta, and Karagiannis 2010; Rogakou et al. 1998), and triggers recruitment of additional repair proteins to the site. Phosphorylated MDC1 recognizes and binds the γ-H2AX modification, acting as an adaptor to facilitate localization of the E3 ubiquitin ligase RNF8 (Mailand et al. 2007; Yu et al. 2016).

Once localized to the damage site, RNF8 and its associated E2 ubiquitin conjugating enzyme, UBC13, attach two ubiquitin molecules to Lys119 of histone H2A (Mailand et al. 2007; Hodge et al. 2016; Yu et al. 2016). RNF8/UBC13 promote K63-linked ubiquitin chains, a variant of the ubiquitin modification that is predominant in DNA damage response (Panier and Durocher 2009). The K63-linked chains are recognized by a second E3 ligase, RNF168, that attaches additional K63-linked ubiquitins to produce a polyubiquitin chain (Doil et al. 2009). The polyubiquitin chain generated by RNF168 is recognized by the BRCA1/RAP80 complex via the tandem ubiquitin interacting motifs of the RAP80 protein (Sobhian et al. 2007; Poulsen et al. 2012; Sato et al. 2009). Binding of the BRCA1 complex initiates recruitment of the

RAD51 protein. This step is critical for progression of the HR pathway, and mutations in either BRCA1 or RAP80 have been associated with decreased RAD51 localization (Sobhian et al. 2007). RAD51 recruitment is also mediated by the BRCA2 protein and a complex comprised of other members of the RAD51 family – RAD51B, RAD51C, RAD51D, and XRCC2 (BCDX2). RAD51 interacts directly with BRCA2 through the conserved BRC repeats along the BRCA2 protein, and mutations in these domains disrupt HR progression (Galkin et al. 2005). A more detailed discussion of the RAD51 protein family is presented in an upcoming section of this chapter.

The BCDX2 complex, in conjunction with BRCA2, promotes RAD51 loading by displacing RPA from the ssDNA, allowing the RAD51 filaments to bind the single strand overhang (Candelli et al. 2014; Short et al. 2016; Xu et al. 2017; Jensen et al. 2013). Loading of RAD51 onto the ssDNA is essential for the homology search and strand invasion (Xu et al. 2017). RAD51 initiates search for a homologous template, usually a sister chromatid, by binding the dsDNA duplex formed during the strand invasion step (Qi et al. 2015). When sufficient homology is reached, RAD51 stabilizes the dsDNA duplex. In yeast, a minimum of 15 nucleotides in the template strand must be homologous to the RAD51-bound ssDNA (Qi et al. 2015), while a minimum of eight homologous nucleotides is required in mammalian cells (Lee et al. 2015; Qi et al. 2015). After a homologous sequence is identified, RAD54 integrates into the RAD51 filament, displacing RAD51, and allowing DNA polymerases to access the DNA and fill in the gap (Sanchez et al. 2013). This replication activity produces Holliday junctions, a cruciform structure that contains the four DNA strands joined together (Holliday 1964). After the DNA has been extended, the Mus81-Mms4 resolvase facilitates cross-over or non-

crossover events that resolve the Holliday junctions and produce two intact DNA strands with no errors (Wyatt and West 2014).

An alternative pathway for repairing IR-induced DSBs is the non-homologous end-joining (NHEJ) pathway. This pathway is active throughout the cell cycle and is considered to be error-prone as the ends of the breaks are re-ligated regardless of homology, which can lead to gene deletions, fusions, and chromosome rearrangements. First, DSBs are recognized by the Ku70/Ku80 heterodimer, which binds the ends of the DNA on both sides of the break. Formation of this heterodimer leads to activation of the catalytic subunit of DNA-dependent protein kinase (DNA-PK), a member of the ATM family of kinases. DNA-PK binds to Ku70 and Ku80 and stabilizes the ends of the DNA. After stabilization, the DNA ligase IV/XRCC4 complex binds and joins the ends of the DNA together, resulting in repair of the DSB (Karran 2000).

The choice to repair DSBs by HR or NHEJ is now known to be regulated by ubiquitination. For example, the E3 ubiquitin ligase RNF138, one of the proteins focused on in this dissertation, also plays a role in promoting HR and inhibiting NHEJ. In response to IR, RNF138 interacts with Ku70/Ku80 and initiates ubiquitination of the Ku80 protein. This modification leads to the degradation of the Ku80 protein, disrupting NHEJ and enhancing HR activity (Ismail et al. 2015). Additionally, in conjunction with the E2 ligase UBE2D, RNF138 ubiquitinates CtIP to promote end resection in the early stages of HR (Schmidt et al. 2015; Ismail et al. 2015).

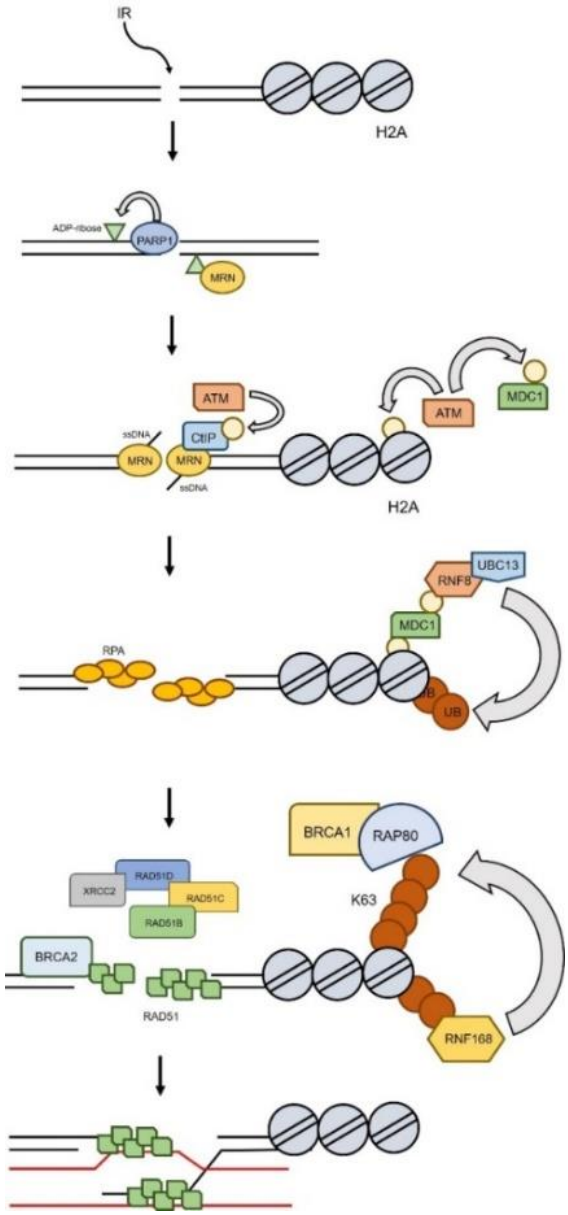

Figure 2.5. Model of homologous recombination-mediated double strand break (DSB) repair. The DSB is indicated by a gap in the two lines. First, PARP recognizes and marks the damage with ADP-ribosylation of the chromatin surrounding the break. The MRN complex binds the ADP-ribose molecule and promotes 5′ to 3′ nucleotide excision in conjunction with CtIP. RPA is recruited and binds the single strand overhang produced by the MRN complex. Concurrently, ubiquitin modifications along the histones surrounding the damage are added by RNF8 and RNF168 E3 ligases. The polyubiquitin chains are bound by the BRCA1/RAP80 complex that promotes recruitment of BRCA2 to the damage site. BRCA2 and the RAD51 paralogs displace RPA to allow RAD51 to bind to the ssDNA and promote strand invasion of the homologous template (modified from Brian D. Yard dissertation).

DNA interstrand crosslink repair during S phase

During DNA replication, two replication forks encounter an interstrand crosslink (ICL), resulting in a stalled replication fork. To remove the lesion, a core complex comprised of Fanconi Anemia (FA) proteins (FANCA, -B, -C, -E, -F, -G, -L, -M) is recruited and binds DNA strands surrounding the lesion (Figure 2.6). The FA core complex stabilizes the lesion and initiates recruitment of the FANCD2/FANCI heterodimer. A crucial step in FA-mediated ICL repair is mono-ubiquitination of FANCD2 and FANCI by the FANCL E3 ligase, a modification that activates the complex (Kim and D'Andrea 2012; Rickman et al. 2015; Liang et al. 2016). Activation of FANCD2/FANCI coordinates recruitment of FANCP/SLX4 and the endonucleases XPF, MUS81/ERCC1, and SLX1. Together, these proteins catalyze the incision of one DNA strand on both sides of the ICL lesion, producing a double strand break and leaving the crosslink as an overhang on the opposite strand (Kottemann and Smogorzewska 2013; Jo and Kim 2015; Knipscheer et al. 2009). The lesion overhang is displaced from the DNA helix and excised by nucleotide excision repair (NER) proteins, and translesion synthesis proteins fill in the gap across the strand (Haynes et al. 2015; Muniandy et al. 2010). Following FA function, the exonuclease CtIP interacts with FANCD2 and excises the DNA surrounding the break to produce a single strand overhang (Unno et al. 2014). BRCA2 and the BCDX2 complex coordinate recruitment of RAD51 to the overhang (Clauson, Scharer, and Niedernhofer 2013). RAD51 initiates strand invasion of the complementary intact dsDNA, allowing DNA polymerases to fill in the gap.

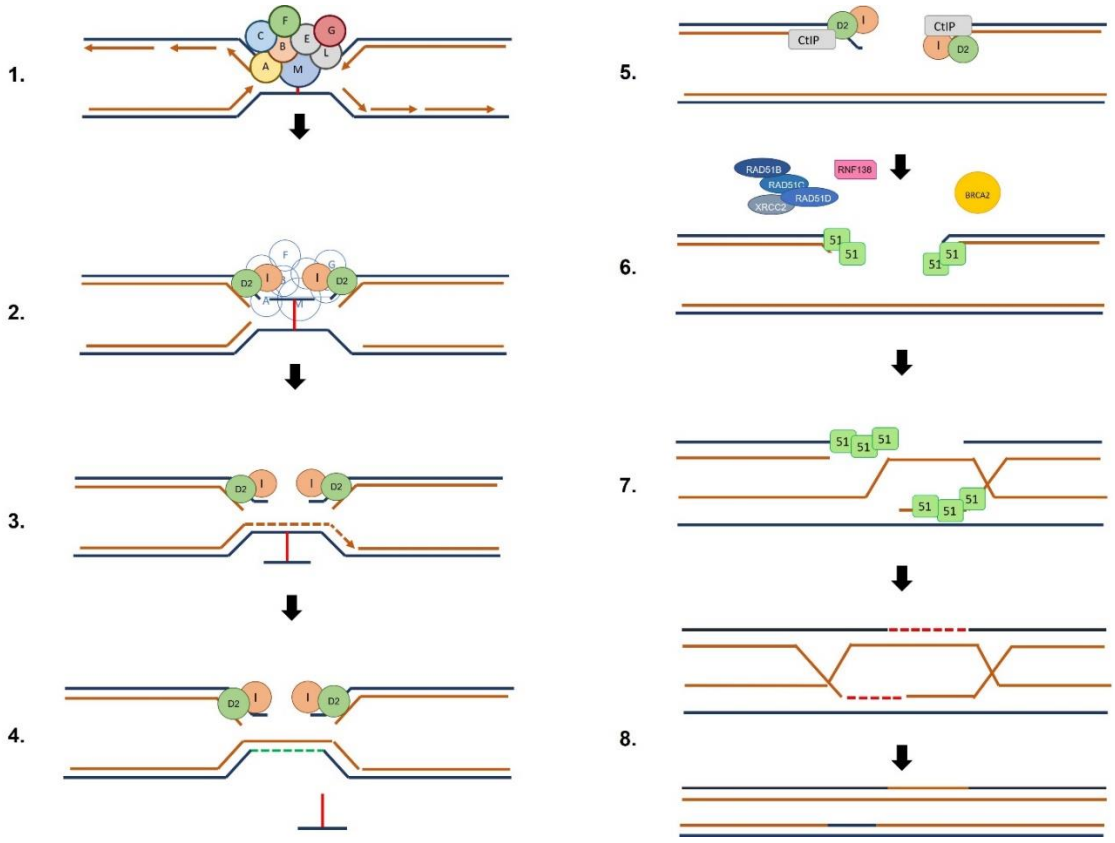

Figure 2.6. Key proteins in multiple pathways repair DNA interstrand crosslinks (modified from (Kim and D'Andrea 2012). (1) The FA core complex binds the lesion and recruits FANCD2/FANCI. (2) FANCD2/FANCI mediate strand incision and 'flip out' of the ICL lesion. (3) Translesion synthesis proteins replicate across the lesion. (4) Nucleotide excision repair proteins remove the lesion and fill in the gap. (5) CtIP interacts with FANCD2/FANCI and excises the DNA to produce a single strand overhang. RPA (not shown) coats the overhang to stabilize the ssDNA. (6) BRCA2 and the BCDX2 complex promote recruitment and binding of RAD51 to the single strand overhang. (7) RAD51 facilitates strand invasion of the homologous template. (8) DNA polymerases fill in the break and the Holliday junctions are resolved by Mus81-Mms84 resolvases.

Repair of mismatched nucleotides

Recognition and repair of DNA base pair mismatches, such as those introduced by 6-thioguanine (6TG), is performed by the mismatch repair (MMR) pathway. In eukaryotes, the mismatch is first recognized by MutSα (MSH2/MSH6), which binds the

mismatch(Casorelli, Russo, and Bignami 2008). Binding of MutSα initiates recruitment of MutLα (MLH1/PMS2) to form a MutSα/MutLα ternary complex (Li and Modrich 1995; Wang and Edelmann 2006). The complex scans along the DNA duplex until it encounters PCNA/RFC that can be either upstream or downstream of the mismatch. Binding activates the endonuclease activity of MutLα which generates an incision in the daughter strand (Kadyrov et al. 2006). The exonuclease 1 (EXO1) protein recognizes the nick and excises the strand in a 5′ to 3′ direction through the mismatch (Li 2008; Kadyrov et al. 2006). RPA binds the ssDNA overhang to stabilize strand that is produced by EXO1. DNA polymerase δ fills in the gap, and DNA ligase I seals the nick (Pena-Diaz and Jiricny 2012; Jiricny 2006). A new mismatch re-activates the MMR proteins, and the process repeats itself (York and Modrich 2006). Prolonged activation of MMR proteins can result in a futile cycle that leads to a double strand break that is repaired by HR proteins (Karran 2001).

The RecA and RAD51 connection

The *Escherichia coli* protein, RecA, is a highly conserved recombinase that promotes recombination-mediated repair of DNA damage (Bell and Kowalczykowski 2016). *In vivo,* RecA forms nucleoprotein filaments that preferentially bind single strand DNA (ssDNA) generated by resection of double strand DNA (dsDNA) during DNA damage response (Bell and Kowalczykowski 2016). RecA nucleofilament formation creates tension along the strand and results in unwinding of the DNA (Singleton and Xiao 2001). Binding of RecA to sites of damage is an essential step in the homologous recombination

(HR) repair pathway (Bell and Kowalczykowski 2016), and this protein functions to facilitate strand invasion of the homologous template during DNA repair (Singleton and Xiao 2001).

The yeast RecA homolog, RAD51, is essential for maintaining genome stability and integrity throughout the mitotic cell cycle and during meiosis (Krogh and Symington 2004; Shinohara, Ogawa, and Ogawa 1992). Similar to RecA, yeast RAD51, forms helical nucleoprotein filaments along ssDNA that promote strand exchange activity in an ATP-dependent manner (Shinohara, Ogawa, and Ogawa 1992; Ogawa et al. 1993; Shinohara and Ogawa 1999; Sung 1994; Conway et al. 2004; Chen et al. 2010). Alanine substitution at lysine 191 in yeast RAD51 (K191A)[1] diminished ATPase function, and decreased mitotic recombination activity of the protein. Additionally, cells expressing the RAD51-K191A mutant were more sensitive to ionizing radiation than wild-type expressing cells (Morgan, Shah, and Symington 2002). Another mutant, RAD51-H352Y, displayed similar ssDNA binding activity as wild-type RAD51, but was defective for nucleotide exchange and strand exchange activity. Structural analysis determined that RAD51-H352Y binding to ssDNA stabilized a nearby phenylalanine (F187) residue and blocked the γ-phosphate binding site of a Walker Box A motif (described below), impairing ATPase activity of the protein (Chen et al. 2010). These data further demonstrated that RAD51 activity is ATP-dependent.

A mammalian homolog of the RecA and yeast RAD51 protein, also named RAD51, is essential for HR in response to ultraviolet radiation (Morita et al. 1993). Early

[1] Note that the nomenclature used to represent amino acid substitutions is the "wild-type single letter amino acid designation" followed by the "residue number" then the "substituted amino acid designation" (e.g. K191A). This nomenclature will be used throughout this dissertation.

studies demonstrated that expressing *Mus musculus* (*MmRad51*) in RAD51-deficient yeast restored cell survival, particularly in response to double strand breaks (DSBs). The mouse *Rad51* gene has approximately 83% and 55% identity with the yeast RAD51 and *E. coli* RecA genes, respectively (Morita et al. 1993). RAD51 monomers interact to form oligomers in free solution prior to binding to ssDNA, and the size of the oligomer affects DNA binding, with smaller oligomers binding more readily to ssDNA than larger oligomers (Sung et al. 2003; Candelli et al. 2014). Structural analysis using cryo-electron microscopy found that RAD51 nucleofilaments form a helical structure around the ssDNA (Xu et al. 2017; Short et al. 2016).

Although RAD51 oligomers have a higher affinity for ssDNA, the ability to bind to dsDNA is essential for promoting homology search and strand exchange during repair (Danilowicz et al. 2014). When bound to dsDNA, RAD51 filaments extend the DNA strand and create tension along the helix and unwinding the DNA (Benson, Stasiak, and West 1994). This tension exposes Watson-Crick base pairings and allows for brief bonding of non-homologous ssDNA to the dsDNA during the homology template search (Danilowicz et al. 2014).

Mammalian RAD51 Paralogs

During homologous recombination (HR), the five RAD51 paralogs – RAD51B, RAD51C, RAD51D, XRCC2, and XRCC3 – alleviate competition between RAD51 and RPA for DNA binding, promoting RAD51 loading onto single stranded DNA (Sigurdsson et al. 2001), and assist in Holliday junction resolution (Liu et al. 2007;

Compton, Ozgur, and Griffith 2010). Each paralog has the conserved Walker Box A and B ATPase motifs, multimer (BRC) interface, and helix-hairpin-helix region discussed below (Figure 2.7) (Miller et al. 2004; Kawabata, Kawabata, and Nishibori 2005).

The Walker Box A and B motifs are ATP binding sites that catalyze the hydrolysis of ATP to promote ssDNA binding activity of the paralogs (Braybrooke et al. 2000; Chen et al. 2010; Gruver et al. 2005; Kawabata, Kawabata, and Nishibori 2005), and mutations in the Walker Box A motif have been shown to decrease ATPase activity and to increase cellular sensitivity to DNA damaging agents. Arginine substitution at a conserved lysine residue in the Walker Box A motif of the RAD51 paralogs decreases recombination activity. Substitution at K113 (K113R) in RAD51D lead to cell death in response to DNA damaging agents in mouse embryonic fibroblasts and Chinese hamster ovarian (CHO) cells (Wiese et al. 2006; Gruver et al. 2005). K113R interaction with RAD51C and XRCC2 was 8- and 2-fold lower than wild-type RAD51D, respectively (Gruver et al. 2005). Substitutions at K113 in Walker Box A of XRCC3 eliminated ATPase activity and lead to prolonged association between XRCC3 and RAD51C, suggesting that ATP hydrolysis activity is required to regulate paralog complex formation (Yamada et al. 2004). Loss of function Walker Box B mutants fail to complement *Rad51d*-deficiency in CHO cells motif in the presence of MMC (Wiese et al. 2006).

The BRC interface is a region of homology between the RAD51 paralogs and the breast cancer associated 2 (BRCA2) protein (Pellegrini et al. 2002; Lo et al. 2003). Interestingly, RAD51 interacts with BRCA2 through this interface, but none of the other paralogs have been shown to bind BRCA2 (Lo et al. 2003). Peptide fragments from the BRC region of BRCA2 act as an inhibitor of RAD51 binding to BRCA2 and prevent

RAD51 nucleoprotein filament formation (Nomme et al. 2008). Furthermore, substitution of Tyr315 in the BRC interface of RAD51 inhibits dsDNA unwinding, presumably through decreased RAD51 filament formation (Takizawa et al. 2004).

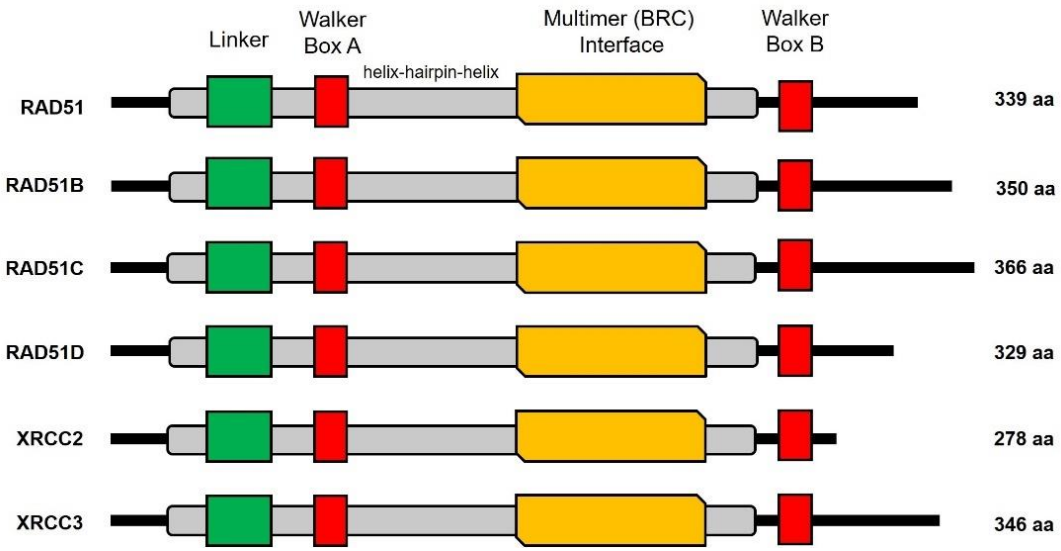

Figure 2.7. RAD51 and its paralogs indicating known domains. The RAD51 family share approximately 20 – 30% identity and have several conserved domains, including a linker region (green) and a helix-hairpin-helix structure (grey). Two Walker Box ATPases motifs (A and B; red) are present in all paralogs and a multimer (BRC) interface domain (yellow) mediates interaction between RAD51 and BCRA2 and is predicted to mediate interactions between the paralogs.

RAD51 paralog complexes

Yeast-two-hybrid protein interaction analysis demonstrated that the five RAD51 paralogs bind in several different combinations: (1) RAD51B with RAD51C, (2) RAD51C with RAD51D, (3) RAD51D with XRCC2, and (4) RAD51C with XRCC3 (Dosanjh et al. 1998; Liu et al. 1998; Braybrooke et al. 2000; Schild et al. 2000). Immunoprecipitation of human RAD51 paralogs further identified two distinct complex formations: RAD51B-

RAD51C-RAD51D-XRCC2 (BCDX2) and RAD51C-XRCC3 (CX3) (Masson et al. 2001; Rajesh et al. 2009). Structural analysis using transmission electron microscopy revealed that both the BCDX2 and CX3 complexes form a multimeric ring structure arranged in a flat disc around DNA Holliday junctions (Compton, Ozgur, and Griffith 2010).

The BCDX2 complex preferentially binds to two distinct DNA structures: Y-shaped DNA and DNA Holliday junctions (Yokoyama et al. 2004), and is required for RAD51 foci formation in response to IR-induced DSBs (Chun, Buechelmaier, and Powell 2013). Depletion of the RAD51D gene decreased RAD51 foci formation, but depletion of XRCC3 did not affect RAD51 foci formation in response to IR suggesting that the BCDX2, not the CX3 complex, is responsible for recruiting RAD51 to damage sites following IR treatment (Chun, Buechelmaier, and Powell 2013). Additionally, the BCDX2 complex stabilizes Holliday junctions and promotes proper resolution of the DNA strands (Liu et al. 2004; Liu et al. 2007; Chun, Buechelmaier, and Powell 2013).

Deletion/disruption mutations of RAD51 paralogs in the mouse genetic model

To date, deletions of the RAD51 protein family have only been generated in mouse embryonic fibroblasts (MEFs), DT40 avian cells, or Chinese hamster ovarian cells, and loss of each gene results in an embryo lethal phenotype (Takata et al. 2001; Deans et al. 2003; Hinz et al. 2006; Griffin et al. 2000; Shu et al. 1999; Pittman and Schimenti 2000; Lim and Hasty 1996; Tsuzuki et al. 1996; Kuznetsov et al. 2009). For the purposes of this dissertation, only mouse gene deletions of the RAD51 paralogs will be discussed.

To study the *Rad51* gene deletion, heterozygous *Rad51* (*Rad51*$^{+/-}$) mice were intercrossed, and out of 148 offspring, zero pups were *Rad51*-null (*Rad51*$^{-/-}$) (Tsuzuki et al. 1996). Early development analysis of potential *Rad51*$^{-/-}$ embryos found that one out of nine 2-cell stage embryos, and one out of 109 4- to 8-cell stage embryos were *Rad51*-null (Tsuzuki et al. 1996). Additionally, blastocysts isolated from *Rad51*$^{-/-}$embryos failed to divide in culture (Tsuzuki et al. 1996; Lim and Hasty 1996). To prolong embryo development, *Rad51*$^{+/-}$ mice were intercrossed with heterozygous *Trp53* (*Trp53*$^{+/-}$) mice, and it was observed that the embryo lethal phenotype can be partially rescued when the *Rad51* gene deletion is generated on a *Trp53*-null (*Trp53*$^{-/-}$) background (Shu et al. 1999; Lim and Hasty 1996). *Rad51*$^{-/-}$*Trp53*$^{-/-}$ embryos were slightly smaller than control littermates (Lim and Hasty 1996), and developed to 8.5 days post conception (dpc) (Tsuzuki et al. 1996). However, out of 41 pups, zero were *Rad51*$^{-/-}$*Trp53*$^{-/-}$, demonstrating that the *Trp53*$^{-/-}$ background did not restore offspring survival (Lim and Hasty 1996). Despite embryo survival being extended by the concurrent deletion of *Trp53*, cells derived from *Rad51*$^{-/-}$*Trp53*$^{-/-}$ embryos did not proliferate in cell culture (Lim and Hasty 1996).

To generate *Rad51c*-deficient mice, heterozygous *Rad51c* (*Rad51c*$^{+/-}$) mice were intercrossed, and no viable pups were obtained. It was also observed that the ratio of live births for wild-type versus *Rad51c*$^{+/-}$ deviated from the Mendelian 2:1 ratio, suggesting that loss of one *Rad51c* allele might affect embryo development (Kuznetsov et al. 2009). *Rad51c* embryos were phenotypically abnormal at 7.5 and 8.5 dpc compared with wild-type *Rad51c* embryos, and TUNEL staining of cells isolated from these embryos showed increased levels of apoptosis. Concurrent deletion of the *Trp53* gene extended embryo

development to 10.5 dpc. These embryos were smaller than littermate controls and did not appear to develop further. MEF cell lines were successfully generated from *Rad51c*$^{-/-}$ *Trp53*$^{-/-}$ embryos (Kuznetsov et al. 2009).

Deletion of the *Rad51d* gene has only been successful in MEFs (Smiraldo et al. 2005) and Chinese hamster ovarian cells (Hinz et al. 2006). Heterozygous *Rad51d* (*Rad51d*$^{+/-}$) mice were intercrossed and out of 102 live births, none were *Rad51d*-deficient (*Rad51d*$^{-/-}$). It was determined that embryo death occurred between 8.5 and 11.5 dpc in *Rad51d*$^{-/-}$ embryos (Pittman and Schimenti 2000). Deletion of the *Trp53* gene in *Rad51d*$^{-/-}$ embryos extended embryo development to 15.5 dpc but did not result in live pups (Smiraldo et al. 2005). *Rad51d*$^{-/-}$ embryos exhibit severe developmental and chromosomal defects compared to *Rad51d*$^{+/-}$ littermates (Smiraldo et al. 2005). Similar to cells isolated from *Rad51*$^{-/-}$ embryos, *Rad51d*$^{-/-}$*Trp53*$^{+/+}$ cells did not grow in culture (Pittman and Schimenti 2000), but *Rad51d*$^{-/-}$*Trp53*$^{-/-}$ cells were able to proliferate in culture (Smiraldo et al. 2005).

Consistent with deletion of other RAD51 paralogs, loss of *Xrcc2* in mice resulted in embryo lethality. Embryo death occurred throughout gestation between 9.5 – 18.5 dpc. The observed neonatal lethality in these embryos appeared to be due to respiratory failure and was attributed to a high frequency of apoptosis in post-mitotic neurons (Deans et al. 2000). Deletion of the *Trp53* gene in *Xrcc2*$^{-/-}$ mice extended embryo development from 12.5 dpc to 18.5 dpc but did not result in any live births. Cells isolated from *Xrcc2*$^{-/-}$ embryos did not proliferate in culture, but consistent with *Rad51c*$^{-/-}$ and *Rad51d*$^{-/-}$ cells, deletion of the *Trp53* gene allowed for *Xrcc2*$^{-/-}$*Trp53*$^{-/-}$ MEF cell lines to be grown in culture (Adam, Deans, and Thacker 2007).

Given the importance of RAD51 paralogs in embryo development and cell survival, it follows that deletion of these genes in human cells would provide further insight into their function. However, to date, no successful attempts to generate RAD51 paralog gene deletions in human cells has been reported. RNA interference has been used to transiently decrease gene expression of RAD51 paralogs in human U2OS, MCF7, HT1080, HeLa, and T84 cells (Jensen et al. 2013; Chun, Buechelmaier, and Powell 2013; Lio et al. 2004; Lee et al. 2014; Wang et al. 2014; Loignon et al. 2007). In human WI38-VA13/2RA cells, depletion of *RAD51D* by two separate siRNAs resulted in apoptosis within seven days of transfection (Tarsounas et al. 2004). A different siRNA used in the same study resulted in cell death at day 5 when only 50% of the RAD51D protein was depleted (Tarsounas et al. 2004). Depletion of the *RAD51D* gene by 84% using siRNA in HT1080 and HEK293 cells increased chemosensitivity of these cells to the DNA damage agent mitomycin C (Jensen et al. 2013). Depletion of RAD51D in human U20S and MCF7 cells also significantly decreased repair of DNA double strand breaks induced by the *Sce*I endonuclease (Chun, Buechelmaier, and Powell 2013).

Disease phenotypes associated with RAD51 genes

The National Institutes of Health provides the ClinVar database, a publicly accessible archive of reports designed to support the evolution of understanding of the relationship between genotypes and clinically observed phenotypes, and to establish the clinical validity of an identified gene variant (Landrum et al. 2016). The mutant alleles listed in the ClinVar database have been identified through clinical testing, research, or extracted from the literature, and have been associated with disease phenotypes. Germline mutations in *Homo sapiens* RAD51, RAD51C, RAD51D, and XRCC3, have been

reported to the NIH ClinVar database and are classified as risk factors for breast, ovarian, and melanoma cancers (Table 2.1).

An intron variant of RAD51 increases disease risk in breast cancer patients that also carried BRCA2, but not BRCA1, mutations (Levy-Lahad et al. 2001). In this study, patients homozygous for the G>C single nucleotide polymorphism had a significant increase in disease risk compared to patients that were heterozygous G/C or homozygous G/G. Risk was further increased in patients that carried mutations in the BRCA2 gene. This mutation modifies splicing in the 5′ UTR of the RAD51 gene and influences RAD51 expression levels in patients (Antoniou et al. 2007). Interestingly, the increased risk in BRCA2-mutant patients was only associated with breast but not ovarian cancer risk (Levy-Lahad et al. 2001).

Three mutations in the RAD51C genes have been linked with an increased risk of cancer, most notably breast and ovarian cancers (Loveday et al. 2011; Loveday et al. 2012; Meindl et al. 2010; Pelttari et al. 2011; Thompson et al. 2012; Kuschel et al. 2002) (Table 2.1). RAD51C germline mutations have long been associated with increased risk for ovarian cancer (Loveday et al. 2012; Meindl et al. 2010; Pelttari et al. 2011; Song et al. 2015), while a connection with breast cancer risk has been debated in the literature (Schnurbein et al. 2013; Thompson et al. 2012). Novel splice-variant mutations that result in truncated RAD51C protein have been identified in both breast and ovarian cancer patients (Neidhardt et al. 2017), and pathogenic RAD51C variants have been detected in patients with a personal history of triple negative breast cancer (Buys et al. 2017). Six RAD51D mutations that increased a patient's risk for developing ovarian cancer, but not breast cancer, have been identified (Kraus et al. 2017; Song et al. 2015; Loveday et al.

2011). Recently, a RAD51D mutant allele was identified in a triple negative breast cancer patient, supporting its classification as a breast cancer susceptibility gene (Kraus et al. 2017).

In addition to increasing a patient's risk for a disease, genetic variants can be used to predict patient response to current chemotherapy agents (Le et al. 2017). Mutations in DNA repair genes, such as RAD51C and RAD51D, conferred cellular sensitivity to platinum-based compounds and to clinically available poly(ADP-ribose) polymerase inhibitors (PARPi) (Pennington et al. 2014; Huang et al. 2013; Loveday et al. 2011; Min et al. 2013). However, one mechanism of drug resistance to chemotherapies is re-activation of mutated DNA repair genes. A study of twelve pairs of pre-treatment and post-progression tumor biopsies from patients in a clinical trial of the PARPi Rucaparib identified secondary somatic mutations in RAD51C and RAD51D that confer resistance to therapy (Kondrashova et al. 2017). Genetic analysis was performed in the twelve paired samples (pre-treatment and post-progression) isolated from patients treated with Rucaparib. Of the twelve pre-treatment samples, six had truncation mutations in RAD51C or RAD51D, and five out of the six corresponding post-progression samples had one or more secondary mutations that restored the open reading frame of the affected gene and increased Rucaparib resistance (Kondrashova et al. 2017).

Table 2.1. RAD51 and paralog mutant alleles classified as "risk factor" as reported to the National Institutes of Health ClinVar database (https://www.ncbi.nlm.nih.gov/clinvar/) (Landrum et al. 2016).

Gene	Mutant Allele	Condition/Disease	Citation(s)
RAD51			
135G>C	intron variant	Breast cancer in BRCA2 mutation carriers	(Antoniou et al. 2007; Levy-Lahad et al. 2001)
760C>T	Arg254Ter	Mirror movements 2	(Depienne et al. 2012; Depienne et al. 2011)
RAD51C/ FANCO			
1-BP Del 93G	Frame shift	Breast/Ovarian Cancer	(Pelttari et al. 2011)
1-BP Del 230G	Frame shift	Breast/Ovarian Cancer	(Thompson et al. 2012)
374G>T	Gly125Val	Breast/Ovarian Cancer	(Meindl et al. 2010)
RAD51D			
345G>C	Gln115His	Breast/Ovarian Cancer	(Loveday et al. 2011)
480+1G>A	Frame shift	Breast/Ovarian Cancer	(Loveday et al. 2011)
803G>A	Trp268Ter	Breast/Ovarian Cancer	(Loveday et al. 2011)
1-BP Del 363A	Frame shift	Breast/Ovarian Cancer	(Loveday et al. 2011)
757C>T	Arg235Ter	Breast/Ovarian Cancer	(Loveday et al. 2011)
556C>T	Arg186Ter	Breast/Ovarian Cancer	(Loveday et al. 2011)
XRCC3			
IVS5 A>G	SNP	Breast cancer	(Kuschel et al. 2002)
722C>T	T241M	Cutaneous malignant melanoma	(Winsey et al. 2000)

Ubiquitin modification of Proteins

DNA damage repair pathways are regulated by post-translational modifications (PTMs). Ubiquitination events during homologous recombination (HR)-mediated double strand break (DSB) repair are essential for pathway progression and accurate repair of the damage. Ubiquitin modification can activate proteins, initiate recruitment and binding of downstream proteins to a damage site, or signal proteasomal-mediated protein degradation (Akutsu, Dikic, and Bremm 2016). A small ubiquitin-like modifier (SUMO) molecule can also be added to proteins, and crosstalk between ubiquitin modifications and SUMO-modifications promotes DNA damage response and repair. These regulatory modifications will be discussed in this section.

Ubiquitin is a conserved 76 amino acid protein expressed throughout the cell. Modifications occur when the ubiquitin molecule is covalently linked at its C-terminus glycine residue (Gly76) to the ε-amine group of a lysine residue or to the N-terminus of the substrate (Busch and Goldknopf 1981). Ubiquitins are attached to a target protein by a three-step enzymatic reaction performed by E1 (ubiquitin-activating), E2 (ubiquitin-conjugating), and E3 (ubiquitin-ligating) enzymes (Figure 2.8A and B) (Pickart 2004; Hershko 1983). Binding of the ubiquitin molecule to an E1 enzyme consumes ATP and activates the ubiquitin by generating a high-energy thioester bond between the C-terminus of the ubiquitin and the cysteine in the E1 active site (Pickart 2004). Following activation, the ubiquitin molecule is transferred to an E2 enzyme. E2s have a core ubiquitin-conjugating domain that forms an active site to bind an activated ubiquitin molecule via a highly conserved cysteine residue. Ubiquitin-bound E2s interact with two

types of E3 ligases: RING (really interesting new gene) or HECT (homologous to the E6-AP carboxyl terminus) (Ye and Rape 2009).

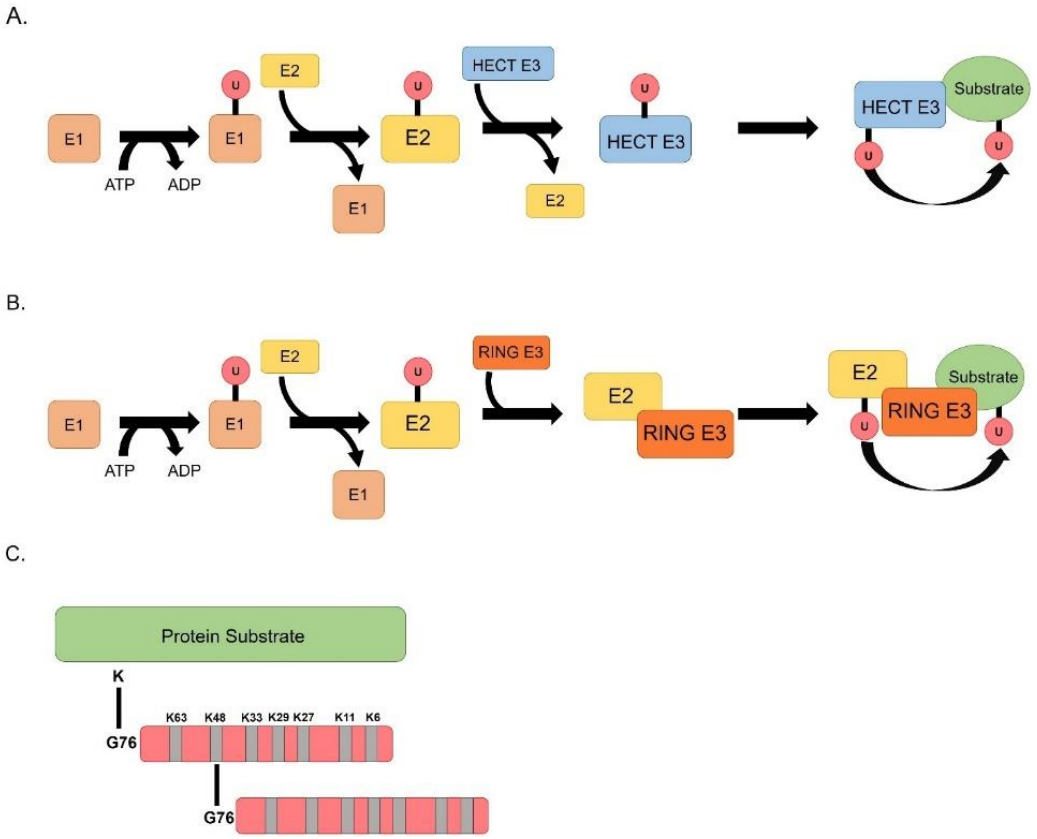

Figure 2.8. Ubiquitin modification of target proteins. (A) Three step enzymatic addition of a ubiquitin molecule to a substrate protein. The ubiquitin is activated and ligated to an E1 enzyme in a reaction that consumes ATP. The activated ubiquitin is transferred to an E2 enzyme that interacts directly with a RING E3 ligase. The RING E3 binds the target protein and promotes the transfer of the ubiquitin molecule from the E2 to the substrate. (B) The activated ubiquitin molecule is transferred from the E2 enzyme directly to the HECT E3 ligase. The HECT interacts with the substrate and facilitates the transfer of the ubiquitin to the protein. (C) Polyubiquitin chains are formed between the terminal glycine of one ubiquitin and one of seven lysine residues (indicated by the grey box) of another ubiquitin molecule.

The E3 ligases provide substrate specificity by binding to the target protein and facilitating the transfer of the ubiquitin (Clague, Heride, and Urbe 2015). HECT E3s are catalytically active and bind the ubiquitin molecule prior to transfer to the substrate

(Figure 2.7A) (Scheffner and Kumar 2014). RING E3 ligases are catalytically inactive, and act as scaffolds between the E2 enzyme and the substrate, promoting E2-dependent ubiquitination of target proteins (Figure 2.7B) (Lorick et al. 1999). The RING domain serves as the interacting region between the E3 and the E2 enzymes. The structure of this domain is a double loop that coordinates binding of two zinc ions, producing a surface for the E2 to bind (Metzger et al. 2014).

Ubiquitins can be added to single or multiple lysine residues along a target protein to produce mono- and multi-mono modifications, or ubiquitin chains can be generated along a single lysine residue. Polyubiquitin chains are formed when multiple ubiquitins are attached directly to each other through isopeptide bonds between a lysine residue on the previous molecule and Gly76 on the subsequent molecule (Figure 2.7C) (Akutsu, Dikic, and Bremm 2016; Swatek and Komander 2016). There are seven lysine residues along the protein that can be used to generate poly-ubiquitin chains (Sloper-Mould et al. 2001). The function of a polyubiquitin chain is determined by the lysine residue along each ubiquitin that forms the isopeptide bond. For example, chains generated between Lys48 of ubiquitin molecules (referred to as K48 linked chains) target a substrate for proteasomal degradation (Akutsu, Dikic, and Bremm 2016).

Ubiquitin chains have characteristic structural conformations that mediate recognition by chain-specific enzymes and binding proteins (Thach et al. 2016; Ikeda, Crosetto, and Dikic 2010). The ‘closed’ conformation occurs when two ubiquitin moieties directly interact via a hydrophobic patch in the middle of the ubiquitin protein. The ‘open’ conformation is observed when two ubiquitins are only linked by the isopeptide bond between the terminal glycine of one molecule and the lysine residue of

the second molecule (Ye et al. 2012). In solution, di-ubiquitin K63 chains adopt both 'open' and compact 'closed' conformations that are recognized by ubiquitin interacting motifs of DNA damage response proteins (Sato et al. 2009). Di-ubiquitin K48 chains predominantly adopt a 'closed' conformation recognized by the 19S subunit of the proteasome and target a protein for proteasomal degradation (Thach et al. 2016; Varadan et al. 2004; Ye et al. 2012; Chau et al. 1989).

The proteolytic component of the proteasome is a 20S unit is comprised of four homologous rings stacked together. The top and bottom rings are formed by seven α-subunits that recognize unfolded protein peptide chains. The two inner rings consist of seven β-subunits and form the proteolytic chamber of the proteasome (Cromm and Crews 2017). In addition to the core particle, there are various 'cap' structures that bind the proteasome. The 19S regulatory particle binds to one or both of the α-subunit rings of the 20S core particle to form the 26S proteasome (Guo and Peng 2013; Cromm and Crews 2017). The 19S subunit recognizes and cleaves ubiquitin chains along a substrate in an ATP-dependent manner. After removal of the ubiquitins, the substrate is shuttled into the proteolytic chamber and is degraded. The active site of the 19S subunit is specific for the 'closed' conformation of K48-linked ubiquitin chains, therefore, only these chains lead to proteasomal degradation (Ye et al. 2012; Chau et al. 1989).

Proteasome inhibition has been a mechanism of disease treatment for several decades. Bortezomib is a proteasome inhibitor approved by the United States Food and Drug Administration for the treatment of multiple myeloma since 2003, and remains a first-line treatment for the disease (Dou and Zonder 2014; Grosicki et al. 2014; Kane et al. 2003; Kouroukis et al. 2014; Schlafer et al. 2017). MG132 is a peptide aldehyde and a

naturally occurring proteasome inhibitor derived from a Chinese medicinal plant. This compound binds the active site of the β-subunits of the 26S proteasome, preventing proteolysis of ubiquitinated substrates (Guo and Peng 2013; Rock et al. 1994).

SUMOylation

Protein modification with SUMO (small ubiquitin-like modifier) molecules has emerged as another regulatory mechanism of DNA damage repair pathways (Nie and Boddy 2016; Pichler et al. 2017). There are five known SUMO paralogs expressed in mammalian cells: SUMO1, SUMO2/3, SUMO4, and SUMO5. SUMO1 has approximately 50% identity with SUMO2 and SUMO3, while the latter two paralogs have above 97% identity, and comprise the majority of the cell pool (Saitoh and Hinchey 2000; Pichler et al. 2017). Before being attached to a substrate, SUMO molecules must be processed by SUMO-specific proteases that cleave the C-terminus to produce a di-glycine motif that can be attached to ε-amine of lysine residues along target proteins (Eifler and Vertegaal 2015). Unlike SUMO1 and SUMO2/3, SUMO4 has a proline residue that prevents processing by any known SUMO-specific proteases and is not thought to modify proteins (Owerbach et al. 2005). SUMO molecules attached to target proteins at a SUMO consensus sequence (ψKxE where ψ is a bulky hydrophobic residue and E is an acidic residue) (Pichler et al. 2017; Hendriks et al. 2017; Bernier-Villamor et al. 2002), often found near phosphorylation sites along substrates (Hendriks et al. 2017).

SUMOylation occurs via a ubiquitination-like mechanism mediated by three enzymes: UBA/AOS1 (SUMO-activating SAE1/E2), UBC9 (E2 SUMO-conjugating), and E3 (SUMO-ligating) enzymes (Figure 2.9).

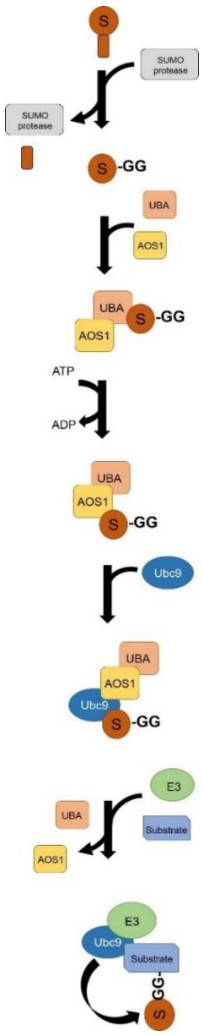

Figure 2.9. Model of the SUMOylation cascade. A SUMO molecule is activated by SUMO proteases that cleave the protein to expose two terminal glycine residues. Activated SUMO is bound by the UBA/AOS1 E1 heterodimer in a reaction that consumes ATP. The E2 Ubc9 binds AOS1 and the SUMO molecule is transferred from UBA to Ubc9. Ubc9 binds an E3 enzyme that has substrate specificity and facilitates the transfer of the SUMO molecule to a lysine residue along the substrate.

First, SUMO is bound by the UBA/AOS1 heterodimer and ATP hydrolysis activates the SUMO molecule. Activated SUMO forms a high-energy thioester bond with a cysteine residue in the active site of the AOS1 enzyme. AOS1 binds the UBC9 E2 enzyme, and SUMO is transferred to the cysteine residue in the active site of UBC9. Unlike in the ubiquitin-proteasome pathway, UBA/AOS1 and UBC9 are the only SUMO-associated E1 and E2 ligases identified in humans (Pichler et al. 2017). The SUMO-bound UBC9 protein interacts with one of several E3 enzymes, which have target specificity, and facilitates SUMO transfer from UBC9 to the substrate (Pichler et al. 2017).

Post-translational modifications along RAD51 proteins

Post-translational modifications (PTMs) play a vital role in promoting accurate repair of DNA damage and are prominent in the homologous recombination (HR) pathway. The six RAD51 paralog proteins are essential for progression of HR, therefore, modifications along these proteins are predicted to be required for HR progression. Proteomics analyses of the RAD51 proteins identified PTMs along each paralog (Figure 2.10) (Mertins et al. 2016; Mertins et al. 2013; Kim et al. 2011; Zhou et al. 2013; Somyajit et al. 2013; Slupianek et al. 2001; Takizawa et al. 2004; Yata et al. 2014; Yata et al. 2012; Yuan et al. 1998). Despite these data, limited experiments have been performed under DNA damage conditions. Given the prevalence of phosphorylation and ubiquitin modifications in DNA damage response, particularly in the HR pathway, and the importance of each paralog in promoting accurate DNA repair, it follows that investigation into these modifications is necessary.

In response to IR, RAD51 activity is regulated by phosphorylation. During S phase, phosphorylation along RAD51 is mediated by c-Abl at Tyr54 and Tyr315 (Yuan et al. 1998; Chen et al. 1999; Subramanyam et al. 2016; Takizawa et al. 2004). RAD51 is activated at the S/G2 junction of the cell cycle by the Chk1-mediated phosphorylation at Thr309 to promote HR (Sorensen et al. 2005). At the G2/M checkpoint, phosphorylation at Thr13 and Ser14 initiates RAD51 binding with the NBS1 protein to recruit RAD51 to the DSB site (Yata et al. 2014).

RAD51 activity during S phase is regulated by c-Abl-mediated phosphorylation at Tyr54 and Tyr315 (Yuan et al. 1998; Chen et al. 1999; Subramanyam et al. 2016; Takizawa et al. 2004). These modifications inhibit RAD51 oligomerization and can enhance its strand exchange activity (Subramanyam et al. 2016; Alligand et al. 2017). In addition to interacting with RAD51, one study identified a direct interaction between BCR-Abl and RAD51B, and found that BCR-Abl phosphorylates RAD51B (Slupianek et al. 2009).

The cell cycle checkpoint kinase Chk1 functions during S phase of the cell cycle (Arnaudeau, Lundin, and Helleday 2001), and directly interacts with RAD51 in response to hydroxyurea (HU)-induced DSBs (Sorensen et al. 2005). Chk1-mediated phosphorylation of RAD51 at Thr309 activates the protein and initiates HR (Sorensen et al. 2005). Cells deficient for Chk1 have decreased RAD51 foci formation in response to HU, and cells expressing a RAD51-T309A mutant that cannot be phosphorylated are hypersensitive to DNA damaging agents including HU and thymidylate synthase inhibitors (Sorensen et al. 2005; Yang, Waldman, and Wyatt 2012).

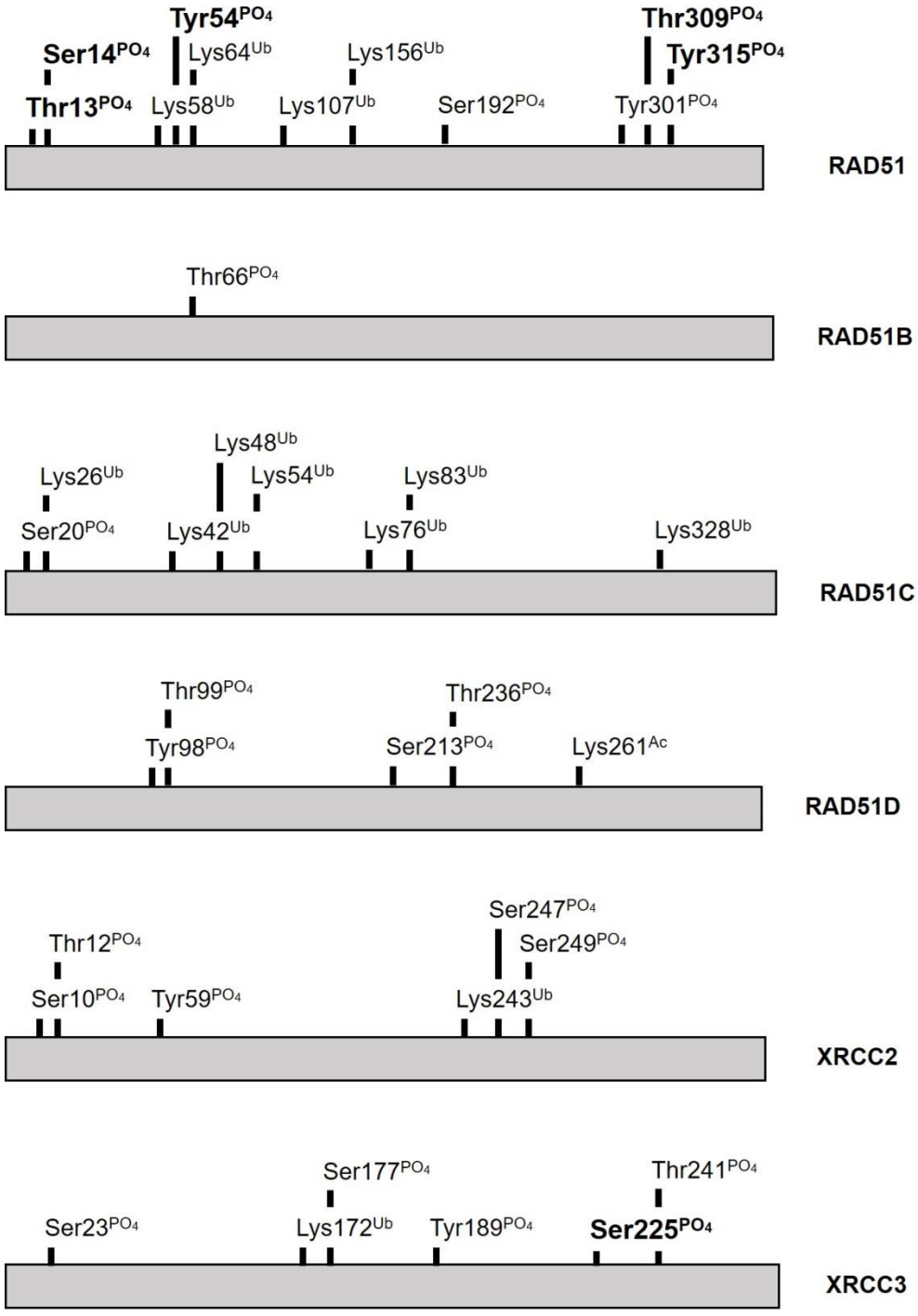

Figure 2.10. Post-translational modifications along RAD51 proteins. Known modifications are shown. Threonine, serine, and tyrosine residues are potential phosphorylation sites, and lysine residues are potential ubiquitination, SUMOylation, and acetylation sites. Bold indicates modifications identified in response to DNA damage.

BRCA2, a known RAD51 binding partner, coordinates the phosphorylation of RAD51 at Ser14 by polo-like kinase 1 (PLK1) in response to DNA damage at the G2/M junction of the cell cycle (Yata et al. 2014). Phosphorylation at Ser14 in turn initiates phosphorylation at Thr13 by casein kinase 2 (CK2), a modification that promotes RAD51 interaction with NBS1, a core component of the MRN complex (Yata et al. 2012). Interaction between RAD51 and NBS1 is important for RAD51 recruitment and binding to DNA damage sites (Yata et al. 2014).

Ubiquitination is another PTM present along RAD51. A novel E3 ubiquitin ligase, RFWD3 ubiquitinates RAD51 in response to DSBs induced by mitomycin C (MMC) as a mechanism of removing the protein from the single strand overhangs (Inano et al. 2017). Inactivation of RFWD3 results in persistent RAD51 foci at the damage site and increased cellular sensitivity to MMC. Additionally, RING mutants of RFWD3 are defective in promoting RAD51 ubiquitination (Inano et al. 2017).

In response to IR, XRCC3 activity during S phase is regulated by ATR-mediated phosphorylation at Ser225. interaction between RAD51C and XRCC3 is required for this modification, and depletion of RAD51C inhibits phosphorylation of XRCC3. This modification is dependent on ATM and is necessary for XRCC3-mediated recruitment of RAD51 to DSBs (Somyajit et al. 2013).

All investigations into the PTMs along RAD51 proteins have been performed in response IR-induced DSBs, and only limited studies have been performed in the presence of other types of damage. RAD51 paralogs, RAD51D specifically, are essential for cell survival in response to DNA ICL-inducing agents, yet knowledge about the PTM regulation of the paralogs in response to ICLs is limited. Further investigation into PTMs

along RAD51 paralogs in response to ICLs and other types of DNA damage will provide insight into the regulatory mechanisms of the HR pathway and offers the potential to identify new targets for clinical therapies.

Summary

Accurate repair of DNA double strand breaks is essential for maintaining genomic integrity and preventing carcinogenesis. The RAD51 family of proteins are key components of the homologous recombination (HR) pathway that functions to recognize and repair DNA DSBs induced by ionizing radiation and through the repair of cisplatin-induced DNA interstrand crosslinks. Post-translational modifications regulate activity of repair proteins, particularly in the HR pathway. Phosphorylation of RAD51 at Thr13 and Ser14 by polo-like kinase 1 and casein kinase 2, respectively, are essential for promoting RAD51 interaction with the NBS1 protein and recruitment of RAD51 to sites of DNA damage. Phosphorylation at Tyr54 and Tyr315 along RAD51 by the c-Abl kinase acts as a negative regulator of RAD51 activity and prevents hyperrecombination that can also lead to detrimental genetic mutations. Ubiquitin modification serves a key regulator of HR activity, and RAD51D has been identified as a ubiquitination target of the HR-associated E3 ubiquitin ligase, RNF138. Both RAD51D and RNF138 are essential for cell survival and promoting HR, suggesting that this modification is another key regulator of HR activity.

Data in Chapter 3 identified regions along RNF138 that mediate its interaction with RAD51D and demonstrated that RAD51D is ubiquitinated. The work presented in Chapter 4 identifies two essential lysine residues (K235 and K298) along RAD51D that

are required for cell survival in response to MMC-induced ICLs and are potential ubiquitination sites. The ubiquitin linkage arrangement along RAD51D is determined, and the stability of RAD51D in the absence of ubiquitinated lysine residues is established. In addition, RAD51D functions downstream of FANCD2 and Ku86 in response to mitomycin C-induced interstrand crosslinks. Chapter 5 demonstrates that RAD51D is required for maintaining telomere stability in response to 6TG, and the work presented in Chapter 6 identifies gene expression differences between *Rad51d*-proficient and *Rad51d*-deficient primary mouse embryonic fibroblasts as determined by microarray and RNA Seq. Together, the data presented in this dissertation will help to establish how RAD51D functions to maintain genome integrity in response to DNA damage, at the telomere region of chromosomes, and during embryogenesis.

CHAPTER 3

RNF138 ZINC FINGER MOTIFS MEDIATES ITS INTERACTION WITH RAD51D[2]

[2]Yard BD, Reilly NM, Bedenbaugh MK, Pittman DL. RNF138 interacts with RAD51D and is required for DNA interstrand crosslink repair and maintaining chromosome integrity. *DNA Repair*, **2016**, 42: 82 – 93.

Preface

Data presented in Chapter 3 were published in or are in addition to the research article entitled "RNF138 Interacts with RAD51D and is Required for DNA Interstrand Crosslink Repair and Maintaining Chromosome Integrity" appearing in *DNA Repair* on April 15, 2016 (Yard et al. 2016). For this manuscript, I generated the data demonstrating these RNF138 splice variants lacking exons 5 and 7 do not interact with RAD51D, and provided data showing that RAD51C is not ubiquitinated.

Introduction

DNA damage repair pathways are regulated by post-translational modifications, and ubiquitination events during homologous recombination (HR)-mediated double strand break repair are essential for pathway progression (Hodge et al. 2016; Mailand et al. 2007; Nakada, Yonamine, and Matsuo 2012; Poulsen et al. 2012). Ubiquitin modifications activate proteins, recruit downstream proteins to damage sites, and signal for proteasomal-mediated protein degradation (Akutsu, Dikic, and Bremm 2016). The RAD51 family of proteins – RAD51, RAD51B, RAD51C, RAD51D, XRCC2, and XRCC3 – function during HR. Five RAD51 paralogs bind in different combinations: (1) RAD51B with RAD51C, (2) RAD51C with RAD51D, (3) RAD51D with XRCC2, and (4) RAD51C with XRCC3 (Dosanjh et al. 1998; Liu et al. 1998; Braybrooke et al. 2000; Schild et al. 2000). Immunoprecipitation of human RAD51 paralogs identified two distinct complex formations: RAD51B-RAD51C-RAD51D-XRCC2 (BCDX2) and RAD51C-XRCC3 (CX3) (Masson et al. 2001; Rajesh et al. 2009).

A yeast-two-hybrid (Y2H) screen was performed in the Pittman laboratory to identify additional RAD51D interacting partners (Yard 2011; Yard et al. 2016). The screen identified 42 clones, two of which – RNF138 and UBC13 – participate in the ubiquitin proteasome pathway (Hodge et al. 2016; Kim and D'Andrea 2012; Nakada 2016; Nakada, Yonamine, and Matsuo 2012; van Twest et al. 2017; Xie et al. 2015). Neither RNF138 nor UBC13 interact with RAD51C or XRCC2, indicating that this interaction is unique to RAD51D (Yard 2011).

RNF138 belongs to a family of E3 ligases characterized by an N-terminal "really interesting new gene" (RING) catalytic domain, three zinc finger (ZF) motifs, and a ubiquitin interacting motif (UIM) (Giannini, Gao, and Bijlmakers 2008). Immunoprecipitation of over-expressed RAD51D and mutant RNF138 (RNF138-H36AC39S) demonstrated that the activity of the RING domain is not required for this interaction (Yard et al. 2016). Expression analysis of mouse tissue samples identified four distinct RNF138 splice variants: full-length, a deletion of exon 5 (RNF138Δ5), a deletion of exon 7 (RNF138Δ7), and a variant retaining intron four with a deletion of exon 7 (RNF138+int4Δ7) (Yard et al. 2016). Expression of the splice variants was similar to full-length in all tissue types except testis, in which expression of RNF138Δ5 and RNF138Δ7 was higher than full length RNF138. RNF138Δ5 is predicted to encode a 226 amino acid protein that remains in-frame and retains all five domains, and RNF138Δ7 is predicted to encode a 209 amino acid protein that lacks one of the C2H2 ZF domains. Y2H analysis demonstrated that the regions encoded by exon 5 and exon 7 of RNF138 are necessary for interaction with RAD51D.

RAD51D forms a complex with other RAD51 paralogs, including RAD51C, and proteomics studies have indicated that RAD51C could also be ubiquitinated (Mertins et al. 2013). To determine whether RAD51C is modified with ubiquitin, *in vivo* ubiquitination assays were performed using both RAD51D and RAD51C. Minimal ubiquitin signal was detected along RAD51C, suggesting that RAD51D is the primary target for this modification.

Materials and Methods

Yeast two hybrid assay

The cDNA of two RNF138 splice variants, one lacking exon 5 (MmRnf138Δ5) and one lacking exon 7 (MmRnf138Δ7), were cloned into the *Bam*HI and *Eco*RI restriction enzyme sites of pGADT7 and pGBKT7 yeast expression vectors. Previously described RAD51D wild-type yeast expression constructs were used for this study (Yard et al. 2016). The AH109 yeast strain was used for all experiments described here, and the genotype is as follows: *MATa, trp1-901, leu2-3, 112, ura3-52, his3-200, gal4Δ, gal80Δ, LYS2::GAL1*$_{UAS}$*-GAL1*$_{TATA}$*-HIS3, MEL1, GAL2*$_{UAS}$*-GAL2*$_{TATA}$*-ADE2, URA3::MEL1*$_{UAS}$*MEL1*$_{TATA}$*-lacZ* (Clontech Laboratories 2009). Each RNF138 splice variant was co-transformed with wild-type RAD51D using the Frozen EZ Yeast Transformation II kit (Zymo Research) per manufacturer's instructions (Schild et al. 2000). The strength of protein interactions was quantified using a liquid β-galactosidase assay (Serebriiskii and Golemis 2000; Gruver et al. 2009). The ortho-Nitrophenyl-β-galactoside (ONPG) substrate is added to yeast cell extracts that express the bait and prey proteins. Direct interaction between the two proteins initiates expression of the *LacZ* gene

which encodes the β-galactosidase protein. This enzyme catalyzes the hydrolysis of the ONPG substrate and produces two products: galactoside and ortho-Nitrophenol (ONP). Release of ONP produces a yellow color that was measured using a spectrophotometer (Beckman, DU 650). The absorbance of ONP was correlated to the strength of the interaction using the following equation:

$$\boldsymbol{\beta - galactosidase\ units} = \frac{(\mathbf{1000} * \boldsymbol{OD420})}{(\boldsymbol{t} * \boldsymbol{V} * \boldsymbol{OD600})}$$

where OD_{420} is the absorbance of the ONP solution, t is the reaction time, V is the total volume of the yeast liquid culture, and OD_{600} is the absorbance of the yeast liquid culture.

Immunoprecipitations

Plasmids containing Myc-tagged RAD51D or RAD51C, and HA-tagged ubiquitin were co-transfected into HeLa cells. Cells were treated with 25 μM MG132 (Sigma) 4 h prior to harvesting. Whole cell extracts were prepared after 24 h using 1X Cell Lysis Buffer (20 mM Tris, 150 mM NaCl, 1 mM EDTA, 1 mM EGTA, 1 mM PMSF, 1% TritonX-100) containing a protease inhibitor cocktail (Complete Mini; Roche Life Sciences). Three to five hundred micrograms of total protein was incubated with anti-myc magnetic beads (9E10; Thermo-Scientific) for 16 h at 4°C with gentle rocking in 1X Cell Lysis Buffer. Precipitated proteins were washed 3 times with 1X Cell Lysis Buffer, eluted by boiling in Laemmli buffer for 10 min, and resolved on 4–20% SDS-PAGE (Bio-Rad).

Immunoblotting

Western blot analysis was performed using mouse monoclonal anti-HA (3F10; Roche) or mouse monoclonal anti-Myc (9E10; Santa Cruz Biotechnology) primary antibodies.

Primary antibody incubations were followed by incubation with the appropriate species-specific IRDye 800CW secondary antibody (Licor). Detection of Myc-tagged RAD51D and RAD51C, and HA-tagged ubiquitin was performed using the Licor Odyssey Sa Imaging System, and densitometry measurements were performed using Licor Image Studio software (v4.0).

Results

Interaction between RAD51D and RNF138 splice variants

To date, a crystal structure of RNF138 has not been produced, therefore, a three-dimensional predicted structure was generated using the I-TASSER prediction program (Yang et al. 2015; Yang and Zhang 2015). This software implements a hierarchical approach to identify template proteins from the Protein Data Bank (PDB) using a multiple threading approach. Iterative template fragment assembly simulations produced full-length atomic models and threading the models through the protein functional database BioLIP derived functional predictions. Full-length RNF138 is predicted to have a linear conformation with the RING domain at the N-terminal, followed by the ZF motifs in the middle of the protein, and the UIM at the end (Figure 3.1A). The predicted structure for the RNF138Δ5 splice variant adopts a circular conformation that appears to disrupt formation of the ZF motifs (Figure 3.1B). The RNF138Δ7 predicted structure maintains a linear conformation similar to full-length but lacks one of the C2H2 ZF motifs (Figure 3.1C).

Yeast-two-hybrid (Y2H) was performed using RNF138 splice variants with a deletion of either exon 5 (*Rnf138Δ5*) or exon 7 (*Rnf138Δ7*) (Figure 3.2A) fused with the

GAL4 DNA binding domain (DBD) or the GAL4 activation domain (AD). Two wild-type RAD51D constructs, one fused with the DBD and one fused with the AD were used. RNF138-DBD splice variants were co-transformed with RAD51D-AD constructs, and RNF138-AD variants were co-transformed with RAD51D-DBD constructs into the AH109 yeast strain. RNF138Δ5 and RNF138Δ7 fused with DBD displayed a 7- and 2-fold decrease in the level of interaction with RAD51D-AD compared to full-length RNF138, respectively. Both RNF138Δ5 and RNF138Δ7 fused with the AD displayed a 5-fold decrease in the level of interaction with RAD51D-DBD compared with RNF138-full length (Figure 3.2B).

RAD51C is not ubiquitinated

RAD51D ubiquitination is mediated, at least in part, by RNF138, and this modification was previously observed when RAD51D was co-expressed with RNF138 and detection was performed using x-ray film (Yard et al. 2016). Here, using the Licor Odyssey system, ubiquitination of RAD51D can now be detected even when RNF138 is not co-transfected (Figure 3.3A). Ubiquitination of the Myc-RAD51D protein was also confirmed using an antibody against ubiquitin (Figure 3.3A; lower blot).

RAD51D directly interacts with two other RAD51 paralogs, RAD51C and XRCC2, to form the BCDX2 complex (Rajesh et al. 2009). Although RNF138 is not known to directly interact with either protein (Yard et al. 2016), RAD51C or XRCC2 could still be ubiquitinated by other E3 ligases or by RNF138 via its interaction with RAD51D. In fact, proteomics studies have identified seven lysine residues along RAD51C as potential ubiquitination sites (Kim et al. 2011; Mertins et al. 2013). To determine if RAD51C is ubiquitinated, Myc-tagged RAD51C was co-expressed in HeLa

cells with HA-tagged ubiquitin. Ubiquitin signal intensity along Myc-RAD51D was nearly 3-fold higher than Myc-RAD51C (Figure 3.3B). These data suggest that RAD51C is not ubiquitinated under these conditions.

Discussion

The RAD51 proteins are essential components of the homologous recombination (HR) pathway, and the fourth member, RAD51D, is required for cell survival in response to ionizing radiation (IR) and DNA interstrand crosslinks (ICLs) (Gruver et al. 2005). A yeast-two-hybrid (Y2H) screen identified a direct interaction with the E3 ubiquitin ligase RNF138 (Yard et al. 2016). Four distinct RNF138 splice variants – full-length, a deletion of exon 5 (RNF138Δ5), a deletion of exon 7 (RNF138Δ7), and a variant retaining intron four and a deletion of exon 7 (RNF138+int4Δ7) – have been identified in mouse tissues (Yard et al. 2016). Y2H analysis of two variants (RN138Δ5 and RNF138Δ7) demonstrated that the regions encoded by these exons mediate the interaction between RNF138 and RAD51D.

RNF138 is required for resistance in response to mitomycin C-induced interstrand crosslinks (ICLs), and loss of RNF138 diminished RAD51 localization (Yard et al. 2016). Ubiquitination is a regulatory mechanism of DNA repair, and RNF138 interaction with RAD51D suggests that this modification may regulate RAD51D function during HR-mediated repair. The stability of RAD51D was increased when RNF138 expression was suppressed by siRNA, demonstrating that RAD51D ubiquitination is mediated by RNF138, and that this modification targets the protein for proteasomal degradation (Yard et al. 2016). Given that both RAD51D and RNF138 are required for resistance to

mitomycin C (MMC) and for RAD51 recruitment, I propose that ubiquitination of RAD51D by RNF138 plays a role in promoting RAD51-mediated HR DNA damage repair.

This modification occurs along lysines, and identification of residues essential for RAD51D function may provide insight into ubiquitination sites along the protein. In conclusion, the data presented in Chapter 3 and published in *DNA Repair* (Yard et al. 2016) provide evidence for RAD51D ubiquitination promoting ICL repair and follow-up investigations into specific lysines along RAD51D required for this function are discussed in Chapter 4.

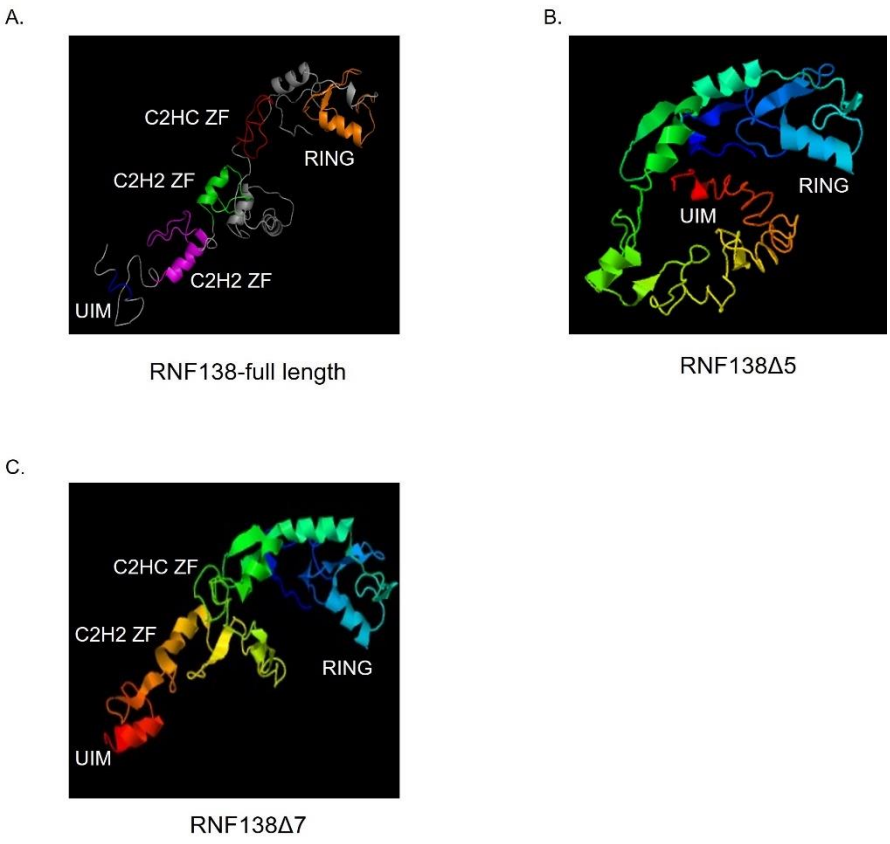

Figure 3.1. Predicted structure of the RNF138 E3 ubiquitin ligase protein. The iTASSER protein structure prediction software (Yang et al. 2015; Yang and Zhang 2015) was used to generate structures of (A) RNF138-full length, (B) RNF138Δ5, and (C) RNF138Δ7. (A) This ligase contains a really interesting new gene (RING) domain (orange), three zinc finger motifs (red, green, purple), and a ubiquitin interacting motif (blue). (B) This protein product maintains the RING domain and UIM. (C) This protein product maintains the RING domain, the C2HC ZF motif, one of the C2H2 ZF motifs, and the UIM.

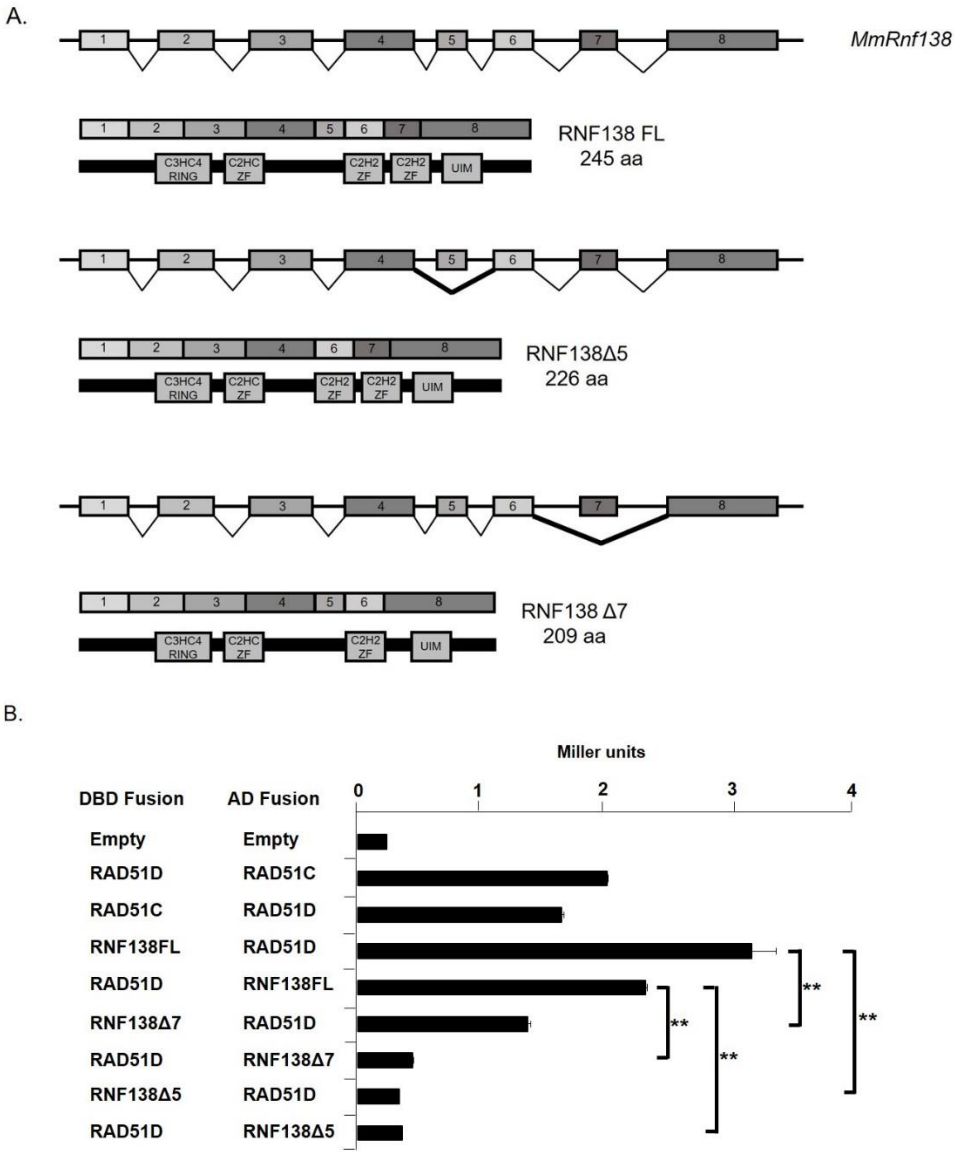

Figure 3.2. (A) Summary of *Mus musculus Rnf138* splice variants. The eight exons of *Rnf138* are displayed as numbered boxes drawn relative to base pair length. The full-length *Rnf138* mRNA transcript is shown along the top, and the alternatively spliced transcripts are displayed below. Note the bold lines indicating the splice sites. Predicted translation products are displayed beneath the transcripts. Open gray boxes mark sequence corresponding to the indicated functional domain. Abbreviations: ZF-zinc finger, UIM-ubiquitin interaction motif, nt-nucleotide, aa-amino acid. (B) Yeast two-hybrid analysis of RNF138 splice variants and full-length RAD51D. Data represent mean +/− SEM from three independent experiments performed in triplicate and ** indicates $p < 0.01$.

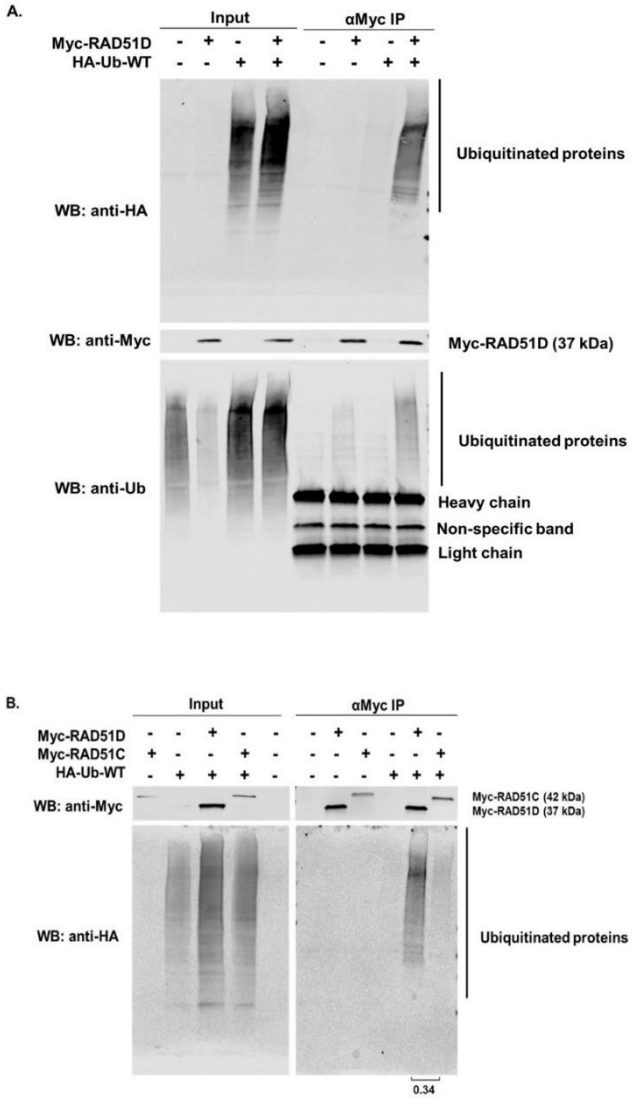

Figure 3.3. Detection of RAD51D ubiquitination in the absence of over-expressed RNF138 and in the presence of MG132. (A) HeLa cells were transfected with Myc-RAD51D, HA-Ub-WT, or both and treated with 25 μM MG132. The top blot represents anti-HA antibody and the lower blot represents anti-ubiquitin. (Note the lower protein concentration in lane 2 of the anti-Ub blot). Heavy and light chains from the anti-Myc beads were detected with the anti-mouse secondary antibody in the lower blot. (B) RAD51C and RAD51D ubiquitination was detected by transfecting HeLa cells with either Myc-RAD51C or Myc-RAD51D and HA-Ub-WT. Densitometry measurements were performed using LiCor Image Studio software (v4.0). The anti-HA signal was normalized to the anti-Myc signal for each corresponding sample. The ratio of anti-HA signal between Myc-RAD51D and Myc-RAD51C is shown beneath the blot.

CHAPTER 4

RAD51D LYSINE RESIDUES 235 AND 298 ARE REQUIRED FOR DNA INTERSTRAND CROSSLINK REPAIR

Abstract

RAD51 proteins are essential components of the homologous recombination (HR) pathway that repairs DNA double strand breaks (DSBs), which can be induced directly by radiation sources or generated during the repair of DNA interstrand crosslinks (ICLs). Deletion of the *Rad51d* HR gene confers increased cellular sensitivity to the ICL-inducing agent mitomycin C (MMC). Previously, a direct interaction between RAD51D and the RNF138 E3 ubiquitin ligase was identified. RNF138 promoted RAD51D ubiquitination, a post-translational modification that occurs primarily along lysine residues, and loss of RNF138 increased RAD51D protein stability. In this study, the lysine residues along RAD51D that are required for protein function and are potential ubiquitin modification sites were identified. Arginine substitution mutations were introduced at each lysine position along RAD51D, and complementation assays were performed using *Rad51d*-deficient mouse embryonic fibroblasts grown in the presence of MMC. Lysine residues 235 (K235R) and 298 (K298R) were essential for ICL repair, but not for interaction with RAD51C, XRCC2, or RNF138 as measured by the yeast-two-hybrid assay. Stability of a lysine-null (K0) mutant was 3-fold higher than wild-type, and K235R and K298R protein stability was 2 to 3-fold higher compared with wild-type RAD51D. Ubiquitination assays identified a 3-ubiquitin modification present along the wild-type but not K0. Finally, neither K235 nor K298 were required for homology-directed repair following *Sce*I-induced DSBs. Overall, these data suggest that K235 and K298 along RAD51D are required for homologous recombination-mediated repair of DNA interstrand crosslinks.

Introduction

Ovarian cancer is the deadliest gynecological cancer (Kuschel et al. 2002; Levy-Lahad et al. 2001; Loveday et al. 2011; Loveday et al. 2012; Meindl et al. 2010; Pelttari et al. 2011; Thompson et al. 2012). Mutations in the *RAD51* gene family increase risk for breast and ovarian cancer (Coulet et al. 2013; Kraus et al. 2017; Loveday et al. 2011; Meindl et al. 2010; Pelttari et al. 2011; Song et al. 2015; Thompson et al. 2013), and the proteins encoded by these genes function during homologous recombination (HR) mediated repair of DNA double strand breaks (DSBs) and interstrand crosslinks (ICLs). Mutations in repair genes also confer increased sensitivity to chemotherapy agents, such as platinum-based drugs (Pennington et al. 2014; Minckwitz et al. 2014; Topp et al. 2014). Cisplatin and mitomycin C (MMC), commonly used treatments for late stage ovarian cancer, and generate DNA intra- and interstrand crosslinks (Dasari and Tchounwou 2014).

Interstrand crosslinks result in a covalent linkage between two complementary DNA strands that can disrupt replication and transcription (Zou, Van Houten, and Farrell 1994). During the S/G2 stages of the cell cycle, Fanconi Anemia (FA) and HR proteins repair ICL damage (Michl, Zimmer, and Tarsounas 2016). A crosslink is first recognized by the FA core complex, which binds to one of the DNA strands on either side of the ICL lesion. Recruitment and ubiquitination of the FANCD2/FANCI heterodimer initiates cleavage of the DNA strand, producing a DSB. Removal of the FANCD2/FANCI complex allows for recognition and binding of HR proteins that use the complementary DNA strand as a homologous template to repair the DSB (Kim and D'Andrea 2012).

Post-translational modifications (PTMs), such as ubiquitination, promote activity of DNA repair pathways (Doil et al. 2009; Gibbs-Seymour et al. 2015; Mailand et al. 2007; Panier and Durocher 2009; Kim and D'Andrea 2012; Hodge et al. 2016). Three recent studies identified an E3 ubiquitin ligase that promotes HR-mediated DSB repair: RNF138 (Ismail et al. 2015; Schmidt et al. 2015; Yard et al. 2016). In response to IR, RNF138 promotes ubiquitination of the NHEJ protein Ku80 and targets it for proteasomal degradation, removing NHEJ proteins from the damage site and allowing HR-mediated repair (Ismail et al. 2015). RNF138 also ubiquitinates the exonuclease CtIP to promote its end-resection activity during the early steps of HR (Schmidt et al. 2015). Furthermore, depletion of RNF138 in mouse embryonic fibroblasts (MEFs) significantly increase sensitivity to the ICL-inducing agent MMC and decreases RAD51 localization to ICL damage (Yard et al. 2016).

As discussed in Chapter 3, RNF138 ubiquitinates RAD51D and signals for its degradation via the proteasome (Yard et al. 2016). Ubiquitin modification occurs at lysine residues along a target protein (Akutsu, Dikic, and Bremm 2016; Swatek and Komander 2016), and there are thirteen lysine residues along the *Mus musculus* RAD51D protein. In this study, single point mutations were generated in *MmRad51d* lysine codons to introduce arginine at those residues. Substitution of two residues – K235R and K298R – along RAD51D conferred sensitivity to MMC but did not affect protein interaction between RAD51D and RAD51C, XRCC2, or RNF138 by yeast-two-hybrid. Stability of a lysine-null mutant (K0) protein was three times higher than wild-type RAD51D, and stability of K235R and K298R was increased 2- and 3-fold, respectively. The K0 mutant includes arginine substitution at K113, a residue in the conserved Walker Box A ATPase

motif. Substitution at this residue eliminates catalytic activity of the protein (Gruver et al. 2005), therefore, the K0 mutant is predicted to be catalytically inactive. *In vivo* ubiquitination assays demonstrated that a band corresponding to three ubiquitin molecules was present in wild-type, but not K0 samples, suggesting a short ubiquitin chain along the protein is no longer present. Foci formation following MMC treatment demonstrated that RAD51D acts downstream of FANCD2 and Ku86, and upstream of RAD51 in response to MMC. Furthermore, homology-directed repair assays demonstrated that neither K235 nor K298 is required for repair of *Sce*I induced DSBs. Overall, these data suggest RAD51D ubiquitination at K235 and K298 is required for repair of DNA interstrand crosslinks.

Materials and Methods

Site-directed mutagenesis

Lysine to arginine substitution point mutations were introduced by PCR-based site-directed mutagenesis using the *Mus musculus Rad51d* cDNA cloned into the pUC19 expression vector (New England BioLabs) (Smiraldo et al. 2005). The primer sequences used are listed in Table 4.1. Each mutation was individually generated to produce single lysine to arginine amino acid substitutions. A lysine-null RAD51D (K0) construct was generated by changing all lysine codons to arginine. A RAD51D-Cpeptide mutant construct representing amino acids 225 to 329 was generated by PCR amplification of the *MmRad51d* wild-type cDNA using the following primers: RAD51D-CpepKpnI Forward and RAD51D-CpepBclI Reverse (Table 4.1). DNA sequencing (Eton Bioscience) confirmed all clones and base substitutions.

Complementation Assays

Each individual RAD51D lysine to arginine mutant construct was cloned into the pcDNA3.1 mammalian expression vector (Invitrogen) containing either the N-terminal Myc or HA epitope tags at the *Kpn*I and *Bam*HI sites. *Rad51d*-deficient (*Rad51d*$^{-/-}$*Trp53*$^{-/-}$) mouse embryonic fibroblasts (MEFs) (Smiraldo et al. 2005) were maintained at 37°C with 5% CO_2 in Dulbecco's Modified Eagle's Medium (DMEM; Hyclone) supplemented with 10% fetal bovine serum (Hyclone), 1% penicillin/streptomycin, and 1% glutamine.

Rad51d-deficient MEFs were transfected with Myc-RAD51D constructs using Lipofectamine LTX Plus reagent (Thermo Fisher). Twenty-four hours following transfection, cells were divided evenly between two 150 mm dishes. Selection was performed using 200 ug/mL hygromycin B (Sigma), and half of the plates were treated with 4 ng/mL mitomycin C as previously described (Gruver et al. 2009). Media was replaced every 3 days for 14 days following initiation of treatment, and both hygromycin B selection and MMC treatment were maintained for the duration of the experiment. Following treatment, the plates were rinsed with 1X PBS, fixed with methanol, and colonies stained with Giemsa. Percent resistance was calculated by dividing the total number of colonies surviving selection with MMC by the number of colonies that grew in the presence of hygromycin B alone.

Protein localization

To generate enhanced green fluorescent protein (EGFP) fusions of the lysine to arginine mutants, each construct was cloned into the *Kpn*I and *Bam*HI sites of the pEGFP-C1 vector (Clontech). EGFP-RAD51D fusion constructs were transiently expressed in *Rad51d*-deficient MEFs grown on glass coverslips as described (Smiraldo et al. 2005).

Twenty-four hours post-transfection, the coverslips were washed with 1X PBS, fixed with 4% paraformaldehyde for 20 minutes at room temperature, and permeabilized with 0.3% Triton-X 100 for 5 minutes. The coverslips were mounted on glass slides with Prolong Gold + DAPI mounting agent (Life Technologies). Slides were viewed using an Evos fluorescent microscope and images captured using a 60x oil immersion objective.

Yeast-two hybrid assays

Each RAD51D lysine construct was cloned into pGADT7 and PGBKT7 (Clontech) at the *Eco*RI and *Bam*HI restriction enzyme sites. Transformations into the AH109 yeast strain was performed using the Frozen EZ Yeast Transformation II kit (Zymo Research) per manufacturer's instructions. Liquid β-galactosidase assays were performed using *ortho*-nitrophenyl-β-galactopyranoside (ONPG; Sigma) as previously described (Gruver et al. 2009).

Immunoprecipitation and in vivo ubiquitination assays

HEK293T and HeLa cells were transfected with Myc-RAD51D or EGFP-RAD51D-Cep and HA-Ubiquitin constructs using TransIT-LTI reagent (Mirus Bio) per manufacturer's instructions. Four hours prior to harvesting, cells were treated with 25 μM MG132 (Selleckchem). Twenty-four hours after transfection, the cells were harvested, and the proteins were extracted using 1X Cell Lysis Buffer (20 mM Tris, 150 mM NaCl, 1 mM EDTA, 1 mM EGTA, 1 mM PMSF, 1% TritonX-100) containing a protease inhibitor cocktail (Thermo Scientific). For protein stability experiments, cycloheximide (Sigma) was added to a final concentration of 10 μg/mL for the indicated times. Three hundred micrograms of whole cell extract were incubated with anti-Myc magnetic beads (9E10;

Thermo-Scientific) or anti-GFP magnetic beads (Chromotek) for 16 h at 4°C with gentle rocking. Precipitated proteins were washed 3 times with dilution buffer (10 mM Tris/Cl, 150 mM NaCl, 0.5 mM EDTA, protease inhibitor cocktail), eluted by boiling in 3X SDS-PAGE buffer (187.5 mM Tris-HCl, 6% w/v SDS, 30% glycerol, 150 mM DTT, 0.03% bromophenol blue) for 7 minutes, and resolved on a 4 - 20% SDS-PAGE (Bio-Rad).

For western blot analysis, primary anti-Myc (9E10; Santa Cruz) mouse polyclonal, anti-Myc (A-14; Santa Cruz) rabbit polyclonal, anti-HA (3F10; Roche) rat polyclonal, anti-β-tubulin (PA5-16863; Invitrogen) rabbit monoclonal, and anti-GFP (SAB4301138; Sigma) rabbit monoclonal antibodies were used. Primary antibody incubations were followed by incubation with the appropriate species-specific IRDye 800CW secondary antibody (Licor). Detection was performed using the Licor Odyssey Sa Imaging System, and densitometry measurements were performed using Licor Image Studio software (v4.0).

Immunofluorescence

Rad51d-proficient and -deficient MEFs were seeded at 3 x 10^5 cells per well on glass coverslips in a 6-well dish. Twelve hours after plating, the cells were treated with either 200 ng/mL (IC_{50} *Rad51d*-proficient) or 2 ng/mL (IC_{50} *Rad51d*-deficient) MMC. Twenty-hours after initiation of treatment, the coverslips were washed with 1X PBS, pre-extracted with 0.5% Triton-X 100 for 4 minutes, fixed with 4% paraformaldehyde for 20 minutes at room temperature, and permeabilized with 0.3% Triton-X 100 for 5 minutes. To block, coverslips were incubated in 5% milk/PBS for 1 hour at room temperature, then washed with 1X PBS three times. Primary antibody incubation was performed in 5% milk/PBS at indicated dilutions in a humid chamber overnight at 4°C. After the primary

incubation, the cells were washed with 1X PBS. Secondary antibody incubations were performed in 5% milk/PBS at the indicated dilutions in a humid chamber for 1 hour at room temperature. The cells were then washed with 1X PBS, and the coverslips were mounted on glass slides with Prolong Gold + DAPI mounting agent (Life Technologies).

For immunofluorescence, primary anti-FANCD2 (ab2187; Abcam; 1:200) rabbit polyclonal, anti-Ku86 (C-20; Santa Cruz; 1:00) goat polyclonal, anti-RAD51 (H-92; Santa Cruz; 1:100) rabbit polyclonal, and secondary antibodies AlexaFluor488 (Sigma; 1:1000) and AlexFluor688 (Sigma; 1:200) were used. Slides were viewed using an Evos fluorescent microscope and images captured using a 60x oil lens objective. Foci per nuclei were scored for each cell line, and nuclei with foci $n \geq 5$ were scored as positive. A minimum of 200 nuclei were scored for each treatment.

Homology directed repair assay

For recombination measurements, 5 x 10^6 HeLa DRGFP cells (Pierce et al. 1999) were co-transfected with 50 ug pCBASce (Rajesh, Baker, et al. 2011) and 25 ug Myc-RAD51D-WT, Myc-RAD51D-K0, Myc-RAD51D-K235R, or Myc-RAD51D-K298R plasmid by electroporation (BTX Harvard Apparatus ECM 630 Electro Cell Manipulator) using the following settings: low voltage, 230V, 500 μF. The medium was replaced every twenty-four hours following transfection. Forty-eight hours after *Sce*I transfection, the cells were viewed on an Evos fluorescent microscope, and images were captured using a 40X objective. Cells were collected and resuspended in 1X PBS for GFP expression analysis using an FC 500 flow cytometer and quantitated using CXP analysis software (Beckman Coulter) (Yang, Waldman, and Wyatt 2012).

Results

Complementation screening of RAD51D lysine to arginine mutants

Our previous work demonstrated that RAD51D is ubiquitinated by the E3 ligase RNF138 (Yard et al. 2016), a modification that occurs at lysine residues (Zee and Garcia 2012). The *Mus musculus* RAD51D protein has thirteen lysine residues, ten of which are conserved with *Homo sapiens* RAD51D (Figure 4.1). Sequence identity between the RAD51 paralogs is approximately 40%, and seven of the lysine residues along MmRAD51D are conserved with another paralog (Figure 4.2). To determine which lysine residues are required for RAD51D function during DNA damage repair, site-directed mutagenesis was performed to individually substitute each lysine codon with an arginine, and a lysine-null (K0) was generated by changing all lysine residues to arginines (Figure 4.3A). The RAD51D constructs are referenced by each lysine to arginine substitution; for example, substitution of lysine 235 and 298 are referred as K235R and K298R, respectively.

Complementation assays were performed to identify the lysine residues essential for resistance to DNA interstrand crosslinks (Smiraldo et al. 2005). Each mutant plasmid was transiently expressed in *Rad51d*-deficient mouse embryonic fibroblasts (MEFs). For each experiment, transfected populations were equally divided and maintained in either the presence of hygromycin B alone or with the addition of the DNA ICL agent mitomycin C (MMC) (Figure 4.3B). K0, K235R, and K298R decreased cellular resistance to MMC by up to 90% compared to wild-type, and expression of K261R decreased cellular resistance by 30%. K24R, K26R, K42R, K48R, and K327R increased cellular resistance to MMC between 10 and 20%, K159R and K201R increased by

approximately 40%, and K76R and K91R were approximately the same as wild-type. Given these data, K235R and K298R were the focus of the subsequent work.

One potential explanation for increased sensitivity in the absence of either residue is that arginine substitution disrupts nuclear localization of the proteins. Using EGFP-tagged RAD51D constructs, cellular localization of RAD51D was not affected by substitution at either K235 or K298 (Figure 4.4).

K235R and K298R interact with RAD51C, XRCC2, and RNF138

RAD51D forms a complex with the paralogs RAD51B, RAD51C, and XRCC2 (BCDX) through direct interactions with RAD51C and XRCC2 (Masson et al. 2001; Rajesh et al. 2009). To determine the effects on protein interaction, yeast-two-hybrid analysis was performed with each lysine mutant and RAD51C (Figure 4.5A, D) or XRCC2 (Figure 4.5B, E). Replica plating results suggest that both RAD51C and XRCC2 interact with K235R and K298R, but not K0. As demonstrated by ONPG analysis, K235R and K298R showed a level of interaction with either RAD51C or XRCC2 similar to wild-type RAD51D. Interestingly, interaction between K201R and RAD51C or XRCC2 was decreased 3- and 4-fold, respectively. Despite decreased interaction with these paralogs, K201R complemented *Rad51d*-deficiency in the presence of MMC.

Previous studies demonstrated that RAD51D directly interacts with the E3 ubiquitin ligase RNF138 (Yard et al. 2016). Replica plating results suggest that RNF138 interacts with K235R and K298R, but not K0. As demonstrated by ONPG analysis, K235R and K298R had a level of interaction with RNF138 similar to wild-type RAD51D, and RNF138 interaction with K0 was decreased to background levels (Figure 4.5C, F). K0 includes arginine substitution at K113 along RAD51D, which was

previously shown to be required for interaction between RAD51D and RNF138 (Gruver et al. 2005; Yard et al. 2016).

Increased stability of K0, K235R, and K298R

To determine if K235 or K298 is a site for degradation specific ubiquitin modification, the stability of Myc-tagged RAD51D mutant proteins after treatment with cycloheximide (CHX) was measured (Figure 4.6A). Two hours after initiation of CHX block, the stability of K0 was 3-fold higher than wild-type ($p<0.05$), and stability of K235R, and K298R were 2-fold and 1.5-fold higher, respectively ($p<0.05$). Four hours after CHX addition, the stability of K0, K235R, and K298R was increased 3-fold, 2-fold, and 2.5-fold, respectively, compared with wild-type RAD51D ($p<0.05$). Six hours after CHX treatment, the protein levels of K0, K235R, and K298R were similar to wild-type, suggesting that degradation of these proteins is delayed, rather than completely eliminated. The stability of HA-tagged RAD51D wild-type and K0 proteins were consistent with these results (Figure 4.6A; lower blots).

The C-terminal region of the RAD51D gene encoding amino acids 225 to 329 (RAD51D-Cpep) was amplified and fused to the gene sequence for enhanced green fluorescent protein. This generated a RAD51D-Cpep-EGFP fusion protein used for subsequent experiments. Stability of Cpep-K0, Cpep-K235R, and Cpep-K298R was decreased to similar levels as wild-type RAD51D-Cpep 4 hours after initiation of a CHX block (Figure 4.6C). This treatment time was selected based on the significant increase in protein stability of the full-length K0, K235R, and K298R mutants (Figure 4.6A). These data are in contrast with the full-length RAD51D that showed increased stability of the

K0, K235R, and K298R compared with wild-type under the same conditions (Figure 4.6A).

Ubiquitin modification of K235R and K298R

Cells expressing K235R and K298R do not complement *Rad51d*-deficiency in the presence of MMC, and these proteins have increased stability compared with wild-type. Loss of a ubiquitin modification at either of these residues could account for MMC sensitivity. To test this hypothesis, Myc-tagged RAD51D lysine to arginine mutant constructs were co-expressed in HEK293T cells with an HA-tagged ubiquitin wild-type plasmid. Signal along K0 was still detected even in the absence of lysine residues. Interestingly, there appears to be a ubiquitin band in the wild-type, K235R, and K298R samples corresponding to approximately 3 ubiquitins (24 kDa increase in molecular weight) that is not present in the K0 sample. This suggests that a specific ubiquitin modification is lost in the absence of any available lysine residues. Ubiquitin patterns along K235R and K298R were similar to wild-type RAD51D (Figure 4.7A).

Ubiquitination assays of the EGFP-RAD51D-Cpep constructs were performed using anti-GFP immunoprecipitation (Figure 4.7B). The absence of ubiquitin signal in the EGFP-only sample indicates that EGFP alone is not ubiquitinated in this system. Ubiquitin signal was detected along the Cpep-K235R and Cpep-K298R consistent with wild-type, indicating that ubiquitin modification occurs along this region of the protein. Ubiquitin signal was detected along the Cpep-K0 (no lysine residues available), suggesting that this region of RAD51D is still ubiquitinated even in the absence of lysine residues. The ubiquitin banding patterns along K0, K235R, and K298R are similar to wild-type.

Ubiquitin chain linkages along RAD51D

Ubiquitin has seven lysines that can be used to form polyubiquitin chains, and the residue used for the peptide bond is indicative of the function of the modification (Akutsu, Dikic, and Bremm 2016; Ohtake and Tsuchiya 2017). For example, polyubiquitin chains formed with lysine 48 (K48) signal for degradation via the proteasome and K63-linked chains promote DNA damage response (Akutsu, Dikic, and Bremm 2016). To identify ubiquitin linkages attached to RAD51D, Myc-tagged RAD51D constructs were co-expressed with HA-tagged ubiquitin mutants that had a single lysine residue available for chain formation and are referred to by that lysine number (Figure 4.7C). Signal was detected when RAD51D was co-expressed with the K48 ubiquitin mutant. These data are consistent with previous experiments showing that stability of RAD51D is increased in the presence of the MG132 proteasome inhibitor (Yard et al. 2016). Ubiquitin signal was detected along RAD51D in the presence of K6, K11, and K27 ubiquitin mutants, indicating that these chain linkages are generated along the RAD51D protein. Decreased ubiquitin signal was detected in the RAD51D samples co-expressed with the K0 and K63 ubiquitin mutants compared with the wild-type ubiquitin mutants. The K0 mutant cannot form isopeptide bonds with subsequent ubiquitin molecules and thus acts as a chain terminator and a negative control for these experiments. K63 chains are generated in the presence of DNA DSBs and the cells used for these experiments were unchallenged with DNA damage.

To determine if RAD51D ubiquitination occurs in response to ICLs induced by MMC, ubiquitin signal along RAD51D was detected 12, 16, 20, and 24 h after MMC treatment. RAD51D ubiquitination levels were increased compared to no treatment at the

16 and 20 h time points and appeared to be highest 16 hours after MMC treatment (Figure 4.7D). These preliminary results suggest that ubiquitination of RAD51D increases in response to MMC treatment.

MMC-induced FANCD2 and Ku86 foci formation in Rad51d-deficient cells

RAD51 is recruited to the sites of ICL damage after the Fanconi Anemia (FA) core complex (Kim and D'Andrea 2012), and RAD51D is required for formation of RAD51 foci in response DSBs (Smiraldo et al. 2005). To determine if RAD51D functions downstream of FA proteins, *Rad51d*-proficient and -deficient MEFs were treated with equitoxic doses of MMC. FANCD2, Ku86, and RAD51 foci were detected by immunofluorescence 24 h after MMC treatment. Thirty percent of nuclei were positive for FANCD2 foci following MMC treatment in both the *Rad51d*-proficient and -deficient cell lines, and the number of positive cells was 2-fold higher than the vehicle treated cells (Figure 4.8A). Fifteen percent of nuclei were Ku86 positive in both cells lines following MMC treatment, and the number of positive cells was 2-fold higher compared with vehicle treated cells (Figure 4.8B). Foci were also detected after forty-eight and seventy-two hours of treatment (Figure 4.8). RAD51 foci were detected in the *Rad51d*-proficient, but not in the *Rad51d*-deficient MEFs, demonstrating that RAD51D is required for RAD51 foci formation in response to MMC.

K235 and K298 are not required for DNA double strand break repair

Complementation assays (Figure 4.3B) demonstrated that K235R and K298R confer sensitivity to MMC, suggesting that these residues are essential for RAD51D function in response to ICLs. To determine if either lysine is also needed for HR-mediated repair of

DSBs, a homology-directed repair assay was performed in cells containing a chromosomally integrated DRGFP recombination reporter (HeLa DRGFP) (Pierce et al. 1999). Expression of the I-*Sce*I endonuclease introduces a DSB in the Sce-GFP gene, and repair by HR reconstitutes a functional GFP gene and GFP expression (Figure 4.9A). HeLa DRGFP cells were co-transfected with the I-SceI plasmid and wild-type RAD51D, K0, K235R, or K298R and allowed to recover for 48 h. GFP positive cells were measured by flow cytometry (Figure 4.9B). The percentage of GFP positive cells was 1.5 in the untransfected cells and 7.5 in the cells transfected with I-SceI only. Cells in which wild-type RAD51D was expressed displayed a GFP-positive population of 8.8%. Cells transfected with K0 displayed a GFP-positive population of 8.7%, similar to WT expressing cells. Expression of K235R and K298R displayed GFP-positive populations of 7.9% and 7.1%, respectively. Arginine substitution at K235 and K298 does not suppress HR-mediated repair of DSBs in this assay, and these data suggest that these residues may be required for RAD51D function specifically in response to ICLs.

Discussion

DNA interstrand crosslinks occur when two complementary DNA strands become covalently linked by endogenous reactive aldehydes or platinum-based drugs. During S phase of the cell cycle, Fanconi Anemia (FA), nucleotide excision repair, and homologous recombination (HR) proteins act in combination to remove ICLs (Alpi et al. 2008; Kim and D'Andrea 2012; Knipscheer et al. 2009; Kottemann and Smogorzewska 2013; Lopez-Martinez, Liang, and Cohn 2016). Post-translational modifications regulate DNA repair pathways, and ubiquitination is prominent in both the FA and HR pathways.

For example, ubiquitin modification of the FANCD2 and FANCI activate the proteins to allow cleavage of the DNA strands flanking an ICL lesion (Kim and D'Andrea 2012; Rickman et al. 2015; Liang et al. 2016). This cleavage generates a DNA double strand break (DSB) that is recognized and repaired by HR proteins (Kim and D'Andrea 2012). During HR-mediated repair of DSBs, the E3 ubiquitin ligase RNF138 ubiquitinates the CtIP endonuclease to promote end resection and HR progression (Schmidt et al. 2015).

We previously demonstrated that loss of RNF138 increases cellular sensitivity to ICL agents, reduces RAD51 foci formation after MMC induced damage, and ubiquitinates RAD51D (Yard et al. 2016). K113 in the Walker Box A motif of RAD51D is also required for cell survival in the presence of MMC (Gruver et al. 2005). In this study, we show that three lysine residues – K235, K261, and K298 – are required for cellular resistance to MMC. K235 is predicted to be in the BRC Interface region along the RAD51D protein, a motif conserved among the RAD51 family members. The BRC interface mediates oligomerization between RAD51 monomers (Pellegrini et al. 2002) and is a potential interaction platform between RAD51 paralogs. K261 is in the mid-region and K298 is located towards the C-terminus of the RAD51D protein. Neither residue is predicted to be near any known motifs or domains.

RNF138-mediated ubiquitination of RAD51D promotes its degradation by the proteasome (Yard et al. 2016). K235R and K298R did not affect interaction between RAD51D and RNF138 but did increase protein stability, suggesting that these residues are sites of proteasomal specific ubiquitin modifications. K0 did not interact with RNF138, consistent with previous work that demonstrated K113 (which is substituted with arginine in K0) is required for this interaction (Yard et al. 2016). Stability of the K0

mutant was increased 3-fold compared to wild-type, although the protein was ultimately degraded. Increased stability of RAD51D could delay or inhibit DNA damage repair in response to MMC and may explain why cells expressing these mutants do not restore cellular resistance to MMC.

RAD51B, RAD51C, RAD51D, and XRCC2 interact to form the BCDX2 complex, and of these proteins, RAD51D directly interacts with RAD51C and XRCC2 (Rajesh et al. 2009). Yeast-two-hybrid analysis demonstrated that K235R and K298R directly interact with RAD51C and XRCC2. Interestingly, K201R did not interact with RAD51C or XRCC2, but complemented the *Rad51d*-deficiency in the presence of MMC, suggesting that the interaction between RAD51C and XRCC2 may not mediate ICL repair.

Ubiquitin signal was detected along the K235R and K298R proteins suggesting that RAD51D is still ubiquitinated in the absence of these residues. Ubiquitin addition along lysine residues is dependent on the availability of the residues, rather than a specific amino acid sequence surrounding the residue and K235 or K298 may not be the only residues available for modification. These data suggest that RAD51D is ubiquitinated in the absence of lysine 235 or 298 and may indicate additional modifications along RAD51D that are required for promoting DNA ICL repair. Ubiquitin signal was detected along the K0 mutant, which has no lysines available for modification, suggesting that non-lysine ubiquitin modifications may be generated along the RAD51D protein.

Increased protein stability in the presence of K0, K235R, and K298R suggests one or more ubiquitin modifications along RAD51D are lost in the absence of lysine residues.

An alternative method for investigating post-translational modifications along proteins using tandem mass spectrometry (MS/MS). This method can be used to identify modifications that occur along specific regions of a protein (Parker et al. 2010). MS/MS analysis can be performed on the wild-type, K0, K235R, and K298R proteins to identify: 1. lysine residues that are modified with ubiquitin, and 2: modifications that are lost in the absence of lysine residues.

To identify specific lysine residues that are required for RAD51D function during DSB repair, I performed a homology-directed repair assay (Pierce et al. 1999) in the presence of K0, K235R, and K298R. Over-expression of wild-type RAD51D increased HR capacity by 2.7% compared with the SceI-only control. HR-capacity of cells expressing K0, K235R, and K298R was similar to wild-type.

Here, we show that two lysine residues along RAD51D – K235 and K298 –are required for cell survival in response to DNA ICLs. I propose that these residues are the sites of degradation specific ubiquitin modifications that remove RAD51D from the site of damage to allow RAD51 to bind and promote HR (Figure 4.10). Following, recognition of a DNA ICL lesion, FA proteins, specifically the FANCD2/FANCI heterodimer, in conjunction with the exonuclease CtIP, function at the site of damage to excise the DNA to produce DNA single strand overhangs surrounding a DNA double strand break. In response to IR, CtIP directly interacts with the E3 ligase RNF138 to promote HR (Schmidt et al. 2015), and a similar mechanism in response to ICLs. In addition to binding CtIP, RNF138 directly interacts with RAD51D of the BCDX2 paralog complex, localizing the complex to the damage. The RAD51 paralog complex initiates recruitment of RAD51 to the site of damage (Chun, Buechelmaier, and Powell

2013). Finally, to remove the BCDX2 complex, RNF138 mediates ubiquitination of RAD51D that targets it to the proteasome for degradation, thereby removing the proteins. Displacement of the BCDX2 complex allows RAD51 to bind single strand DNA overhangs generated by CtIP and for HR-mediated repair of the ICL damage to progress.

Future studies will identify lysine residues along RAD51D necessary for RAD51 foci formation in the presence of MMC. Wild-type RAD51D, K0, K235R, and K298R can be expressed in *Rad51d*-deficient MEFs treated with non-lethal doses of IR and RAD51 foci formation measured using immunofluorescence. K0 and K298R are predicted to be needed for RAD51 foci formation in response to IR-induced DSBs given that HDR is suppressed in the presence of these mutants, and over-expression of K235R is not expected to affect RAD51 foci formation. K201R should also be included in these experiments, since this mutant had decreased interaction with both RAD51C and XRCC2 by the yeast-two-hybrid assay, suggesting that the BCDX2 complex does not properly form when Lys201 is not present. Loss of RAD51 foci in the presence of K201R would suggest that the function of RAD51D differs in response to ICLs versus 'traditional' DSBs.

Acknowledgements

The HeLa DRGFP cells were a generous gift from Dr. Andrew Pierce. We thank Dr. Jason Stewart for assistance with fluorescence microscopy, Dr. Lydia E. Matesic and Dr. Heather Mentrup for assistance with ubiquitin linkage experiments, Dr. Alex Gasparian for assistance with EGFP immunoprecipitation experiments, and Dr. Chang-Uk Lim for assistance with flow cytometry. This research was supported primarily by the National

Institutes of Health under Award Number R15GM110615. Additional support was provided by a Support to Promote Advancement of Research and Creativity (SPARC) Graduate Research Grant from the Office of the Vice President for Research at the University of South Carolina to NMR and Magellan Scholarship Awards from the Office of Undergraduate Research at the University of South Carolina to MGM, CLC, and MEI. DOA and JG were supported by a Summer Minority Undergraduate Research Fellowship in the Center for Colon Cancer Research at USC (P30 GM103336).

Table 4.1. Sequences of primers used for *MmRad51d* cDNA site-directed mutagenesis. The lysine to arginine change is indicated by the residue number. The bold and underline indicates site of the changed base. Note that the base pair change introduced in the K235 codon introduces a *Bam*HI restriction enzyme site.

Primer Name	**Sequence**
K24R Forward	5’ – CTTCTCAGAGGCCGAA**G**GATAAAAACAGTGGCAG – 3’
K24R Reverse	5’ – CTGCCACTGTTTTTATC**C**TTCGGCCTCTGAGAAG – 3’
K26R Forward	5’ – GGCCGAAAGATAA**G**AACAGTGGCAGACCTGGC – 3’
K26R Reverse	5’ – GCCAGGTCTGCCACTGTT**C**TTATCTTTCGGCC – 3’
K42R Forward	5’ – CTTGGAGGAAGTAGCCCAGA**G**GTGTGGCTTGTCCTAC – 3’
K42R Reverse	5’ – GTAGGACAAGCCACAC**C**TCTGGGCTACTTCCTCCAAG – 3’
K48R Forward	5’ – GAAGTGTGGCTTGTCCTACA**G**GGCCCTCGTTGCCCTGAG – 3’
K48R Reverse	5’ – CTCAGGGCAACGAGGGCC**C**TGTAGGACAAGCCACACTTC – 3’
K76R Forward	5’ – CTCTATGAGGAACTGA**G**GACTTCCACGGCCATCC – 3’
K76R Reverse	5’ – GGATGGCCGTGGAAGTC**C**TCAGTTCCTCATAGAG – 3’
K91R Forward	5’ – CATCGGAAGCCTGGACA**G**ACTACTTGATGCTGGCC – 3’
K91R Reverse	5’ – GGCCAGCATCAAGTAGT**C**TGTCCAGGCTTCCGATG – 3’
K113R Forward	5’ – GCCCAGGTAGCGGCA**G**AACCCAGGTGTGTCTCTG – 3’
K113R Reverse	5’ – CAGAGACACACCTGGGTT**C**TGCCGCTACCTGGGC – 3’
K159R Forward	5’ – CCCAAGATGAGGAGA**G**ACAGGCAAGTGCTCTC – 3’
K159R Reverse	5’ – GGAGAGCACTTGCCT**C**TGTCTCCTCATCTTGG – 3’
K201R Forward	5’ – CTTCAGGCGCCGTGA**G**GGTTGTGATTGTGGAC – 3’
K201R Reverse	5’ – GTCCACAATCACAACC**C**TCACGGCGCCTGAAG – 3’
K235R Forward	5’ – CCCGAGAGCTCA**G**GATCCTGGCCCG – 3’
K235R Reverse	5’ – CGGGCCAGGATC**C**TGAGCTCTCGGG – 3’
K261R Forward	5’ – GATGGTAGAAGATTCA**G**ACCTGCCCTTGGACGA – 3’
K261R Reverse	5’ – GCGTCCAAGGGCAGGT**C**TGAATCTTCTACCATC – 3’
K298R Forward	5’ – CACAGTATGTCTGACCA**G**GTCTCCCCGCCAGCC – 3’
K298R Reverse	5’ – GGCTGGCGGGGAGAC**C**TGGTCAGACATACTGTG – 3’
K327R Forward	5’ – CAGAATTACCTGGCA**G**GCAGACGTGACACTGTTG – 3’
K327R Reverse	5’ – CAACAGTGTCACGTCTGC**C**TGCCAGGTAATTCTG – 3’
K24/26R Forward	5’ – CTTCTCAGAGGCCGAA**G**GATAA**G**AACAGTGGCAG – 3’
K24/26R Reverse	5’ – CTGCCACTGTT**C**TTATC**C**TTCGGCCTCTGAGAAG – 3’
K42/48R Forward	5’ – GGAAGTAGCCCAGA**G**GTGTGGCTTGTCCTACA**G**GGCCCTC GTTGCCCTG – 3’
K42/48R Reverse	5’ –

	CAGGGCAACGAGGGCC**C**TGTAGGACAAGCCACA**C**CTCTGG GCTACTTCC – 3’
CpepKpnI Forward	5’ – CGTATCGGTACCGCCTTGATGATGCAGCTGG – 3’
CpepBclI Reverse	5’ – GTGGCCTTGATCAACTGGACTAGTGGATCCCAATC – 3’

```
HsRAD51D        MGVLRVGLCPGLTEEMIQLLRSHRIKTVVDLVSADLEEVAQKCGLSYKALVALRRVLLAQ
MmRAD51D        MGMLRAGLCPGLTEETVQLLRGRKIKTVADLAAADLEEVAQKCGLSYKALVALRRVLLAQ
                                  24 26              42  48

HsRAD51D        FSAFPVNGADLYEELKTSTAILSTGIGSLDKLLDAGLYTGEVTEIVGGPGSGKTQVCLCM
MmRAD51D        FSAFPLNGADLYEELKTSTAILSTGIGSLDKLLDAGLYTGEVTEIVGGPGSGKTQVCLCV
                          76              91                 113

HsRAD51D        AANVAHGLQQNVLYVDSNGGLTASRLLQLLQAKTQDEEEQAEALRRIQVVHAFDIFQMLD
MmRAD51D        AANVAHSLQQNVLYVDSNGGMTASRLLQLLQARTQDEEKQASALQRIQVVRSFDIFRMLD
                                                 159

HsRAD51D        VLQELRGTVAQQVTGSSGTVKVVVVDSVTAVVSPLLGGQQREGLALMMQLARELKTLARD
MmRAD51D        MLQDLRGTIAQQEATSSGAVKVVIVDSVTAVVAPLLGGQQREGLALMMQLARELKILARD
                                201                                235

HsRAD51D        LGMAVVVTNHITRDRDSGRLKPALGRSWSFVPSTRILLDTIEGAGASGG-RRMACLAKSS
MmRAD51D        LGVAVVVTNHLTRDWDGRRFKPALGRSWSFVPSTRILLDVTEGAGTLGSSQRTVCLTKSP
                                261                                298

HsRAD51D        RQPTGFQEMVDIGTWGTSEQSATLQGDQT
MmRAD51D        RQPTGLQEMIDIGTLGTEEQSPELPGKQT
                                327
```

Figure 4.1. Alignment between *Homo sapiens* RAD51D (328 amino acids) and *Mus musculus* (C57BL/6) RAD51D (329 amino acids) protein sequences. Lysines are indicated by the residue number in the *Mus musculus* sequence and conserved residues indicated by bold.

Figure 4.2. Conserved lysine residues between *Mus musculus* RAD51 family members. Conserved residues are boxed, and the numbers are in reference to the RAD51D protein.

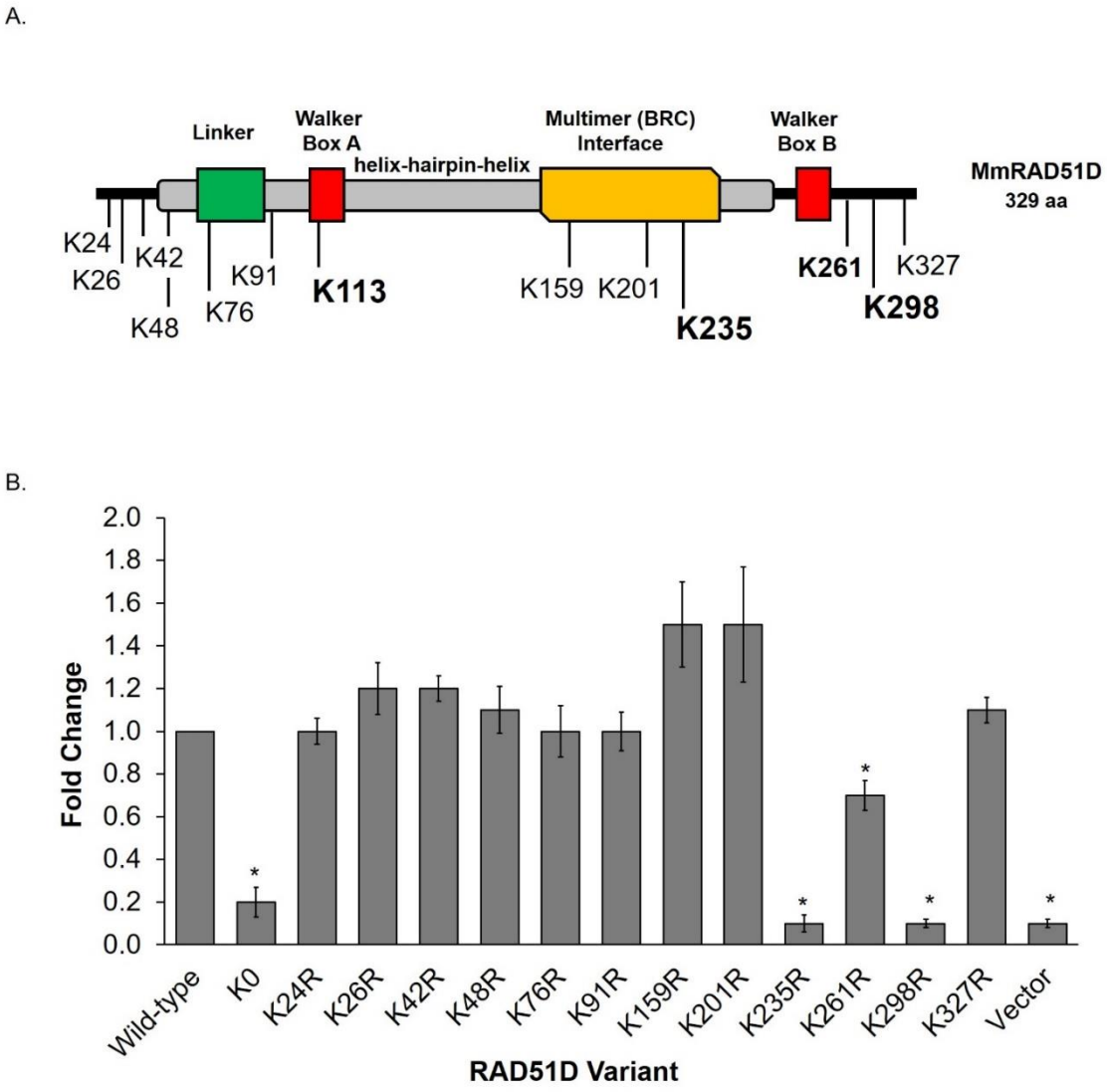

Figure 4.3. Complementation analysis of RAD51D lysine to arginine substituted alleles. (A) Box structure of RAD51D illustrating the conserved domains and lysine residues. Linker region (green), Walker Box ATPase motifs (red), helix-hairpin-helix motif (grey), and BRC interface (yellow). Essential lysine residues 113 (Gruver et al. 2005), 235, and 298 are bold. (B) *Rad51d*-deficient MEFs were transfected with RAD51D-lysine to arginine mutant constructs, treated with 4 ng/mL MMC. Colonies were counted 14 days following treatment. Fold change as compared to wild-type is shown for three independent experiments. Error bars represent SEM and * indicates $p<0.05$ calculated using a Student's T-test.

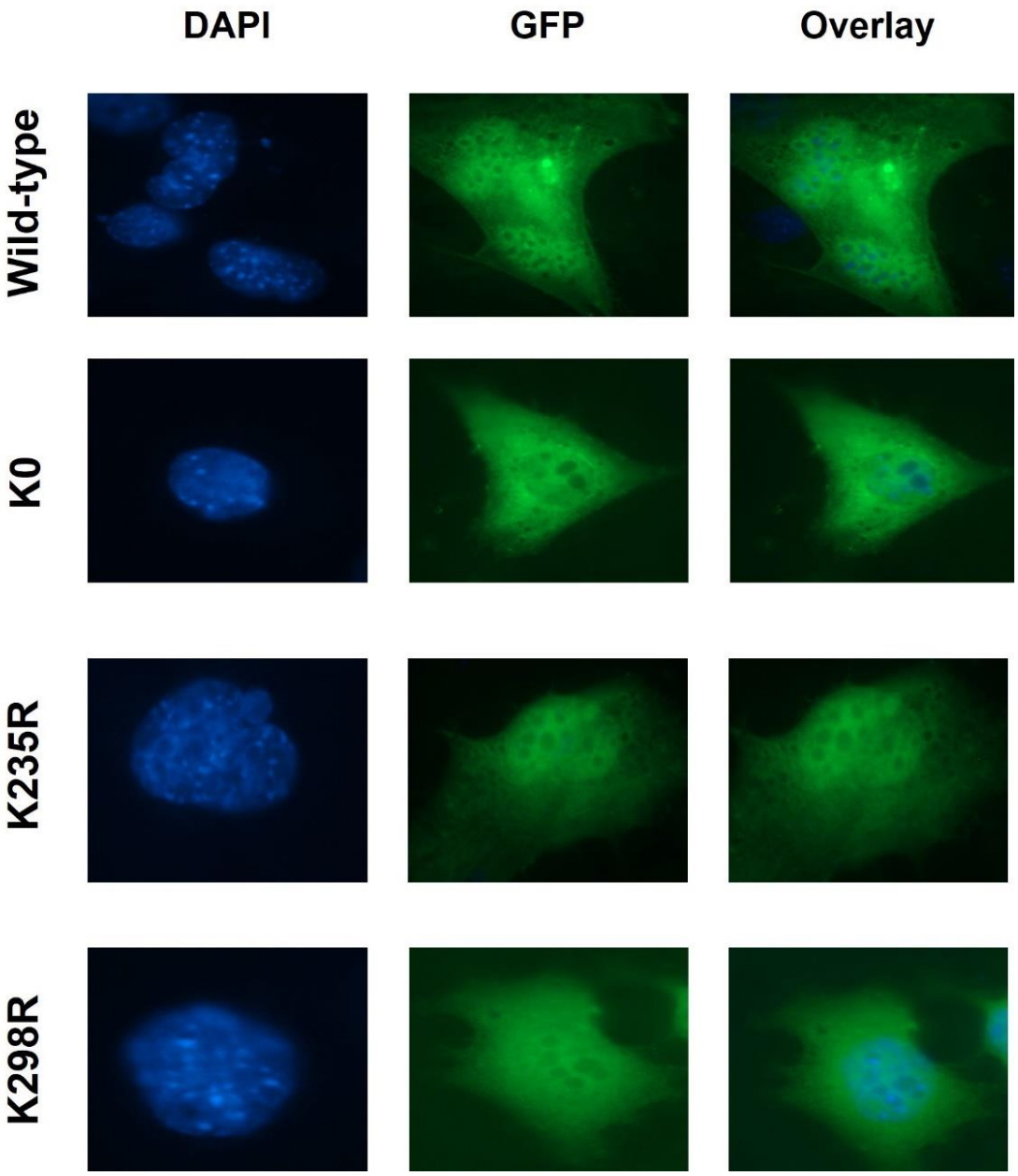

Figure 4.4. Intracellular localization of RAD51D mutant proteins. EGFP-tagged RAD51D variants were expressed in *Rad51d*-deficient mouse embryonic fibroblasts for 24 h.

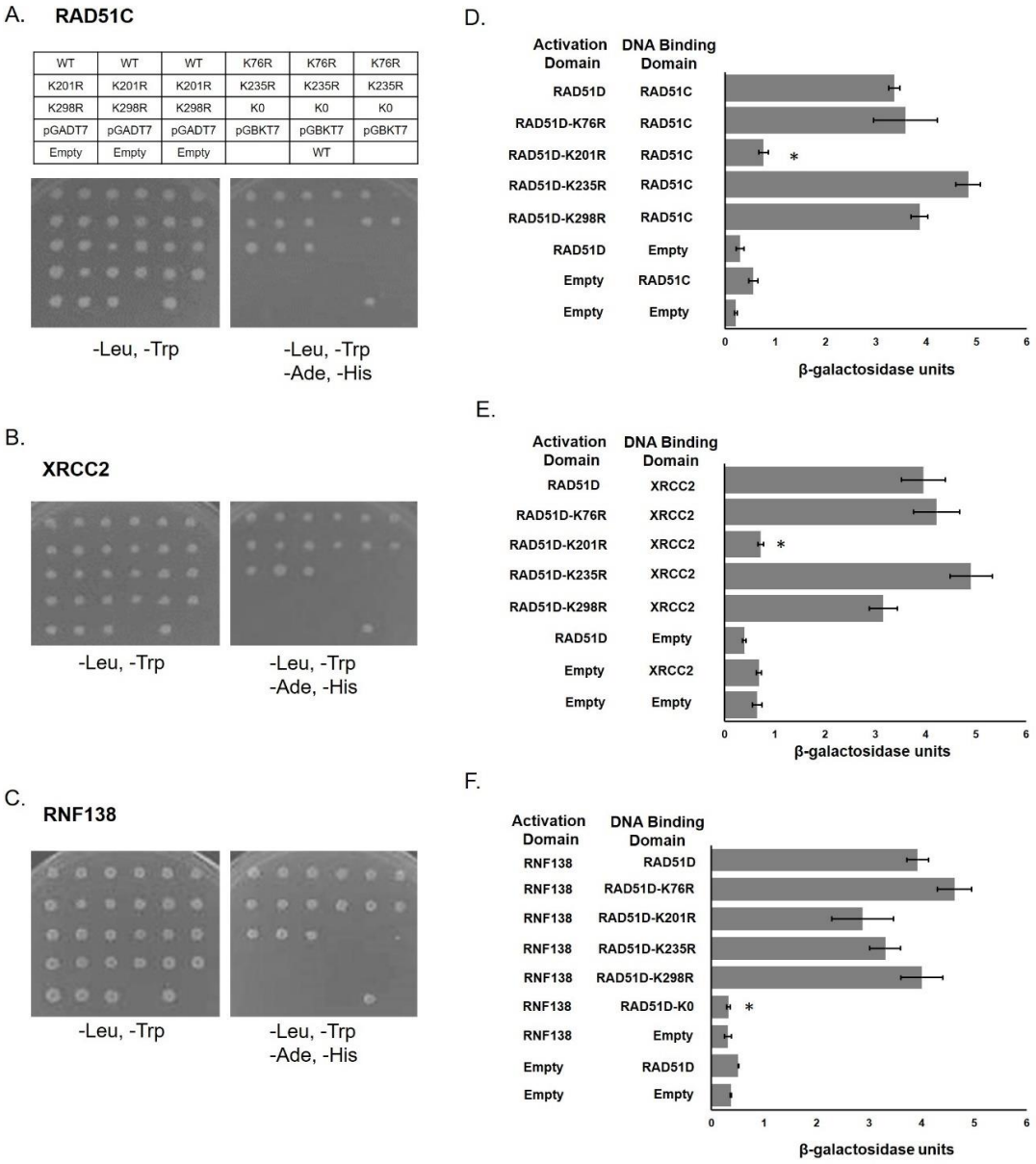

Figure 4.5. Yeast-two-hybrid protein interaction analysis between RAD51D variants with RAD51C, XRCC2, and RNF138. (A-C) Yeast-two-hybrid interactions were tested by replica-plating AH109 strains co-transformed with RAD51D variants and (A) RAD51C, (B) XRCC2, and (C) RNF138 on selective growth medium lacking leucine and tryptophan (left plate) or adenine, histidine, leucine, tryptophan (right plate). (D-F) ONPG analysis of the AH109 yeast strain transformed with the indicated RAD51D variants and (D) RAD51C full-length, (E) XRCC2 full-length, and (F) RNF138 full-length expression constructs. Data represent the mean of two independent experiments performed in triplicate, error bars represent SEM and * indicates $p<0.05$ compared to wild-type.

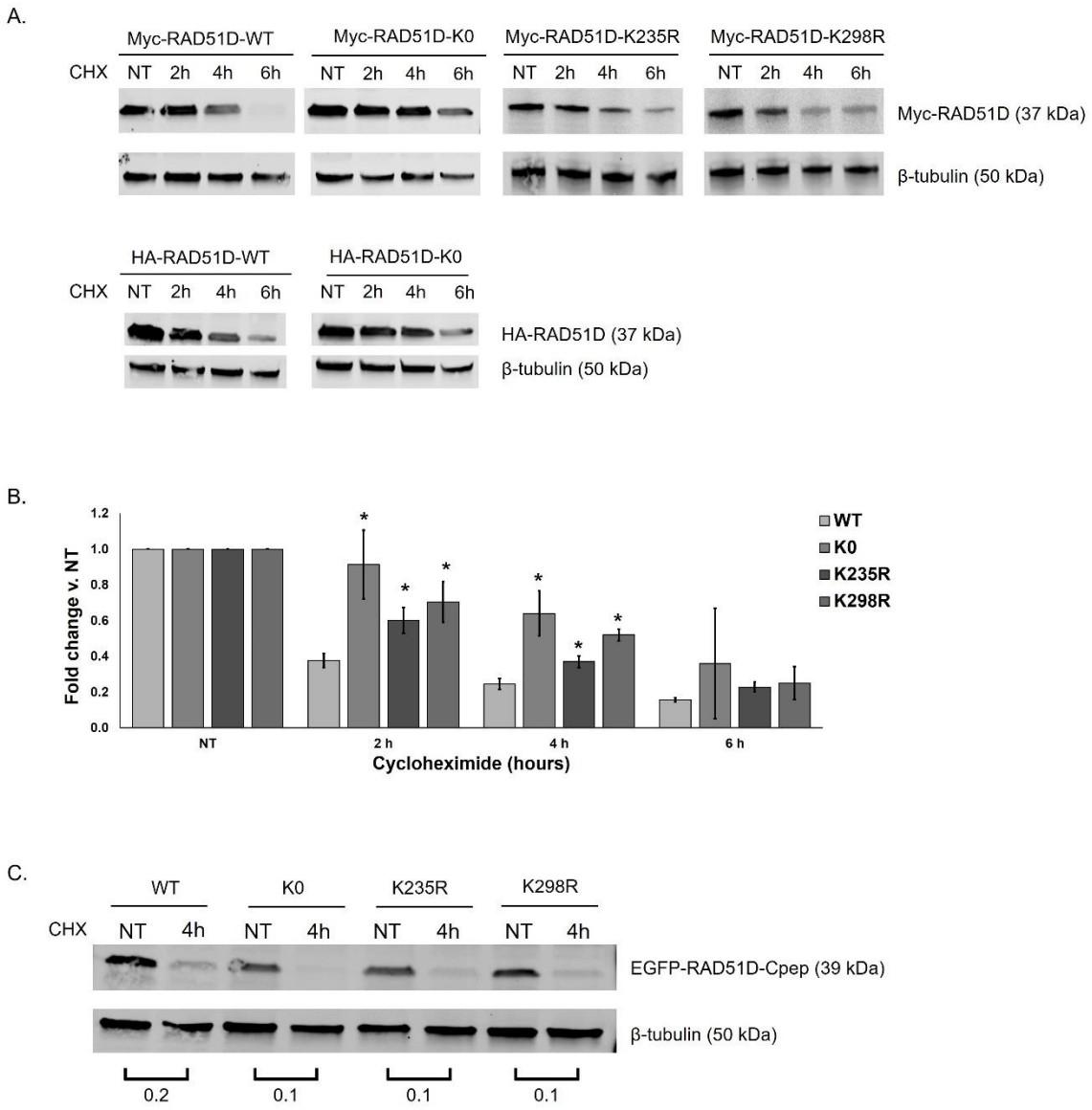

Figure 4.6. Stability and ubiquitination of RAD51D variants. (A) Myc-RAD51D protein levels were assessed 24 hours post-transfection, and 2, 4, and 6 h following the addition of cycloheximide (CHX). (B) Densitometry analysis of band intensity was performed using Image Studio (Licor version 4.0). Myc-RAD51D band intensity was normalized to β-tubulin and graphed as fold-change versus no treatment (NT) for each time point. Data represent the mean from two independent experiments, error bars represent SEM, and * indicates $p<0.05$ compared with wild-type. (C) EGFP-RAD51D-Cpep protein levels were assessed 4 h following CHX block. EGFP-RAD51D-Cpep band intensity was normalized to β-tubulin and fold change versus NT was calculated. Data is representative of two independent experiments.

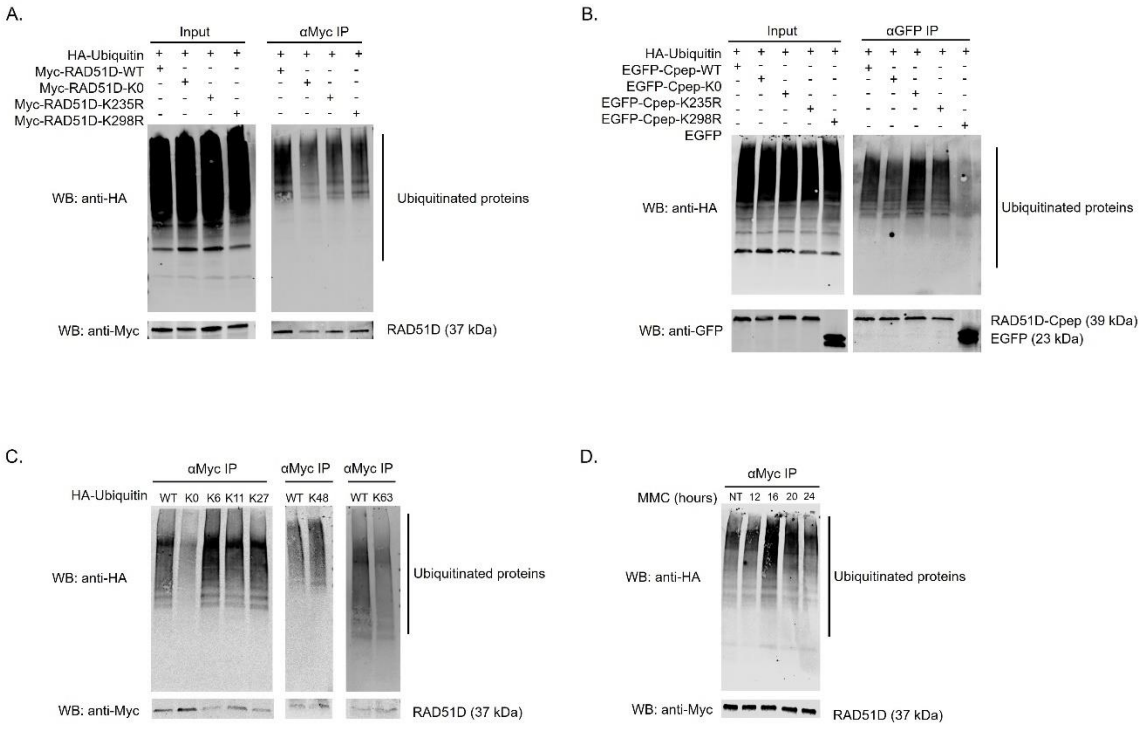

Figure 4.7. Ubiquitination signaling along RAD51D. (A) Analysis of RAD51D ubiquitination *in vivo.* Myc-tagged RAD51D variants were co-expressed with HA-tagged ubiquitin constructs, and anti-Myc immunoprecipitation was performed. Data are representative of three independent experiments. (B) Analysis of ubiquitination of RAD51D C-terminus. EGFP-tagged RAD51D variants were co-expressed with HA-tagged ubiquitin constructs and anti-GFP immunoprecipitation was performed. Data are representative of two independent experiments. (C) Myc-tagged RAD51D was co-expressed with HA-tagged ubiquitin mutant constructs containing single lysine residues (indicated by the number). Anti-Myc immunoprecipitation was performed to detect ubiquitin chain linkages along RAD51D. (D) HeLa cells were transfected with Myc-tagged RAD51D wild-type and HA-tagged ubiquitin then treated with 160 ng/mL MMC 12 h after transfection. RAD51D ubiquitination levels were assessed 12 h, 16 h, 20 h, and 24 h following MMC treatment.

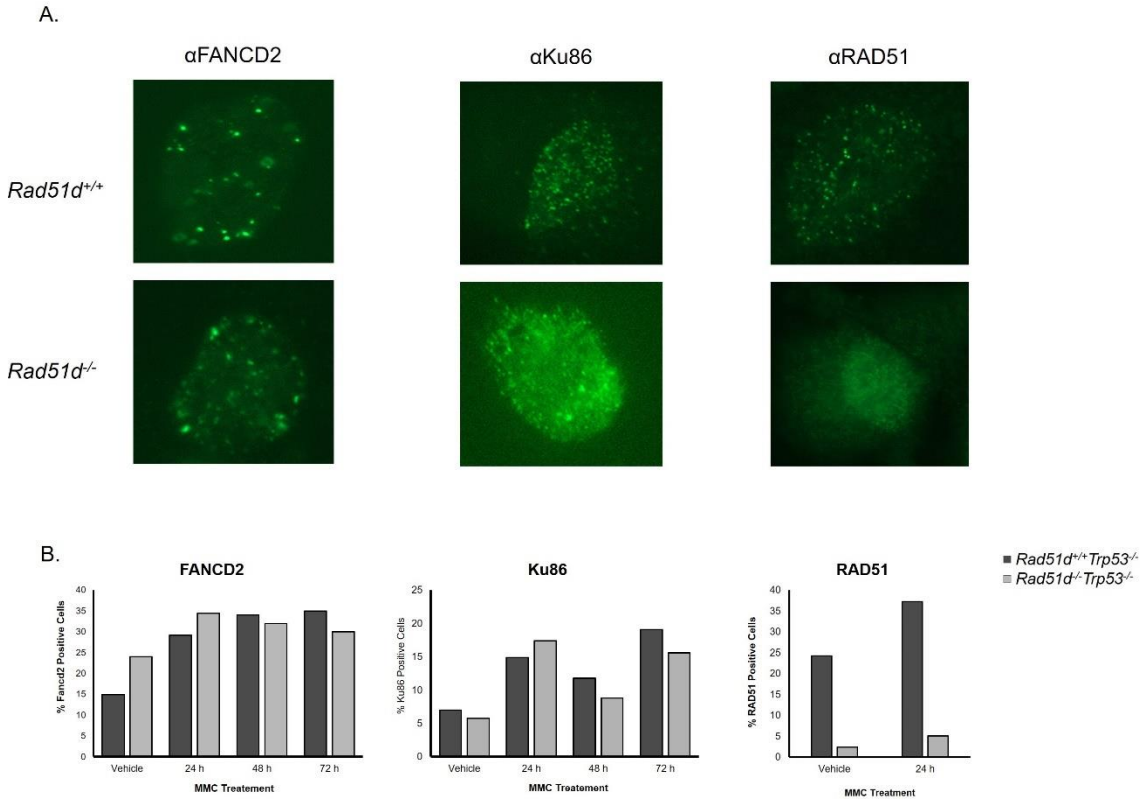

Figure 4.8. Recruitment of FANCD2, Ku86, and RAD51 to MMC-induced DNA damage. *Rad51d*$^{+/+}$*Trp53*$^{-/-}$ and *Rad51d*$^{-/-}$*Trp53*$^{-/-}$ MEFs were treated mitomycin C (MMC) for 24 h, 48 h, or 72 h. Equitoxic doses of MMC were used: *Rad51d*$^{+/+}$*Trp53*$^{-/-}$ (200 ng/mL) and *Rad51d*$^{-/-}$*Trp53*$^{-/-}$ (2 ng/mL). (A) Representative images of FANCD2, Ku86, and RAD51 foci in *Rad51d*$^{+/+}$*Trp53*$^{-/-}$ and *Rad51d*$^{-/-}$*Trp53*$^{-/-}$ MEFs. (B) Quantitation of FANCD2, Ku86, and RAD51 foci in *Rad51d*$^{+/+}$*Trp53*$^{-/-}$ and *Rad51d*$^{-/-}$ *Trp53*$^{-/-}$ MEFs. Nuclei with >5 foci were scored as positive, and a minimum 200 nuclei were scored for each timepoint.

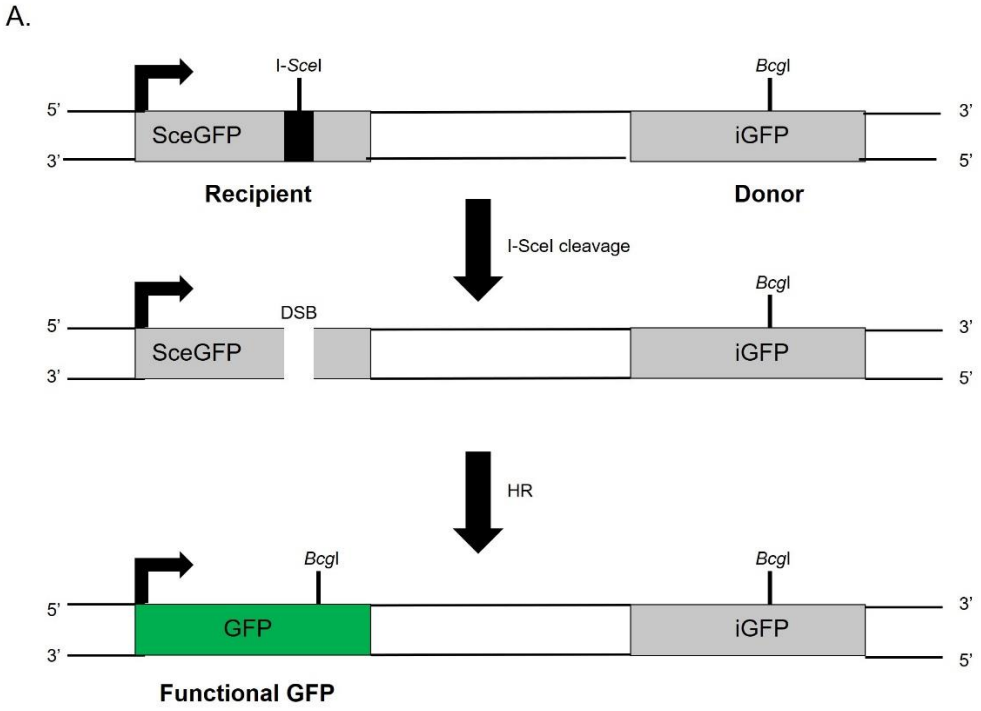

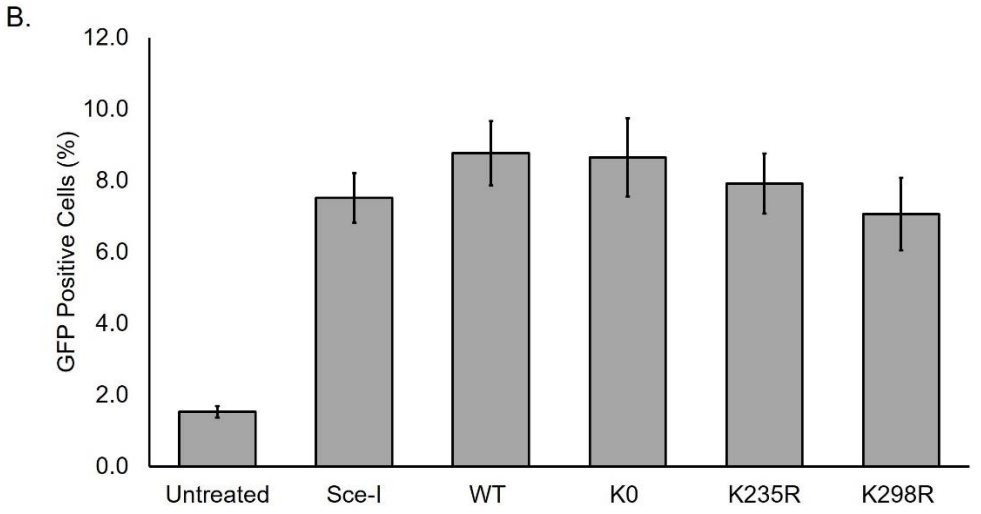

Figure 4.9. Measurement of HR by reconstitution of GFP fluorescence in HeLa DRGFP cells**.** (A) Homology-directed GFP repair assay (Pierce et al. 1999). A modified GFP gene is expressed in HeLa cells (HeLa-DRGFP). This gene encodes the enhanced green fluorescent protein (EGFP) expressed from an hCMV enhancer/chicken β-actin promoter (arrow) that is modified to contain an I-SceI site and in-frame termination codon. Downstream of the SceGFP is iGFP, a 5′ and 3′ truncated GFP gene that includes a

*Bcg*I restriction enzyme site. HeLa-DRGFP cells are transfected with an I-SceI plasmid that encodes the I-SceI enzyme, leading to DNA cleavage within the SceGFP gene and a double stranded break. Homologous recombination proteins repair the break using the iGFP gene as a homologous template, producing an intact GFP gene. (B) Bar graph showing the percentage of GFP positive cells (two experiments performed in triplicate) after electroporation with buffer (untreated), Sce-I plasmid only, or each Myc-tagged RAD51D construct and Sce-I plasmid. Statistical significance was not achieved using one-way ANOVA analysis.

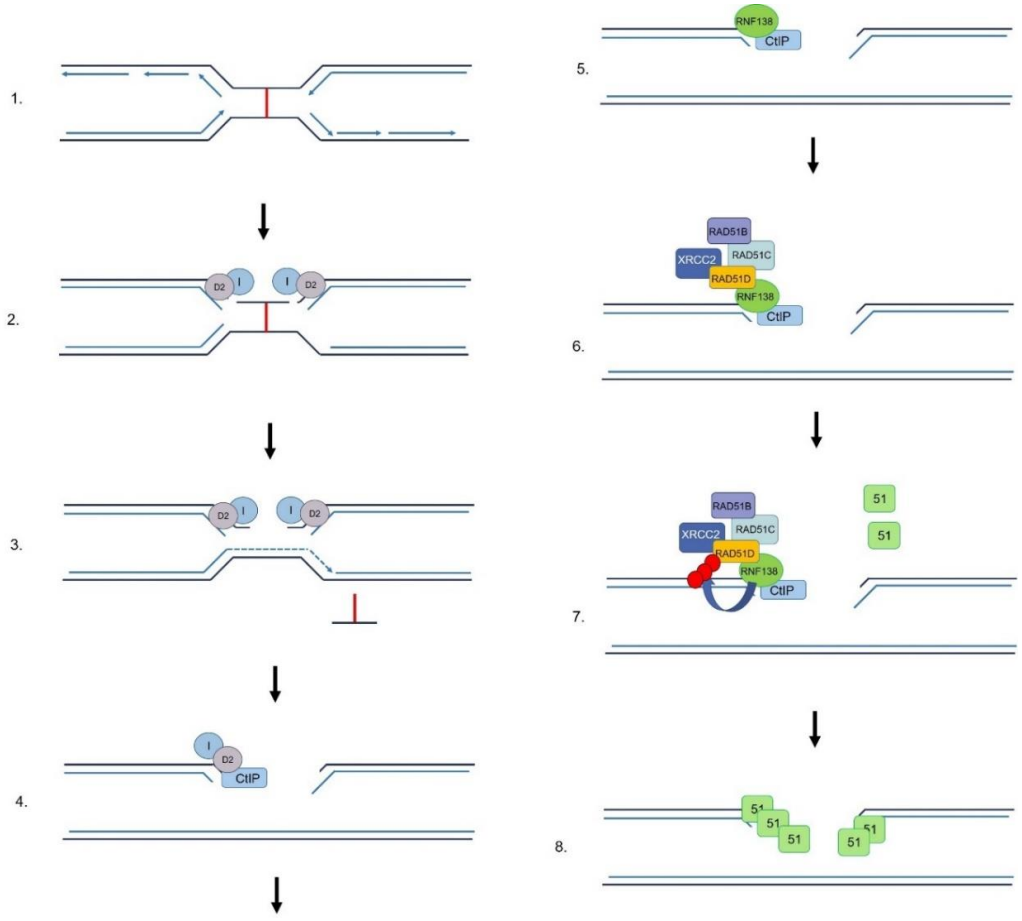

Figure 4.10. Proposed model of RAD51D ubiquitination during DNA interstrand crosslink repair. (1) An interstrand crosslink inhibits DNA replication, which is represented by the arrows showing directions of replication machinery during S phase. (2) FANCD2/FANCI mediate strand incision and 'flip out' of the ICL lesion. (3) Nucleotide excision repair proteins remove the lesion and translesion synthesis proteins replicate across the break represented by a red line, producing an intact DNA strand and a double strand break (DSB). (4) CtIP interacts with FANCD2/FANCI and excises the DNA to produce a single strand overhang (shown on the right side of the double strand break). (5) RNF138 binds to CtIP to further promote strand nucleotide excision. (6) The BCDX2 complex is localized to the DSB through the interaction between RAD51D and RNF138. (7) BCDX2 initiates recruitment of RAD51 to the break. Polyubiquitination of RAD51D leads to removal of the proteins from the break and further loading of RAD51. Absence of K235 and K298 are proposed to prevent RAD51D polyubiquitination, leading to the BCDX2 complex remaining at the damage site and blocking the next step. (8) RAD51 filaments coat the single strand overhang to prepare for homology search and strand invasion.

CHAPTER 5

THIOPURINE-INDUCED TELOMERIC DAMAGE IN RAD51D-DEFICIENT MAMMALIAN CELLS[3]

[3]Michael D. Wyatt, Nicole M. Reilly, Shikha Patel, Preeti Rajesh, Gary P. Schools, Phillip G. Smiraldo, Douglas L. Pittman. Thiopurine-induced mitotic catastrophe in *Rad51d*-deficient mammalian cells. *Environmental and Molecular Mutagenesis*, **2017**, 59: 38 – 48.

Preface

The data in this Chapter were published in the research article titled "Thiopurine-induced mitotic catastrophe in *Rad51d*-deficient mammalian cells" appearing in *Environmental and Molecular Mutagenesis* on September 25, 2017 (Wyatt et al.). For the purposes of this dissertation, the data that I contributed to the manuscript are reported.

Abstract

Thiopurines are part of a clinical regimen used for the treatment of autoimmune disorders and childhood acute lymphoblastic leukemia. However, despite these successes, there are also unintended consequences such as therapy-induced cancer in long-term survivors. Therefore, a better understanding of cellular responses to thiopurines will lead to improved and personalized treatment strategies. RAD51D is an important component of homologous recombination (HR), and our previous work established that mammalian cells defective for RAD51D are more sensitive to the thiopurine 6-thioguanine (6TG) and have dramatically increased numbers of multinucleated cells and chromosome instability. 6TG is capable of being incorporated into telomeres, and interestingly, RAD51D contributes to telomere maintenance, although the precise function of RAD51D at the telomeres remains unclear. We sought here to investigate: 1) the activity of RAD51D at telomeres, 2) the contribution of RAD51D to protect against 6TG-induced telomere damage, and 3) the fates of *Rad51d*-deficient cells following 6TG treatment. These results demonstrate that RAD51D is required for maintaining the telomeric 3´ overhangs. As measured by γ-H2AX induction and foci formation, 6TG-induced DNA damage in *Rad51d*-proficient and *Rad51d*-deficient cells. However, the extent of γ-H2AX telomere

localization following 6TG treatment was higher in *Rad51d*-deficient cells than in *Rad51d*-proficient cells. Using live-cell imaging of 6TG-treated *Rad51d*-deficient cells, two predominant forms of mitotic catastrophe were found to contribute to the formation of multinucleated cells, failed division and restitution. Collectively, these findings provide a unique window into the role of the RAD51D HR protein during thiopurine induction of mitotic catastrophe.

Introduction

Thiopurines have a long history of clinical usage as immunosuppressants and in cancer chemotherapy. Combination therapy including mercaptopurine for childhood acute lymphoblastic leukemia (ALL) treatment is an amazing success story, with cure or long-term remission rates now being greater than 90%. Although the metabolism of thiopurines is well known (Krynetski and Evans 2003), surprisingly little is understood about the mechanism by which thiopurines induce DNA damage and kill cancer cells. When thiopurines are metabolized into active nucleotide forms, the predominant mechanism of action is incorporation into DNA (Karran 2006). During replication, the thiopurine 6-thioguanine (6TG) causes base mispairing, which is then recognized by DNA mismatch repair (MMR) proteins. As part of a poorly understood process, the MMR machinery causes DNA strand breaks and invokes homologous recombination (HR) mediated repair. Inactivation or loss of MMR thus alleviates killing and chromosomal instability caused by thiopurines (Armstrong and Galloway 1997; Buermeyer et al. 1999; Rajesh, Litvinchuk, et al. 2011).

RAD51D is one of the RAD51 family members indispensable for HR. RAD51D is now an established ovarian cancer susceptibility gene (Loveday et al. 2011; Song et al. 2015; Thompson et al. 2013), and BRCA2-defective cancer cells are also sensitized to 6TG (Issaeva et al. 2010). Indeed, a recent phase II clinical trial, NCT01432145, explored the use of a thiopurine in BRCA2-defective tumors; based upon genetic signatures, thiopurines might be used in other HR-defective cancers. At this time, there have been no reports of the successful generation of human *knockout* cells for any of the RAD51 paralogs. In fact, vertebrate cells deficient in any of the RAD51 paralogs have only been generated in mouse embryonic fibroblasts, DT40 avian cells, and Chinese hamster ovary cells (Deans et al. 2003; Hinz et al. 2006; Lim and Hasty 1996; Takata et al. 2001; Tsuzuki et al. 1996). Even though RNA interference mediated knockdowns of several of the RAD51 family members in human cancer cells have been attempted, none achieved a substantially reduced expression (e.g., RAD51 by Wyatt and coworkers (Yang, Waldman, and Wyatt 2008)). In all cases examined, decreased expression of the RAD51 paralogs exhibited a similar sensitivity to DNA damaging agents and chromosome instability.

Our previous work established that RAD51D-dependent HR is protective downstream of MMR following 6TG treatment (Rajesh, Litvinchuk, et al. 2011). Specifically, *Rad51d*-deficient cells were extremely sensitive to 6TG, and there was a substantial increase in the frequency of chromosomal aberrations, particularly radials. There was also an increase in multinucleation and chromosomal aneuploidy in the *Rad51d*-deficient cells following 6TG treatment. The loss of MLH1 alleviated these phenotypes, demonstrating that the induced damage depends on functional MMR. The

roles of RAD51D in genomic maintenance include telomere stability (Tarsounas et al. 2004). In this regard, it is interesting to note that deoxy-thioguanine nucleotides can be incorporated into DNA by telomerase (Marathias, Sawicki, and Bolton 1999; Mender et al. 2015; Tendian and Parker 2000). These observations prompted our investigation into three related topics. First, we sought to better understand the specific telomeric defect associated with *Rad51d*-deficient cells. Here, it was found that RAD51D is required for maintaining the telomeric 3´ overhangs in mammalian cells. Second, we investigated telomeric DNA damage caused by 6TG. Chromosome fusions were induced by 6TG, some of which contained telomeric labeling. In *Rad51d*-deficient cells, there was increased co-localization of telomere probes with γ-H2AX foci compared to *Rad51d*-proficient cells, which further increased upon treatment with 6TG. Lastly, we investigated via live cell imaging multi-nucleation induced by 6TG treatment of *Rad51d*-deficient cells. Note that, similar to this *Rad51d*-deficient cellular phenotype, different leukemias and lymphomas are known to have increased aneuploidy and multinucleation, and also telomere defects (Knecht et al. 2009; Knecht et al. 2010). These findings provide a unique window into the formation of multinucleated *Rad51d*-deficient cells and demonstrate that RAD51D provides a protective role against the telomeric DNA damage and chromosomal instability that thiopurine treatment causes.

Materials and methods

Cell lines

Mice heterozygous for a mutation in the *Mlh1* gene and mice heterozygous for null-alleles in *Rad51d* and *Trp53* were crossed to generate murine embryonic fibroblasts (MEFs) with different combinations of the three mutated genes (Rajesh, Litvinchuk, et al. 2011; Rajesh et al. 2010; Smiraldo et al. 2005). Primary and immortalized mouse embryonic fibroblasts (MEFs) were grown in DMEM (Corning, Corning, NY USA) supplemented with 7.5% fetal bovine serum (Atlanta Biologicals, Flowery Branch, GA USA), 7.5% newborn calf serum (GE Life Sciences, Pittsburgh, PA USA), and antibiotics (GE) as previously described (Smiraldo et al. 2005). The following immortalized cell lines used for these studies were *Rad51d*$^{+/+}$*Trp53*$^{-/-}$ (C53), *Rad51d*$^{-/-}$ *Trp53*$^{-/-}$ (310), and *Rad51d*$^{-/-}$*Trp53*$^{-/-}$*Mlh1*$^{-/-}$ (T3) cells. Note that because it was only possible to generate immortalized MEFs that were *Rad51d*$^{-/-}$ on a *Trp53*$^{-/-}$ background (Smiraldo et al. 2005), all work in immortalized MEFs occurred in *Trp53*$^{-/-}$ cells. For simplicity, genotypes of the immortalized MEFs are referred to throughout the manuscript as *Rad51d* or *Mlh1* status.

Western blot analysis of γ-H2AX induction

Immortalized *Rad51d*$^{+/+}$, *Rad51d*$^{-/-}$, and *Rad51d*$^{-/-}$ *Mlh1*$^{-/-}$ MEFs were plated in a 6-well dish at a concentration of 6 x 10^4 cells per well and, after 24 h, treated with 50 or 100 nM 6TG (Sigma Aldrich, St. Louis, MO USA) for 48 and 72 h. Following treatment, cells were trypsinized and proteins extracted in 1X cell lysis buffer (20 mM Tris, 150 mM NaCl, 1 mM EDTA, 1 mM EGTA, 1 mM PMSF, 1% Triton X-100) containing protease inhibitor cocktail (Thermo Fisher, Waltham, MA USA). Thirty micrograms of whole-cell

protein extracts were separated using a 4–20% gradient gel (Bio-Rad, Hercules, CA USA). Western blot analysis was performed using rabbit polyclonal anti-γ-H2AX (A300-081, Bethyl, Montgomery, TX USA) or rabbit monoclonal anti-GAPDH (D16H11, Cell Signaling, Danvers, MA USA). Primary incubations were followed with species specific IR Dye 800CW secondary antibody (Licor, Lincoln, NE USA), and signal detection was performed using a Licor Odyssey Sa Imaging System. Quantitative analysis of band intensity was performed using Image Studio software (LiCor, version 4.0, Lincoln NE, USA).

Immunofluorescence, telomere staining, and chromosome fusions

For the detection of γ-H2AX foci and telomere co-localization, sub-confluent cells, grown on sterile glass microscope slides or cover slips (VWR, Radnor, PA USA), were treated for the indicated times with 6TG. Following treatment, cells were fixed in 4% paraformaldehyde (Affymetrix, Santa Clara, CA USA), permeabilized with a 0.2% Triton X-100 solution, and incubated in block solution (5% dry milk in 1x PBS) at room temperature. This was followed by incubation with the anti-phospho-Histone H2AX (Ser139) mouse monoclonal antibody (1:600; Bethyl) and Oregon Green 488 goat anti-mouse IgG secondary (1:1000; Molecular Probes (Thermo Fisher), Waltham, MA USA). Telomeres were visualized with the peptide nucleic acid probe Cy3-$(CCCTAA)_3$ (PNA Bio, Thousand Oaks, CA USA) and chromatin visualized by DAPI (Sigma).

For studies using primary MEFs to detect γ-H2AX foci, cells containing ≥ 5 distinct γ-H2AX foci were defined as foci-positive, and the percentage of γ-H2AX foci at telomeres was calculated as [(number of γ-H2AX foci at telomeres) / (number of γ-H2AX foci)]* 100% for each cell. Statistical significance was determined by comparing

the mean number of γ-H2AX foci at telomeres per cell for each genotype by ANOVA. Follow-up comparisons were performed using the Tukey HSD post hoc test. For studies using immortalized MEFs and 6TG-induced damage, cells containing ≥ 10 distinct γ-H2AX foci were defined as foci-positive, and the percentage of γ-H2AX positive cells was calculated as [(number of γ-H2AX positive cells)/(total number of cells)]*100. An EvosFL fluorescence microscope (Life Technologies, Carlsbad, CA USA) under a 60X oil objective was used to detect γ-H2AX foci. Individual cells were manually scored through depth-of-field for foci, identified based upon signal intensity above general background staining levels and present within the nucleus as assessed by DAPI staining. Metaphase chromosome spreads were prepared as described previously (Smiraldo et al. 2005). The percent of fusions per chromosome was calculated as [(number of fusions)/(number of chromosomes)]*100 per metaphase spread. Statistical significance of the experimental data was determined by calculating a z-score. The presence of a telomere at a fusion was scored positive, and the percent telomere associated fusions was calculated as [(number of telomere positive fusions)/(number of fusions)]*100.

For detection of telomeres at chromosome fusions, an Axiovert 200 with Axiovision (Zeiss, Oberkochen, Germany) fluorescence microscope and 100X oil objective was used. For detection of γ-H2AX foci at telomeres, cells were treated as described above and the telomere $(CCCTAA)_3$ probe added after γ-H2AX antibody incubation. Individual cells were scored for co-localized foci by manual scanning through the cellular depth. Cells were scored positive when overlapping signals were observed within the nucleus. The number of γ-H2AX foci co-localized with telomere signal was counted per nuclei and grouped into three categories: 0 to 2 co-localized foci, 3 to 7 co-

localized foci, or ≥8 co-localized foci. A minimum of 200 nuclei were counted for each genotype and treatment.

Results

H2AX phosphorylation in response to 6TG treatment

Induction of γ-H2AX following 6TG treatment was assessed by Western blotting and immunofluorescence in immortalized *Rad51d*-proficient and *Rad51d*-deficient MEFs both in a *Trp53*-deficient background. Following treatment with 50 nM 6TG, an increase of γ-H2AX at 48 and 72 h in the *Rad51d*-proficient cells and in the *Rad51d*-deficient cells was observed (Figure 5.1A). At this dose and time point of 48 h, quantitation revealed that γ-H2AX was not statistically different in *Rad51d*-proficient and *Rad51d*-deficient cells (Figure 5.1B, grey bars, ~2.5 fold). At a 50 nM dose for 72 h, γ-H2AX was higher in *Rad51d*-proficient cells (Figure 5.1B, black bars, 4.5-fold compared to 2.5-fold in *Rad51d*-deficient cells). Treatment with 100 nM 6TG at 48 and 72 hours induced γ-H2AX to a greater extent than that seen with 50 nM 6TG in all genotypes. No statistically significant differences were seen between *Rad51d*-proficient and *Rad51d*-deficient cells (Figure 5.1C). Our prior work established that in the absence of MLH1, *Rad51d*-deficient cells were less sensitive to killing and chromosomal instability caused by 6TG (Rajesh, Litvinchuk, et al. 2011). In the *Rad51d*$^{-/-}$*Mlh1*$^{-/-}$ cells, there was no measurable γ-H2AX increase in the *Rad51d*$^{-/-}$*Mlh1*$^{-/-}$ cells at 50 nM 6TG at either time point (Figure 5.1B). At 100 nM 6TG, there was a modest induction of γ-H2AX at 100 nM 6TG that was lower compared to MLH1-proficient cells regardless of RAD51D status (Figure 5.1C). This is consistent with prior observations and further supports idea that the specificity of the

clastogenic damage caused by 6TG in the absence of RAD51D depends on functional MMR.

Using immunofluorescence microscopy, nuclei with ten or more γ-H2AX foci after 72 h 6TG treatment were scored as positive. The untreated *Rad51d*-deficient cells had a basal level of 15% γ-H2AX foci, whereas no γ-H2AX positive *Rad51d*-proficient cells were observed (Figure 5.1D, white bars), indicative of the extensive genome instability associated with *Rad51d* deficiency. Following treatment with 50 nM 6TG, γ-H2AX foci positive cells increased to 42% in *Rad51d*-proficient cells, whereas in *Rad51d*-deficient cells the γ-H2AX foci positivity went from a basal level of 15% to 27% (Figure 5.1D, grey bars). This agreed with muted induction of H2AX by 6TG in the absence of RAD51D as observed by Western blotting in Figure 5.2B. At the higher dose of 100 nM 6TG, the increase in γ-H2AX foci positive cells was similar in both genotypes following treatment with 100 nM 6TG (Figure 5.1D, black bars). In examining the *Rad51d*$^{-/-}$*Mlh1*$^{-/-}$ cells for γ-H2AX foci, the results were entirely consistent with the observations by Western blotting for γ-H2AX in Figure 5.1A and B. Specifically, Figure 5.2C shows that there was no γ-H2AX foci induction above basal levels at 50 nM 6TG, whereas at the higher dose of 100 nM, a statistically significant but lessened induction of foci was observed in *Rad51d*$^{-/-}$ *Mlh1*$^{-/-}$ cells compared to the *Mlh1*$^{+/+}$ cells.

γH2AX and telomere co-localization in response to 6TG treatment

To determine whether γ-H2AX foci were associated with telomeres in response to 6TG, immortalized MEFs containing ≥5 γ-H2AX foci were scored after 6TG treatment (Figure 5.2A). Co-localization of the telomere probe with γ-H2AX foci was grouped into three categories (0-2, 3-7, and ≥8 foci/nuclei, Figure 5.2B). In vehicle treated, a majority (80%)

of *Rad51d*-proficient cells contained between zero and two co-localized foci per nucleus (Figure 5.2B, left panel, white portion of bar). In contrast, the majority (>60%) of vehicle-treated *Rad51d*-deficient cells contained three or more co-localized foci per nucleus (Figure 5.2B, middle panel, grey portion) indicative of an elevated basal level of DNA damage in the absence of RAD51D. In response to 50 nM 6TG treatment, there was an induction of co-localized foci per nucleus in *Rad51d*-proficient cells (Figure 5.2B, left panel). In *Rad51d*-deficient cells, 50 nM 6TG treatment caused a large increase in the number of cells with 8+ co-localized foci (Figure 5.3B, middle panel, black portion). The higher dose of 100 nM induced an equivalent co-localization in *Rad51d*-proficient and *Rad51d*-deficient cells (Figure 5.2B, left versus middle panel). These data demonstrate that 6TG induced DNA damage as visualized by γ-H2AX at telomeres in a dose-dependent manner, and at least at the lower dose of 6TG, there is more telomeric damage in the absence of RAD51D. Figure 5.2B (right panel) also shows that γ-H2AX localization at telomeres is reduced in the absence of MLH1, which is consistent with prior work showing that MMR recognition of 6TG damage promotes clastogenic events.

Previously, we reported a striking induction of radial chromosomes in *Rad51d*-deficient cells following 6TG treatment (Rajesh, Litvinchuk, et al. 2011). To determine whether chromosome fusions were associated with telomere ends, telomere associated fusions were examined in metaphase spreads. As expected, no fusions were detected in vehicle treated *Rad51d*-proficient cells (Table 1; n=1005 scored). After treatment with 50 or 100 nM 6TG, the number of fusions observed in *Rad51d*-proficient cells was detectable but, as expected, remained low, 0.4 and 0.8%, respectively (Figure 5.3, white bars). Too few fusions were observed to clearly determine telomere association (Table

5.1). In the vehicle-treated *Rad51d*-deficient cells, a basal level of 1.1% chromosome fusions was detected, which increased to 2.7% and 6.9% following treatment with 50 and 100 nM 6TG, respectively (Figure 5.3, grey bars, $p<0.05$). In vehicle-treated *Rad51d*-deficient cells, telomere-associated fusions were detectable and do appear to increase following 6TG treatment, but the level of fusions regardless of telomere association was too few to make any statistically meaningful conclusions (Table 5.1). Lastly, a basal level of 0.6% chromosome fusions was detected in the *Rad51d*$^{-/-}$*Mlh1*$^{-/-}$ cells, which increased by a statistically insignificant amount to 0.9% and 1.6% following treatment with 50 and 100 nM 6TG, respectively (Figure 5.3, black bars). The data showing that 6TG-induced fusions was reduced in *Mlh1*-deficient cells agreed with prior data from us and others that the cytogenetic damage caused by 6TG is dependent at least in part on functional MMR (Armstrong and Galloway 1997; Rajesh, Litvinchuk, et al. 2011).

6-Thioguanine induces multinucleation in Rad51d-deficient cells

Our prior work demonstrated that treatment with 100 nM 6TG induced aneuploidy and multinucleation in *Rad51d*-deficient cells (Rajesh, Litvinchuk, et al. 2011). Here, the induction of multinucleated cells was verified following treatment with a lower dose of 50 nM 6TG (Figure 5.4). Note also we investigated whether there was an unequal distribution of telomeric DNA in the multinucleated cells because of such observations in a prior report (Knecht et al. 2009). However, we show that the multinucleated cells contained an equal distribution of telomeric DNA in this experimental system (Figure 5.5).

Discussion

Thiopurines induce a G2 arrest, which presumably prevents cells with damaged DNA from entering what would otherwise become an abnormal mitosis (Armstrong and Galloway 1997; Buermeyer et al. 1999; Rajesh, Litvinchuk, et al. 2011). However, co-treatment with caffeine or UCN-01 to block ATM/ATR signaling can override the G2 arrest, from which cells subsequently enter tetraploid G1 arrest (Rajesh, Litvinchuk, et al. 2011). In *Rad51d*-deficient cells, the G2 arrest caused by 6TG was heightened but transient; by 72 h, both *Rad51d*-deficient and *Rad51d*-proficient cells progressed into mitosis, as demonstrated by flow cytometry and phospho-histone H3 staining (Yan et al. 2004). One implication is that release from this G2 checkpoint does not require the resolution/completion of HR, and as such might help explain how cancer cells achieve aneuploidy. 6TG treatment induced aneuploidy and multinucleated cells (Rajesh, Litvinchuk, et al. 2011). Similar to this *Rad51d*-deficient cellular phenotype, different leukemia and lymphomas are known to have increased aneuploidy and multinucleation. One notable example is Reed-Sternberg (RS) cells associated with the pathology of Hodgkin's lymphoma (Mauch 2006). The data presented here demonstrates that multinucleation following 6TG treatment occurs via mitotic catastrophe in two ways: failed division and restitution. In this system, mitotic catastrophe resulted in multinucleated cells that do not undergo apoptosis over the duration of the observations here. When treated with the 50 nM 6TG dose, a larger percentage of multinucleated *Rad51d*-deficient cells undergo mitotic catastrophe, which was not observed in cells at the 100 nM dose presumably because of the heightened arrest. These results suggest that a percentage of cells progress into mitosis at the lower dose of 6TG. In fact,

multinucleation and mitotic catastrophe is proposed to be a favored cell death mechanism after cell cycle arrest (Castedo et al. 2004; Fragkos and Beard 2011).

Phosphorylation of Serine-139 on H2AX was measured as a marker of DNA damage, and 6TG induced γ-H2AX as measured by Western blotting and immunofluorescence in both *Rad51d*-deficient and *Rad51d*-proficient cells. It was interesting to note that, as detected by Western blotting and immunofluorescence, γ-H2AX induction seemed muted in the *Rad51d*-deficient cells at the lower dose of 50 nM. It is tempting to speculate that the absence of RAD51D disrupts not just HR repair but also associated DNA damage signaling. In fact, a role for the paralog RAD51C in checkpoint signaling was demonstrated (Badie et al. 2009). However, note that γ-H2AX induction is a highly dynamic process intertwined with yet to be clarified connections with the induction of apoptosis and a broader epigenetic reprogramming in cancer (Cook et al. 2009; Liu et al. 2016; Lu et al. 2006; Monteiro et al. 2014; Xiao et al. 2009).

RAD51D, a protein required for HR, was demonstrated previously to have a role in telomere protection (Tarsounas et al. 2004). Loss of RAD51D conferred extensive chromosome instability, increased chromosome fusions, and accelerated telomere attrition (Smiraldo et al. 2005; Tarsounas et al. 2004). To further examine the role of RAD51D at telomeres, we analyzed the length of the 3´ telomeric overhanging tail in *Rad51d*-deficient MEFs. *Rad51d*-deficient cells had an approximately 40 percent increase in overhang signal intensity. These data demonstrate that loss of RAD51D affects the length of the 3´ telomeric overhang and suggest that RAD51D is required for the regulation of telomere termini. Telomere dysfunction is known to activate DNA damage responses, and loss of murine exonuclease 1 (Exo1) alleviated deleterious

cellular responses in telomere dysfunctional mice (Schaetzlein et al. 2007). This implies that damage disrupting the normal telomere protective mechanisms can expose chromosome ends to exonucleolytic processing that can promote chromosome fusions. Exo1 deletion also conferred cellular resistance to killing by 6TG (Schaetzlein et al. 2007), which implicates telomeric damage as a mechanism of action for 6TG. Because mammalian telomeres contain a G_3 repeat in its canonical sequence, 6TG (as the deoxynucleoside triphosphate) can become incorporated into telomeric DNA by telomerase (Marathias, Sawicki, and Bolton 1999; Tendian and Parker 2000). It was more recently reported that the deoxynucleoside of 6TG can directly damage telomeric DNA, and that hTERT positive cells are sensitized to this treatment (Mender et al. 2015). We measured the distribution of telomeres in the multinucleated *Rad51d*-deficient cells because prior reports have shown structural telomeric defects and unequal distribution in multinucleated Reed-Sternberg cells (Knecht et al. 2009; Knecht et al. 2010). However, no unequal telomere distribution was observed in the *Rad51d*-deficient MEFs after 6TG treatment. Collectively, this work contributes to the understanding of 6TG-induced telomere damage and the negative consequences for chromosomal instability in the absence of RAD51D-dependent processes at telomeres.

RAD51D is a RAD51 family member broadly appreciated to be indispensable for HR; yet, the specialized functions of the individual protein products have evaded full elucidation. Components of HR are recruited to stalled replication forks and inter-strand crosslinks (ICLs), as well as DNA double strand breaks (DSBs). Recently, a dominant RAD51 mutation in a patient with Fanconi anemia-like phenotypes was characterized and uncovered a role for RAD51 in ICL repair independent of HR (Wang et al. 2015),

suggesting there is much more to learn about these highly related yet potentially separable processes. Human variant alleles of the RAD51 paralogs confer cancer susceptibility, for example RAD51B mutations are associated with breast cancer (Golmard et al. 2013; Pelttari et al. 2016), RAD51C mutations are associated with breast and ovarian cancer , and RAD51D mutations are associated with ovarian cancer (Coulet et al. 2013; Meindl et al. 2010; Song et al. 2015; Vaz et al. 2010). There are many more mutations of unknown significance in these paralogs. Our results suggest that clinical variability in how patients respond to thiopurine treatment, as well as their potential risk for a future, therapy-related secondary dysplasia might include the status of RAD51D-dependent processing of telomeres.

Table 5.1. Cytological analysis of MEFs treated with 6TG.

(A) Vehicle treated MEFs			
Genotype	*Rad51d*$^{+/+}$	*Rad51d*$^{-/-}$	*Rad51d*$^{-/-}$*Mlh1*$^{-/-}$
Number of chromosomes	1005	462	980
End-to-end fusions[a]	0(0)	0.01(5)	0.01(6)
-TTAGGG[b]	0(0)	0.60(3)	0.33(2)
+TTAGGG[b]	0(0)	0.40(2)	0.67(4)
(B) 50 nM 6TG treated MEFs			
Genotype	*Rad51d*$^{+/+}$	*Rad51d*$^{-/-}$	*Rad51d*$^{-/-}$*Mlh1*$^{-/-}$
Number of chromosomes	552	587	572
End-to-end fusions[a]	0(2)	0.03(16)	0.01(5)
-TTAGGG[b]	1(2)	0.75(12)	0(0)
+TTAGGG[b]	0(0)	0.25(4)	1(5)
(C) 100 nM 6TG treated MEFs			
Genotype	*Rad51d*$^{+/+}$	*Rad51d*$^{-/-}$	*Rad51d*$^{-/-}$*Mlh1*$^{-/-}$
Number of chromosomes	522	463	632
End-to-end fusions[a]	0.01(4)	0.07(32)	0.02(10)
-TTAGGG[b]	0.75(3)	0.66(21)	0(0)
+TTAGGG[b]	0.25(1)	0.34(11)	1(10)

[a]Frequency of end-to-end fusions represented as the percentage of the total number of chromosomes scored for that sample. The total number is shown in parentheses.

[b]+TTAGGG and -TTAGGG refer to the presence or absence of telomeric repeats at the fusion point.

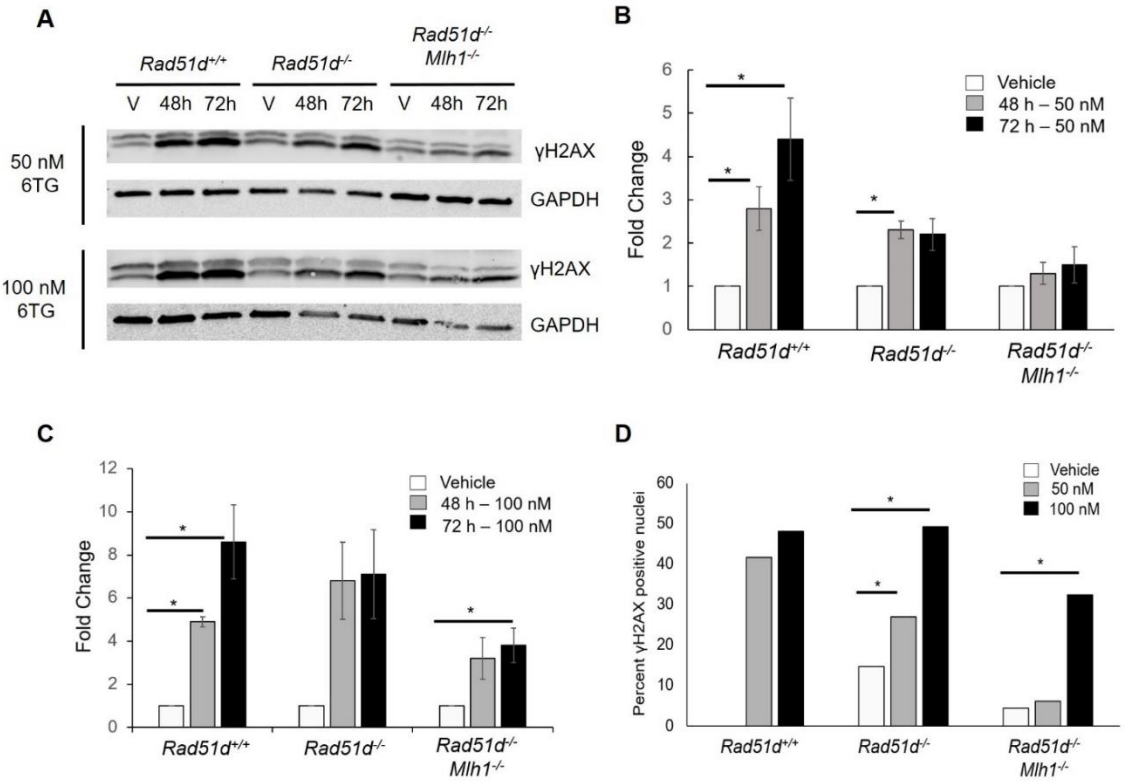

Figure 5.1. Induction of γ-H2AX following treatment with 6TG. (A) The γ-H2AX signal (lower band) was determined by Western blot analysis after 6TG treatment for 48 and 72 h at the doses indicated in *Rad51d*$^{+/+}$ (lanes 1 – 3) and *Rad51d*$^{-/-}$ (lanes 4 – 6) and *Rad51d*$^{-/-}$*Mlh1*$^{-/-}$ MEFs (lanes 7 – 9). (B & C) Quantification of γ-H2AX band intensities from untreated cells (□), or cells treated for 48 h (■) or 72 h (■) that were normalized to GAPDH (*$p<0.05$) after 50 nM (B) or 100 nM (C) 6TG treatment. (D) Quantitation of cellular γ-H2AX foci from untreated cells (□), or cells treated with 50 (■) or 100 nM (■) 6TG. Nuclei with ten or more γ-H2AX foci were scored as positive, and at least 100 nuclei were counted for each sample.

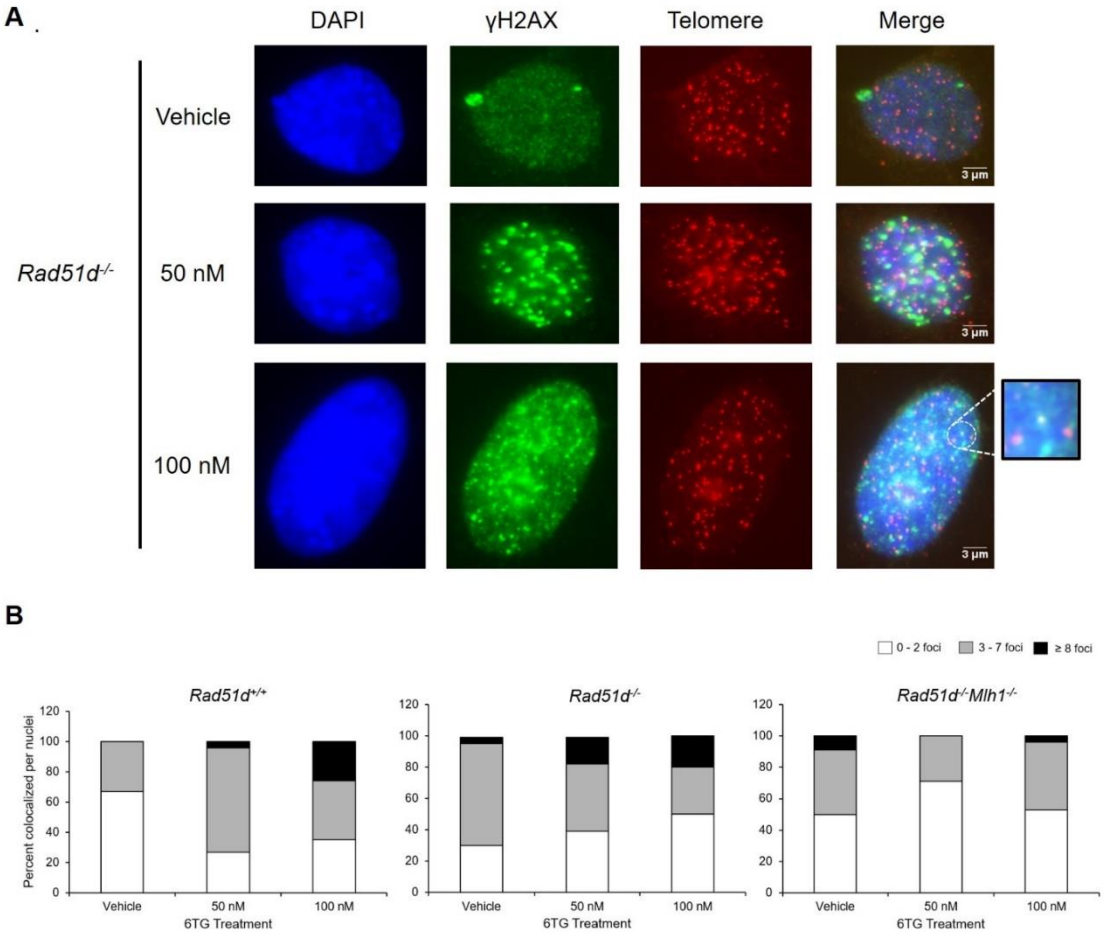

Figure 5.2. (A) Representative images of *Rad51d*$^{-/-}$ cells mock treated or treated with 50 or 100 nM 6TG. Blue panels are DAPI stained nuclei. Green panels are stained with anti-γ-H2AX antibody. Red panels are stained with the telomere probe. Merge is the overlay of each panel. White arrowheads indicate the co-localization of γ-H2AX foci at telomeres. (B) Localization of γ-H2AX foci co-localized with telomere signal at telomeres in immortalized MEFs after treatment with vehicle alone, 50 nM, or 100 nM 6TG. The three categories are 0 to 2 co-localized foci (□), 3 to 7 co-localized foci (■), or ≥8 co-localized foci (■) per nuclei.

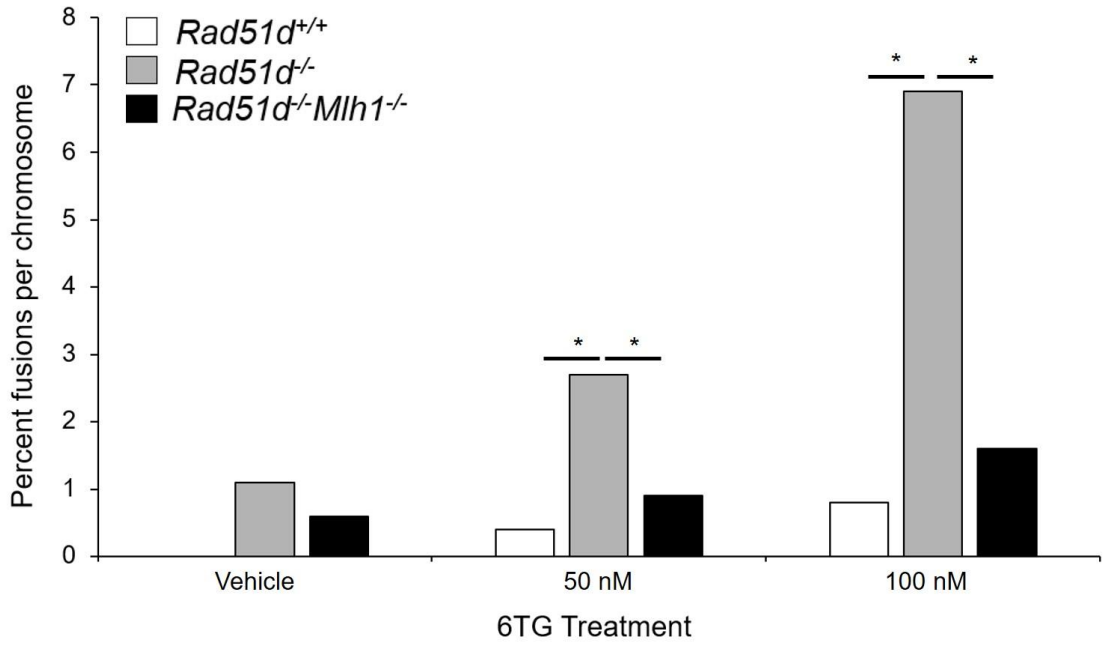

Figure 5.3. 6TG induced chromosome fusions in *Rad51d*-deficient immortalized MEFs. After treatment for 72 hours, chromosomes were stained with DAPI. The number of chromosome fusions was scored as a percent of the total number of chromosomes in vehicle, 50 nM, or 100 nM 6TG-treated *Rad51d*$^{+/+}$ (□), and *Rad51d*$^{-/-}$ (■) and *Rad51d*$^{-/-}$ *Mlh1*$^{-/-}$ MEFs (■) Statistical significance was determined by calculating a z-score; *indicates $p<0.05$.

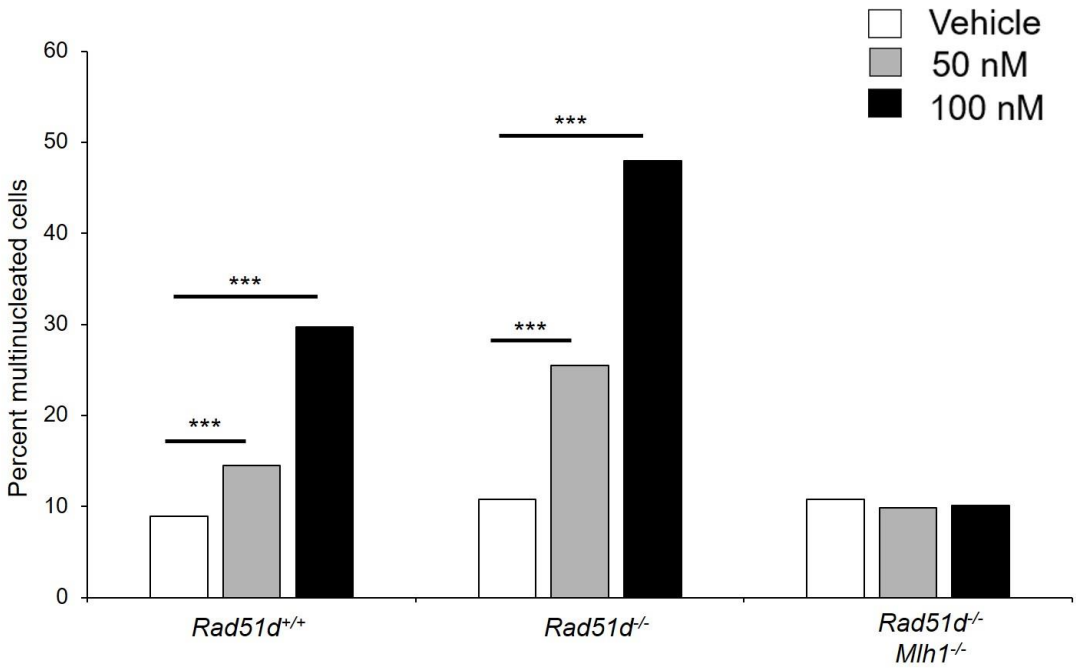

Figure 5.4. 6-TG treatment induces increased multinucleation in *Rad51d*-deficient and *Mlh1*-proficient MEFs. *Rad51d*$^{+/+}$, *Rad51d*$^{-/-}$, and *Rad51d*$^{-/-}$*Mlh1*$^{-/-}$ MEFs were treated with vehicle, 50 nM 6-TG, and 100 nM 6-TG for 72 hours. Cells containing more than one nuclei were scored positive. Statistical significance was determined by a z-test (***$p<0.001$).

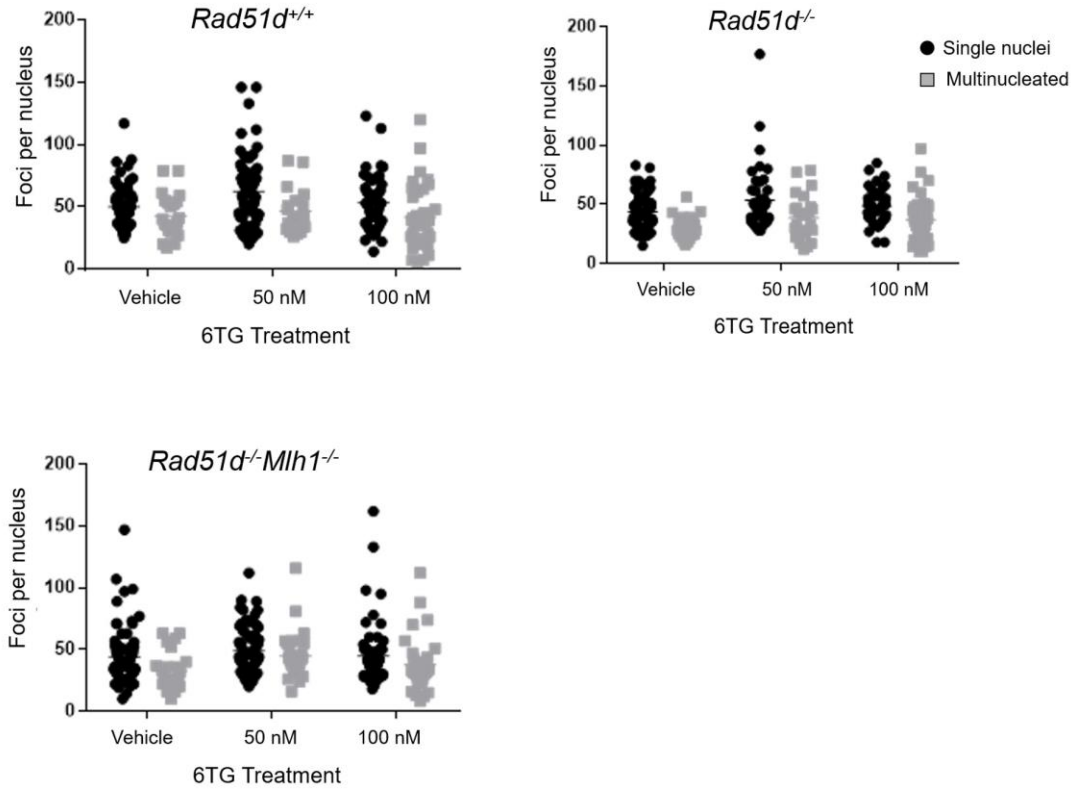

Figure 5.5. 6-TG treatment does not affect the telomere distribution across nuclei within multinucleated cells. *Rad51d*$^{+/+}$, *Rad51d*$^{-/-}$, and *Rad51d*$^{-/-}$*Mlh1*$^{-/-}$ MEFs were treated with vehicle, 50 nM 6-TG, and 100 nM 6-TG for 72 hours then incubated with a fluorescent telomere-specific probe (CCCTAA). The number of telomere foci were counted for each nucleus in both single or multinucleated cells.

CHAPTER 6

GENOME-WIDE IDENTIFICATION AND EXPRESSION ANALYSIS OF GENE DIFFERENCES BETWEEN RAD51D PROFICIENT AND DEFICIENT PRIMARY MOUSE EMBRYONIC FIBROBLASTS

Abstract

One of the hallmarks of cancer is replicative immortality, and an enabling characteristic is genome instability that increases the prevalence of acquired gene mutations. Mutations in genes associated with the homologous recombination (HR) repair pathway increases genomic instability and are found in approximately 50% of ovarian cancers. Patients that carry mutations in the *RAD51D* HR gene are up to 12 times more likely to develop this cancer. Loss of *Rad51d* in mouse embryos confers mid-gestation embryo death, and cells isolated from *Rad51d*$^{-/-}$ embryos fail to proliferate in culture. Concurrent deletion of the *Trp53* gene extends embryo development up to 7 days, and *Rad51d*$^{-/-}$*Trp53*$^{-/-}$ (*Rad51d*-deficient) MEF cell lines have been successfully generated. *Rad51d*-deficient cells have extensive chromosomal aberrations, such as fusions and telomere shortening, and similar defects are often observed in ovarian cancer cells. For this reason, *Rad51d*-deficient MEFs were used as a model for genomic unstable ovarian cancers. The gene expression profiles of primary MEFs derived from *Rad51d*$^{+/+}$*Trp53*$^{-/-}$ (*Rad51d*-proficient) and *Rad51d*-deficient embryos were analyzed by both microarray and RNA Seq. Microarray identified 489 genes with higher expression and 129 genes with lower expression in *Rad51d*-deficient MEFs compared with *Rad51d*-proficient MEFs. RNA Seq analysis identified 449 genes with higher expression, and 479 genes with lower expression in the absence of *Rad51d*. In both analyses, the highest proportion of genes were associated with cellular growth and proliferation. Twenty-one genes associated with cell cycle progression were identified by microarray including *Id1*, *Id2*, and *Cdkn1a(p21)* that had higher expression in *Rad51d*-deficient MEFs. Analysis using the TopHat function on the Illumina platform identified two intra-chromosomal gene fusions, one along

Chromosome 4 and one along Chromosome 17, in the *Rad51d*-proficient cell line, and three inter-chromosomal fusions all involving Chromosome 10. Only the fusion involving Chromosome 4 was also identified in the *Rad51d*-deficient MEFs, and no fusions were identified only in the *Rad51d*-deficient cell lines. Together these data provide insight into gene expression compromises that support cell proliferation in the absence of *Rad51d*.

Introduction

Approximately 50% of ovarian cancers carry mutations in genes associated with the homologous recombination (HR) pathway, and exhibit extensive chromosome instability (Coulet et al. 2013; Eoh et al. 2016; Konstantinopoulos et al. 2015; Konstantinopoulos et al. 2014; Loveday et al. 2011; Meindl et al. 2010; Prakash et al. 2015; Song et al. 2015; Tedaldi et al. 2017; Thompson et al. 2013). The *RAD51* gene family – *RAD51*, *RAD51B*, *RAD51C*, *RAD51D*, *XRCC2*, and *XRCC3* – encode proteins that are part of the HR pathway. These proteins are essential for maintaining chromosome integrity and repairing DNA damage, and loss of any RAD51 paralog confers cellular sensitivity to DNA damaging agents (Andreassen and Ren 2009; Baumann and West 1998; Kim and D'Andrea 2012; Chirnomas et al. 2006; Rajesh, Litvinchuk, et al. 2011; Konstantinopoulos et al. 2014). RAD51D, the fourth member of the RAD51 family of genes, is a known breast and ovarian cancer susceptibility gene (Loveday et al. 2011; Song et al. 2015; Tedaldi et al. 2017; Thompson et al. 2013).

Early investigations into *Mus musculus Rad51d* demonstrated that loss of the gene confers an embryo lethal phenotype beginning at 8.5 days post conception (dpc) (Pittman and Schimenti 2000). A concurrent deletion of the *Trp53* gene extends embryo development to 15.5 dpc (Smiraldo et al. 2005). In addition to embryo defects, null alleles of *Rad51d* lead to chromosomal defects in the form of breaks, gaps, and translocations, telomere shortening, and telomere-specific end-to-end fusions (Tarsounas et al. 2004; Smiraldo et al. 2005). Spectral karyotype analysis of cells isolated from a *Rad51d*-deficient embryo identified a large number of fusions – for example, between chromosomes 9 and 12, and chromosomes 2 and 19 (Smiraldo et al. 2005). Despite the extensive genomic instability and embryo lethality observed when the *Rad51d* gene is deleted, mouse embryonic fibroblasts (MEFs) were able to proliferate in culture when the *Trp53* gene was deleted concurrently (Smiraldo et al. 2005).

In this study, gene expression profiles of $Rad51d^{+/+}Trp53^{-/-}$ (*Rad51d*-proficient) and $Rad51d^{-/-}Trp53^{-/-}$ (*Rad51d*-deficient) primary MEF cell lines were assessed by microarray and RNA Seq analyses. Microarray identified 618 genes with differential expression between the *Rad51d*-deficient and -proficient cell lines, and 21 of the identified genes are associated with cell cycle progression. RNA Seq analysis of *Rad51d*-proficient and -deficient cell lines identified 928 genes that were differentially expressed. Five gene fusions were identified in the *Rad51d*-proficient cell lines, but only one of these fusions was also present in the *Rad51d*-deficient samples. Comparison between the two data sets identified 135 genes that were differentially expressed between *Rad51d*-proficient and -deficient cell lines. Together these data provide insight into gene expression compromises that support cell division in a chromosomal unstable cell line.

Materials and Methods

Cell Culture

Rad51d$^{+/-}$*Trp53*$^{+/-}$ mice were intercrossed, and primary MEFs were generated from mid-gestation embryos (Smiraldo et al. 2005). MEFs isolated from *Rad51d*$^{+/+}$*Trp53*$^{-/-}$ (MEFPR1) and two independent *Rad51d*$^{-/-}$*Trp53*$^{-/-}$ (MEFT11 and MEFT34) embryos were maintained at 37°C with 5% CO_2 in Dulbecco's Modified Eagle's Medium (DMEM; Fisher Scientific) supplemented with 10% fetal bovine serum (Atlanta Biologicals), 1% penicillin/streptomycin, and 1% glutamine. For these experiments, primary MEFs were used only up until three passages.

RNA Isolation and RT-PCR of Rad51d

Total RNA was isolated using the miRNeasy Mini Kit (Cat. #: 217004; Qiagen) according to the manufacturer's protocol. RNA quality was assessed using an Agilent 2100 Bioanalyzer and RNA Integrity Numbers for all samples used ranged from 9.0 to 10.0. First-strand reverse transcription for each RNA sample was performed using a ProScriptII First Strand DNA Synthesis Kit (NEB). Gene specific primers for *MmRad51d* spanning exon 1 to exon 4, and for *MmGapdh* were used: Rad51d SS1 5'-(GCGAGCGCCCAAGTGACAGA)-3', Rad51d SS2 (5'-GCTACCTGGGCCACCCACAA-3'), Gapdh left (5'-AACTTTGGCATTGTGGAAG-3'), Gapdh right (5'-GGATGCAGGGATGATGTTCT-3'). PCR reactions were performed under the following conditions: 30 cycles at 94°C for 30 seconds, 57°C for 30 seconds, and 72°C for 1 minute.

Microarray Analysis

Microarray experiments were performed using the Affymetrix platform. Total RNA samples were amplified and biotinylated using GeneChip WT PLUS Reagent Kit (Affymetrix, Santa Clara, CA). One hundred nanograms of total RNA per sample was reverse transcribed into ds-cDNA using random hexamers, and the remaining RNA was degraded using RNase H. Single strand cDNA was then fragmented and labelled with biotin. The amplified and labeled samples were hybridized to Mouse Transcriptome Arrays 1.0 (Affymetrix, Santa Clara, CA) for 16 h at 45°C using a GeneChip Hybridization Oven 640 and a GeneChip Hybridization, Wash, and Stain Kit (Affymetrix, Santa Clara, CA). Hybridized arrays were washed and stained using a GeneChip Fluidics Stations 450. Arrays (8 total) were scanned using a GeneChip Scanner 3000 7G system and computer workstation equipped with GeneChip Command Console 4.0 software (Affymetrix, Santa Clara, CA).

Following completion of array scans, probe cell intensity (CEL) files were imported into Expression Console Software (Affymetrix, Santa Clara, CA) and processed at the gene-level using the Robust Multichip Analysis (RMA) algorithm to generate CHP files. After confirming data quality within Expression Console, CHP files containing log2 expression signals for each probe were imported into Transcriptome Analysis Console Software version 3.0.0.466 (Affymetrix, Santa Clara, CA) to analyze cell type specific transcriptional responses using one-way between-subject analysis of variance (ANOVA). A p-value of 0.05 and a fold change of 1.5 were used as cutoff parameters. Subsequently, pathway analysis of the differentially expressed genes was performed using Ingenuity Pathway Analysis software (Qiagen, Hilden, Germany).

RNA Sequencing Library Preparation

RNA-seq libraries were constructed using TruSeq® Stranded mRNA LT (Cat. #: RS-122-2101; Illumina) according to the manufacturer's protocol. Briefly, the mRNA was purified by two rounds of polyA selection from the total RNA. The mRNA was reverse transcribed into first strand cDNA using reverse transcriptase and random primers. The second strand cDNA was synthesized using PCR. A single "A" nucleotide was added to the 3' ends of the blunt fragments and ligated with multiple single "T" indexing adapters to the ends of the double strand cDNA. DNA libraries were enriched by PCR amplification, qualified using an Agilent Technologies 2100 Bioanalyzer, and quantitated by qPCR in a Bio-Rad iCycler using a Bio-Rad iCyclerTM qPCR Master Mix (Cat. #: KK4844; Kapa Biosystems). After denaturation, libraries were diluted to 1.8 pM with hybridization buffer. Paired end 75 bp sequencing was performed on the Illumina NextSeq 500 using NSQ® 500 High Output KT v2 (150 CYS; Cat. #: FC-404-2002; Illumina) per manufacturer's protocol.

RNA Sequencing Analysis

Expression analysis was performed on the Illumina BaseSpace platform (Illumina). The iGenome reference dataset used for analysis was the University of California – Santa Cruz (UCSC) M*us musculus* reference genome (mm10). Uniquely mapped reads were assembled into transcripts guided by the UCSC *Mus musculus* mm10 RefSeq & Gencode gene annotation using the TopHat function on the Illumina platform. Expression differences between conditions were evaluated using DESeq2 (Love, Huber, and Anders 2014; Schurch et al. 2016). The analysis was generated using Partek® software (St. Louis, MO, USA). Annotation of significantly different transcripts and enrichment analysis was

performed with DAVID. This is a bioinformatic resource, supported by the National Institutes of Allergy and Infectious Disease, that uses integrated biological knowledgebases to systematically extract biological meaning from large data sets (Huang da, Sherman, and Lempicki 2009). The hierarchical clustering analysis of the global gene expression pattern in different samples was carried out using heatmap.2 function (gplots package) in R. Gene set enrichment was analyzed with GSEA software (Subramanian et al. 2005).

Results

Microarray gene expression analysis of primary mouse embryonic fibroblasts

The main goal of this study was to identify expression profile differences between low-passage primary mouse embryonic fibroblasts (MEFs) generated from individual *Rad51d*-deficient and *Rad51d*-proficient embryos (described previously (Smiraldo et al. 2005)) using an Affymetrix microarray platform. RNA was isolated, and the *Rad51d* status of each cell line was confirmed by RT-PCR (Figure 6.1A). Differences in gene expression levels were determined by comparing the *Rad51d*-deficient sample with the *Rad51d*-proficient (control) sample. Genes with greater than 1.5-fold difference are reported. Of the 65,956 genes represented on the array, 618 were differentially expressed between the samples (Table A.1); 489 genes had higher expression, and 129 had lower expression in the *Rad51d*-deficient cell line compared with the *Rad51d*-proficient cell line.

The transcripts represented on the array encoded only for known protein products and predicted genes based on Ensembl data sets. Of the genes with higher expression in

the *Rad51d*-deficient cell line, 207 encode known protein products. A proteomics screen performed by the Pittman laboratory identified 75 proteins that co-precipitate with RAD51D (Rajesh et al. 2009). The genes that encode two of the proteins identified in this screen – *Ifit1* and *Rnf213* – had lower expression in the *Rad51d*-deficient cell line. Expression of *Ifit1* was 2.35 times lower in the absence of *Rad51d*. In the *Mus musculus* genome, this gene maps to chromosome 19 and encodes for the interferon-induced protein with tetratricopeptide repeats 1 (IFIT1) protein that is expressed in mouse large intestine, liver, small intestine, and bladder (Yue et al. 2014). In a study of breast cancer patients, expression of IFIT1 was associated with improved local relapse-free survival and has been shown to mediate chemotherapy and radiation resistance (Danish et al. 2013). *Rnf213* maps to chromosome 11 and is most highly expressed in ovary, mammary gland, and thymus tissues (Yue et al. 2014). This gene encodes for the RING finger 213 (RNF213) E3 ubiquitin ligase protein. In humans, small nucleotide polymorphisms in this gene is associated with increased risk for moyamoya disease (Hu, Luo, and Chen 2017).

The Ingenuity Pathway Analysis (IPA) tool was used to sort genes into known biological functions (Figure 6.2). This software is designed to "integrate previously observed cause-effect relationships reported in the literature" with a gene expression data set using Ingenuity Knowledge Base, a "collection of observations from various experimental contexts curated from biomedical literature" (Kramer et al. 2014). For this study, IPA was used to categorized genes into known biological functions. Ninety-one genes with differential expression between the *Rad51d*-deficient and *Rad51d*-proficient cell lines were associated with "cellular growth and proliferation" (Table 6.1).

One of the main goals of this project was to understand how expression compromises in the absence of *Rad51d* promote cell division and proliferation when the genome is unstable. Twenty-one genes associated with "cell cycle progression" (18 included in the "cellular growth and proliferation" group) had altered gene expression in the absence of *Rad51d* (Table 6.2). Expression of *Stat1* was 1.6-fold lower in the *Rad51d*-deficient cell line than the *Rad51d*-proficient. The STAT1 protein encoded by this gene is activated in response to extracellular signals, including cytokines and growth factors, and acts as a transcription factor that activates expression of over 1000 gene targets (Calo et al. 2003; Satoh and Tabunoki 2013). Two members of the DNA binding and/or differentiation (Id) family – *Id1* and *Id2* – had 1.5- and 2.3-fold higher expression in the absence of *Rad51d*, respectively. The proteins encoded by these genes, ID1 and ID2, block binding of helix-loop-helix (HLH) transcription factors during the S phase of the cell cycle to prevent cell differentiation (Jogi et al. 2002). Expression of the *Cdkn1a* gene was 1.6-fold higher in the *Rad51d*-deficient cell line. This gene encodes the cell-cycle dependent kinase p21 that can function independently of p53 to initiate cell cycle arrest in response to DNA damage and cellular stress (Georgakilas, Martin, and Bonner 2017).

RNA Seq gene expression analysis of primary mouse embryonic fibroblasts

Microarray is a useful tool for identifying genes with differential expression between cell lines, however, analysis is limited to gene transcripts represented on the array. RNA Seq allows for genome-wide detection of gene expression levels with low background compared to microarray (Wang, Gerstein, and Snyder 2009). For this reason, we chose to

analyze gene expression in an independent *Rad51d*-deficient and the *Rad51d*-proficient cell lines using RNA Seq.

Nine hundred twenty-eight genes were differentially expressed between the *Rad51d*-deficient and *Rad51d*-proficient samples (Table A.2). Of the genes identified, 449 genes had higher expression and 479 had lower expression in the absence of *Rad51d*. The *Cd52* gene had 11.56 times lower expression in the *Rad51d*-deficient cell line compared with the *Rad51d*-proficient cell line. This gene maps to Chromosome 4 and encodes the CD52 glycoprotein that is expressed on the surface of normal and leukemic immune cells (Vojdeman et al. 2017). The *Stra6* gene had 3.17 times lower expression in the *Rad51d*-deficient cell line. This gene maps to Chromosome 9 and encodes the integral membrane receptor protein STRA6 that mediates uptake of vitamin A (Chen et al. 2016).

IPA was used to sort the genes identified by RNA Seq into categories based on known biological functions (Figure 6.3). The categories are defined based on literature data, and 156 genes with differential expression between the *Rad51d*-deficient and *Rad51d*-proficient cell lines were associated with "cellular growth and proliferation" (Table 6.3), and 146 genes were associated with "cell death and survival." These data suggest that the loss of *Rad51d* affects expression of genes that regulate cell proliferation.

Chromosome fusion points identified by RNA Seq

One advantage of RNA Seq is the ability to identify transcriptome boundaries, such as the connectivity between two exons (Wang, Gerstein, and Snyder 2009). The TopHat-Fusion algorithm is designed to identify both intra- and inter-chromosome fusions (Kim and Salzberg 2011), and was used to identify gene fusions in the *Rad51d*-proficient and *Rad51d*-deficient samples (Table 6.4). Five gene fusions were identified in the *Rad51d*-

proficient sample; two intra- and three inter-chromosome gene fusions. The first intra-chromosome fusion was along Chromosome 4 and resulted in a fusion between the coding region for the *Faf1* gene and a non-coding region within the chromosome. The second was along Chromosome 17 and resulted in a fusion between the coding regions for the *Acat3* and *Acat2* genes. The other three fusions were inter-chromosome fusions that all involved different regions along Chromosome 10. The fusions occurred at different points along Chromosome 10, suggesting that multiple breaks had occurred. The first inter-chromosome fusion occurred at the coding region for the *Nap1l1* gene along Chromosome 10 and a non-coding region of the Chromosome 1. The second fusion occurred at the coding regions for the *Hmga2* gene along Chromosome 10 and the *Sdccag8* gene along Chromosome 1. The third fusion occurred along the coding region for *H2afy2* along Chromosome 10 and the *Pvt1* gene along Chromosome 15.

One intra-chromosome fusion was identified in the *Rad51d*-deficient sample along Chromosome 4 between the coding region for the *Faf1* gene and a non-coding region. This same fusion was identified in the *Rad51d*-proficient. We hypothesized that more gene fusions would be identified in the *Rad51d*-deficient cell line, and that these fusions would be unique to the *Rad51d*$^{-/-}$ genotype. However, this analysis did not identify any novel fusions in the *Rad51d*-deficient sample compared with the *Rad51d*-proficient cell line.

Genes with altered expression identified by both microarray and RNA Seq

Microarray and RNA Seq analysis identified 618 and 928 genes, respectively, that were differentially expressed between *Rad51d*-deficient and *Rad51d*-proficient cell lines. Of those genes, 111 were identified in both analyses (Table 6.5). The genes are listed by

increasing fold change (*Rad51d*-deficient v. *Rad51d*-proficient) as determined by the microarray, and only genes that code for a known protein product are included. IPA identified 91 and 156 genes by microarray and RNA Seq, respectively, that are associated with the "cellular growth and proliferation." Of these, 18 genes were identified by both analyses (Table 6.6). Of the 21 cell cycle regulatory genes identified by microarray, 8 were also identified by RNA Seq, including *Cdkn1a* (Table 6.7). The *Ifit1* gene was identified by microarray and by RNA Seq as being differentially expressed in the absence of *Rad51d*. In a proteomics study, the IFIT1 protein was identified as an interacting protein with RAD51D (Rajesh et al. 2009). Interestingly, the expression differences were inconsistent between the independent *Rad51d*-deficient samples. Expression of *Ifit1* was determined to be 2.35 times lower by microarray and 1.09 times higher by RNA Seq, respectively, in the *Rad51d*-deficient cell line compared with the *Rad51d*-proficient cell line.

Discussion

Hanahan and Weinberg classified six identifiable biological characteristics of tumor development that they termed the "hallmarks of cancer" (Hanahan and Weinberg 2000). In addition to these features, cancer cells acquire 'enabling characteristics' that contribute to carcinogenesis. In 2011, Hanahan and Weinberg classified 'genome instability' as an enabling characteristic, and argued that tumor growth can often be attributed to acquisition of mutations that promote cell proliferation and inhibit cell death (Hanahan and Weinberg 2011). The observation that cancer is a mutation-driven disease also led to the "Mutator Phenotype Hypothesis." First described by Lawrence Loeb, this hypothesis

stated that "mutations occurred randomly throughout the genome, and among these would be mutations in genes that guarantee the fidelity of DNA replication… and repair" (Loeb, Springgate, and Battula 1974). Together, these ideas have led to the current belief that "defects in genome maintenance are… instrumental for tumor progression" (Hanahan and Weinberg 2011).

The *RAD51D* gene encodes a protein that functions during homologous recombination (HR)-mediated repair of DNA double strand breaks and interstrand crosslinks, and is essential for maintaining chromosome and telomere stability (Gruver et al. 2005; Hinz et al. 2006; Rajesh, Litvinchuk, et al. 2011; Rajesh et al. 2010; Smiraldo et al. 2005; Tarsounas et al. 2004; Wyatt et al. ; Yard et al. 2016). Loss of the *Rad51d* gene induces an embryo lethal phenotype in mice, and cells isolated from these embryos exhibit extensive chromosomal defects (Pittman and Schimenti 2000; Smiraldo et al. 2005). Despite chromosome instability, *Rad51d*$^{-/-}$ cells proliferate in culture when the *Trp53* gene is also deleted (Smiraldo et al. 2005). For these reasons, *Rad51d*$^{-/-}$*Trp53*$^{-/-}$ (*Rad51d*-deficient) mouse embryonic fibroblast (MEF) cell lines serve as a model of chromosomally unstable mammalian cells and can be utilized to identify expression compromises that promote cell growth under genome unstable conditions. For this study, gene expression analysis of *Rad51d*-deficient and *Rad51d*-proficient primary mouse embryonic fibroblast cell lines was performed using both microarray and RNA Seq technologies.

Microarray is a high-throughput bioinformatics technique that boasts the ability to analyze expression of tens of thousands of genes at once (Govindarajan et al. 2012). In this study, microarray analysis identified 618 genes with differential expression between

Rad51d-deficient and *Rad51d*-proficient cell lines. Ingenuity Pathway Analysis (IPA) performed on the microarray data set identified 91 genes that are associated with "cellular growth and proliferation," and 21 genes associated with cell cycle progression. The cell cycle genes include *Id1*, *Id2*, and *Cdkn1a(p21)* are discussed below.

The *Id1* and *Id2* genes encode proteins that promote abnormal cell proliferation. ID1 forms a heterodimer with the ETS-1 transcription factor to preventing binding and activation of target genes. One target of ETS-1 is p16, a tumor suppressor that activates cell cycle arrest. Binding of ID1 to ETS-1 suppresses transcription of p16, leading to increased expression of CDKs that promote cell cycle progression and cell differentiation (Perk, Iavarone, and Benezra 2005). Overexpression of ID1 has been linked with increased development of several cancer types, and approximately 70% of ovarian cancers have abnormal expression of ID1 that has been correlated with cancer cell proliferation and resistance to apoptosis (Zhang et al. 2004). Consistent with these previous observations, increased expression of *Id1* and *Id2* in *Rad51d*-deficient cells may contribute to cell proliferation and growth, despite the extensive genomic instability.

The *Cdkn1a(p21)* gene encodes the p21 protein that induces cell growth arrest and inhibits cell cycle progression in response to DNA damage and cellular stress (Abbas and Dutta 2009). The cell lines used for these studies are *Trp53*-null, therefore, expression of *Cdkn1a(p21)* in these cells is independent of p53. In a p53-deficient environment, p21 leads to dysregulation of replication machinery, increased genome instability, and high levels of cell proliferation (Georgakilas, Martin, and Bonner 2017). Furthermore, these data provide an explanation for how ovarian cancers that carry mutations in the *RAD51D* gene proliferate in the presence of genome instability.

Advancement in bioinformatics technologies have led to the rise of an alternative high-throughput method for analyzing gene expression: RNA Seq. This method provides more precise measurements of gene expression levels than microarray, and is not limited to detecting transcripts that correspond to reference sequences on an array (Wang, Gerstein, and Snyder 2009). In this study, 928 genes with altered expression in the *Rad51d*-deficient cell line compared with the *Rad51d*-proficient cell line were identified by RNA Seq. Previous studies showed increased levels of chromosome breaks, fusions, and translocations in *Rad51d*-deficient cells (Smiraldo et al. 2005), and we hypothesized that certain regions of the genome would be more susceptible to fusions in the absence of *Rad51d.* Using the TopHat-Fusion algorithm in the Illumina platform, gene fusions present in the *Rad51d*-deficient and -proficient cell lines were identified. Two intra-chromosomal and three inter-chromosomal gene fusions were detected in the *Rad51d*-proficient sample, and only one intra-chromosomal fusion was observed in the *Rad51d*-deficient sample. The fusion identified in the *Rad51d*-deficient sample occurred along Chromosome 4 between the coding region for *Faf1* and a non-coding region. This fusion has never been reported but may be present in the mouse germline as it was identified in both the *Rad51d*-proficient and -deficient cells. Previous spectral karyotyping of *Rad51d*-deficient cells identified chromosomal fusions, for example between chromosomes 9 and 12, and chromosomes 2 and 19 (Smiraldo et al. 2005); however, these specific translocations were not detected in this study. These data did not support my assertion that loss of *Rad51d* would affect specific regions along the genome.

Future studies would complement the data presented here by investigating how loss of other RAD51 paralogs affects genome stability. Loss of either *Rad51c* or *Xrcc2* in

embryos also disrupts development mid-gestation and induces an embryo lethal phenotype. Consistent with *Rad51d*-deficient cells, loss of *Rad51c* or *Xrcc2* inhibits proliferation in culture unless *Trp53* is deleted concurrently (Kuznetsov et al. 2009; Adam, Deans, and Thacker 2007). Analyzing gene expression profiles of primary MEF cell lines that lack *Rad51c* or *Xrcc2* could provide additional insight into how loss of other HR DNA repair genes affects gene expression and promotes tumor growth.

Additional future studies could include testing inhibitors of p21 in the *Rad51d*-proficient and -deficient cell lines. The McInnes laboratory at the University of South Carolina has successfully synthesized a 16-mer peptide that competes with the p21 binding site along the proliferating cell nuclear antigen (PCNA) protein and provides evidence for a potential target site that will disrupt this interaction (Kontopidis et al. 2005). Interaction between p21 and PCNA delays replication in the presence of DNA damage. Inhibitors that disrupt p21 binding with PCNA will prevent DNA repair and promote apoptosis (Abbas and Dutta 2009). If increased expression of p21 is a compensatory mechanism that promotes cell survival in the absence of *Rad51d*, then inhibiting the activity of this protein offers the potential to induce apoptosis in these cells. This type of therapeutic approach would offer a myriad of benefits in the clinic, particularly for treating ovarian cancer patients that increased p21 expression in conjunction with mutations in *RAD51D* and/or *TP53*.

Acknowledgements

NMR performed RNA isolation, data analysis, and contributed to writing the manuscript. DA performed the RNA quality analysis and ran the microarray. CL prepared the samples

for RNA Seq and ran the analysis. PR generated the *Rad51d*-proficient and *Rad51d*-deficient primary cell lines used in this paper. PJB performed data analysis using Partek software. DLP contributed to experimental design and manuscript preparation. This research was supported by a South Carolina IDeA Networks of Biomedical Research Excellence (INBRE) Grant to DLP, the National Institutes of Health under Award Number R15GM110615, and a Support to Promote Advancement of Research and Creativity (SPARC) Graduate Research Grant from the Office of the Vice President for Research at the University of South Carolina to NMR. The content is solely the responsibility of the authors and does not necessarily represent the official views of the National Institutes of Health.

Table 6.1. List of genes associated with "cellular growth and proliferation" identified by Ingenuity Pathway Analysis of the microarray data set. The q-value shown is an adjusted p-value accounting for the false discovery rate (FDR) which is necessary when analyzing large data sets.

Gene	Fold Change (*Rad51d*-proficient v. *Rad51d*-deficient)	q-value
Rad51d	2.66	2.59E-03
Il1rl1	2.38	2.59E-03
Usp18	2.16	1.72E-01
Adam12	1.95	8.41E-03
Fcer1g	1.95	3.62E-02
Csf1r	1.72	2.11E-02
Adm	1.72	4.55E-02
Itgam	1.71	2.14E-02
Ccl9	1.71	8.68E-02
Adam8	1.7	1.09E-01
Myd88	1.7	3.17E-01
Slit2	1.65	2.11E-02
Ldlr	1.64	1.85E-02
Stat1	1.63	3.07E-01
Serpine1	1.6	3.92E-03
Tnfsf9	1.6	2.15E-01
Tnc	1.59	2.11E-02
Plac8	1.58	4.32E-02
Lsp1	1.57	4.29E-02
Msr1	1.57	7.16E-02
Tlr7	1.53	9.05E-02
Tyrobp	1.52	1.38E-01
Tfap2b	1.51	2.77E-02
Rarb	-1.51	1.22E-02
Plp1	-1.51	2.53E-02
Nr4a1	-1.51	2.85E-02
Nfkbia	-1.51	3.01E-02
Epha4	-1.51	3.54E-01
Cyp26b1	-1.52	2.64E-02
Pdgfra	-1.52	1.76E-01
Des	-1.53	1.55E-01
Msx2	-1.53	1.56E-01
Ptprq	-1.53	2.36E-01
Mdk	-1.54	2.18E-02
Id1	-1.54	4.14E-02
Hist1h1c	-1.54	5.47E-02
Peg3	-1.54	3.47E-01
Krt8	-1.55	2.11E-02
Tgfb2	-1.55	1.64E-01
Dusp4	-1.56	1.87E-02
Rcan1	-1.56	2.15E-02
Smad6	-1.56	3.54E-02

Pdgfb	-1.56	4.70E-02
Tnnt2	-1.56	4.81E-02
Grem1	-1.56	2.34E-01
Ngfr	-1.57	1.22E-02
Gpx7	-1.58	1.03E-02
Fas	-1.59	3.11E-02
Cyp1b1	-1.59	1.89E-01
Lims2	-1.6	4.72E-02
Bmp4	-1.6	1.69E-01
Cdkn1a	-1.61	1.22E-02
Fabp3	-1.61	2.58E-02
Perp	-1.63	8.40E-02
Gabrb3	-1.64	1.36E-01
Ddit3	-1.65	2.39E-02
Edn1	-1.65	6.08E-02
Casp4	-1.65	2.93E-01
Myrf	-1.66	2.59E-03
Nupr1	-1.67	1.22E-02
Krt18	-1.68	1.49E-02
Serpinb6b	-1.68	3.57E-02
Thbd	-1.68	7.71E-02
Myh11	-1.7	1.20E-02
Mmp2	-1.72	1.46E-02
Cp	-1.73	6.45E-02
Dusp6	-1.75	4.94E-02
Cd55	-1.75	1.33E-01
Rorb	-1.77	1.77E-01
Dlx2	-1.81	4.66E-02
Crip1	-1.84	4.14E-02
Sfrp1	-1.84	1.40E-01
Serpine2	-1.88	2.49E-02
Eng	-1.9	3.92E-03
Dsp	-1.93	1.17E-02
Hmox1	-1.97	1.22E-02
Gas6	-1.98	5.39E-03
Clu	-2	1.26E-02
Ppargc1a	-2.12	3.94E-02
Ptgs1	-2.14	3.51E-03
Nqo1	-2.25	6.62E-03
Id2	-2.28	1.37E-02
Kif1a	-2.33	3.92E-03
Aldh1a1	-2.53	2.91E-03
Serpinb9b	-2.55	1.91E-02
Ptn	-2.65	3.87E-01
Dcn	-2.72	1.51E-02

Table 6.2. Genes identified by microarray analysis in *Rad51d*-deficient primary cell lines associated with cell cycle progression.

Gene Symbol	Fold Change (*Rad51d*-proficient v. *Rad51d*-deficient)
Rad51d	2.66
Adam12	1.95
Adm	1.72
Csf1r	1.72
Stat1	1.63
Nfkbia	-1.51
Nr4a1	-1.51
Rarb	-1.51
Trnp1	-1.51
Pdgfra	-1.52
Id1	-1.54
Ptx3	-1.54
Tgfb2	-1.55
Ifnz	-1.57
Cdkn1a (p21)	-1.61
Nupr1	-1.67
Krt18	-1.68
Dlx2	-1.81
Gas6	-1.98
Id2	-2.28
Ly6a	-2.37

Table 6.3. List of genes associated with "cellular growth and proliferation" identified by Ingenuity Pathway Analysis of the RNA Seq data set. The q-value shown is an adjusted p-value taking into account the false discovery rate (FDR) and is necessary when analyzing large sets of data.

Gene Symbol	Fold Change (*Rad51d*-proficient v. *Rad51d*-deficient)	q value
Vav1	5.38	2.72E-03
Spi1	4.91	1.42E-02
Laptm5	4.88	1.51E-03
Trem2	4.87	1.51E-03
Dock2	4.87	2.72E-03
Itgam	4.76	1.51E-03
C5ar1	4.75	1.51E-03
Tyrobp	4.69	1.51E-03
Fcer1g	4.59	1.51E-03
Inpp5d	4.58	1.51E-03
Col2a1	4.41	1.51E-03
Ncf1	4.35	1.51E-03
Cd37	4.32	3.20E-02
Itgal	4.17	1.51E-03
Csf1r	3.60	1.51E-03
Pik3ap1	3.54	1.51E-03
C3ar1	3.36	1.51E-03
Irf8	2.81	1.51E-03
Nckap1l	2.73	1.51E-03
Plac8	2.48	1.51E-03
Dok2	2.46	1.51E-03
Slfn2	2.21	1.51E-03
Ptpn6	2.19	1.51E-03
Zic1	2.04	1.51E-03
Itgb2	1.80	1.51E-03
C1qtnf3	1.79	1.51E-03
Foxc2	1.74	1.51E-03
Coro1a	1.70	1.51E-03
Ptpre	1.51	1.51E-03
Krt7	1.50	1.51E-03
Hoxb4	1.49	1.51E-03
Egr2	1.37	1.51E-03
Ret	1.36	1.51E-03
Cspg4	1.33	1.51E-03
Ucp2	1.31	1.51E-03
Dmrta2	1.26	1.51E-03
Skap1	1.25	1.51E-03
Ctsh	1.19	1.51E-03
Lims2	1.15	1.51E-03
Serpine1	1.14	1.51E-03
Egr1	1.08	1.51E-03
Ctgf	1.01	1.51E-03

Cd14	1.01	1.51E-03
Klf5	0.99	1.51E-03
Hspb1	0.95	1.51E-03
Krt19	0.90	1.51E-03
Csf1	0.89	1.51E-03
Nog	0.88	1.51E-03
Junb	0.88	1.51E-03
Igsf9	0.86	1.51E-03
Gas7	0.85	1.51E-03
Cblb	0.85	1.51E-03
Cited2	0.83	1.51E-03
Klf2	0.83	1.51E-03
Hlx	0.83	2.72E-03
Runx1	0.82	1.51E-03
Plaur	0.82	1.51E-03
Kdr	0.81	1.51E-03
Flt1	0.81	1.51E-03
Phlpp1	0.79	1.51E-03
Syk	0.76	1.51E-03
Twist2	0.73	1.51E-03
Gadd45g	0.73	1.51E-03
Arhgdib	0.72	1.51E-03
Rtn4r	0.72	2.16E-02
Ngf	0.69	3.86E-03
Bcar1	0.68	2.72E-03
Epha2	0.67	1.51E-03
Ptk2b	0.67	7.91E-03
Runx3	0.67	3.03E-02
Flt4	0.65	5.04E-03
Errfi1	0.64	3.86E-03
Adm	0.61	1.24E-02
Srf	0.60	8.90E-03
Etv6	0.60	9.82E-03
Pim3	0.60	2.16E-02
Sema7a	0.59	4.22E-02
Jund	0.53	2.52E-02
Tgfb1	0.53	3.54E-02
Rhob	0.51	3.77E-02
Cav2	-0.55	2.44E-02
Idh1	-0.68	2.72E-03
Net1	-0.72	1.51E-03
Sfrp1	-0.75	1.51E-03
Fgf10	-0.76	5.04E-03
Gadd45a	-0.76	7.00E-03
Crem	-0.76	9.82E-03
Cdon	-0.79	1.51E-03
Rgs4	-0.84	1.51E-03
Lrrn1	-0.87	4.97E-02
Ackr3	-0.88	1.51E-03
Sfrp2	-0.88	1.51E-03
Pappa	-0.88	1.51E-03
Lpin1	-0.90	1.51E-03
Irf1	-0.99	1.51E-03

Nupr1	-1.01	1.51E-03
Mt2	-1.01	1.51E-03
Grem1	-1.03	1.51E-03
Ppargc1a	-1.03	1.51E-03
Sprr1a	-1.07	1.51E-03
Penk	-1.07	1.51E-03
Pax3	-1.08	1.51E-03
Ccl2	-1.10	1.51E-03
Angpt1	-1.14	2.85E-02
Gas1	-1.16	1.51E-03
C3	-1.17	2.72E-03
Ptgs1	-1.20	1.51E-03
Igfbp3	-1.21	1.51E-03
Plat	-1.21	1.51E-03
Nrep	-1.26	1.51E-03
Tmem119	-1.29	1.51E-03
Snca	-1.29	1.51E-03
Spp1	-1.35	1.51E-03
Axin2	-1.36	1.51E-03
Mst1r	-1.38	3.03E-02
Mmp9	-1.42	1.51E-03
Rarb	-1.52	1.51E-03
Il33	-1.52	6.03E-03
Igfbp5	-1.61	1.51E-03
Eln	-1.64	1.51E-03
Gfra2	-1.70	1.51E-03
Dcn	-1.74	1.51E-03
Dkk3	-1.77	1.51E-03
Cd34	-1.79	1.51E-03
Osr2	-1.80	1.51E-03
Ptn	-1.84	1.51E-03
Tnfsf18	-1.85	1.51E-03
Wisp2	-1.92	1.51E-03
Icam1	-2.05	1.51E-03
Barx1	-2.06	1.51E-03
Lgr5	-2.08	2.72E-03
Mmp3	-2.16	1.51E-03
Dlx5	-2.20	1.51E-03
Lum	-2.47	1.51E-03
Dlx6	-3.05	3.86E-03

Table 6.4. Chromosome fusions identified in the RNA Seq samples by TopHat-Fusion. The "Gene" and "Chr." columns lists the genes on the "left" and "right" side of the fusion. The "Pos." column lists the coordinates for the respective gene.

***Rad51d*$^{+/+}$ *Trp53*$^{-/-}$**					
Gene (left)	**Chr. (left)**	**Pos. (left)**	**Gene (right)**	**Chr. (right)**	**Pos. (right)**
Faf1	4	109,710,857	---	4	109,656,436
Nap1l1	10	111,495,360	---	1	135,233,180
Hmga2	10	120,476,118	*Sdccag8*	1	176,835,817
H2afy2	10	61,743,005	*Pvt1*	15	62,218,557
Acat3	17	12,939,874	*Acat2*	17	12,948,657
***Rad51d*$^{-/-}$ *Trp53*$^{-/-}$**					
Gene (left)	**Chr. (left)**	**Pos. (left)**	**Gene (right)**	**Chr. (right)**	**Pos. (right)**
Faf1	4	109,710,857	---	4	109,656,436

Table 6.5. List of genes identified in both microarray and RNA Seq analysis. Genes are listed by increasing fold change as determined by microarray and only genes with known protein products are listed.

Gene	Description	Fold Change (*Rad51d*-proficient v. *Rad51d*-deficient)
Lyz2	lysozyme 2	2.90
Rad51d	RAD51 homolog D	2.66
C1qb	complement component 1, q subcomponent, beta polypeptide	2.53
Il1rl1	interleukin 1 receptor-like 1	2.38
Ifit1	interferon-induced protein with tetratricopeptide repeats 1	2.35
Usp18	ubiquitin specific peptidase 18	2.16
Slc7a8	solute carrier family 7 (cationic amino acid transporter, y+ system), member 8	1.96
Fcer1g	Fc receptor, IgE, high affinity I, gamma polypeptide	1.95
Cdh10	cadherin 10	1.94
Asb5	ankyrin repeat and SOCs box-containing 5	1.92
Slc16a3	solute carrier family 16 (monocarboxylic acid transporters), member 3	1.89
Htr1b	5-hydroxytryptamine (serotonin) receptor 1B	1.78
Csf1r	colony stimulating factor 1 receptor	1.72
Adm	adrenomedullin	1.72
Bcl2a1b	B cell leukemia/lymphoma 2 related protein A1b	1.72
Itgam	integrin alpha M	1.71
Ccl9	chemokine (C-C motif) ligand 9	1.71
Adam8	a disintegrin and metallopeptidase domain 8	1.70
Lrrc15	leucine rich repeat containing 15	1.67
Lcp1	lymphocyte cytosolic protein 1	1.65
Slc1a6	solute carrier family 1 (high affinity aspartate/glutamate transporter), member 6	1.65
Slfn2	schlafen 2	1.63
Alox5ap	arachidonate 5-lipoxygenase activating protein	1.62
Serpine1	serine (or cysteine) peptidase inhibitor, clade E, member 1	1.60
Grem2	gremlin 2 homolog, cysteine knot superfamily (Xenopus laevis)	1.60
Nipal1	NIPA-like domain containing 1	1.60
Plac8	placenta-specific 8	1.58
Tnn	tenascin N	1.58
Msr1	macrophage scavenger receptor 1	1.57
C1qc	complement component 1, q subcomponent, C chain	1.57
Tll1	tolloid-like	1.55
Xaf1	XIAP associated factor 1	1.55
Phlpp1	PH domain and leucine rich repeat protein phosphatase 1	1.54
Tlr7	toll-like receptor 7	1.53
Specc1	sperm antigen with calponin homology and coiled-coil domains 1; cytospin B	1.53

Flt4	FMS-like tyrosine kinase 4	1.53
Ulbp1	UL16 binding protein 1	1.53
Tyrobp	TYRO protein tyrosine kinase binding protein	1.52
Rtp4	receptor transporter protein 4	1.52
Rarb	retinoic acid receptor, beta	-1.51
Nr4a1	nuclear receptor subfamily 4, group A, member 1	-1.51
Epha4	Eph receptor A4	-1.51
Ccdc3	coiled-coil domain containing 3	-1.51
Ackr3	atypical chemokine receptor 3	-1.52
AW551984	expressed sequence AW551984	-1.52
Des	desmin	-1.53
Msx2	msh homeobox 2; homeo box, msh-like 2	-1.53
Prss12	protease, serine 12 neurotrypsin (motopsin)	-1.53
Mxd4	Max dimerization protein 4	-1.53
Lrrn1	leucine rich repeat protein 1, neuronal	-1.53
Id1	inhibitor of DNA binding 1	-1.54
Ptx3	pentraxin related gene	-1.54
Mdk	midkine; midkine (Mdk), transcript variant 1, mRNA.	-1.54
Rragd	Ras-related GTP binding D	-1.55
Grem1	gremlin 1	-1.56
Dlx5	distal-less homeobox 5	-1.56
Tbx2	T-box 2	-1.56
Ngfr	nerve growth factor receptor (TNFR superfamily, member 16)	-1.57
Anxa8	annexin A8	-1.57
Ndrg2	N-myc downstream regulated gene 2	-1.58
Rhoj	ras homolog gene family, member J	-1.58
Myo16	myosin XVI	-1.59
Lims2	LIM and senescent cell antigen like domains 2	-1.60
Acot13	acyl-CoA thioesterase 13	-1.60
Pmp22	peripheral myelin protein 22	-1.61
Gsta4	glutathione S-transferase, alpha 4	-1.61
Mgst1	microsomal glutathione S-transferase 1	-1.63
Igfbp6	insulin-like growth factor binding protein 6	-1.63
Ddit3	DNA-damage inducible transcript 3	-1.65
Casp4	caspase 4, apoptosis-related cysteine peptidase	-1.65
Dhrs3	dehydrogenase/reductase (SDR family) member 3	-1.65
Popdc2	popeye domain containing 2	-1.66
Nupr1	nuclear protein transcription regulator 1	-1.67
Aqp5	aquaporin 5	-1.69
Myh11	myosin, heavy polypeptide 11, smooth muscle	-1.70
Nnt	nicotinamide nucleotide transhydrogenase	-1.70
Sparcl1	SPARC-like 1	-1.71
Mmp2	matrix metallopeptidase 2	-1.72
Pgf	placental growth factor	-1.72
Dusp6	dual specificity phosphatase 6	-1.75
Ptprb	protein tyrosine phosphatase, receptor type, B	-1.76
Rorb	RAR-related orphan receptor beta	-1.77
Tnfsf18	tumor necrosis factor (ligand) superfamily, member 18	-1.77
Cotl1	coactosin-like 1 (Dictyostelium)	-1.78
Cdo1	cysteine dioxygenase 1, cytosolic	-1.80

Mgst3	microsomal glutathione S-transferase 3	-1.81
Pgm5	phosphoglucomutase 5	-1.81
Efemp1	epidermal growth factor-containing fibulin-like extracellular matrix protein 1	-1.82
Sulf2	sulfatase 2	-1.82
Sfrp1	secreted frizzled-related protein 1	-1.84
Crip1	cysteine-rich protein 1 (intestinal)	-1.84
Vat1l	vesicle amine transport protein 1 homolog-like (T. californica)	-1.85
Srpx2	sushi-repeat-containing protein, X-linked 2	-2.00
Cd34	CD34 antigen	-2.01
Hspb8	heat shock protein 8	-2.03
Ppargc1a	peroxisome proliferative activated receptor, gamma, coactivator 1 alpha	-2.12
Sorbs2	sorbin and SH3 domain containing 2	-2.13
Ptgs1	prostaglandin-endoperoxide synthase 1	-2.14
Ly6c1	lymphocyte antigen 6 complex, locus C1	-2.21
Mmp3	matrix metallopeptidase 3	-2.28
Stmn2	stathmin-like 2	-2.33
Serping1	serine (or cysteine) peptidase inhibitor, clade G, member 1	-2.33
Ly6a	lymphocyte antigen 6 complex, locus A	-2.37
Rgs4	regulator of G-protein signaling 4	-2.40
Crip2	cysteine rich protein 2	-2.55
Ptn	pleiotrophin	-2.65
Dcn	decorin	-2.72
Atoh8	atonal homolog 8 (Drosophila)	-2.73
Ly6c2	lymphocyte antigen 6 complex, locus C2	-2.80
Gpr50	G-protein-coupled receptor 50	-2.96
Erdr1	erythroid differentiation regulator 1	-3.12
Akr1c18	aldo-keto reductase family 1, member C18	-3.25
Tgfbi	transforming growth factor, beta induced	-3.62

Table 6.6. Genes associated with "cellular growth and proliferation" as defined by Ingenuity Pathway Analysis identified by both microarray and RNA Seq.

Gene Symbol	Description	Fold Change (*Rad51d*-proficient v. *Rad51d*-deficient)
Fcer1g	Fc receptor, IgE, high affinity I, gamma polypeptide	1.95
Csf1r	colony stimulating factor 1 receptor	1.72
Adm	adrenomedullin	1.72
Itgam	integrin alpha M	1.71
Serpine1	serine (or cysteine) peptidase inhibitor, clade E, member 1	1.60
Plac8	placenta-specific 8	1.58
Tyrobp	TYRO protein tyrosine kinase binding protein	1.52
Rarb	retinoic acid receptor, beta	-1.51
Grem1	gremlin 1	-1.56
Lims2	LIM and senescent cell antigen like domains 2	-1.60
Nupr1	nuclear protein transcription regulator 1	-1.67
Sfrp1	secreted frizzled-related protein 1	-1.84
Clu	clusterin	-2.00
Ppargc1a	peroxisome proliferative activated receptor, gamma, coactivator 1 alpha	-2.12
Ptgs1	prostaglandin-endoperoxide synthase 1	-2.14
Ptn	pleiotrophin	-2.65
Dcn	decorin	-2.72

Table 6.7. Cell cycle progression genes identified by microarray and RNA Seq analysis. Genes are listed by decreasing fold change according to microarray analysis.

Gene Symbol	Description	Fold Change (*Rad51d*-proficient v. *Rad51d*-deficient)
Rad51d	RAD51 homolog D	2.66
Csf1r	colony stimulating factor 1 receptor	1.72
Adm	adrenomedullin	1.72
Rarb	retinoic acid receptor, beta	-1.51
Ptx3	pentraxin related gene	-1.54
Nupr1	nuclear protein transcription regulator 1	-1.67

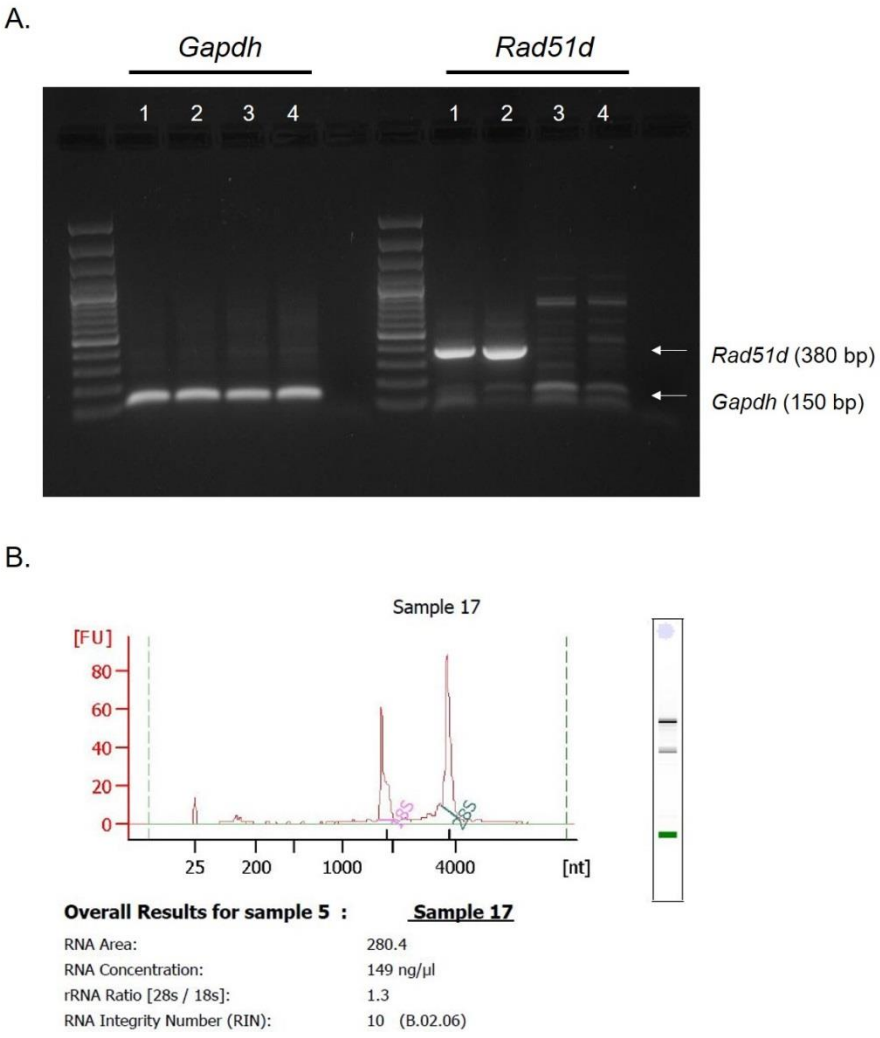

Figure 6.1. *Rad51d* expression and RNA quality assessment. (A) *Rad51d* expression was confirmed by RT-PCR. Amplification of a 380 bp gene product indicates the presence and expression of the *Rad51d* gene. Lanes 1 and 2 are *Rad51d*-proficient, and lanes 3 and 4 are *Rad51d*-deficient MEFs. Amplification of *Gapdh* was used as a control. (B) Representative read-out of RNA Quality Assessment of one sample using an Agilent 2100 Bioanalyzer and determination of RNA Integrity Number (RIN).

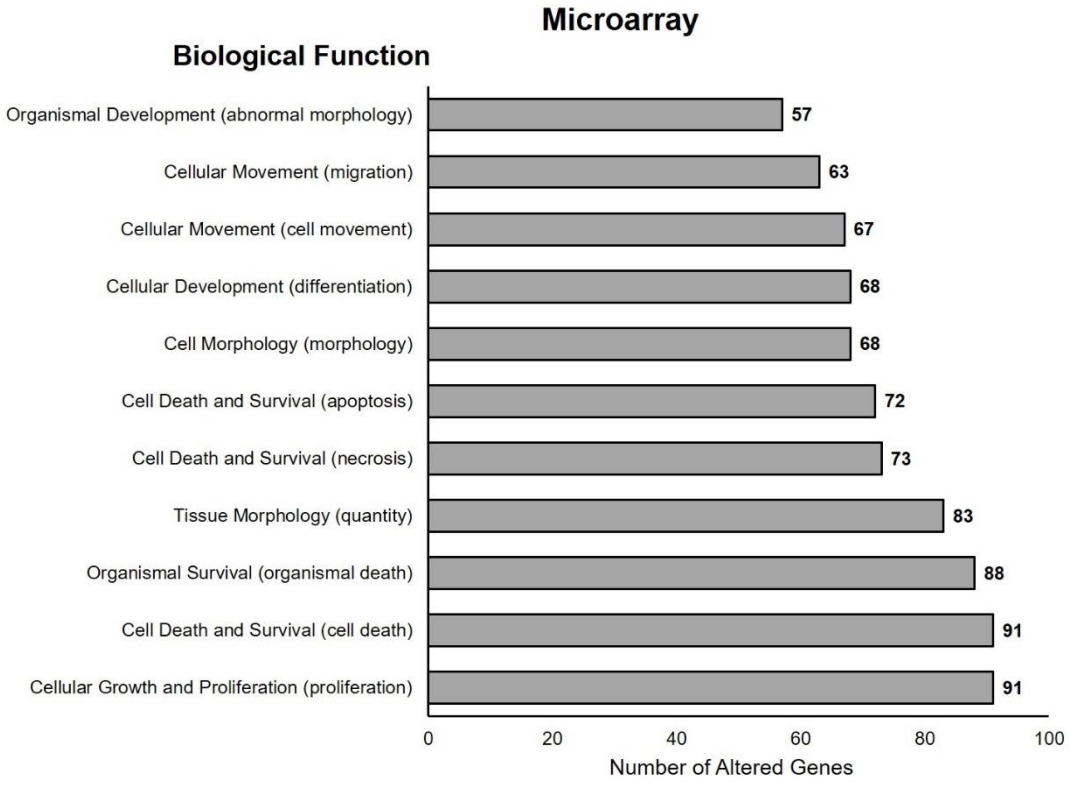

Figure 6.2. Biological functions as identified by Ingenuity Pathway Analysis (IPA) for the microarray data set. Genes with differential expression between *Rad51d*-proficient and *Rad51d*-deficient cells were categorized using IPA. The categories are defined based on the Ingenuity Knowledge Base that integrates bioinformatics data with literature. Parentheses indicate the specific cellular function associated with the genes in each category. Eleven categories with the most number of genes are displayed.

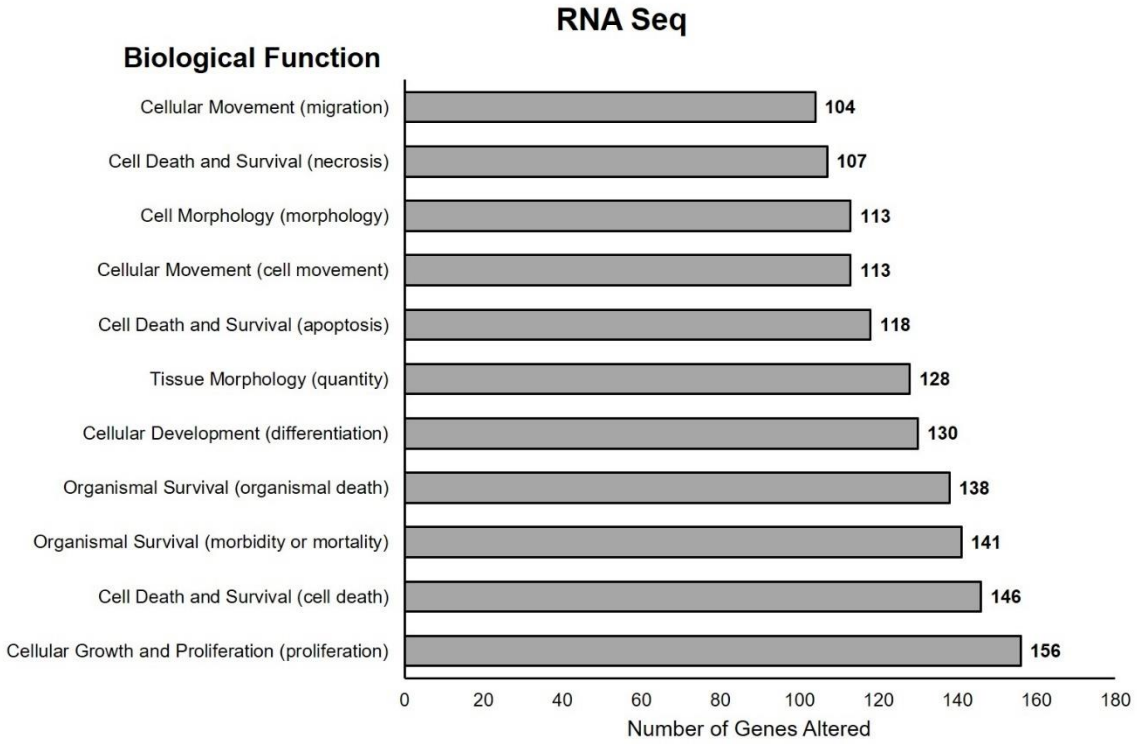

Figure 6.3. Biological functions as identified by Ingenuity Pathway Analysis (IPA) for the RNA Seq data set. Genes with differential expression between *Rad51d*-proficient and *Rad51d*-deficient cells were categorized using IPA. The categories are defined based on Ingenuity Knowledge Base that integrates bioinformatics data with literature. Parentheses indicate the specific cellular function associated with the genes in each category. Eleven categories with the most number of genes are displayed.

CHAPTER 7

DISCUSSION

Ovarian cancer is the deadliest of the five main types of gynecological cancer and leads to over 14,000 deaths per year in the United States (American Cancer Society, 2017). One characteristic of ovarian cancer is genome instability associated with mutations in DNA repair genes (Wang et al. 2012). In 2012 when these projects were initiated, there were three known ovarian cancer susceptibility genes: *BRCA1*, *BRCA2*, and the newly identified *RAD51D*. The two BRCA genes were also associated with an increased risk for breast cancer, but *RAD51D* was only recently confirmed as a breast cancer susceptibility gene (Kraus et al. 2017). Mutations in other DNA repair genes were also more recently associated with breast and ovarian cancers, including RAD51C (Coulet et al. 2013; Loveday et al. 2011; Pelttari et al. 2011; Thompson et al. 2012).

The data presented in this dissertation elucidate mechanisms by which RAD51D functions to maintain genome integrity. In Chapter 3, I presented data that were published in the research article entitled "RNF138 interacts with RAD51D and is required for DNA interstrand crosslink repair." This work identified a direct interaction between RAD51D and the novel E3 ubiquitin ligase RNF138 and demonstrated that the regions encoded by exons 5 and 7 along RNF138 are required for this interaction. In Chapter 4, I demonstrated that expression of two RAD51D missense mutations – K235R and K298R – confer cellular sensitivity to mitomycin C (MMC) in *Rad51d*-deficient mouse embryonic fibroblast (MEFs). Arginine substitution at these residues increased RAD51D

stability, suggesting that these residues are sites of ubiquitin modifications that target RAD51D for proteasomal degradation. Neither K235 nor K298 was required for homology directed repair of *Sce*I induced double strand breaks, suggesting that these residues are required for RAD51D function specifically in response to crosslinks. In Chapter 5, I investigated how RAD51D protects the telomeres specifically in the presence of the DNA damaging agent 6-thioguanine (6TG). γ-H2AX foci were detected at the telomere regions more frequently in *Rad51d*-deficient compared with *Rad51d*-proficient MEFs, and a higher frequency of 6TG-induced chromosome fusions were observed in *Rad51d*-deficient MEFs. In Chapter 6, gene expression profiles between *Rad51d*-proficient and -deficient MEFs were analyzed by microarray and RNA Seq. Ninety-one genes associated with "cell growth and proliferation" were differentially expressed in the *Rad51d*-deficient cells compared with the *Rad51d*-proficient cells. Further sorting of the data identified 21 genes that were associated specifically with "cell cycle progression."

Identification of lysine residues that confer sensitivity to thiopurine damage

The complementation assays presented in Chapter 4 provide evidence that K235 and K298 along RAD51D promote HR-mediated repair of ICLs. I also investigated the function of RAD51D in response to 6TG induced damage, based on previous work demonstrating that *Rad51d*-deficient cells are more sensitive to 6TG treatment (Rajesh, Litvinchuk, et al. 2011). Follow-up experiments should include performing the complementation assays in the presence of 6TG to identify lysine residues along RAD51D necessary for function in response to these types of damage. I expect that

expression of K235R, but not K113R or K298R, in *Rad51d*-deficient MEFs will restore cellular resistance in the presence of 6TG.

Lysine residues along RAD51D mediate interaction with RAD51C and XRCC2

I hypothesized that increased MMC sensitivity in the presence of the K235R and K298R variants was due to disruption of the BCDX2 complex. As discussed in Chapter 2, the five RAD51 paralogs – RAD51B, RAD51C, RAD51D, XRCC2, and XRCC3 – form two distinct complexes in mammalian cells, and RAD51D specifically interacts with RAD51C and XRCC2 (Masson et al. 2001). Yeast-two-hybrid (Y2H) analysis was performed to determine if any of the variants fail to interact with either RAD51C or XRCC2. Arginine substitution at K235 and K298 did not affect interaction with RAD51C and XRCC2, suggesting that the BCDX2 complex is formed even in the absence of these residues. K201R did not interact with XRCC2 but possibly maintains interaction with RAD51C, and K261R interacted with RAD51C but not with XRCC2. These data offer insight into specific residues along RAD51D that mediate the interactions with other paralogs that has not previously been reported (Figure 7.1). Validation by co-immunoprecipitation methods in mammalian cells is necessary.

Interestingly, these data present a conundrum. Y2H data suggest the BCDX2 complex is not formed in the presence of K261R, however, cellular resistance to MMC was decreased by 30%, but not eliminated, when K261R was expressed in *Rad51d*-deficient MEFs. The data suggest that disruption of the interaction between RAD51D and XRCC2 is sufficient to decrease HR-mediated repair of ICLs, but not to fully eliminate repair. Therefore, these data are hinting towards a potential separation of function and suggest an alternative complex might form during HR-mediated repair of ICLs.

The RAD51 paralogs have approximately 30% identity between them, and only three lysine residues are conserved between RAD51D and other proteins in the BCDX2 complex: K201 and K235 are conserved with RAD51B, and K298 is conserved with RAD51C. To further elucidate the function of each paralog within this complex, arginine substitutions in RAD51B and RAD51C at these positions can be introduced. Complementation assays using *Rad51b*- and *Rad51c*-deficient cells can be performed to determine if these conserved residues are required for cellular resistance to DNA damaging agents, and Y2H analysis would determine if these residues mediate interaction between the paralogs.

Lysine residues are not required for repair of Sce-I induced double strand breaks

Data in Chapter 4 present evidence that HR activity is similar in the presence of over-expressed K0, K235R, and K298R compared with wild-type (Figure 4.9B), suggesting that lysine residues along RAD51D are not required for HR-mediated repair of double strand breaks (DSBs). K261R and K201R had decreased interaction with XRCC2 but not with RAD51C, and complemented *Rad51d*-deficiency in the presence of MMC. Follow-up experiments should include these variants to confirm that HR-activity is not affected in the presence of these mutant proteins. I propose that arginine substitution at these residues leads to formation of a new RAD51 paralog complex comprised of RAD51B-RAD51C-RAD51D (BCD) (Figure 7.1E). Exclusion of XRCC2 from this complex is predicted to diminish the activity of the paralogs during crosslink repair but may not be necessary for HR-mediated repair of DSBs. I would hypothesize that the activity of the BCD complex will be sufficient to repair *Sce*I-induced DSBs.

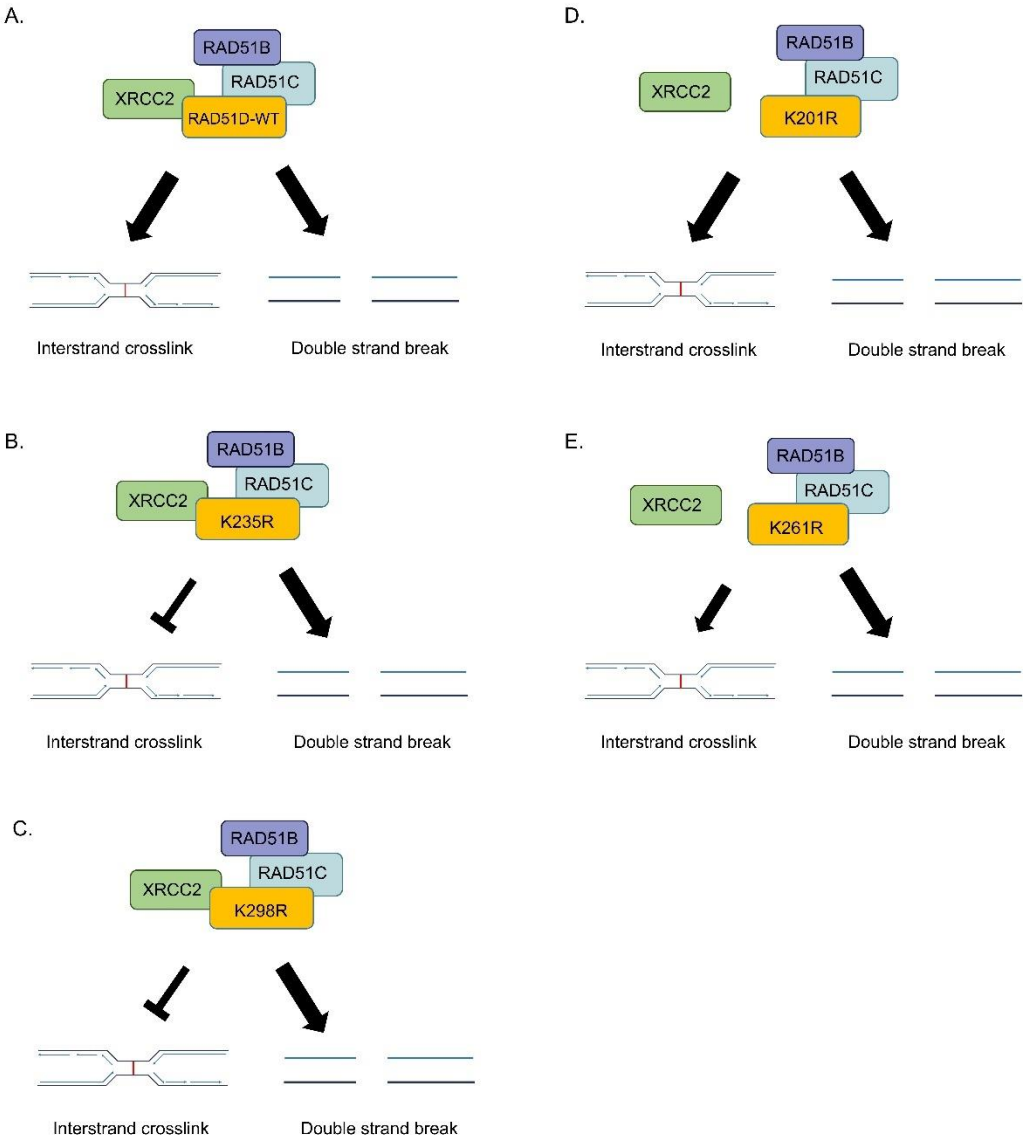

Figure 7.1 Proposed RAD51 paralog complexes that function in response to interstrand crosslinks and double strand breaks. (A) RAD51D wild-type interacts with RAD51C and XRCC2 to form the BCDX2 complex that functions during homologous recombination-mediated repair of interstrand crosslinks and double strand breaks. (B) RAD51D-K235R interacts with RAD51C and XRCC2. Repair of interstrand crosslinks is inhibited, and repair of double strand breaks is decreased (indicated by the small arrow). (C) RAD51D-K298R interacts with RAD51C and XRCC2 repair of interstrand crosslinks is inhibited, and repair of double strand breaks is inhibited. (D) RAD51D-K201R does not interact with either RAD51C or XRCC2 and still functions to repair interstrand crosslinks. I propose that double strand breaks will not be repaired in the presence of this variant. (E) RAD51D-K261R does not interact with XRCC2 but does interact with RAD51C to form a BCD complex. I propose that repair of double strand breaks will not occur in the presence of this variant.

Lysine combinations that restore RAD51D function

Lysine residues can be reintroduced along K0 in different combinations to further elucidate the function of these residues during DNA repair. Site-directed mutagenesis should be performed to reintroduce K113 (RAD51D-SingleK113), K235 (RAD51D-SingleK235), and K298 (RAD51D-SingleK298) into K0. A second lysine residue can be reintroduced in each SingleK mutant in the following combinations: K113 and K235 (RAD51D-DoubleK113235), K113 and K298 (RAD51D-DoubleK113298), and K235 and K298 (RAD51D-DoubleK235298). Finally, a RAD51D-TripleK can be generated by re-introducing K113 in RAD51D-DoubleK235298. Complementation assays using the newly generated lysine combination mutants can be performed in *Rad51d*-deficient MEFs as described in Chapter 4. It is predicted that none of the SingleK or DoubleK mutants will restore cellular resistance to MMC since each of them retains arginine substitution at one or more essential lysine residue. Complementation with the TripleK in the presence of MMC is predicted to restore cellular sensitivity to MMC. These data would indicate that only K113, K235, and K298 are required for RAD51D function during ICL repair.

I also investigated ubiquitination along RAD51D as a regulatory mechanism of RAD51D. This post-translational modification (PTM) occurs along substrate proteins at lysine residues and at the N-terminus (Akutsu, Dikic, and Bremm 2016). RAD51D is ubiquitinated by the E3 ligase RNF138 (Yard et al. 2016), and K235 and K298 are potential ubiquitination sites. Lysine residue(s) targeted with the proteasome specific ubiquitin modification can be identified by measuring the stability of each RAD51D-SingleK and -DoubleK variant. I propose that K235 and K298 along RAD51D are the

only sites of K48 chain addition along RAD51D. It is predicted that the stability of SingleK235 will be similar to K298R, and SingleK298 stability will be consistent with K235R. I expect that stability of RAD51D-DoubleK235298 will be consistent with wild-type, further demonstrating that K48 chains are attached at these residues (Figure 7.2). Arginine substitution at both K235 and K298 was introduced to generate a RAD51D-DoubleR235298 construct. If these two residues are the only sites of K48 ubiquitin chain addition, one would predict that proteasomal degradation of the DoubleR235298 protein would be inhibited and protein stability would increase (Figure 7.2D).

Ubiquitin modification occurs along surface lysine residues rather than within a consensus sequence. In the absence of either K235 or K298, another residue may be modified. *In vivo* ubiquitination assays can be performed using each Myc-tagged SingleK113, SingleK235, SingleK298, DoubleK113235, DoubleK113298, DoubleK235298, or TripleK113235298 RAD51D constructs and HA-tagged ubiquitin to identify modification sites along each protein. It is expected that the ubiquitin pattern along RAD51D-SingleK113 will resemble K0, SingleK235 will be consistent with K298R, and SingleK298 will be similar to K235R. I hypothesize that ubiquitin signal along the RAD51D-DoubleK235298 will be stronger than SingleK235, SingleK298, and K0. These data will indicate that both residues are modified with separate ubiquitin chains. I hypothesize that K113 is not ubiquitinated, therefore, it is expected that RAD51D-DoubleK113235 and RAD51D-DoubleK113298 will have the same ubiquitin signal as the SingleK mutants. Furthermore, data presented in Chapter 4 suggests that a 3-ubiquitin modification is absent along the K0 compared with wild-type, K235R, and

K298R proteins. I predict that these experiments will identify the lysine residue(s) that are modified with this specific ubiquitin chain.

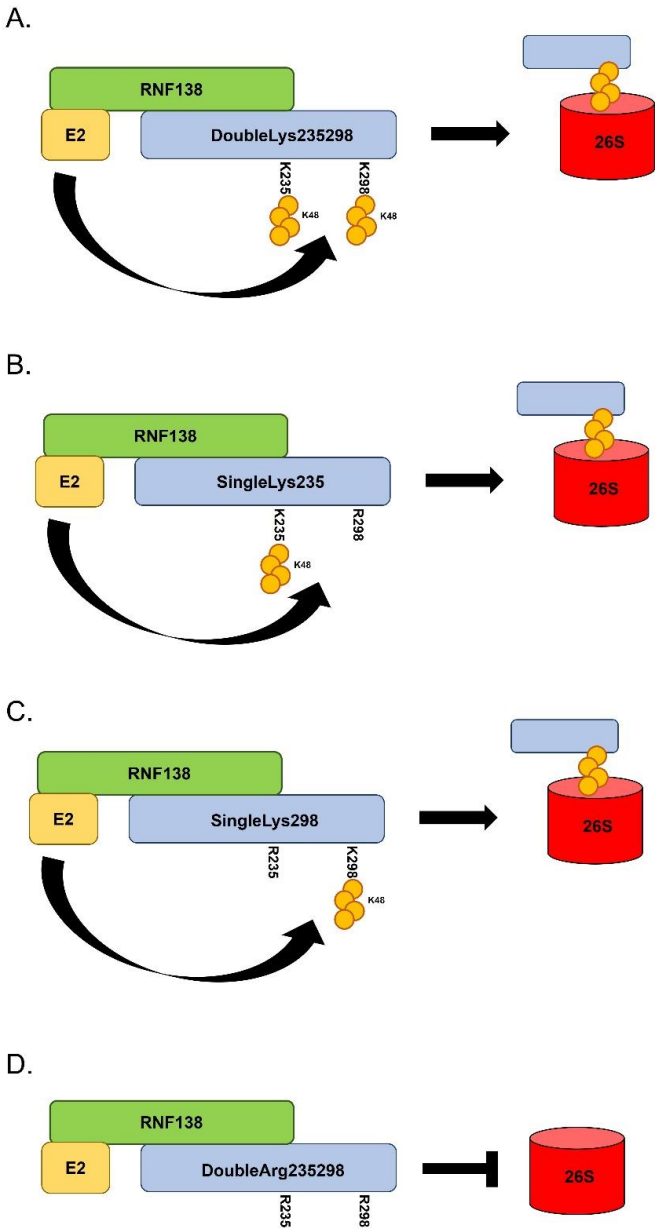

Figure 7.2. Stability of RAD51D protein variants. (A) RAD51D wild-type is modified with proteasomal specific (K48) ubiquitin chains at K235 and K298 and is degraded by the 26S proteasome. (B) SingleK235 is modified with a K48 chain at K235 and the protein is degraded. (C) SingleK298 is modified with K48 chain at K298 and the protein is degraded. (D) Arginine substitution at both K235 and K298 (DoubleR235298) eliminates the addition of K48 ubiquitin chain and inhibits proteasomal degradation of RAD51D.

Post-translational modifications along RAD51D by mass spectrometry

Of the 20 amino acids, lysine is modified with the highest number of possible PTMs (Zee and Garcia 2012). One method for identifying ubiquitinated residues along a protein is tandem mass spectrometry (MS/MS) (Calderon-Celis, Encinar, and Sanz-Medel 2017). I propose that MS/MS analysis be performed on K0, K235R, and K298R to identify alternative modifications that occur in the absence of one or more lysine residues. Analysis of these RAD51D variants will confirm loss of a specific modification when a lysine residue is substituted with an arginine. Protein stability experiments demonstrated that K235R and K298R are more stable than wild-type, suggesting that a degradation specific ubiquitin modification has been lost. It is predicted that MS/MS analysis will identify a ubiquitin molecule attached to each of these lysine residues in the wild-type protein.

To perform these experiments, RAD51D constructs can be expressed in mammalian cells, isolated by co-immunoprecipitation, trypsin digested, and analyzed using MS/MS. The trypsin digestion will cleave the isopeptide bond along a protein after lysine residues, producing protein fragments that have only a single lysine residue. When a ubiquitinated fragment is digested, a portion of the ubiquitin molecule remains on the residue, producing two β and γ ions for that fragment rather than one produced by an unmodified peptide. Thus, the fragmentation pattern of RAD51D can be used to identify lysine residues that have a ubiquitin molecule attached. MS/MS analysis of RAD51D wild-type will identify lysine residues along the protein that are modified with ubiquitin. I hypothesize that K235 and K298 will be modified with a ubiquitin molecule.

One limitation of MS/MS is that it cannot identify the chain type that is attached to a specific residue. To identify specific chains attached to lysine residues, *in vitro* ubiquitination assays could be performed. Myc-tagged RAD51D can be incubated with ubiquitin mutants that have only a single lysine residue available for chain elongation. RAD51D can be immunoprecipitated and analyzed by MS/MS. RAD51D is targeted for degradation by the proteasome and is ubiquitinated with K48 specific chain linkages, therefore, I expect one lysine residue along wild-type RAD51D to be modified with a K48 ubiquitin molecule. To further elucidate the dynamics of this modification, K0, K235R, and K298R can also be analyzed to determine if the K48 ubiquitin is added to an alternative lysine residue in the absence of either K235 or K298. Additionally, it will be interesting to test the K113R variant to determine if loss of ATPase activity affects the proteasomal specific ubiquitin modification.

Ubiquitination is not the only PTM that can occur at lysine residues along a protein. Other modifications include SUMOylation, acetylation, and glycosylation, and can be identified by MS/MS analysis (Zee and Garcia 2012). K261 along RAD51D is predicted to be acetylated (Mertins et al. 2013). The data presented in Chapter 4 demonstrated that K261R decreases cellular resistance to MMC by 30% and disrupts RAD51D interaction with XRCC2. K261 can be substituted with glutamine to generate a K261Q mutant that will mimic acetylation at this residue (Kamieniarz and Schneider 2009) and can be tested in the complementation assay. These data will determine if acetylation at this residue is required for cellular resistance to MMC.

Identification of E2 ligases that interact with RNF138 to ubiquitinate RAD51D

In addition to being modified by K48-linked chains and targeted for proteasomal degradation, RAD51D is also modified with other chain linkage types (Figure 4.7C). The E2 enzymes that interact with RNF138 to promote these alternative linkage arrangements remain unknown and performing a screen of E2 enzymes will provide further information into RAD51D ubiquitination. A screen performed in the laboratory of Stephen Jackson identified the UBE2D E2 enzyme as directly interacting with RNF138 (Schmidt et al. 2015). The UBE2D family of E2 conjugating enzymes promotes several ubiquitin linkages along target proteins. For example, UBE2N catalyzes the addition of K63-linked ubiquitin chains to promote DNA repair (Sato et al. 2012). The yeast-two-hybrid (Y2H) screen that identified RNF138, also identified UBE2N/UBC13 as a direct interacting protein with RAD51D (Yard 2011), and I hypothesize that this E2 promotes K63-linkages along RAD51D, which could be tested in future studies.

K235 and K298 requirement for RAD51 and BRCA1 localization sites of damage

Data presented in Chapter 4 demonstrated that loss of *Rad51d* decreases RAD51 foci formation in the presence of MMC. It is predicted that K235 and K298 fail to complement *Rad51d*-deficiency in the presence of MMC because they are required for RAD51 recruitment to the site of damage, and disruption of RAD51 localization prevents HR progression. To test this hypothesis, K235R and K298R can be expressed in *Rad51d*-deficient MEFs and RAD51 foci can be detected by immunofluorescence 24 h, 48 h, and 72 h after MMC treatment. It is expected that cells expressing K235R and K298R will have less RAD51 foci positive nuclei compared with cells expressing wild-type RAD51D. These experiments will determine if each lysine is required specifically for

RAD51 recruitment to damage sites. K113R can be included in these experiments to determine if the ATPase activity of RAD51D mediates RAD51 recruitment in response to ICLs.

In addition to the BCDX2 complex, other proteins function during HR to recruit RAD51 to damage. In response to DNA crosslinks, BRCA1 is required for RAD51 recruitment to damage (Bhattacharyya et al. 2000), and it is hypothesized that the BCDX2 complex functions upstream of BRCA1. To investigate this, BRCA1 foci formation after MMC treatment can be detected in *Rad51d*-deficient and -proficient MEFs. It is expected that the number of BRCA1 positive nuclei will be higher in *Rad51d*-proficient MEFs compared with *Rad51d*-deficient MEFs when challenged with MMC. K235R and K298R can be expressed in *Rad51d*-deficient MEFs treated with MMC and BRCA1 foci can be detected. These experiments will determine if K235 or Ly298 specifically mediate BRCA1 localization in the presence of interstrand crosslinks.

Generating K235R and K298R substitutions in RAD51D using CRISPR-Cas9

Within the past 5 years, a new scientific tool – known as CRISPR (clustered regularly interspaced short palindromic repeats) – has become available that allows for mutations to be introduced in genome of a cell (Cong et al. 2013). This technology uses an endonuclease, Cas9, to generate nicks in DNA strands at a specific locus. Briefly, eukaryotic cells are transfected with a plasmid encoding the Cas9 enzyme and a short guide RNA (sgRNA) complementary to a sequence along the genome is targeted. The sgRNA localizes the Cas9 enzyme where it generates a nick in the DNA and introduces the desired point mutations within a gene. Mutations can now be introduced into a locus without generating a nick in the DNA strand using a catalytically inactive Cas9 (Gaudelli

et al. 2017). For applications in my work, CRISPR can be used to introduce arginine substitution at the codons along RAD51D for K113 (MEF-RAD51DK113R), K235 (MEF-RAD51DK235R), K298 (MEF-RAD51DK298R), and all lysines (MEF-RAD51DK0) in the *Rad51d* gene of *Rad51d*-proficient MEFs. As a positive control cell line, arginine substitution can be introduced at Lys159 (MEF-K159R) along RAD51D; this residue is non-conserved between *Mus musculus* and *Homo sapiens* and is predicted to be non-essential for RAD51D function.

First, cell survival assays in the presence of DNA damaging agents, such as MMC and 6TG, could be performed in these newly generated cell lines. Second, to identify lysine residue(s) required for RAD51 recruitment, each cell line could be challenged with MMC and IR, and foci formation detected as described in Chapter 4. My hypothesis is that RAD51 foci will only form in the MEF-K159R cell line, and not in the other mutant cell lines. Loss of RAD51 foci in the MEF-K113R cell lines will indicate that ATPase activity of RAD51D is necessary for RAD51 recruitment. Each lysine mutant cell line can be challenged with 6TG and telomere stability can be measured as described in Chapter 5. I hypothesize that MEFs expressing K0 and K113R will have telomeric defects, such as fusions, the presence of 6TG. These data would determine if ATPase activity of RAD51D is necessary for its activity in maintaining telomere integrity.

Investigations into RNF138 mediated interstrand crosslink repair

Most of the work presented in this dissertation has focused on lysine residues along RAD51D that are required for cellular resistance to DNA damaging agents, and on detecting ubiquitination of RAD51D, a PTM mediated by the E3 ligase RNF138. The Pittman laboratory and two other groups have demonstrated that RNF138 promotes HR-

mediated repair of ICLs and DSBS, and further investigations into RNF138 will provide insight into how it functions during DNA damage repair. RNF138 contains a really interesting new gene (RING) catalytic domain, three zinc finger (ZF) motifs, and a ubiquitin interacting motif (UIM). Mutations in the RING domain decrease RAD51D ubiquitination and increase its stability (Yard et al. 2016), and deletion of the ZFs inhibits RNF138-mediated ubiquitination of Ku80 (Ismail et al. 2015).

To date, no investigations into the UIM of RNF138 have been reported. This motif is characterized by a 20-amino acid protein sequence: X-**Ac**-**Ac**-**Ac**-**Ac**-ϕ-X-X-**Ala**-X-X-X-**Ser**-X-X-**Ac**-X-*X*-X-X, where ϕ represents a hydrophobic residue, **Ac** represents an acidic residue, and X represents non-conserved residues (Fisher et al. 2003; Hofmann and Falquet 2001). UIMs bind mono-ubiquitin modifications along proteins (Fisher et al. 2003; Woelk et al. 2006), a function important for E3 ligase activity. For example, mutations in the UIM domains of BRCA1/RAP80 prevent its binding to K63-linked chains generated by RNF168 and inhibits HR progression (Kim, Chen, and Yu 2007). I propose that the UIM along RNF138 has a similar function and is required for RNF318 interaction with the CtIP endonuclease. Site-directed mutagenesis can be performed to introduce amino acid substitutions at Ala236 and Ser240 in the UIM of RNF138. Immunoprecipitation experiments can be performed to determine if RNF138 UIM mutants fail to interact with CtIP. To determine if the UIM is required for cellular resistance to interstrand crosslinks, each UIM mutant can be expressed in MEFs that do not express endogenous RNF138 in the presence of MMC. Together, these data will determine 1. if the UIM along RNF138 mediates its interaction with CtIP, and 2. if this motif is required for crosslink repair.

Proposed model of RAD51D ubiquitination during interstrand crosslink repair

In this dissertation, I described work towards understanding mechanisms of RAD51D that promote genomic stability. These studies identified two lysine residues – Lys 235 and K298 – along RAD51D required for cellular resistance to MMC and demonstrated that the protein is stabilized when a mutation occurs at these positions. From the data collected, I propose that RAD51D ubiquitination is essential for recruitment of RAD51 to the double strand break during homologous recombination-mediated repair of interstrand crosslinks (Figure 7.3).

As described in Chapter 2, the interstrand crosslink (ICL) is first bound by the Fanconi Anemia (FA) core complex (Figure 2.6). The FANCD2/FANCI heterodimer initiates excision of the crosslink from the top DNA strands, and nucleotide excision repair and translesion synthesis proteins facilitate removal of the lesion. Following activity of FANCD2/FANCI, the CtIP endonuclease is recruited to the newly generated double strand break (DSB). Studies performed in the laboratory of Stephen Jackson identified a direct interaction between RNF138 and the CtIP exonuclease in response to IR (Schmidt et al. 2015), and I propose that this interaction occurs during ICL repair (Figure 7.3). Localization of RNF138 to the DSB promotes recruitment of the BCDX2 complex through the RNF138/RAD51D interaction. I hypothesize that RNF138 generates K63-linked ubiquitin chains along RAD51D as a mechanism to recruit the BRCA1/RAP80 complex and RAD51 to the damage site. Following RAD51 localization, I propose that RAD51D is ubiquitinated at K235 and K298 to target the protein for proteasomal degradation, effectively removing the BCDX2 complex from the DNA. In the presence of K235R or K298R, RAD51D will not be targeted for degradation and

RAD51 loading will be inhibited. Clearing the BCDX2 complex for the break will allow RAD51 to bind the single strand overhang generated by CtIP, and to facilitate the homology search using the second DNA double helix as a template.

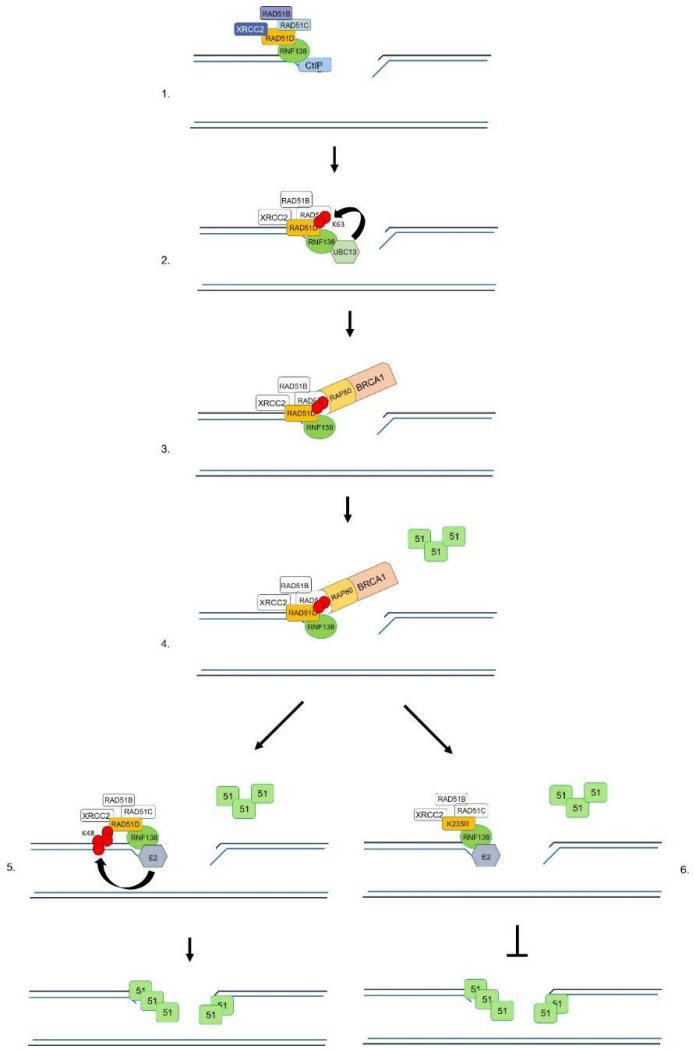

Figure 7.3. Proposed model of RAD51D ubiquitination during DNA interstrand crosslink repair. (1) Following activity of FA, NER, and TLS proteins, RNF138 binds to CtIP and, the BCDX2 complex is localized to the DSB through the interaction between RAD51D and RNF138. (2) RAD51D is ubiquitinated by RNF138/UBC13 with K63 linked ubiquitin. (3) The RAP80 subunit of the BRCA1/RAP80 complex binds the ubiquitin chain along RAD51D to recruit the complex to the damage. (4) Following BRCA1 localization, RAD51 is recruited to the DSB. (5) RNF138 promotes K48 linked ubiquitin chain formation along wild-type RAD51D to target the protein to the proteasome. This degradation is a mechanism of removing the BCDX2 complex from the damage site.

RAD51 filaments coat the single strand overhang to prepare for homology search and strand invasion. (6) Arginine substitution at K235 (K235R) or K298 (not shown) prevents ubiquitination of RAD51D, preventing the BCDX2 complex from being cleared from the break and inhibiting RAD51-mediated homology search.

REFERENCES

Abbas, T., and A. Dutta. 2009. 'p21 in cancer: intricate networks and multiple activities', *Nat Rev Cancer*, 9: 400-14.

Adam, J., B. Deans, and J. Thacker. 2007. 'A role for Xrcc2 in the early stages of mouse development', *DNA Repair (Amst)*, 6: 224-34.

Akutsu, M., I. Dikic, and A. Bremm. 2016. 'Ubiquitin chain diversity at a glance', *J Cell Sci*, 129: 875-80.

Alligand, B., M. Le Breton, D. Marquis, F. Vallette, and F. Fleury. 2017. 'Functional effects of diphosphomimetic mutations at cAbl-mediated phosphorylation sites on Rad51 recombinase activity', *Biochimie*.

Alpi, A. F., P. E. Pace, M. M. Babu, and K. J. Patel. 2008. 'Mechanistic insight into site-restricted monoubiquitination of FANCD2 by Ube2t, FANCL, and FANCI', *Mol Cell*, 32: 767-77.

Andreassen, P. R., and K. Ren. 2009. 'Fanconi anemia proteins, DNA interstrand crosslink repair pathways, and cancer therapy', *Curr Cancer Drug Targets*, 9: 101-17.

Antoniou, A. C., O. M. Sinilnikova, J. Simard, M. Leone, M. Dumont, S. L. Neuhausen, J. P. Struewing, D. Stoppa-Lyonnet, L. Barjhoux, D. J. Hughes, I. Coupier, M. Belotti, C. Lasset, V. Bonadona, Y. J. Bignon, T. R. Rebbeck, T. Wagner, H. T. Lynch, S. M. Domchek, K. L. Nathanson, J. E. Garber, J. Weitzel, S. A. Narod, G. Tomlinson, O. I. Olopade, A. Godwin, C. Isaacs, A. Jakubowska, J. Lubinski, J. Gronwald, B. Gorski, T. Byrski, T. Huzarski, S. Peock, M. Cook, C. Baynes, A. Murray, M. Rogers, P. A. Daly, H. Dorkins, R. K. Schmutzler, B. Versmold, C. Engel, A. Meindl, N. Arnold, D. Niederacher, H. Deissler, A. B. Spurdle, X. Chen, N. Waddell, N. Cloonan, T. Kirchhoff, K. Offit, E. Friedman, B. Kaufmann, Y. Laitman, G. Galore, G. Rennert, F. Lejbkowicz, L. Raskin, I. L. Andrulis, E. Ilyushik, H. Ozcelik, P. Devilee, M. P. Vreeswijk, M. H. Greene, S. A. Prindiville, A. Osorio, J. Benitez, M. Zikan, C. I. Szabo, O. Kilpivaara, H. Nevanlinna, U. Hamann, F. Durocher, A. Arason, F. J. Couch, D. F. Easton, and G. Chenevix-Trench. 2007. 'RAD51 135G-->C modifies breast cancer risk among BRCA2 mutation carriers: results from a combined analysis of 19 studies', *Am J Hum Genet*, 81: 1186-200.

Armstrong, M. J., and S. M. Galloway. 1997. 'Mismatch repair provokes chromosome aberrations in hamster cells treated with methylating agents or 6-thioguanine, but not with ethylating agents', *Mutat Res*, 373: 167-78.

Arnaudeau, C., C. Lundin, and T. Helleday. 2001. 'DNA double-strand breaks associated with replication forks are predominantly repaired by homologous recombination involving an exchange mechanism in mammalian cells', *J Mol Biol*, 307: 1235-45.

Badie, S., C. Liao, M. Thanasoula, P. Barber, M. A. Hill, and M. Tarsounas. 2009. 'RAD51C facilitates checkpoint signaling by promoting CHK2 phosphorylation', *J Cell Biol*, 185: 587-600.

Baumann, P., and S. C. West. 1998. 'Role of the human RAD51 protein in homologous recombination and double-stranded-break repair', *Trends Biochem Sci*, 23: 247-51.

Bell, J. C., and S. C. Kowalczykowski. 2016. 'RecA: Regulation and Mechanism of a Molecular Search Engine', *Trends Biochem Sci*, 41: 491-507.

Benson, F. E., A. Stasiak, and S. C. West. 1994. 'Purification and characterization of the human Rad51 protein, an analogue of E. coli RecA', *Embo j*, 13: 5764-71.

Bernier-Villamor, V., D. A. Sampson, M. J. Matunis, and C. D. Lima. 2002. 'Structural basis for E2-mediated SUMO conjugation revealed by a complex between ubiquitin-conjugating enzyme Ubc9 and RanGAP1', *Cell*, 108: 345-56.

Bhattacharyya, A., U. S. Ear, B. H. Koller, R. R. Weichselbaum, and D. K. Bishop. 2000. 'The breast cancer susceptibility gene BRCA1 is required for subnuclear assembly of Rad51 and survival following treatment with the DNA cross-linking agent cisplatin', *J Biol Chem*, 275: 23899-903.

Bohon, J., and C. R. de los Santos. 2003. 'Structural effect of the anticancer agent 6-thioguanine on duplex DNA', *Nucleic Acids Res*, 31: 1331-8.

———. 2005. 'Effect of 6-thioguanine on the stability of duplex DNA', *Nucleic Acids Res*, 33: 2880-86.

Boudaiffa, B., P. Cloutier, D. Hunting, M. A. Huels, and L. Sanche. 2000. 'Resonant formation of DNA strand breaks by low-energy (3 to 20 eV) electrons', *Science*, 287: 1658-60.

Boveri, T. 2008. 'Concerning the origin of malignant tumours by Theodor Boveri. Translated and annotated by Henry Harris', *J Cell Sci*, 121 Suppl 1: 1-84.

Braybrooke, J. P., K. G. Spink, J. Thacker, and I. D. Hickson. 2000. 'The RAD51 family member, RAD51L3, is a DNA-stimulated ATPase that forms a complex with XRCC2', *J Biol Chem*, 275: 29100-6.

Buermeyer, A.B., C. Wilson-Van Patten, S. M. Baker, and R. M. Liskay. 1999. 'The human MLH1 cDNA complements DNA mismatch repair defects in Mlh1-deficient mouse embryonic fibroblasts', *Cancer Res*, 59: 538-41.

Busch, H., and I. L. Goldknopf. 1981. 'Ubiquitin - protein conjugates', *Mol Cell Biochem*, 40: 173-87.

Buys, S. S., J. F. Sandbach, A. Gammon, G. Patel, J. Kidd, K. L. Brown, L. Sharma, J. Saam, J. Lancaster, and M. B. Daly. 2017. 'A study of over 35,000 women with breast cancer tested with a 25-gene panel of hereditary cancer genes', *Cancer*.

Calderon-Celis, F., J. R. Encinar, and A. Sanz-Medel. 2017. 'Standardization approaches in absolute quantitative proteomics with mass spectrometry', *Mass Spectrom Rev*.

Calo, V., M. Migliavacca, V. Bazan, M. Macaluso, M. Buscemi, N. Gebbia, and A. Russo. 2003. 'STAT proteins: from normal control of cellular events to tumorigenesis', *J Cell Physiol*, 197: 157-68.

Candelli, A., J. T. Holthausen, M. Depken, I. Brouwer, M. A. Franker, M. Marchetti, I. Heller, S. Bernard, E. B. Garcin, M. Modesti, C. Wyman, G. J. Wuite, and E. J. Peterman. 2014. 'Visualization and quantification of nascent RAD51 filament

formation at single-monomer resolution', *Proc Natl Acad Sci U S A*, 111: 15090-5.
Casorelli, I., M. T. Russo, and M. Bignami. 2008. 'Role of mismatch repair and MGMT in response to anticancer therapies', *Anticancer Agents Med Chem*, 8: 368-80.
Castedo, M., J. L. Perfettini, T. Roumier, K. Andreau, R. Medema, and G. Kroemer. 2004. 'Cell death by mitotic catastrophe: a molecular definition', *Oncogene*, 23: 2825-37.
Chau, V., J. W. Tobias, A. Bachmair, D. Marriott, D. J. Ecker, D. K. Gonda, and A. Varshavsky. 1989. 'A multiubiquitin chain is confined to specific lysine in a targeted short-lived protein', *Science*, 243: 1576-83.
Chen, G., S. S. Yuan, W. Liu, Y. Xu, K. Trujillo, B. Song, F. Cong, S. P. Goff, Y. Wu, R. Arlinghaus, D. Baltimore, P. J. Gasser, M. S. Park, P. Sung, and E. Y. Lee. 1999. 'Radiation-induced assembly of Rad51 and Rad52 recombination complex requires ATM and c-Abl', *J Biol Chem*, 274: 12748-52.
Chen, J., N. Villanueva, M. A. Rould, and S. W. Morrical. 2010. 'Insights into the mechanism of Rad51 recombinase from the structure and properties of a filament interface mutant', *Nucleic Acids Res*, 38: 4889-906.
Chen, Y., O. B. Clarke, J. Kim, S. Stowe, Y. K. Kim, Z. Assur, M. Cavalier, R. Godoy-Ruiz, D. C. von Alpen, C. Manzini, W. S. Blaner, J. Frank, L. Quadro, D. J. Weber, L. Shapiro, W. A. Hendrickson, and F. Mancia. 2016. 'Structure of the STRA6 receptor for retinol uptake', *Science*, 353.
Chirnomas, D., T. Taniguchi, M. de la Vega, A. P. Vaidya, M. Vasserman, A. R. Hartman, R. Kennedy, R. Foster, J. Mahoney, M. V. Seiden, and A. D. D'Andrea. 2006. 'Chemosensitization to cisplatin by inhibitors of the Fanconi anemia/BRCA pathway', *Mol Cancer Ther*, 5: 952-61.
Chun, J., E. S. Buechelmaier, and S. N. Powell. 2013. 'Rad51 paralog complexes BCDX2 and CX3 act at different stages in the BRCA1-BRCA2-dependent homologous recombination pathway', *Mol Cell Biol*, 33: 387-95.
Ciccia, A., and S. J. Elledge. 2010. 'The DNA damage response: making it safe to play with knives', *Mol Cell*, 40: 179-204.
Clague, M. J., C. Heride, and S. Urbe. 2015. 'The demographics of the ubiquitin system', *Trends Cell Biol*, 25: 417-26.
Clauson, C., O. D. Scharer, and L. Niedernhofer. 2013. 'Advances in understanding the complex mechanisms of DNA interstrand cross-link repair', *Cold Spring Harb Perspect Biol*, 5: a012732.
Clontech Laboratories, Inc. 2009. *Yeast Protocols Handbook*.
Compton, S. A., S. Ozgur, and J. D. Griffith. 2010. 'Ring-shaped Rad51 paralog protein complexes bind Holliday junctions and replication forks as visualized by electron microscopy', *J Biol Chem*, 285: 13349-56.
Cong, L., F. A. Ran, D. Cox, S. Lin, R. Barretto, N. Habib, P. D. Hsu, X. Wu, W. Jiang, L. A. Marraffini, and F. Zhang. 2013. 'Multiplex genome engineering using CRISPR/Cas systems', *Science*, 339: 819-23.
Conway, A. B., T. W. Lynch, Y. Zhang, G. S. Fortin, C. W. Fung, L. S. Symington, and P. A. Rice. 2004. 'Crystal structure of a Rad51 filament', *Nat Struct Mol Biol*, 11: 791-6.

Cook, P. J., B. G. Ju, F. Telese, X. Wang, C. K. Glass, and M. G. Rosenfeld. 2009. 'Tyrosine dephosphorylation of H2AX modulates apoptosis and survival decisions', *Nature*, 458: 591-6.

Coulet, F., A. Fajac, C. Colas, M. Eyries, A. Dion-Miniere, R. Rouzier, S. Uzan, J. P. Lefranc, M. Carbonnel, F. Cornelis, A. Cortez, and F. Soubrier. 2013. 'Germline RAD51C mutations in ovarian cancer susceptibility', *Clin Genet*, 83: 332-6.

Coulthard, S., and L. Hogarth. 2005. 'The thiopurines: An update', *Investigational New Drugs*, 23: 523-32.

Cromm, P. M., and C. M. Crews. 2017. 'The Proteasome in Modern Drug Discovery: Second Life of a Highly Valuable Drug Target', *ACS Cent Sci*, 3: 830-38.

Danilowicz, C., A. Peacock-Villada, J. Vlassakis, A. Facon, E. Feinstein, N. Kleckner, and M. Prentiss. 2014. 'The differential extension in dsDNA bound to Rad51 filaments may play important roles in homology recognition and strand exchange', *Nucleic Acids Res*, 42: 526-33.

Danish, H. H., S. Goyal, N. K. Taunk, H. Wu, M. S. Moran, and B. G. Haffty. 2013. 'Interferon-induced protein with tetratricopeptide repeats 1 (IFIT1) as a prognostic marker for local control in T1-2 N0 breast cancer treated with breast-conserving surgery and radiation therapy (BCS + RT)', *Breast J*, 19: 231-9.

Dasari, S., and P. B. Tchounwou. 2014. 'Cisplatin in cancer therapy: molecular mechanisms of action', *Eur J Pharmacol*, 740: 364-78.

Deans, B., C. S. Griffin, M. Maconochie, and J. Thacker. 2000. 'Xrcc2 is required for genetic stability, embryonic neurogenesis and viability in mice', *Embo j*, 19: 6675-85.

Deans, B., C. S. Griffin, P. O'Regan, M. Jasin, and J. Thacker. 2003. 'Homologous recombination deficiency leads to profound genetic instability in cells derived from Xrcc2-knockout mice', *Cancer Res*, 63: 8181-7.

Depienne, C., D. Bouteiller, A. Meneret, S. Billot, S. Groppa, S. Klebe, F. Charbonnier-Beaupel, J. C. Corvol, J. P. Saraiva, N. Brueggemann, K. Bhatia, M. Cincotta, V. Brochard, C. Flamand-Roze, W. Carpentier, S. Meunier, Y. Marie, M. Gaussen, G. Stevanin, R. Wehrle, M. Vidailhet, C. Klein, I. Dusart, A. Brice, and E. Roze. 2012. 'RAD51 haploinsufficiency causes congenital mirror movements in humans', *Am J Hum Genet*, 90: 301-7.

Depienne, C., M. Cincotta, S. Billot, D. Bouteiller, S. Groppa, V. Brochard, C. Flamand, C. Hubsch, S. Meunier, F. Giovannelli, S. Klebe, J. C. Corvol, M. Vidailhet, A. Brice, and E. Roze. 2011. 'A novel DCC mutation and genetic heterogeneity in congenital mirror movements', *Neurology*, 76: 260-4.

Dodson, G. E., O. Limbo, D. Nieto, and P. Russell. 2010. 'Phosphorylation-regulated binding of Ctp1 to Nbs1 is critical for repair of DNA double-strand breaks', *Cell Cycle*, 9: 1516-22.

Doil, C., N. Mailand, S. Bekker-Jensen, P. Menard, D. H. Larsen, R. Pepperkok, J. Ellenberg, S. Panier, D. Durocher, J. Bartek, J. Lukas, and C. Lukas. 2009. 'RNF168 binds and amplifies ubiquitin conjugates on damaged chromosomes to allow accumulation of repair proteins', *Cell*, 136: 435-46.

Dosanjh, M. K., D. W. Collins, W. Fan, G. G. Lennon, J. S. Albala, Z. Shen, and D. Schild. 1998. 'Isolation and characterization of RAD51C, a new human member of the RAD51 family of related genes', *Nucleic Acids Res*, 26: 1179-84.

Dou, Q. P., and J. A. Zonder. 2014. 'Overview of proteasome inhibitor-based anti-cancer therapies: perspective on bortezomib and second generation proteasome inhibitors versus future generation inhibitors of ubiquitin-proteasome system', *Curr Cancer Drug Targets*, 14: 517-36.

Eifler, K., and A. C. Vertegaal. 2015. 'Mapping the SUMOylated landscape', *Febs j*, 282: 3669-80.

Eoh, K. J., H. S. Park, J. S. Park, S. T. Lee, J. Han, J. Y. Lee, S. W. Kim, S. Kim, Y. T. Kim, and E. J. Nam. 2016. 'Comparison of Clinical Outcomes of BRCA1/2 Pathologic Mutation, Variants of Unknown Significance, or Wild Type Epithelial Ovarian Cancer Patients', *Cancer Res Treat*.

Fisher, R. D., B. Wang, S. L. Alam, D. S. Higginson, H. Robinson, W. I. Sundquist, and C. P. Hill. 2003. 'Structure and ubiquitin binding of the ubiquitin-interacting motif', *J Biol Chem*, 278: 28976-84.

Fragkos, M., and P. Beard. 2011. 'Mitotic catastrophe occurs in the absence of apoptosis in p53-null cells with a defective G1 checkpoint', *PLoS One*, 6: e22946.

Galkin, V. E., F. Esashi, X. Yu, S. Yang, S. C. West, and E. H. Egelman. 2005. 'BRCA2 BRC motifs bind RAD51-DNA filaments', *Proc Natl Acad Sci U S A*, 102: 8537-42.

Gaudelli, N. M., A. C. Komor, H. A. Rees, M. S. Packer, A. H. Badran, D. I. Bryson, and D. R. Liu. 2017. 'Programmable base editing of A*T to G*C in genomic DNA without DNA cleavage', *Nature*, 551: 464-71.

Georgakilas, A. G., O. A. Martin, and W. M. Bonner. 2017. 'p21: A Two-Faced Genome Guardian', *Trends Mol Med*, 23: 310-19.

Giannini, A. L., Y. Gao, and M. J. Bijlmakers. 2008. 'T-cell regulator RNF125/TRAC-1 belongs to a novel family of ubiquitin ligases with zinc fingers and a ubiquitin-binding domain', *Biochem J*, 410: 101-11.

Gibbs-Seymour, I., Y. Oka, E. Rajendra, B. T. Weinert, L. A. Passmore, K. J. Patel, J. V. Olsen, C. Choudhary, S. Bekker-Jensen, and N. Mailand. 2015. 'Ubiquitin-SUMO circuitry controls activated fanconi anemia ID complex dosage in response to DNA damage', *Mol Cell*, 57: 150-64.

Golmard, L., V. Caux-Moncoutier, G. Davy, E. Al Ageeli, B. Poirot, C. Tirapo, D. Michaux, C. Barbaroux, C. D. d'Enghien, A. Nicolas, L. Castera, X. Sastre-Garau, M. H. Stern, C. Houdayer, and D. Stoppa-Lyonnet. 2013. 'Germline mutation in the RAD51B gene confers predisposition to breast cancer', *BMC Cancer*, 13: 484.

Govindarajan, R., J. Duraiyan, K. Kaliyappan, and M. Palanisamy. 2012. 'Microarray and its applications', *J Pharm Bioallied Sci*, 4: S310-2.

Griffin, C. S., P. J. Simpson, C. R. Wilson, and J. Thacker. 2000. 'Mammalian recombination-repair genes XRCC2 and XRCC3 promote correct chromosome segregation', *Nat Cell Biol*, 2: 757-61.

Grosicki, S., A. Barchnicka, A. Jurczyszyn, and A. Grosicka. 2014. 'Bortezomib for the treatment of multiple myeloma', *Expert Rev Hematol*, 7: 173-85.

Gruver, A. M., K. A. Miller, C. Rajesh, P. G. Smiraldo, S. Kaliyaperumal, R. Balder, K. M. Stiles, J. S. Albala, and D. L. Pittman. 2005. 'The ATPase motif in RAD51D is required for resistance to DNA interstrand crosslinking agents and interaction with RAD51C', *Mutagenesis*, 20: 433-40.

Gruver, A. M., B. D. Yard, C. McInnes, C. Rajesh, and D. L. Pittman. 2009. 'Functional characterization and identification of mouse Rad51d splice variants', *BMC Mol Biol*, 10: 27.

Guo, N., and Z. Peng. 2013. 'MG132, a proteasome inhibitor, induces apoptosis in tumor cells', *Asia Pac J Clin Oncol*, 9: 6-11.

Haince, J. F., D. McDonald, A. Rodrigue, U. Dery, J. Y. Masson, M. J. Hendzel, and G. G. Poirier. 2008. 'PARP1-dependent kinetics of recruitment of MRE11 and NBS1 proteins to multiple DNA damage sites', *J Biol Chem*, 283: 1197-208.

Hanahan, D., and R. A. Weinberg. 2000. 'The hallmarks of cancer', *Cell*, 100: 57-70.

———. 2011. 'Hallmarks of cancer: the next generation', *Cell*, 144: 646-74.

Hansford, S., and D. G. Huntsman. 2014. 'Boveri at 100: Theodor Boveri and genetic predisposition to cancer', *J Pathol*, 234: 142-5.

Haynes, B., N. Saadat, B. Myung, and M. P. Shekhar. 2015. 'Crosstalk between translesion synthesis, Fanconi anemia network, and homologous recombination repair pathways in interstrand DNA crosslink repair and development of chemoresistance', *Mutat Res Rev Mutat Res*, 763: 258-66.

Hendriks, I. A., D. Lyon, C. Young, L. J. Jensen, A. C. Vertegaal, and M. L. Nielsen. 2017. 'Site-specific mapping of the human SUMO proteome reveals co-modification with phosphorylation', *Nat Struct Mol Biol*, 24: 325-36.

Hershko, A. 1983. 'Ubiquitin: roles in protein modification and breakdown', *Cell*, 34: 11-2.

Hieda, K. 1994. 'DNA-DAMAGE INDUCED BY VACUUM AND SOFT-X-RAY PHOTONS FROM SYNCHROTRON-RADIATION', *International Journal of Radiation Biology*, 66: 561-67.

Hinz, J. M., R. S. Tebbs, P. F. Wilson, P. B. Nham, E. P. Salazar, H. Nagasawa, S. S. Urbin, J. S. Bedford, and L. H. Thompson. 2006. 'Repression of mutagenesis by Rad51D-mediated homologous recombination', *Nucleic Acids Res*, 34: 1358-68.

Hitchings, G. H., and G. B. Elion. 1954. 'The chemistry and biochemistry of purine analogs', *Ann N Y Acad Sci*, 60: 195-9.

Hodge, C. D., I. H. Ismail, R. A. Edwards, G. L. Hura, A. T. Xiao, J. A. Tainer, M. J. Hendzel, and J. N. Glover. 2016. 'RNF8 E3 Ubiquitin Ligase Stimulates Ubc13 E2 Conjugating Activity That Is Essential for DNA Double Strand Break Signaling and BRCA1 Tumor Suppressor Recruitment', *J Biol Chem*, 291: 9396-410.

Hofmann, K., and L. Falquet. 2001. 'A ubiquitin-interacting motif conserved in components of the proteasomal and lysosomal protein degradation systems', *Trends Biochem Sci*, 26: 347-50.

Holliday, R. 1964. 'THE INDUCTION OF MITOTIC RECOMBINATION BY MITOMYCIN C IN USTILAGO AND SACCHAROMYCES', *Genetics*, 50: 323-35.

Hu, J., J. Luo, and Q. Chen. 2017. 'The Susceptibility Pathogenesis of Moyamoya Disease', *World Neurosurg*, 101: 731-41.

Huang da, W., B. T. Sherman, and R. A. Lempicki. 2009. 'Systematic and integrative analysis of large gene lists using DAVID bioinformatics resources', *Nat Protoc*, 4: 44-57.

Huang, H., L. Zhu, B. R. Reid, G. P. Drobny, and P. B. Hopkins. 1995. 'Solution structure of a cisplatin-induced DNA interstrand cross-link', *Science*, 270: 1842-5.
Huang, J. W., Y. Wang, K. K. Dhillon, P. Calses, E. Villegas, P. S. Mitchell, M. Tewari, C. J. Kemp, and T. Taniguchi. 2013. 'Systematic screen identifies miRNAs that target RAD51 and RAD51D to enhance chemosensitivity', *Mol Cancer Res*, 11: 1564-73.
Huen, M. S., S. M. Sy, and J. Chen. 2010. 'BRCA1 and its toolbox for the maintenance of genome integrity', *Nat Rev Mol Cell Biol*, 11: 138-48.
Ikeda, F., N. Crosetto, and I. Dikic. 2010. 'What determines the specificity and outcomes of ubiquitin signaling?', *Cell*, 143: 677-81.
Inano, S., K. Sato, Y. Katsuki, W. Kobayashi, H. Tanaka, K. Nakajima, S. Nakada, H. Miyoshi, K. Knies, A. Takaori-Kondo, D. Schindler, M. Ishiai, H. Kurumizaka, and M. Takata. 2017. 'RFWD3-Mediated Ubiquitination Promotes Timely Removal of Both RPA and RAD51 from DNA Damage Sites to Facilitate Homologous Recombination', *Mol Cell*, 66: 622-34.e8.
Ismail, I. H., J. P. Gagne, M. M. Genois, H. Strickfaden, D. McDonald, Z. Xu, G. G. Poirier, J. Y. Masson, and M. J. Hendzel. 2015. 'The RNF138 E3 ligase displaces Ku to promote DNA end resection and regulate DNA repair pathway choice', *Nat Cell Biol*, 17: 1446-57.
Issaeva, N., H. D. Thomas, T. Djurenovic, J. E. Jaspers, I. Stoimenov, S. Kyle, N. Pedley, P. Gottipati, R. Zur, K. Sleeth, V. Chatzakos, E. A. Mulligan, C. Lundin, E. Gubanova, A. Kersbergen, A. L. Harris, R. A. Sharma, S. Rottenberg, N. J. Curtin, and T. Helleday. 2010. '6-thioguanine selectively kills BRCA2-defective tumors and overcomes PARP inhibitor resistance', *Cancer Res*, 70: 6268-76.
Iyer, R. R., A. Pluciennik, V. Burdett, and P. L. Modrich. 2006. 'DNA mismatch repair: functions and mechanisms', *Chem Rev*, 106: 302-23.
Jensen, R. B., A. Ozes, T. Kim, A. Estep, and S. C. Kowalczykowski. 2013. 'BRCA2 is epistatic to the RAD51 paralogs in response to DNA damage', *DNA Repair (Amst)*, 12: 306-11.
Jiricny, J. 2006. 'MutLalpha: at the cutting edge of mismatch repair', *Cell*, 126: 239-41.
Jo, U., and H. Kim. 2015. 'Exploiting the Fanconi Anemia Pathway for Targeted Anti-Cancer Therapy', *Mol Cells*, 38: 669-76.
Jogi, A., P. Persson, A. Grynfeld, S. Pahlman, and H. Axelson. 2002. 'Modulation of basic helix-loop-helix transcription complex formation by Id proteins during neuronal differentiation', *J Biol Chem*, 277: 9118-26.
Kadyrov, F. A., L. Dzantiev, N. Constantin, and P. Modrich. 2006. 'Endonucleolytic function of MutLalpha in human mismatch repair', *Cell*, 126: 297-308.
Kamieniarz, K., and R. Schneider. 2009. 'Tools to tackle protein acetylation', *Chem Biol*, 16: 1027-9.
Kane, R. C., P. F. Bross, A. T. Farrell, and R. Pazdur. 2003. 'Velcade: U.S. FDA approval for the treatment of multiple myeloma progressing on prior therapy', *Oncologist*, 8: 508-13.
Karran, P. 2000. 'DNA double strand break repair in mammalian cells', *Curr Opin Genet Dev*, 10: 144-50.
———. 2001. 'Mechanisms of tolerance to DNA damaging therapeutic drugs', *Carcinogenesis*, 22: 1931-7.

———. 2006. 'Thiopurines, DNA damage, DNA repair and therapy-related cancer', *Br Med Bull*, 79-80: 153-70.
Karran, P., and N. Attard. 2008. 'Thiopurines in current medical practice: molecular mechanisms and contributions to therapy-related cancer', *Nat Rev Cancer*, 8: 24-36.
Kawabata, M., T. Kawabata, and M. Nishibori. 2005. 'Role of recA/RAD51 family proteins in mammals', *Acta Med Okayama*, 59: 1-9.
Kim, D., and S. L. Salzberg. 2011. 'TopHat-Fusion: an algorithm for discovery of novel fusion transcripts', *Genome Biol*, 12: R72.
Kim, H., J. Chen, and X. Yu. 2007. 'Ubiquitin-binding protein RAP80 mediates BRCA1-dependent DNA damage response', *Science*, 316: 1202-5.
Kim, H., and A. D. D'Andrea. 2012. 'Regulation of DNA cross-link repair by the Fanconi anemia/BRCA pathway', *Genes Dev*, 26: 1393-408.
Kim, M. Y., T. Zhang, and W. L. Kraus. 2005. 'Poly(ADP-ribosyl)ation by PARP-1: 'PAR-laying' NAD+ into a nuclear signal', *Genes Dev*, 19: 1951-67.
Kim, W., E. J. Bennett, E. L. Huttlin, A. Guo, J. Li, A. Possemato, M. E. Sowa, R. Rad, J. Rush, M. J. Comb, J. W. Harper, and S. P. Gygi. 2011. 'Systematic and quantitative assessment of the ubiquitin-modified proteome', *Mol Cell*, 44: 325-40.
Knecht, H., B. Sawan, D. Lichtensztejn, B. Lemieux, R. J. Wellinger, and S. Mai. 2009. 'The 3D nuclear organization of telomeres marks the transition from Hodgkin to Reed-Sternberg cells', *Leukemia*, 23: 565-73.
Knecht, H., B. Sawan, Z. Lichtensztejn, D. Lichtensztejn, and S. Mai. 2010. '3D Telomere FISH defines LMP1-expressing Reed-Sternberg cells as end-stage cells with telomere-poor 'ghost' nuclei and very short telomeres', *Lab Invest*, 90: 611-9.
Knipscheer, P., M. Raschle, A. Smogorzewska, M. Enoiu, T. V. Ho, O. D. Scharer, S. J. Elledge, and J. C. Walter. 2009. 'The Fanconi anemia pathway promotes replication-dependent DNA interstrand cross-link repair', *Science*, 326: 1698-701.
Kondrashova, O., M. Nguyen, K. Shield-Artin, A. V. Tinker, N. N. H. Teng, M. I. Harrell, M. J. Kuiper, G. Y. Ho, H. Barker, M. Jasin, R. Prakash, E. M. Kass, M. R. Sullivan, G. J. Brunette, K. A. Bernstein, R. L. Coleman, A. Floquet, M. Friedlander, G. Kichenadasse, D. M. O'Malley, A. M. Oza, J. X. Sun, L. Robillard, L. Maloney, D. D. L. Bowtell, H. Giordano, M. J. Wakefield, S. H. Kaufmann, A. D. Simmons, T. C. Harding, M. Raponi, I. A. McNeish, E. M. Swisher, K. Lin, and C. L. Scott. 2017. 'Secondary Somatic Mutations Restoring RAD51C and RAD51D Associated with Acquired Resistance to the PARP Inhibitor Rucaparib in High-grade Ovarian Carcinoma', *Cancer Discov*.
Konstantinopoulos, P. A., R. Ceccaldi, G. I. Shapiro, and A. D. D'Andrea. 2015. 'Homologous Recombination Deficiency: Exploiting the Fundamental Vulnerability of Ovarian Cancer', *Cancer Discov*, 5: 1137-54.
Konstantinopoulos, P. A., A. J. Wilson, J. Saskowski, E. Wass, and D. Khabele. 2014. 'Suberoylanilide hydroxamic acid (SAHA) enhances olaparib activity by targeting homologous recombination DNA repair in ovarian cancer', *Gynecol Oncol*, 133: 599-606.
Kontopidis, G., S. Y. Wu, D. I. Zheleva, P. Taylor, C. McInnes, D. P. Lane, P. M. Fischer, and M. D. Walkinshaw. 2005. 'Structural and biochemical studies of

human proliferating cell nuclear antigen complexes provide a rationale for cyclin association and inhibitor design', *Proc Natl Acad Sci U S A*, 102: 1871-6.

Kottemann, M. C., and A. Smogorzewska. 2013. 'Fanconi anaemia and the repair of Watson and Crick DNA crosslinks', *Nature*, 493: 356-63.

Kouroukis, C. T., F. G. Baldassarre, A. E. Haynes, K. Imrie, D. E. Reece, and M. C. Cheung. 2014. 'Bortezomib in multiple myeloma: a practice guideline', *Clin Oncol (R Coll Radiol)*, 26: 110-9.

Kramer, A., J. Green, J. Pollard, Jr., and S. Tugendreich. 2014. 'Causal analysis approaches in Ingenuity Pathway Analysis', *Bioinformatics*, 30: 523-30.

Kraus, C., J. Hoyer, G. Vasileiou, M. Wunderle, M. P. Lux, P. A. Fasching, M. Krumbiegel, S. Uebe, M. Reuter, M. W. Beckmann, and A. Reis. 2017. 'Gene panel sequencing in familial breast/ovarian cancer patients identifies multiple novel mutations also in genes others than BRCA1/2', *Int J Cancer*, 140: 95-102.

Krogh, B. O., and L. S. Symington. 2004. 'Recombination proteins in yeast', *Annu Rev Genet*, 38: 233-71.

Krynetski, E., and W. E. Evans. 2003. 'Drug methylation in cancer therapy: lessons from the TPMT polymorphism', *Oncogene*, 22: 7403-13.

Kuschel, B., A. Auranen, S. McBride, K. L. Novik, A. Antoniou, J. M. Lipscombe, N. E. Day, D. F. Easton, B. A. Ponder, P. D. Pharoah, and A. Dunning. 2002. 'Variants in DNA double-strand break repair genes and breast cancer susceptibility', *Hum Mol Genet*, 11: 1399-407.

Kuznetsov, S. G., D. C. Haines, B. K. Martin, and S. K. Sharan. 2009. 'Loss of Rad51c leads to embryonic lethality and modulation of Trp53-dependent tumorigenesis in mice', *Cancer Res*, 69: 863-72.

Lando, D. Y., C. L. Chang, A. S. Fridman, I. E. Grigoryan, E. N. Galyuk, Y. W. Hsueh, and C. K. Hu. 2014. 'Comparative thermal and thermodynamic study of DNA chemically modified with antitumor drug cisplatin and its inactive analog transplatin', *J Inorg Biochem*, 137: 85-93.

Landrum, M. J., J. M. Lee, M. Benson, G. Brown, C. Chao, S. Chitipiralla, B. Gu, J. Hart, D. Hoffman, J. Hoover, W. Jang, K. Katz, M. Ovetsky, G. Riley, A. Sethi, R. Tully, R. Villamarin-Salomon, W. Rubinstein, and D. R. Maglott. 2016. 'ClinVar: public archive of interpretations of clinically relevant variants', *Nucleic Acids Res*, 44: D862-8.

Le, D. T., J. N. Durham, K. N. Smith, H. Wang, B. R. Bartlett, L. K. Aulakh, S. Lu, H. Kemberling, C. Wilt, B. S. Luber, F. Wong, N. S. Azad, A. A. Rucki, D. Laheru, R. Donehower, A. Zaheer, G. A. Fisher, T. S. Crocenzi, J. J. Lee, T. F. Greten, A. G. Duffy, K. K. Ciombor, A. D. Eyring, B. H. Lam, A. Joe, S. P. Kang, M. Holdhoff, L. Danilova, L. Cope, C. Meyer, S. Zhou, R. M. Goldberg, D. K. Armstrong, K. M. Bever, A. N. Fader, J. Taube, F. Housseau, D. Spetzler, N. Xiao, D. M. Pardoll, N. Papadopoulos, K. W. Kinzler, J. R. Eshleman, B. Vogelstein, R. A. Anders, and L. A. Diaz, Jr. 2017. 'Mismatch repair deficiency predicts response of solid tumors to PD-1 blockade', *Science*, 357: 409-13.

Lee, J. Y., T. Terakawa, Z. Qi, J. B. Steinfeld, S. Redding, Y. Kwon, W. A. Gaines, W. Zhao, P. Sung, and E. C. Greene. 2015. 'DNA RECOMBINATION. Base triplet stepping by the Rad51/RecA family of recombinases', *Science*, 349: 977-81.

Lee, P. S., J. Fang, L. Jessop, T. Myers, P. Raj, N. Hu, C. Wang, P. R. Taylor, J. Wang, J. Khan, M. Jasin, and S. J. Chanock. 2014. 'RAD51B Activity and Cell Cycle Regulation in Response to DNA Damage in Breast Cancer Cell Lines', *Breast Cancer (Auckl)*, 8: 135-44.

Levy-Lahad, E., A. Lahad, S. Eisenberg, E. Dagan, T. Paperna, L. Kasinetz, R. Catane, B. Kaufman, U. Beller, P. Renbaum, and R. Gershoni-Baruch. 2001. 'A single nucleotide polymorphism in the RAD51 gene modifies cancer risk in BRCA2 but not BRCA1 carriers', *Proc Natl Acad Sci U S A*, 98: 3232-6.

Li, G. M. 1999. 'The role of mismatch repair in DNA damage-induced apoptosis', *Oncol Res*, 11: 393-400.

———. 2008. 'Mechanisms and functions of DNA mismatch repair', *Cell Res*, 18: 85-98.

Li, G. M., and P. Modrich. 1995. 'Restoration of mismatch repair to nuclear extracts of H6 colorectal tumor cells by a heterodimer of human MutL homologs', *Proc Natl Acad Sci U S A*, 92: 1950-4.

Liang, C. C., Z. Li, D. Lopez-Martinez, W. V. Nicholson, C. Venien-Bryan, and M. A. Cohn. 2016. 'The FANCD2-FANCI complex is recruited to DNA interstrand crosslinks before monoubiquitination of FANCD2', *Nat Commun*, 7: 12124.

Lim, D. S., and P. Hasty. 1996. 'A mutation in mouse rad51 results in an early embryonic lethal that is suppressed by a mutation in p53', *Mol Cell Biol*, 16: 7133-43.

Lio, Y. C., D. Schild, M. A. Brenneman, J. L. Redpath, and D. J. Chen. 2004. 'Human Rad51C deficiency destabilizes XRCC3, impairs recombination, and radiosensitizes S/G2-phase cells', *J Biol Chem*, 279: 42313-20.

Liu, F., L. Wang, F. Perna, and S. D. Nimer. 2016. 'Beyond transcription factors: how oncogenic signalling reshapes the epigenetic landscape', *Nat Rev Cancer*, 16: 359-72.

Liu, N., J. E. Lamerdin, R. S. Tebbs, D. Schild, J. D. Tucker, M. R. Shen, K. W. Brookman, M. J. Siciliano, C. A. Walter, W. Fan, L. S. Narayana, Z. Q. Zhou, A. W. Adamson, K. J. Sorensen, D. J. Chen, N. J. Jones, and L. H. Thompson. 1998. 'XRCC2 and XRCC3, new human Rad51-family members, promote chromosome stability and protect against DNA cross-links and other damages', *Mol Cell*, 1: 783-93.

Liu, Y., J. Y. Masson, R. Shah, P. O'Regan, and S. C. West. 2004. 'RAD51C is required for Holliday junction processing in mammalian cells', *Science*, 303: 243-6.

Liu, Y., M. Tarsounas, P. O'Regan, and S. C. West. 2007. 'Role of RAD51C and XRCC3 in genetic recombination and DNA repair', *J Biol Chem*, 282: 1973-9.

Lo, T., L. Pellegrini, A. R. Venkitaraman, and T. L. Blundell. 2003. 'Sequence fingerprints in BRCA2 and RAD51: implications for DNA repair and cancer', *DNA Repair (Amst)*, 2: 1015-28.

Loeb, L. A., C. F. Springgate, and N. Battula. 1974. 'Errors in DNA replication as a basis of malignant changes', *Cancer Res*, 34: 2311-21.

Loignon, M., L. Amrein, M. Dunn, and R. Aloyz. 2007. 'XRCC3 depletion induces spontaneous DNA breaks and p53-dependent cell death', *Cell Cycle*, 6: 606-11.

Lopez-Martinez, D., C. C. Liang, and M. A. Cohn. 2016. 'Cellular response to DNA interstrand crosslinks: the Fanconi anemia pathway', *Cell Mol Life Sci*.

Lorick, K. L., J. P. Jensen, S. Fang, A. M. Ong, S. Hatakeyama, and A. M. Weissman. 1999. 'RING fingers mediate ubiquitin-conjugating enzyme (E2)-dependent ubiquitination', *Proc Natl Acad Sci U S A*, 96: 11364-9.

Love, M. I., W. Huber, and S. Anders. 2014. 'Moderated estimation of fold change and dispersion for RNA-seq data with DESeq2', *Genome Biol*, 15: 550.

Loveday, C., C. Turnbull, E. Ramsay, D. Hughes, E. Ruark, J. R. Frankum, G. Bowden, B. Kalmyrzaev, M. Warren-Perry, K. Snape, J. W. Adlard, J. Barwell, J. Berg, A. F. Brady, C. Brewer, G. Brice, C. Chapman, J. Cook, R. Davidson, A. Donaldson, F. Douglas, L. Greenhalgh, A. Henderson, L. Izatt, A. Kumar, F. Lalloo, Z. Miedzybrodzka, P. J. Morrison, J. Paterson, M. Porteous, M. T. Rogers, S. Shanley, L. Walker, D. Eccles, D. G. Evans, A. Renwick, S. Seal, C. J. Lord, A. Ashworth, J. S. Reis-Filho, A. C. Antoniou, and N. Rahman. 2011. 'Germline mutations in RAD51D confer susceptibility to ovarian cancer', *Nat Genet*, 43: 879-82.

Loveday, C., C. Turnbull, E. Ruark, R. M. Xicola, E. Ramsay, D. Hughes, M. Warren-Perry, K. Snape, D. Eccles, D. G. Evans, M. Gore, A. Renwick, S. Seal, A. C. Antoniou, and N. Rahman. 2012. 'Germline RAD51C mutations confer susceptibility to ovarian cancer', *Nat Genet*, 44: 475-6; author reply 76.

Lu, C., F. Zhu, Y. Y. Cho, F. Tang, T. Zykova, W. Y. Ma, A. M. Bode, and Z. Dong. 2006. 'Cell apoptosis: requirement of H2AX in DNA ladder formation, but not for the activation of caspase-3', *Mol Cell*, 23: 121-32.

Mah, L. J., A. El-Osta, and T. C. Karagiannis. 2010. 'gammaH2AX: a sensitive molecular marker of DNA damage and repair', *Leukemia*, 24: 679-86.

Mailand, N., S. Bekker-Jensen, H. Faustrup, F. Melander, J. Bartek, C. Lukas, and J. Lukas. 2007. 'RNF8 ubiquitylates histones at DNA double-strand breaks and promotes assembly of repair proteins', *Cell*, 131: 887-900.

Malinge, J. M., M. J. Giraud-Panis, and M. Leng. 1999. 'Interstrand cross-links of cisplatin induce striking distortions in DNA', *J Inorg Biochem*, 77: 23-9.

Marathias, V. M., M. J. Sawicki, and P. H. Bolton. 1999. '6-Thioguanine alters the structure and stability of duplex DNA and inhibits quadruplex DNA formation', *Nucleic Acids Res*, 27: 2860-7.

Marechal, A., and L. Zou. 2015. 'RPA-coated single-stranded DNA as a platform for post-translational modifications in the DNA damage response', *Cell Res*, 25: 9-23.

Masson, J. Y., M. C. Tarsounas, A. Z. Stasiak, A. Stasiak, R. Shah, M. J. McIlwraith, F. E. Benson, and S. C. West. 2001. 'Identification and purification of two distinct complexes containing the five RAD51 paralogs', *Genes Dev*, 15: 3296-307.

Mauch, P. M., Weiss, L., Armitage, J.O. 2006. 'Hodgkin Disease.' in D. W. Kufe, Bast, R.C., Hait, W. N, Hong, W. K., Pollock, R. E., Weichselbaum, R.R., Holland, J. F., Frei, E. (ed.), *Cancer Medicine* (BC Decker: Hamilton, Ontario Canada).

Meindl, A., H. Hellebrand, C. Wiek, V. Erven, B. Wappenschmidt, D. Niederacher, M. Freund, P. Lichtner, L. Hartmann, H. Schaal, J. Ramser, E. Honisch, C. Kubisch, H. E. Wichmann, K. Kast, H. Deissler, C. Engel, B. Muller-Myhsok, K. Neveling, M. Kiechle, C. G. Mathew, D. Schindler, R. K. Schmutzler, and H. Hanenberg. 2010. 'Germline mutations in breast and ovarian cancer pedigrees establish RAD51C as a human cancer susceptibility gene', *Nat Genet*, 42: 410-4.

Mender, I., S. Gryaznov, Z. G. Dikmen, W. E. Wright, and J. W. Shay. 2015. 'Induction of telomere dysfunction mediated by the telomerase substrate precursor 6-thio-2'-deoxyguanosine', *Cancer Discov*, 5: 82-95.

Mertins, P., D. R. Mani, K. V. Ruggles, M. A. Gillette, K. R. Clauser, P. Wang, X. Wang, J. W. Qiao, S. Cao, F. Petralia, E. Kawaler, F. Mundt, K. Krug, Z. Tu, J. T. Lei, M. L. Gatza, M. Wilkerson, C. M. Perou, V. Yellapantula, K. L. Huang, C. Lin, M. D. McLellan, P. Yan, S. R. Davies, R. R. Townsend, S. J. Skates, J. Wang, B. Zhang, C. R. Kinsinger, M. Mesri, H. Rodriguez, L. Ding, A. G. Paulovich, D. Fenyo, M. J. Ellis, and S. A. Carr. 2016. 'Proteogenomics connects somatic mutations to signalling in breast cancer', *Nature*, 534: 55-62.

Mertins, P., J. W. Qiao, J. Patel, N. D. Udeshi, K. R. Clauser, D. R. Mani, M. W. Burgess, M. A. Gillette, J. D. Jaffe, and S. A. Carr. 2013. 'Integrated proteomic analysis of post-translational modifications by serial enrichment', *Nat Methods*, 10: 634-7.

Metzger, M. B., J. N. Pruneda, R. E. Klevit, and A. M. Weissman. 2014. 'RING-type E3 ligases: master manipulators of E2 ubiquitin-conjugating enzymes and ubiquitination', *Biochim Biophys Acta*, 1843: 47-60.

Michl, J., J. Zimmer, and M. Tarsounas. 2016. 'Interplay between Fanconi anemia and homologous recombination pathways in genome integrity', *Embo j*, 35: 909-23.

Miller, K. A., D. Sawicka, D. Barsky, and J. S. Albala. 2004. 'Domain mapping of the Rad51 paralog protein complexes', *Nucleic Acids Res*, 32: 169-78.

Min, A., S. A. Im, Y. K. Yoon, S. H. Song, H. J. Nam, H. S. Hur, H. P. Kim, K. H. Lee, S. W. Han, D. Y. Oh, T. Y. Kim, M. J. O'Connor, W. H. Kim, and Y. J. Bang. 2013. 'RAD51C-deficient cancer cells are highly sensitive to the PARP inhibitor olaparib', *Mol Cancer Ther*, 12: 865-77.

Minckwitz, Gunter Von, Eric Hahnen, Peter A. Fasching, Jan Hauke, Andreas Schneeweiss, Christoph Salat, Mahdi Rezai, Jens U. Blohmer, Dirk Michael Zahm, Christian Jackisch, Bernd Gerber, Peter Klare, Sherko Kummel, Holger Eidtmann, Stefan Paepke, Valentina Nekljudova, Sibylle Loibl, Michael Untch, Rita K. Schmutzler, GBG, and AGO-B Study Groups. 2014. 'Pathological complete response (pCR) rates after carboplatin-containing neoadjuvant chemotherapy in patients with germline BRCA (gBRCA) mutation and triple-negative breast cancer (TNBC): Results from GeparSixto', *Journal of Clinical Oncology*, 32: 1005-05.

Monteiro, F. L., T. Baptista, F. Amado, R. Vitorino, C. Jeronimo, and L. A. Helguero. 2014. 'Expression and functionality of histone H2A variants in cancer', *Oncotarget*, 5: 3428-43.

Morgan, E. A., N. Shah, and L. S. Symington. 2002. 'The requirement for ATP hydrolysis by Saccharomyces cerevisiae Rad51 is bypassed by mating-type heterozygosity or RAD54 in high copy', *Mol Cell Biol*, 22: 6336-43.

Morita, T., Y. Yoshimura, A. Yamamoto, K. Murata, M. Mori, H. Yamamoto, and A. Matsushiro. 1993. 'A mouse homolog of the Escherichia coli recA and Saccharomyces cerevisiae RAD51 genes', *Proc Natl Acad Sci U S A*, 90: 6577-80.

Muniandy, P. A., J. Liu, A. Majumdar, S. T. Liu, and M. M. Seidman. 2010. 'DNA interstrand crosslink repair in mammalian cells: step by step', *Crit Rev Biochem Mol Biol*, 45: 23-49.

Munshi, P. N., M. Lubin, and J. R. Bertino. 2014. '6-Thioguanine: A Drug With Unrealized Potential for Cancer Therapy', *Oncologist*, 19: 760-65.

Nakada, S. 2016. 'Opposing roles of RNF8/RNF168 and deubiquitinating enzymes in ubiquitination-dependent DNA double-strand break response signaling and DNA-repair pathway choice', *J Radiat Res*, 57 Suppl 1: i33-i40.

Nakada, S., R. M. Yonamine, and K. Matsuo. 2012. 'RNF8 regulates assembly of RAD51 at DNA double-strand breaks in the absence of BRCA1 and 53BP1', *Cancer Res*, 72: 4974-83.

Neidhardt, G., A. Becker, J. Hauke, J. Horvath, N. Bogdanova Markov, S. Heilmann-Heimbach, H. Hellebrand, H. Thiele, J. Altmuller, P. Nurnberg, A. Meindl, K. Rhiem, B. Blumcke, B. Wappenschmidt, R. K. Schmutzler, and E. Hahnen. 2017. 'The RAD51C exonic splice-site mutations c.404G>C and c.404G>T are associated with familial breast and ovarian cancer', *Eur J Cancer Prev*, 26: 165-69.

Nie, M., and M. N. Boddy. 2016. 'Cooperativity of the SUMO and Ubiquitin Pathways in Genome Stability', *Biomolecules*, 6: 14.

Nomme, J., Y. Takizawa, S. F. Martinez, A. Renodon-Corniere, F. Fleury, P. Weigel, K. Yamamoto, H. Kurumizaka, and M. Takahashi. 2008. 'Inhibition of filament formation of human Rad51 protein by a small peptide derived from the BRC-motif of the BRCA2 protein', *Genes Cells*, 13: 471-81.

Ogawa, T., X. Yu, A. Shinohara, and E. H. Egelman. 1993. 'Similarity of the yeast RAD51 filament to the bacterial RecA filament', *Science*, 259: 1896-9.

Ohtake, F., and H. Tsuchiya. 2017. 'The emerging complexity of ubiquitin architecture', *J Biochem*, 161: 125-33.

Owerbach, D., E. M. McKay, E. T. Yeh, K. H. Gabbay, and K. M. Bohren. 2005. 'A proline-90 residue unique to SUMO-4 prevents maturation and sumoylation', *Biochem Biophys Res Commun*, 337: 517-20.

Panier, S., and D. Durocher. 2009. 'Regulatory ubiquitylation in response to DNA double-strand breaks', *DNA Repair (Amst)*, 8: 436-43.

Parker, C. E., V. Mocanu, M. Mocanu, N. Dicheva, and M. R. Warren. 2010. 'Frontiers in Neuroscience

Mass Spectrometry for Post-Translational Modifications.' in O. Alzate (ed.), *Neuroproteomics* (CRC Press/Taylor & Francis

Llc.: Boca Raton (FL)).

Pellegrini, L., D. S. Yu, T. Lo, S. Anand, M. Lee, T. L. Blundell, and A. R. Venkitaraman. 2002. 'Insights into DNA recombination from the structure of a RAD51-BRCA2 complex', *Nature*, 420: 287-93.

Pelttari, L. M., T. Heikkinen, D. Thompson, A. Kallioniemi, J. Schleutker, K. Holli, C. Blomqvist, K. Aittomaki, R. Butzow, and H. Nevanlinna. 2011. 'RAD51C is a susceptibility gene for ovarian cancer', *Hum Mol Genet*, 20: 3278-88.

Pelttari, L. M., S. Khan, M. Vuorela, J. I. Kiiski, S. Vilske, V. Nevanlinna, S. Ranta, J. Schleutker, R. Winqvist, A. Kallioniemi, T. Dork, N. V. Bogdanova, J. Figueroa, P. D. Pharoah, M. K. Schmidt, A. M. Dunning, M. Garcia-Closas, M. K. Bolla, J. Dennis, K. Michailidou, Q. Wang, J. L. Hopper, M. C. Southey, E. H. Rosenberg,

P. A. Fasching, M. W. Beckmann, J. Peto, I. Dos-Santos-Silva, E. J. Sawyer, I. Tomlinson, B. Burwinkel, H. Surowy, P. Guenel, T. Truong, S. E. Bojesen, B. G. Nordestgaard, J. Benitez, A. Gonzalez-Neira, S. L. Neuhausen, H. Anton-Culver, H. Brenner, V. Arndt, A. Meindl, R. K. Schmutzler, H. Brauch, T. Bruning, A. Lindblom, S. Margolin, A. Mannermaa, J. M. Hartikainen, G. Chenevix-Trench, L. Van Dyck, H. Janssen, J. Chang-Claude, A. Rudolph, P. Radice, P. Peterlongo, E. Hallberg, J. E. Olson, G. G. Giles, R. L. Milne, C. A. Haiman, F. Schumacher, J. Simard, M. Dumont, V. Kristensen, A. L. Borresen-Dale, W. Zheng, A. Beeghly-Fadiel, M. Grip, I. L. Andrulis, G. Glendon, P. Devilee, C. Seynaeve, M. J. Hooning, M. Collee, A. Cox, S. S. Cross, M. Shah, R. N. Luben, U. Hamann, D. Torres, A. Jakubowska, J. Lubinski, F. J. Couch, D. Yannoukakos, N. Orr, A. Swerdlow, H. Darabi, J. Li, K. Czene, P. Hall, D. F. Easton, J. Mattson, C. Blomqvist, K. Aittomaki, and H. Nevanlinna. 2016. 'RAD51B in Familial Breast Cancer', *PLoS One*, 11: e0153788.

Pena-Diaz, J., and J. Jiricny. 2012. 'Mammalian mismatch repair: error-free or error-prone?', *Trends Biochem Sci*, 37: 206-14.

Pennington, K. P., T. Walsh, M. I. Harrell, M. K. Lee, C. C. Pennil, M. H. Rendi, A. Thornton, B. M. Norquist, S. Casadei, A. S. Nord, K. J. Agnew, C. C. Pritchard, S. Scroggins, R. L. Garcia, M. C. King, and E. M. Swisher. 2014. 'Germline and somatic mutations in homologous recombination genes predict platinum response and survival in ovarian, fallopian tube, and peritoneal carcinomas', *Clin Cancer Res*, 20: 764-75.

Perk, J., A. Iavarone, and R. Benezra. 2005. 'Id family of helix-loop-helix proteins in cancer', *Nat Rev Cancer*, 5: 603-14.

Pichler, A., C. Fatouros, H. Lee, and N. Eisenhardt. 2017. 'SUMO conjugation - a mechanistic view', *Biomol Concepts*, 8: 13-36.

Pickart, C. M. 2004. 'Back to the future with ubiquitin', *Cell*, 116: 181-90.

Pierce, A. J., R. D. Johnson, L. H. Thompson, and M. Jasin. 1999. 'XRCC3 promotes homology-directed repair of DNA damage in mammalian cells', *Genes Dev*, 13: 2633-8.

Pittman, D. L., and J. C. Schimenti. 2000. 'Midgestation lethality in mice deficient for the RecA-related gene, Rad51d/Rad51l3', *Genesis*, 26: 167-73.

Poulsen, M., C. Lukas, J. Lukas, S. Bekker-Jensen, and N. Mailand. 2012. 'Human RNF169 is a negative regulator of the ubiquitin-dependent response to DNA double-strand breaks', *J Cell Biol*, 197: 189-99.

Prakash, R., Y. Zhang, W. Feng, and M. Jasin. 2015. 'Homologous recombination and human health: the roles of BRCA1, BRCA2, and associated proteins', *Cold Spring Harb Perspect Biol*, 7: a016600.

Qi, Z., S. Redding, J. Y. Lee, B. Gibb, Y. Kwon, H. Niu, W. A. Gaines, P. Sung, and E. C. Greene. 2015. 'DNA sequence alignment by microhomology sampling during homologous recombination', *Cell*, 160: 856-69.

Rajesh, C., D. K. Baker, A. J. Pierce, and D. L. Pittman. 2011. 'The splicing-factor related protein SFPQ/PSF interacts with RAD51D and is necessary for homology-directed repair and sister chromatid cohesion', *Nucleic Acids Res*, 39: 132-45.

Rajesh, C., A. M. Gruver, V. Basrur, and D. L. Pittman. 2009. 'The interaction profile of homologous recombination repair proteins RAD51C, RAD51D and XRCC2 as determined by proteomic analysis', *Proteomics*, 9: 4071-86.

Rajesh, P., A. V. Litvinchuk, D. L. Pittman, and M. D. Wyatt. 2011. 'The homologous recombination protein RAD51D mediates the processing of 6-thioguanine lesions downstream of mismatch repair', *Mol Cancer Res*, 9: 206-14.

Rajesh, P., C. Rajesh, M. D. Wyatt, and D. L. Pittman. 2010. 'RAD51D protects against MLH1-dependent cytotoxic responses to O(6)-methylguanine', *DNA Repair (Amst)*, 9: 458-67.

Rappaport, H. P. 1993. 'Replication of the base pair 6-thioguanine/5-methyl-2-pyrimidine with the large Klenow fragment of Escherichia coli DNA polymerase I', *Biochemistry*, 32: 3047-57.

Rickman, K. A., F. P. Lach, A. Abhyankar, F. X. Donovan, E. M. Sanborn, J. A. Kennedy, C. Sougnez, S. B. Gabriel, O. Elemento, S. C. Chandrasekharappa, D. Schindler, A. D. Auerbach, and A. Smogorzewska. 2015. 'Deficiency of UBE2T, the E2 Ubiquitin Ligase Necessary for FANCD2 and FANCI Ubiquitination, Causes FA-T Subtype of Fanconi Anemia', *Cell Rep*, 12: 35-41.

Rock, K. L., C. Gramm, L. Rothstein, K. Clark, R. Stein, L. Dick, D. Hwang, and A. L. Goldberg. 1994. 'Inhibitors of the proteasome block the degradation of most cell proteins and the generation of peptides presented on MHC class I molecules', *Cell*, 78: 761-71.

Rogakou, E. P., D. R. Pilch, A. H. Orr, V. S. Ivanova, and W. M. Bonner. 1998. 'DNA double-stranded breaks induce histone H2AX phosphorylation on serine 139', *J Biol Chem*, 273: 5858-68.

Saitoh, H., and J. Hinchey. 2000. 'Functional heterogeneity of small ubiquitin-related protein modifiers SUMO-1 versus SUMO-2/3', *J Biol Chem*, 275: 6252-8.

Sanchez, H., A. Kertokalio, S. van Rossum-Fikkert, R. Kanaar, and C. Wyman. 2013. 'Combined optical and topographic imaging reveals different arrangements of human RAD54 with presynaptic and postsynaptic RAD51-DNA filaments', *Proc Natl Acad Sci U S A*, 110: 11385-90.

Sato, Y., A. Yamagata, S. Goto-Ito, K. Kubota, R. Miyamoto, S. Nakada, and S. Fukai. 2012. 'Molecular basis of Lys-63-linked polyubiquitination inhibition by the interaction between human deubiquitinating enzyme OTUB1 and ubiquitin-conjugating enzyme UBC13', *J Biol Chem*, 287: 25860-8.

Sato, Y., A. Yoshikawa, H. Mimura, M. Yamashita, A. Yamagata, and S. Fukai. 2009. 'Structural basis for specific recognition of Lys 63-linked polyubiquitin chains by tandem UIMs of RAP80', *Embo j*, 28: 2461-8.

Satoh, J., and H. Tabunoki. 2013. 'A Comprehensive Profile of ChIP-Seq-Based STAT1 Target Genes Suggests the Complexity of STAT1-Mediated Gene Regulatory Mechanisms', *Gene Regul Syst Bio*, 7: 41-56.

Schaetzlein, S., N. R. Kodandaramireddy, Z. Ju, A. Lechel, A. Stepczynska, D. R. Lilli, A. B. Clark, C. Rudolph, F. Kuhnel, K. Wei, B. Schlegelberger, P. Schirmacher, T. A. Kunkel, R. A. Greenberg, W. Edelmann, and K. L. Rudolph. 2007. 'Exonuclease-1 deletion impairs DNA damage signaling and prolongs lifespan of telomere-dysfunctional mice', *Cell*, 130: 863-77.

Scheffner, M., and S. Kumar. 2014. 'Mammalian HECT ubiquitin-protein ligases: biological and pathophysiological aspects', *Biochim Biophys Acta*, 1843: 61-74.
Schild, D., Y. C. Lio, D. W. Collins, T. Tsomondo, and D. J. Chen. 2000. 'Evidence for simultaneous protein interactions between human Rad51 paralogs', *J Biol Chem*, 275: 16443-9.
Schlafer, D., K. S. Shah, E. H. Panjic, and S. Lonial. 2017. 'Safety of proteasome inhibitors for treatment of multiple myeloma', *Expert Opin Drug Saf*, 16: 167-83.
Schmidt, C. K., Y. Galanty, M. Sczaniecka-Clift, J. Coates, S. Jhujh, M. Demir, M. Cornwell, P. Beli, and S. P. Jackson. 2015. 'Systematic E2 screening reveals a UBE2D-RNF138-CtIP axis promoting DNA repair', *Nat Cell Biol*, 17: 1458-70.
Schnurbein, G., J. Hauke, B. Wappenschmidt, N. Weber-Lassalle, S. Engert, H. Hellebrand, L. Garbes, A. Becker, G. Neidhardt, K. Rhiem, A. Meindl, R. K. Schmutzler, and E. Hahnen. 2013. 'RAD51C deletion screening identifies a recurrent gross deletion in breast cancer and ovarian cancer families', *Breast Cancer Res*, 15: R120.
Schurch, N. J., P. Schofield, M. Gierlinski, C. Cole, A. Sherstnev, V. Singh, N. Wrobel, K. Gharbi, G. G. Simpson, T. Owen-Hughes, M. Blaxter, and G. J. Barton. 2016. 'How many biological replicates are needed in an RNA-seq experiment and which differential expression tool should you use?', *RNA*, 22: 839-51.
Serebriiskii, I. G., and E. A. Golemis. 2000. 'Uses of lacZ to study gene function: evaluation of beta-galactosidase assays employed in the yeast two-hybrid system', *Anal Biochem*, 285: 1-15.
Shinohara, A., H. Ogawa, and T. Ogawa. 1992. 'Rad51 protein involved in repair and recombination in S. cerevisiae is a RecA-like protein', *Cell*, 69: 457-70.
Shinohara, A., and T. Ogawa. 1999. 'Rad51/RecA protein families and the associated proteins in eukaryotes', *Mutat Res*, 435: 13-21.
Short, J. M., Y. Liu, S. Chen, N. Soni, M. S. Madhusudhan, M. K. Shivji, and A. R. Venkitaraman. 2016. 'High-resolution structure of the presynaptic RAD51 filament on single-stranded DNA by electron cryo-microscopy', *Nucleic Acids Res*, 44: 9017-30.
Shu, Z., S. Smith, L. Wang, M. C. Rice, and E. B. Kmiec. 1999. 'Disruption of muREC2/RAD51L1 in mice results in early embryonic lethality which can Be partially rescued in a p53(-/-) background', *Mol Cell Biol*, 19: 8686-93.
Sigurdsson, S., S. Van Komen, W. Bussen, D. Schild, J. S. Albala, and P. Sung. 2001. 'Mediator function of the human Rad51B-Rad51C complex in Rad51/RPA-catalyzed DNA strand exchange', *Genes Dev*, 15: 3308-18.
Singh, K., B. GrothVasselli, P. N. Farnsworth, and D. K. Rai. 1996. 'Effect of thiobase incorporation into duplex DNA during the polymerization reaction', *Research Communications in Molecular Pathology and Pharmacology*, 94: 129-40.
Singleton, S. F., and J. Xiao. 2001. 'The stretched DNA geometry of recombination and repair nucleoprotein filaments', *Biopolymers*, 61: 145-58.
Sloper-Mould, K. E., J. C. Jemc, C. M. Pickart, and L. Hicke. 2001. 'Distinct functional surface regions on ubiquitin', *J Biol Chem*, 276: 30483-9.
Slupianek, A., S. K. Jozwiakowski, E. Gurdek, and T. Skorski. 2009. 'BCR/ABL kinase interacts with and phosphorylates the RAD51 paralog, RAD51B', *Leukemia*, 23: 2308-10.

Slupianek, A., C. Schmutte, G. Tombline, M. Nieborowska-Skorska, G. Hoser, M. O. Nowicki, A. J. Pierce, R. Fishel, and T. Skorski. 2001. 'BCR/ABL regulates mammalian RecA homologs, resulting in drug resistance', *Mol Cell*, 8: 795-806.

Smiraldo, P. G., A. M. Gruver, J. C. Osborn, and D. L. Pittman. 2005. 'Extensive chromosomal instability in Rad51d-deficient mouse cells', *Cancer Res*, 65: 2089-96.

Sobhian, B., G. Shao, D. R. Lilli, A. C. Culhane, L. A. Moreau, B. Xia, D. M. Livingston, and R. A. Greenberg. 2007. 'RAP80 targets BRCA1 to specific ubiquitin structures at DNA damage sites', *Science*, 316: 1198-202.

Somerville, L., E. Y. Krynetski, N. F. Krynetskaia, R. D. Beger, W. X. Zhang, C. A. Marhefka, W. E. Evans, and R. W. Kriwacki. 2003. 'Structure and dynamics of thioguanine-modified duplex DNA', *Journal of Biological Chemistry*, 278: 1005-11.

Somyajit, K., S. Basavaraju, R. Scully, and G. Nagaraju. 2013. 'ATM- and ATR-mediated phosphorylation of XRCC3 regulates DNA double-strand break-induced checkpoint activation and repair', *Mol Cell Biol*, 33: 1830-44.

Song, H., E. Dicks, S. J. Ramus, J. P. Tyrer, M. P. Intermaggio, J. Hayward, C. K. Edlund, D. Conti, P. Harrington, L. Fraser, S. Philpott, C. Anderson, A. Rosenthal, A. Gentry-Maharaj, D. D. Bowtell, K. Alsop, M. S. Cicek, J. M. Cunningham, B. L. Fridley, J. Alsop, M. Jimenez-Linan, E. Hogdall, C. K. Hogdall, A. Jensen, S. K. Kjaer, J. Lubinski, T. Huzarski, A. Jakubowska, J. Gronwald, S. Poblete, S. Lele, L. Sucheston-Campbell, K. B. Moysich, K. Odunsi, E. L. Goode, U. Menon, I. J. Jacobs, S. A. Gayther, and P. D. Pharoah. 2015. 'Contribution of Germline Mutations in the RAD51B, RAD51C, and RAD51D Genes to Ovarian Cancer in the Population', *J Clin Oncol*, 33: 2901-7.

Sorensen, C. S., L. T. Hansen, J. Dziegielewski, R. G. Syljuasen, C. Lundin, J. Bartek, and T. Helleday. 2005. 'The cell-cycle checkpoint kinase Chk1 is required for mammalian homologous recombination repair', *Nat Cell Biol*, 7: 195-201.

Subramanian, A., P. Tamayo, V. K. Mootha, S. Mukherjee, B. L. Ebert, M. A. Gillette, A. Paulovich, S. L. Pomeroy, T. R. Golub, E. S. Lander, and J. P. Mesirov. 2005. 'Gene set enrichment analysis: a knowledge-based approach for interpreting genome-wide expression profiles', *Proc Natl Acad Sci U S A*, 102: 15545-50.

Subramanyam, S., M. Ismail, I. Bhattacharya, and M. Spies. 2016. 'Tyrosine phosphorylation stimulates activity of human RAD51 recombinase through altered nucleoprotein filament dynamics', *Proc Natl Acad Sci U S A*, 113: E6045-e54.

Suchankova, T., K. Kubicek, J. Kasparkova, V. Brabec, and J. Kozelka. 2012. 'Platinum-DNA interstrand crosslinks: molecular determinants of bending and unwinding of the double helix', *J Inorg Biochem*, 108: 69-79.

Sung, P. 1994. 'Catalysis of ATP-dependent homologous DNA pairing and strand exchange by yeast RAD51 protein', *Science*, 265: 1241-3.

Sung, P., L. Krejci, S. Van Komen, and M. G. Sehorn. 2003. 'Rad51 recombinase and recombination mediators', *J Biol Chem*, 278: 42729-32.

Swatek, K. N., and D. Komander. 2016. 'Ubiquitin modifications', *Cell Res*, 26: 399-422.

Takata, M., M. S. Sasaki, S. Tachiiri, T. Fukushima, E. Sonoda, D. Schild, L. H. Thompson, and S. Takeda. 2001. 'Chromosome instability and defective

recombinational repair in knockout mutants of the five Rad51 paralogs', *Mol Cell Biol*, 21: 2858-66.

Takizawa, Y., T. Kinebuchi, W. Kagawa, S. Yokoyama, T. Shibata, and H. Kurumizaka. 2004. 'Mutational analyses of the human Rad51-Tyr315 residue, a site for phosphorylation in leukaemia cells', *Genes Cells*, 9: 781-90.

Tarsounas, M., P. Munoz, A. Claas, P. G. Smiraldo, D. L. Pittman, M. A. Blasco, and S. C. West. 2004. 'Telomere maintenance requires the RAD51D recombination/repair protein', *Cell*, 117: 337-47.

Tedaldi, G., M. Tebaldi, V. Zampiga, R. Danesi, V. Arcangeli, M. Ravegnani, I. Cangini, F. Pirini, E. Petracci, A. Rocca, F. Falcini, D. Amadori, and D. Calistri. 2017. 'Multiple-gene panel analysis in a case series of 255 women with hereditary breast and ovarian cancer', *Oncotarget*.

Tendian, S. W., and W. B. Parker. 2000. 'Interaction of deoxyguanosine nucleotide analogs with human telomerase', *Mol Pharmacol*, 57: 695-9.

Thach, T. T., D. Shin, S. Han, and S. Lee. 2016. 'New conformations of linear polyubiquitin chains from crystallographic and solution-scattering studies expand the conformational space of polyubiquitin', *Acta Crystallogr D Struct Biol*, 72: 524-35.

Thompson, E. R., S. E. Boyle, J. Johnson, G. L. Ryland, S. Sawyer, D. Y. Choong, kConFab, G. Chenevix-Trench, A. H. Trainer, G. J. Lindeman, G. Mitchell, P. A. James, and I. G. Campbell. 2012. 'Analysis of RAD51C germline mutations in high-risk breast and ovarian cancer families and ovarian cancer patients', *Hum Mutat*, 33: 95-9.

Thompson, E. R., S. M. Rowley, S. Sawyer, kConfab, D. M. Eccles, A. H. Trainer, G. Mitchell, P. A. James, and I. G. Campbell. 2013. 'Analysis of RAD51D in ovarian cancer patients and families with a history of ovarian or breast cancer', *PLoS One*, 8: e54772.

Topp, M. D., L. Hartley, M. Cook, V. Heong, E. Boehm, L. McShane, J. Pyman, O. McNally, S. Ananda, M. Harrell, D. Etemadmoghadam, L. Galletta, K. Alsop, G. Mitchell, S. B. Fox, J. B. Kerr, K. J. Hutt, S. H. Kaufmann, Study Australian Ovarian Cancer, E. M. Swisher, D. D. Bowtell, M. J. Wakefield, and C. L. Scott. 2014. 'Molecular correlates of platinum response in human high-grade serous ovarian cancer patient-derived xenografts', *Mol Oncol*, 8: 656-68.

Tsuzuki, T., Y. Fujii, K. Sakumi, Y. Tominaga, K. Nakao, M. Sekiguchi, A. Matsushiro, Y. Yoshimura, and MoritaT. 1996. 'Targeted disruption of the Rad51 gene leads to lethality in embryonic mice', *Proc Natl Acad Sci U S A*, 93: 6236-40.

Unno, J., A. Itaya, M. Taoka, K. Sato, J. Tomida, W. Sakai, K. Sugasawa, M. Ishiai, T. Ikura, T. Isobe, H. Kurumizaka, and M. Takata. 2014. 'FANCD2 binds CtIP and regulates DNA-end resection during DNA interstrand crosslink repair', *Cell Rep*, 7: 1039-47.

van Twest, S., V. J. Murphy, C. Hodson, W. Tan, P. Swuec, J. J. O'Rourke, J. Heierhorst, W. Crismani, and A. J. Deans. 2017. 'Mechanism of Ubiquitination and Deubiquitination in the Fanconi Anemia Pathway', *Mol Cell*, 65: 247-59.

Varadan, R., M. Assfalg, A. Haririnia, S. Raasi, C. Pickart, and D. Fushman. 2004. 'Solution conformation of Lys63-linked di-ubiquitin chain provides clues to functional diversity of polyubiquitin signaling', *J Biol Chem*, 279: 7055-63.

Vaz, F., H. Hanenberg, B. Schuster, K. Barker, C. Wiek, V. Erven, K. Neveling, D. Endt, I. Kesterton, F. Autore, F. Fraternali, M. Freund, L. Hartmann, D. Grimwade, R. G. Roberts, H. Schaal, S. Mohammed, N. Rahman, D. Schindler, and C. G. Mathew. 2010. 'Mutation of the RAD51C gene in a Fanconi anemia-like disorder', *Nat Genet*, 42: 406-9.

Vojdeman, F. J., S. E. M. Herman, N. Kirkby, A. Wiestner, M. B. van T' Veer, G. E. Tjonnfjord, M. A. Itala-Remes, E. Kimby, M. Z. Farooqui, A. Polliack, K. L. Wu, J. K. Doorduijn, W. G. Alemayehu, S. Wittebol, T. Kozak, J. Walewski, M. C. J. Abrahamse-Testroote, M. H. J. van Oers, C. H. Geisler, and C. U. Niemann. 2017. 'Soluble CD52 is an indicator of disease activity in chronic lymphocytic leukemia', *Leuk Lymphoma*, 58: 2356-62.

Wang, A. T., T. Kim, J. E. Wagner, B. A. Conti, F. P. Lach, A. L. Huang, H. Molina, E. M. Sanborn, H. Zierhut, B. K. Cornes, A. Abhyankar, C. Sougnez, S. B. Gabriel, A. D. Auerbach, S. C. Kowalczykowski, and A. Smogorzewska. 2015. 'A Dominant Mutation in Human RAD51 Reveals Its Function in DNA Interstrand Crosslink Repair Independent of Homologous Recombination', *Mol Cell*, 59: 478-90.

Wang, J. Y., and W. Edelmann. 2006. 'Mismatch repair proteins as sensors of alkylation DNA damage', *Cancer Cell*, 9: 417-8.

Wang, Q., Y. Wang, L. Du, C. Xu, Y. Sun, B. Yang, Z. Sun, Y. Fu, L. Cai, S. Fan, F. Fan, and Q. Liu. 2014. 'shRNA-mediated XRCC2 gene knockdown efficiently sensitizes colon tumor cells to X-ray irradiation in vitro and in vivo', *Int J Mol Sci*, 15: 2157-71.

Wang, Z. C., N. J. Birkbak, A. C. Culhane, R. Drapkin, A. Fatima, R. Tian, M. Schwede, K. Alsop, K. E. Daniels, H. Piao, J. Liu, D. Etemadmoghadam, A. Miron, H. B. Salvesen, G. Mitchell, A. DeFazio, J. Quackenbush, R. S. Berkowitz, J. D. Iglehart, D. D. Bowtell, and U. A. Matulonis. 2012. 'Profiles of genomic instability in high-grade serous ovarian cancer predict treatment outcome', *Clin Cancer Res*, 18: 5806-15.

Wang, Z., M. Gerstein, and M. Snyder. 2009. 'RNA-Seq: a revolutionary tool for transcriptomics', *Nat Rev Genet*, 10: 57-63.

Wiese, C., J. M. Hinz, R. S. Tebbs, P. B. Nham, S. S. Urbin, D. W. Collins, L. H. Thompson, and D. Schild. 2006. 'Disparate requirements for the Walker A and B ATPase motifs of human RAD51D in homologous recombination', *Nucleic Acids Res*, 34: 2833-43.

Winsey, S. L., N. A. Haldar, H. P. Marsh, M. Bunce, S. E. Marshall, A. L. Harris, F. Wojnarowska, and K. I. Welsh. 2000. 'A variant within the DNA repair gene XRCC3 is associated with the development of melanoma skin cancer', *Cancer Res*, 60: 5612-6.

Woelk, T., B. Oldrini, E. Maspero, S. Confalonieri, E. Cavallaro, P. P. Di Fiore, and S. Polo. 2006. 'Molecular mechanisms of coupled monoubiquitination', *Nat Cell Biol*, 8: 1246-54.

Wu, Y., D. Bhattacharyya, C. L. King, I. Baskerville-Abraham, S. H. Huh, G. Boysen, J. A. Swenberg, B. Temple, S. L. Campbell, and S. G. Chaney. 2007. 'Solution structures of a DNA dodecamer duplex with and without a cisplatin 1,2-d(GG)

intrastrand cross-link: comparison with the same DNA duplex containing an oxaliplatin 1,2-d(GG) intrastrand cross-link', *Biochemistry*, 46: 6477-87.

Wyatt, H. D., and S. C. West. 2014. 'Holliday junction resolvases', *Cold Spring Harb Perspect Biol*, 6: a023192.

Wyatt, M. D., N. M. Reilly, S. Patel, P. Rajesh, G. P. Schools, P. G. Smiraldo, and D. L. Pittman. 2017. 'Thiopurine-induced mitotic catastrophe in Rad51d-deficient mammalian cells', *Environ Mol Mutagen*.

Wyatt, Michael D., Nicole M. Reilly, Shikha Patel, Preeti Rajesh, Gary P. Schools, Phillip G. Smiraldo, and Douglas L. Pittman. 'Thiopurine-induced mitotic catastrophe in Rad51d-deficient mammalian cells', *Environmental and Molecular Mutagenesis*: n/a-n/a.

Xiao, A., H. Li, D. Shechter, S. H. Ahn, L. A. Fabrizio, H. Erdjument-Bromage, S. Ishibe-Murakami, B. Wang, P. Tempst, K. Hofmann, D. J. Patel, S. J. Elledge, and C. D. Allis. 2009. 'WSTF regulates the H2A.X DNA damage response via a novel tyrosine kinase activity', *Nature*, 457: 57-62.

Xie, J., H. Kim, L. A. Moreau, S. Puhalla, J. Garber, M. Al Abo, S. Takeda, and A. D. D'Andrea. 2015. 'RNF4-mediated polyubiquitination regulates the Fanconi anemia/BRCA pathway', *J Clin Invest*, 125: 1523-32.

Xu, J., L. Zhao, Y. Xu, W. Zhao, P. Sung, and H. W. Wang. 2017. 'Cryo-EM structures of human RAD51 recombinase filaments during catalysis of DNA-strand exchange', *Nat Struct Mol Biol*, 24: 40-46.

Yamada, N. A., J. M. Hinz, V. L. Kopf, K. D. Segalle, and L. H. Thompson. 2004. 'XRCC3 ATPase activity is required for normal XRCC3-Rad51C complex dynamics and homologous recombination', *J Biol Chem*, 279: 23250-4.

Yan, T., A. B. Desai, J. W. Jacobberger, R. M. Sramkoski, T. Loh, and T. J. Kinsella. 2004. 'CHK1 and CHK2 are differentially involved in mismatch repair-mediated 6-thioguanine-induced cell cycle checkpoint responses', *Mol Cancer Ther*, 3: 1147-57.

Yang, J., R. Yan, A. Roy, D. Xu, J. Poisson, and Y. Zhang. 2015. 'The I-TASSER Suite: protein structure and function prediction', *Nat Methods*, 12: 7-8.

Yang, J., and Y. Zhang. 2015. 'Protein Structure and Function Prediction Using I-TASSER', *Curr Protoc Bioinformatics*, 52: 5.8.1-15.

Yang, Z., A. S. Waldman, and M. D. Wyatt. 2008. 'DNA damage and homologous recombination signaling induced by thymidylate deprivation', *Biochem Pharmacol*, 76: 987-96.

———. 2012. 'Expression and regulation of RAD51 mediate cellular responses to chemotherapeutics', *Biochem Pharmacol*, 83: 741-6.

Yard, B. D. 2011. 'Regulation of RAD51D in Homologous Recombination DNA Repair by Alternative Splicing and Ubiquitin Modification', Dissertation, University of South Carolina.

Yard, B. D., N. M. Reilly, M. K. Bedenbaugh, and D. L. Pittman. 2016. 'RNF138 interacts with RAD51D and is required for DNA interstrand crosslink repair and maintaining chromosome integrity', *DNA Repair (Amst)*, 42: 82-93.

Yata, K., J. Y. Bleuyard, R. Nakato, C. Ralf, Y. Katou, R. A. Schwab, W. Niedzwiedz, K. Shirahige, and F. Esashi. 2014. 'BRCA2 coordinates the activities of cell-cycle kinases to promote genome stability', *Cell Rep*, 7: 1547-59.

Yata, K., J. Lloyd, S. Maslen, J. Y. Bleuyard, M. Skehel, S. J. Smerdon, and F. Esashi. 2012. 'Plk1 and CK2 act in concert to regulate Rad51 during DNA double strand break repair', *Mol Cell*, 45: 371-83.

Ye, Y., G. Blaser, M. H. Horrocks, M. J. Ruedas-Rama, S. Ibrahim, A. A. Zhukov, A. Orte, D. Klenerman, S. E. Jackson, and D. Komander. 2012. 'Ubiquitin chain conformation regulates recognition and activity of interacting proteins', *Nature*, 492: 266-70.

Ye, Y., and M. Rape. 2009. 'Building ubiquitin chains: E2 enzymes at work', *Nat Rev Mol Cell Biol*, 10: 755-64.

Yokoyama, H., N. Sarai, W. Kagawa, R. Enomoto, T. Shibata, H. Kurumizaka, and S. Yokoyama. 2004. 'Preferential binding to branched DNA strands and strand-annealing activity of the human Rad51B, Rad51C, Rad51D and Xrcc2 protein complex', *Nucleic Acids Res*, 32: 2556-65.

York, S. J., and P. Modrich. 2006. 'Mismatch repair-dependent iterative excision at irreparable O6-methylguanine lesions in human nuclear extracts', *J Biol Chem*, 281: 22674-83.

You, Z., and J. M. Bailis. 2010. 'DNA damage and decisions: CtIP coordinates DNA repair and cell cycle checkpoints', *Trends Cell Biol*, 20: 402-9.

Yu, M., K. Liu, Z. Mao, J. Luo, W. Gu, and W. Zhao. 2016. 'USP11 Is a Negative Regulator to gammaH2AX Ubiquitylation by RNF8/RNF168', *J Biol Chem*, 291: 959-67.

Yuan, B., and Y. Wang. 2008. 'Mutagenic and cytotoxic properties of 6-thioguanine, S6-methylthioguanine, and guanine-S6-sulfonic acid', *J Biol Chem*, 283: 23665-70.

Yuan, Z. M., Y. Huang, T. Ishiko, S. Nakada, T. Utsugisawa, S. Kharbanda, R. Wang, P. Sung, A. Shinohara, R. Weichselbaum, and D. Kufe. 1998. 'Regulation of Rad51 function by c-Abl in response to DNA damage', *J Biol Chem*, 273: 3799-802.

Yue, F., Y. Cheng, A. Breschi, J. Vierstra, W. Wu, T. Ryba, R. Sandstrom, Z. Ma, C. Davis, B. D. Pope, Y. Shen, D. D. Pervouchine, S. Djebali, R. E. Thurman, R. Kaul, E. Rynes, A. Kirilusha, G. K. Marinov, B. A. Williams, D. Trout, H. Amrhein, K. Fisher-Aylor, I. Antoshechkin, G. DeSalvo, L. H. See, M. Fastuca, J. Drenkow, C. Zaleski, A. Dobin, P. Prieto, J. Lagarde, G. Bussotti, A. Tanzer, O. Denas, K. Li, M. A. Bender, M. Zhang, R. Byron, M. T. Groudine, D. McCleary, L. Pham, Z. Ye, S. Kuan, L. Edsall, Y. C. Wu, M. D. Rasmussen, M. S. Bansal, M. Kellis, C. A. Keller, C. S. Morrissey, T. Mishra, D. Jain, N. Dogan, R. S. Harris, P. Cayting, T. Kawli, A. P. Boyle, G. Euskirchen, A. Kundaje, S. Lin, Y. Lin, C. Jansen, V. S. Malladi, M. S. Cline, D. T. Erickson, V. M. Kirkup, K. Learned, C. A. Sloan, K. R. Rosenbloom, B. Lacerda de Sousa, K. Beal, M. Pignatelli, P. Flicek, J. Lian, T. Kahveci, D. Lee, W. J. Kent, M. Ramalho Santos, J. Herrero, C. Notredame, A. Johnson, S. Vong, K. Lee, D. Bates, F. Neri, M. Diegel, T. Canfield, P. J. Sabo, M. S. Wilken, T. A. Reh, E. Giste, A. Shafer, T. Kutyavin, E. Haugen, D. Dunn, A. P. Reynolds, S. Neph, R. Humbert, R. S. Hansen, M. De Bruijn, L. Selleri, A. Rudensky, S. Josefowicz, R. Samstein, E. E. Eichler, S. H. Orkin, D. Levasseur, T. Papayannopoulou, K. H. Chang, A. Skoultchi, S. Gosh, C. Disteche, P. Treuting, Y. Wang, M. J. Weiss, G. A. Blobel, X. Cao, S. Zhong, T. Wang, P. J. Good, R. F. Lowdon, L. B. Adams, X. Q. Zhou, M. J. Pazin, E. A. Feingold, B. Wold, J. Taylor, A. Mortazavi, S. M. Weissman, J.

A. Stamatoyannopoulos, M. P. Snyder, R. Guigo, T. R. Gingeras, D. M. Gilbert, R. C. Hardison, M. A. Beer, and B. Ren. 2014. 'A comparative encyclopedia of DNA elements in the mouse genome', *Nature*, 515: 355-64.

Zee, B. M., and B. A. Garcia. 2012. 'Discovery of lysine post-translational modifications through mass spectrometric detection', *Essays Biochem*, 52: 147-63.

Zhang, X., M. T. Ling, H. Feng, Y. C. Wong, S. W. Tsao, and X. Wang. 2004. 'Id-I stimulates cell proliferation through activation of EGFR in ovarian cancer cells', *Br J Cancer*, 91: 2042-7.

Zhou, H., S. Di Palma, C. Preisinger, M. Peng, A. N. Polat, A. J. Heck, and S. Mohammed. 2013. 'Toward a comprehensive characterization of a human cancer cell phosphoproteome', *J Proteome Res*, 12: 260-71.

Zou, Y., B. Van Houten, and N. Farrell. 1994. 'Sequence specificity of DNA-DNA interstrand cross-link formation by cisplatin and dinuclear platinum complexes', *Biochemistry*, 33: 5404-10.

APPENDIX A

GENES WITH DIFFERENTIAL EXPRESSION IN THE ABSENCE OF RAD51D IDENTIFIED BY MICROARRAY

Table A.1. Genes identified by microarray analysis with differential expression between *Rad51d*-proficient and *Rad51d*-deficient primary mouse embryonic fibroblast cell lines. Genes are listed in order of increasing fold change.

Gene Symbol	Description	Fold Change (*Rad51d*-proficient v. *Rad51d*-deficient)	FDR p-value	Group
Lyz2	lysozyme 2	2.90	0.045698	Coding
Rad51d	RAD51 homolog D	2.66	0.002589	Complex
Slfn9	schlafen 9	2.63	0.060793	Coding
C1qb	complement component 1, q subcomponent, beta polypeptide	2.53	0.064458	Coding
		2.49	0.063475	NonCoding
		2.42	0.083478	NonCoding
Il1rl1	interleukin 1 receptor-like 1	2.38	0.002589	Coding
Ifit1	interferon-induced protein with tetratricopeptide repeats 1	2.35	0.224665	Coding
2010300F17Rik	RIKEN cDNA 2010300F17 gene	2.28	0.012221	NonCoding
Lyz1	lysozyme 1	2.28	0.03706	Coding
		2.21	0.056045	NonCoding
Dynap	dynactin associated protein	2.18	0.042872	Coding
Usp18	ubiquitin specific peptidase 18	2.16	0.171789	Coding
Hoxd13	homeobox D13	2.13	0.006665	Coding
Rnf213	ring finger protein 213	2.04	0.100862	Complex
Slfn10-ps	schlafen 10, pseudogene	1.98	0.032321	Complex
Uck2	uridine-cytidine kinase 2	1.96	0.012221	Coding
Slc7a8	solute carrier family 7 (cationic amino acid transporter, y+ system), member 8	1.96	0.018935	Coding
		1.96	0.021149	NonCoding
Adam12	a disintegrin and metallopeptidase domain 12 (meltrin alpha)	1.95	0.008406	Complex
Fcer1g	Fc receptor, IgE, high affinity I, gamma polypeptide	1.95	0.036185	Complex
Cdh10	cadherin 10	1.94	0.008153	Complex
Loxl3	lysyl oxidase-like 3	1.93	0.041649	Complex
Asb5	ankyrin repeat and SOCs box-containing 5	1.92	0.006665	Coding
		1.90	0.026432	NonCoding
		1.90	0.027718	NonCoding
Lilrb4	leukocyte immunoglobulin-like receptor, subfamily B, member 4	1.90	0.226172	Coding
Slc16a3	solute carrier family 16	1.89	0.00868	Complex

	(monocarboxylic acid transporters), member 3			
Speer8-ps1	spermatogenesis associated glutamate (E)-rich protein 8, pseudogene 1	1.87	0.012722	Complex
Gm6091	predicted pseudogene 6091	1.87	0.018935	Pseudogene
Lipg	lipase, endothelial	1.85	0.012221	Complex
Bst2	bone marrow stromal cell antigen 2	1.79	0.30203	Coding
Angptl7	angiopoietin-like 7	1.78	0.02546	Coding
Gm21847	predicted gene, 21847	1.78	0.027453	Complex
Htr1b	5-hydroxytryptamine (serotonin) receptor 1B	1.78	0.05327	Complex
Gm11116	predicted gene 11116	1.77	0.3617	Coding
Mfsd2a	major facilitator superfamily domain containing 2A	1.75	0.007187	Complex
Rasal2	RAS protein activator like 2	1.75	0.029268	Complex
Gm16464	predicted gene 16464	1.73	0.005385	Pseudogene
Csf1r	colony stimulating factor 1 receptor	1.72	0.021149	Complex
Adm	adrenomedullin	1.72	0.045499	Coding
Bcl2a1b	B cell leukemia/lymphoma 2 related protein A1b	1.72	0.113603	Coding
		1.72	0.129933	NonCoding
Itgam	integrin alpha M	1.71	0.021372	Coding
Col12a1	collagen, type XII, alpha 1	1.71	0.066342	Complex
Ccl9	chemokine (C-C motif) ligand 9	1.71	0.086773	Complex
Ccnyl1	cyclin Y-like 1	1.70	0.003613	Complex
Speer7-ps1	spermatogenesis associated glutamate (E)-rich protein 7, pseudogene 1	1.70	0.040525	Complex
Adam8	a disintegrin and metallopeptidase domain 8	1.70	0.10941	Complex
Gm24325	predicted gene, 24325	1.70	0.25208	NonCoding
Myd88	myeloid differentiation primary response gene 88	1.70	0.31687	Complex
		1.69	0.140823	NonCoding
		1.69	0.160967	NonCoding
Lgals3bp	lectin, galactoside-binding, soluble, 3 binding protein	1.69	0.234481	Complex
Htr2a	5-hydroxytryptamine (serotonin) receptor 2A	1.69	0.286288	Coding
Mir380	microRNA 380	1.69	0.345875	NonCoding
Cd180	CD180 antigen	1.68	0.15251	Coding
		1.67	0.120419	NonCoding
Lrrc15	leucine rich repeat containing 15	1.67	0.256253	Coding
		1.66	0.190557	NonCoding
		1.66	0.359297	NonCoding
Herc3	hect domain and RLD 3	1.65	0.012221	Complex
Lcp1	lymphocyte cytosolic	1.65	0.013723	Complex

	protein 1			
Hmga2-ps1	high mobility group AT-hook 2, pseudogene 1	1.65	0.015471	Complex
Slit2	slit homolog 2 (Drosophila)	1.65	0.021149	Complex
Slc1a6	solute carrier family 1 (high affinity aspartate/glutamate transporter), member 6	1.65	0.036394	Coding
		1.65	0.125997	NonCoding
Gp49a	glycoprotein 49 A	1.65	0.168662	Complex
		1.65	0.171385	NonCoding
Ldlr	low density lipoprotein receptor	1.64	0.018459	Coding
Lrrc32	leucine rich repeat containing 32	1.64	0.108744	Coding
Slfn2	schlafen 2	1.63	0.014916	Coding
		1.63	0.065511	NonCoding
		1.63	0.100342	NonCoding
Stat1	signal transducer and activator of transcription 1	1.63	0.306519	Coding
Alox5ap	arachidonate 5-lipoxygenase activating protein	1.62	0.100537	Coding
		1.62	0.265718	NonCoding
		1.61	0.118276	NonCoding
		1.61	0.325426	Other
Spcs3	signal peptidase complex subunit 3 homolog (S. cerevisiae)	1.60	0.002589	Coding
Serpine1	serine (or cysteine) peptidase inhibitor, clade E, member 1	1.60	0.003921	Coding
Dok1	docking protein 1	1.60	0.014694	Complex
Grem2	gremlin 2 homolog, cysteine knot superfamily (Xenopus laevis)	1.60	0.024993	Coding
Nipal1	NIPA-like domain containing 1	1.60	0.035013	Coding
		1.60	0.074161	NonCoding
Tnfsf9	tumor necrosis factor (ligand) superfamily, member 9	1.60	0.215125	Coding
Tnc	tenascin C; tenascin C (hexabrachion)	1.59	0.021149	Coding
		1.59	0.293309	NonCoding
		1.59	0.293309	NonCoding
		1.59	0.293309	NonCoding
		1.59	0.293309	NonCoding
Plac8	placenta-specific 8	1.58	0.043229	Complex
		1.58	0.059964	NonCoding
		1.58	0.14483	NonCoding
		1.58	0.166231	NonCoding
Tnn	tenascin N	1.58	0.320986	Coding
Lsp1	lymphocyte specific 1	1.57	0.042888	Complex

Msr1	macrophage scavenger receptor 1	1.57	0.071559	Complex
Gm12957	predicted gene 12957	1.57	0.133047	Complex
C1qc	complement component 1, q subcomponent, C chain	1.57	0.154394	Complex
		1.57	0.233862	NonCoding
Gm22889	predicted gene, 22889	1.56	0.045764	NonCoding
		1.56	0.138796	NonCoding
		1.56	0.15867	NonCoding
Phf11d	PHD finger protein 11D	1.55	0.090001	Complex
Slfn8	schlafen 8	1.55	0.096014	Coding
Tll1	tolloid-like	1.55	0.132532	Coding
		1.55	0.168775	NonCoding
		1.55	0.337992	NonCoding
Xaf1	XIAP associated factor 1	1.55	0.346964	Complex
Phlpp1	PH domain and leucine rich repeat protein phosphatase 1	1.54	0.008675	Complex
Clec2d	C-type lectin domain family 2, member d	1.54	0.037978	Coding
C1ql3	C1q-like 3	1.54	0.079766	Complex
Bcl2a1a	B cell leukemia/lymphoma 2 related protein A1a	1.54	0.109343	Coding
		1.54	0.176695	NonCoding
Specc1	sperm antigen with calponin homology and coiled-coil domains 1; cytospin B	1.53	0.005385	Complex
Flt4	FMS-like tyrosine kinase 4	1.53	0.023519	Complex
Tlr7	toll-like receptor 7	1.53	0.090471	Complex
Ulbp1	UL16 binding protein 1	1.53	0.095694	Coding
Samd9l	sterile alpha motif domain containing 9-like	1.53	0.357599	Coding
		1.52	0.120116	NonCoding
Tyrobp	TYRO protein tyrosine kinase binding protein	1.52	0.137837	Coding
Rtp4	receptor transporter protein 4	1.52	0.188955	Coding
		1.52	0.276675	NonCoding
Gm23536	predicted gene, 23536	1.52	0.333575	NonCoding
		1.52	0.357777	NonCoding
Gm26652	predicted gene, 26652	1.52	0.383691	NonCoding
Tfap2b	transcription factor AP-2 beta	1.51	0.027738	Complex
Ifih1	interferon induced with helicase C domain 1	1.51	0.142591	Complex
Rarb	retinoic acid receptor, beta	-1.51	0.012221	Complex
Trnp1	TMF1-regulated nuclear protein 1	-1.51	0.023945	Complex
Plp1	proteolipid protein (myelin) 1	-1.51	0.025322	Complex
Nr4a1	nuclear receptor subfamily 4, group A, member 1	-1.51	0.028479	Coding
Rnf166	ring finger protein 166	-1.51	0.029746	Complex
Nfkbia	nuclear factor of kappa light	-1.51	0.030054	Coding

	polypeptide gene enhancer in B cells inhibitor, alpha			
Gm26437	predicted gene, 26437	-1.51	0.031461	NonCoding
Zdhhc15	zinc finger, DHHC domain containing 15	-1.51	0.073282	Coding
Rnu3b4	U3B small nuclear RNA 4	-1.51	0.088601	NonCoding
Gm13105	predicted gene 13105	-1.51	0.132926	Complex
		-1.51	0.141666	NonCoding
Ccdc3	coiled-coil domain containing 3	-1.51	0.181439	Coding
Gm21860	predicted gene, 21860	-1.51	0.202291	Coding
Gm21748	predicted gene, 21748	-1.51	0.202291	Coding
mt-Ts2	mitochondrially encoded tRNA serine 2	-1.51	0.245861	NonCoding
Epha4	Eph receptor A4	-1.51	0.354087	Complex
Tmem59l	transmembrane protein 59-like	-1.52	0.008675	Coding
Mdk-ps1	midkine pseudogene 1	-1.52	0.00868	Complex
Gm21857	predicted gene, 21857	-1.52	0.0103	Complex
Cyp26b1	cytochrome P450, family 26, subfamily b, polypeptide 1	-1.52	0.026432	Coding
Dcaf12l1	DDB1 and CUL4 associated factor 12-like 1	-1.52	0.065748	Coding
Ackr3	atypical chemokine receptor 3	-1.52	0.074004	Coding
		-1.52	0.118988	NonCoding
Gm6665	predicted gene 6665	-1.52	0.135963	Coding
Gm23690	predicted gene, 23690	-1.52	0.155074	NonCoding
AW551984	expressed sequence AW551984	-1.52	0.161282	Complex
Pdgfra	platelet derived growth factor receptor, alpha polypeptide	-1.52	0.175798	Complex
Tmlhe	trimethyllysine hydroxylase, epsilon	-1.52	0.311299	Coding
Gm22130	predicted gene, 22130	-1.52	0.312939	NonCoding
		-1.52	0.369061	NonCoding
Sord	sorbitol dehydrogenase	-1.53	0.0103	Coding
Prss12	protease, serine 12 neurotrypsin (motopsin)	-1.53	0.035401	Coding
Klf4	Kruppel-like factor 4 (gut)	-1.53	0.042838	Coding
Mxd4	Max dimerization protein 4	-1.53	0.049785	Complex
Lrrn1	leucine rich repeat protein 1, neuronal	-1.53	0.090325	Complex
Gm13295	predicted gene 13295	-1.53	0.100342	Complex
Rnu11	U11 small nuclear RNA	-1.53	0.142063	NonCoding
Des	desmin	-1.53	0.155258	Complex
Msx2	msh homeobox 2; homeo box, msh-like 2	-1.53	0.156102	Coding
Gm23815	predicted gene, 23815	-1.53	0.17101	NonCoding
Gm26465	predicted gene, 26465	-1.53	0.173336	NonCoding
Gm25021	predicted gene, 25021	-1.53	0.173336	NonCoding

Gm24864	predicted gene, 24864	-1.53	0.173336	NonCoding
Gm24424	predicted gene, 24424	-1.53	0.173336	NonCoding
Gm24389	predicted gene, 24389	-1.53	0.173336	NonCoding
Serpinb9g	serine (or cysteine) peptidase inhibitor, clade B, member 9g	-1.53	0.176221	Coding
Ptprq	protein tyrosine phosphatase, receptor type, Q	-1.53	0.236494	Coding
Snord118	small nucleolar RNA, C/D box 118	-1.53	0.280828	NonCoding
Csn3	casein kappa	-1.54	0.018459	Complex
Mdk	midkine; midkine (Mdk), transcript variant 1, mRNA.	-1.54	0.021825	Coding
Wwtr1	WW domain containing transcription regulator 1	-1.54	0.034744	Coding
Id1	inhibitor of DNA binding 1	-1.54	0.041352	Coding
Gm6644	predicted gene 6644	-1.54	0.054684	Pseudogene
Hist1h1c	histone cluster 1, H1c; histone 1, H1c	-1.54	0.054695	Coding
Ptx3	pentraxin related gene	-1.54	0.071195	Complex
		-1.54	0.09568	NonCoding
Peg3	paternally expressed 3	-1.54	0.346899	Complex
Snord45b	small nucleolar RNA, C/D box 45B	-1.54	0.384319	NonCoding
Gm16418	predicted pseudogene 16418	-1.54	0.39616	Pseudogene
Krt8	keratin 8	-1.55	0.021149	Coding
Rragd	Ras-related GTP binding D	-1.55	0.048207	Complex
Gstk1	glutathione S-transferase kappa 1	-1.55	0.054695	Complex
Gm12177	predicted gene 12177	-1.55	0.067603	Complex
Tgfb2	transforming growth factor, beta 2	-1.55	0.163647	Coding
		-1.55	0.176143	NonCoding
		-1.56	0.012415	NonCoding
Lrrn4	leucine rich repeat neuronal 4	-1.56	0.013606	Complex
Dusp4	dual specificity phosphatase 4	-1.56	0.018732	Coding
Rcan1	regulator of calcineurin 1	-1.56	0.021547	Coding
Dlx5	distal-less homeobox 5	-1.56	0.023147	Coding
Tbx2	T-box 2	-1.56	0.024189	Coding
Smad6	SMAD family member 6	-1.56	0.035412	Complex
Pdgfb	platelet derived growth factor, B polypeptide	-1.56	0.046955	Coding
Tnnt2	troponin T2, cardiac	-1.56	0.048122	Coding
4833412C05Rik	RIKEN cDNA 4833412C05 gene	-1.56	0.127455	NonCoding
Grem1	gremlin 1	-1.56	0.234481	Complex
		-1.56	0.251222	NonCoding
		-1.56	0.264247	NonCoding
Gm25107	predicted gene, 25107	-1.56	0.35493	NonCoding
Scrn1	secernin 1	-1.57	0.006665	Complex

Slc43a3	solute carrier family 43, member 3	-1.57	0.008406	Complex
Ngfr	nerve growth factor receptor (TNFR superfamily, member 16)	-1.57	0.012221	Coding
Ank	progressive ankylosis	-1.57	0.021252	Complex
Anxa8	annexin A8	-1.57	0.027453	Coding
Apod	apolipoprotein D	-1.57	0.071206	Complex
Ifnz	interferon zeta	-1.57	0.111888	Coding
		-1.57	0.137222	NonCoding
		-1.57	0.222824	NonCoding
Snord111	small nucleolar RNA, C/D box 111	-1.57	0.253654	NonCoding
		-1.57	0.279724	NonCoding
Gpx7	glutathione peroxidase 7	-1.58	0.0103	Coding
Ndrg2	N-myc downstream regulated gene 2	-1.58	0.011736	Coding
Rhoj	ras homolog gene family, member J	-1.58	0.012221	Complex
Myo16	myosin XVI	-1.59	0.011736	Complex
2810047C21Rik1	RIKEN cDNA 2810047C21 gene 1	-1.59	0.012221	Complex
Gm12138	predicted gene 12138	-1.59	0.02012	Pseudogene
Chac1	ChaC, cation transport regulator 1	-1.59	0.021844	Coding
Fas	Fas (TNF receptor superfamily member 6)	-1.59	0.03111	Coding
Gm7040	predicted gene 7040	-1.59	0.040076	Coding
Gm26251	predicted gene, 26251	-1.59	0.143099	NonCoding
Cyp1b1	cytochrome P450, family 1, subfamily b, polypeptide 1	-1.59	0.189484	Coding
		-1.59	0.242176	NonCoding
		-1.59	0.367489	NonCoding
Vmn1r90	vomeronasal 1 receptor 90	-1.60	0.006574	Complex
Acot13	acyl-CoA thioesterase 13	-1.60	0.026432	Coding
Lims2	LIM and senescent cell antigen like domains 2	-1.60	0.047196	Coding
Bmp4	bone morphogenetic protein 4	-1.60	0.168775	Complex
Gm24518	predicted gene, 24518	-1.60	0.198184	NonCoding
Prr32	proline rich 32	-1.60	0.280683	Coding
Impact	impact, RWD domain protein	-1.60	0.302947	Complex
D130007C19Rik	RIKEN cDNA D130007C19 gene	-1.60	0.394347	Complex
Pmp22	peripheral myelin protein 22	-1.61	0.010973	Complex
Cdkn1a	cyclin-dependent kinase inhibitor 1A (P21)	-1.61	0.012221	Coding
Gsta4	glutathione S-transferase, alpha 4	-1.61	0.021149	Complex
Fabp3	fatty acid binding protein 3, muscle and heart	-1.61	0.025827	Coding
Gstm2	glutathione S-transferase,	-1.61	0.030189	Complex

	mu 2			
Gm13606	predicted gene 13606	-1.61	0.061815	Complex
G530011O06 Rik	RIKEN cDNA G530011O06 gene	-1.61	0.068059	NonCoding
Ly6i	lymphocyte antigen 6 complex, locus I	-1.61	0.114041	Coding
Gm12840	predicted gene 12840	-1.61	0.134048	NonCoding
Mmp13	matrix metallopeptidase 13	-1.61	0.387046	Coding
Gm6736	predicted gene 6736	-1.62	0.022682	Pseudogene
Mgst1	microsomal glutathione S-transferase 1	-1.63	0.005341	Complex
Serpinb8	serine (or cysteine) peptidase inhibitor, clade B, member 8	-1.63	0.014313	Complex
Igfbp6	insulin-like growth factor binding protein 6	-1.63	0.019098	Coding
Perp	PERP, TP53 apoptosis effector	-1.63	0.083962	Coding
Gm24310	predicted gene, 24310	-1.63	0.203398	NonCoding
DQ267102	snoRNA DQ267102	-1.64	0.109678	NonCoding
Gabrb3	gamma-aminobutyric acid (GABA) A receptor, subunit beta 3	-1.64	0.135992	Complex
Snora31	small nucleolar RNA, H/ACA box 31	-1.64	0.171789	NonCoding
Gm25934	predicted gene, 25934	-1.64	0.291397	NonCoding
Zim1	zinc finger, imprinted 1	-1.64	0.390479	Coding
Gm24289	predicted gene, 24289	-1.64	0.393882	NonCoding
F11r	F11 receptor	-1.65	0.021149	Complex
Mest	mesoderm specific transcript	-1.65	0.02163	Complex
Heg1	HEG homolog 1 (zebrafish)	-1.65	0.02333	Complex
Ddit3	DNA-damage inducible transcript 3	-1.65	0.023934	Complex
Gm11496	predicted gene 11496	-1.65	0.056358	NonCoding
Edn1	endothelin 1	-1.65	0.060793	Coding
Pcp4l1	Purkinje cell protein 4-like 1	-1.65	0.071348	Coding
Dhrs3	dehydrogenase/reductase (SDR family) member 3	-1.65	0.072086	Complex
Casp4	caspase 4, apoptosis-related cysteine peptidase	-1.65	0.292732	Complex
Myrf	myelin regulatory factor	-1.66	0.002589	Coding
Popdc2	popeye domain containing 2	-1.66	0.021149	Complex
Car3	carbonic anhydrase 3	-1.66	0.087357	Complex
Sncg	synuclein, gamma	-1.66	0.11119	Coding
Nupr1	nuclear protein transcription regulator 1	-1.67	0.012221	Complex
Gm15242	predicted gene 15242	-1.67	0.033042	Complex
Gm12892	predicted gene 12892	-1.67	0.051954	Pseudogene
Gm26230	predicted gene, 26230	-1.67	0.10993	NonCoding
Gm26498	predicted gene, 26498	-1.67	0.10993	NonCoding
Sprr2k	small proline-rich protein	-1.67	0.354951	Coding

	2K			
Prl2c5	prolactin family 2, subfamily c, member 5	-1.68	0.013826	Complex
Krt18	keratin 18	-1.68	0.014916	Coding
Serpinb6b	serine (or cysteine) peptidase inhibitor, clade B, member 6b	-1.68	0.035718	Complex
Gm6175	predicted gene 6175	-1.68	0.047339	Pseudogene
Thbd	thrombomodulin	-1.68	0.077084	Coding
Aqp5	aquaporin 5	-1.69	0.005385	Coding
Prg4	proteoglycan 4 (megakaryocyte stimulating factor, articular superficial zone protein)	-1.69	0.02854	Coding
Gm22496	predicted gene, 22496	-1.69	0.0688	NonCoding
Prex2	phosphatidylinositol-3,4,5-trisphosphate-dependent Rac exchange factor 2	-1.69	0.168246	Complex
Nnt	nicotinamide nucleotide transhydrogenase	-1.70	0.003352	Complex
Myh11	myosin, heavy polypeptide 11, smooth muscle	-1.70	0.011994	Coding
Neto1	neuropilin (NRP) and tolloid (TLL)-like 1	-1.70	0.024189	Coding
Acot2	acyl-CoA thioesterase 2	-1.70	0.039102	Coding
		-1.70	0.039102	NonCoding
		-1.70	0.039102	NonCoding
Cemip	cell migration inducing protein, hyaluronan binding	-1.71	0.023945	Complex
Sparcl1	SPARC-like 1	-1.71	0.071248	Coding
Gm26087	predicted gene, 26087	-1.71	0.267255	NonCoding
Ly96	lymphocyte antigen 96	-1.71	0.395858	Coding
Gstm1	glutathione S-transferase, mu 1	-1.72	0.011717	Coding
Mmp2	matrix metallopeptidase 2	-1.72	0.014609	Coding
Gdf6	growth differentiation factor 6	-1.72	0.014916	Coding
Pgf	placental growth factor	-1.72	0.017884	Coding
Usp11	ubiquitin specific peptidase 11	-1.73	0.014599	Complex
Cp	ceruloplasmin	-1.73	0.064458	Complex
Gm24969	predicted gene, 24969	-1.73	0.068663	NonCoding
Fabp3-ps1	fatty acid binding protein 3, muscle and heart, pseudogene 1	-1.74	0.051895	Pseudogene
Scarna8	small Cajal body-specific RNA 8	-1.74	0.314417	NonCoding
Ifi30	interferon gamma inducible protein 30	-1.75	0.006665	Coding
Dusp6	dual specificity phosphatase 6	-1.75	0.049369	Coding
Cd55	CD55 antigen	-1.75	0.133246	Complex
Gm12245	predicted gene 12245	-1.76	0.024291	Complex
Ptprb	protein tyrosine	-1.76	0.029955	Complex

	phosphatase, receptor type, B			
Snord71	small nucleolar RNA, C/D box 71	-1.76	0.306059	NonCoding
Tubb4a	tubulin, beta 4A class IVA	-1.77	0.025826	Coding
		-1.77	0.083962	NonCoding
Tnfsf18	tumor necrosis factor (ligand) superfamily, member 18	-1.77	0.125146	Coding
Rorb	RAR-related orphan receptor beta	-1.77	0.176695	Complex
Cotl1	coactosin-like 1 (Dictyostelium)	-1.78	0.072889	Complex
Qpct	glutaminyl-peptide cyclotransferase (glutaminyl cyclase)	-1.79	0.016241	Coding
Gpm6a	glycoprotein m6a	-1.79	0.020827	Complex
A630033H20 Rik	RIKEN cDNA A630033H20 gene	-1.79	0.215518	Coding
2610528A11R ik	RIKEN cDNA 2610528A11 gene	-1.80	0.011736	Complex
Cdo1	cysteine dioxygenase 1, cytosolic	-1.80	0.020827	Coding
Scel	sciellin	-1.80	0.034574	Coding
Fmod	fibromodulin	-1.80	0.133696	Coding
Scarna6	small Cajal body-specific RNA 6	-1.80	0.390479	NonCoding
Bex1	brain expressed gene 1	-1.81	0.018459	Complex
Mgst3	microsomal glutathione S-transferase 3	-1.81	0.029475	Complex
Dlx2	distal-less homeobox 2	-1.81	0.04662	Complex
Pgm5	phosphoglucomutase 5	-1.81	0.083962	Complex
Gm24983	predicted gene, 24983	-1.81	0.106914	NonCoding
Efemp1	epidermal growth factor-containing fibulin-like extracellular matrix protein 1	-1.82	0.0103	Complex
Gm21738	predicted gene, 21738	-1.82	0.033199	Coding
Sulf2	sulfatase 2	-1.82	0.112245	Complex
Ddit3	DNA-damage inducible transcript 3	-1.83	0.034853	Coding
		-1.83	0.137354	Other
Crip1	cysteine-rich protein 1 (intestinal)	-1.84	0.041352	Coding
Sfrp1	secreted frizzled-related protein 1	-1.84	0.140458	Coding
Ildr2	immunoglobulin-like domain containing receptor 2	-1.85	0.01739	Complex
Vat1l	vesicle amine transport protein 1 homolog-like (T. californica)	-1.85	0.019083	Complex
		-1.85	0.081573	Coding
Klhl24	kelch-like 24	-1.85	0.095252	Complex

H2afv	H2A histone family, member V	-1.86	0.01056	Coding
Apela	apelin receptor early endogenous ligand; novel gene	-1.86	0.013723	NonCoding
Gm22289	predicted gene, 22289	-1.87	0.017021	NonCoding
Gm11168	predicted gene 11168	-1.87	0.050922	Coding
Leprel1	leprecan-like 1	-1.88	0.009385	Complex
Parm1	prostate androgen-regulated mucin-like protein 1	-1.88	0.013723	Complex
Serpine2	serine (or cysteine) peptidase inhibitor, clade E, member 2	-1.88	0.024869	Complex
Nrk	Nik related kinase	-1.88	0.220637	Complex
Gm22422	predicted gene, 22422	-1.88	0.34072	NonCoding
2610318N02Rik	RIKEN cDNA 2610318N02 gene	-1.89	0.016472	Coding
Gm11382	predicted pseudogene 11382	-1.89	0.066342	Pseudogene
Gm25492	predicted gene, 25492	-1.89	0.095333	NonCoding
Eng	endoglin	-1.90	0.003921	Complex
Gm10719	predicted gene 10719	-1.91	0.026432	Coding
Gm10718	predicted gene 10718; predicted gene 10722	-1.92	0.036475	Complex
Dsp	desmoplakin	-1.93	0.011736	Complex
Gm25121	predicted gene, 25121	-1.95	0.067782	NonCoding
Rorb	RAR-related orphan receptor beta	-1.95	0.162511	Coding
Chchd10	coiled-coil-helix-coiled-coil-helix domain containing 10	-1.96	0.008235	Coding
Megf10	multiple EGF-like-domains 10	-1.96	0.061275	Complex
Hmox1	heme oxygenase (decycling) 1	-1.97	0.012221	Complex
Gas6	growth arrest specific 6	-1.98	0.005385	Coding
		-1.98	0.098489	NonCoding
Gm23145	predicted gene, 23145	-1.99	0.247351	NonCoding
Tinagl1	tubulointerstitial nephritis antigen-like 1	-2.00	0.00679	Complex
Clu	clusterin	-2.00	0.012632	Complex
Srpx2	sushi-repeat-containing protein, X-linked 2	-2.00	0.013723	Complex
Gm11351	predicted gene 11351	-2.00	0.182704	NonCoding
Cd34	CD34 antigen	-2.01	0.012221	Complex
Gm10715	predicted gene 10715	-2.01	0.032737	Coding
Gm17535	predicted gene, 17535	-2.01	0.040503	Coding
Lce1g	late cornified envelope 1G	-2.01	0.073604	Coding
Hspb8	heat shock protein 8	-2.03	0.009357	Complex
		-2.03	0.014329	NonCoding
Jam2	junction adhesion molecule 2	-2.03	0.021149	Complex
Gm15035	predicted gene 15035	-2.04	0.02583	Complex
Gm10720	predicted gene 10720	-2.05	0.029437	Coding

Gm10717	predicted gene 10717	-2.05	0.060156	Coding
Cdh19	cadherin 19, type 2	-2.06	0.061704	Coding
		-2.07	0.104126	NonCoding
Gm11274	predicted gene 11274	-2.09	0.012221	NonCoding
Snord89	small nucleolar RNA, C/D box 89	-2.09	0.092197	NonCoding
Gm10721	predicted gene 10721	-2.11	0.031947	Coding
Gm13086	predicted gene 13086	-2.12	0.014313	Complex
Ppargc1a	peroxisome proliferative activated receptor, gamma, coactivator 1 alpha	-2.12	0.039398	Complex
Sorbs2	sorbin and SH3 domain containing 2	-2.13	0.012221	Complex
Ptgs1	prostaglandin-endoperoxide synthase 1	-2.14	0.003508	Complex
Dlk1	delta-like 1 homolog (Drosophila)	-2.15	0.012221	Complex
		-2.15	0.02583	NonCoding
		-2.15	0.041051	NonCoding
Gm26337	predicted gene, 26337	-2.16	0.160047	NonCoding
Gm22131	predicted gene, 22131	-2.17	0.029957	NonCoding
Gm26365	predicted gene, 26365	-2.19	0.01056	NonCoding
Pdk4	pyruvate dehydrogenase kinase, isoenzyme 4	-2.19	0.019534	Complex
Ly6c1	lymphocyte antigen 6 complex, locus C1	-2.21	0.021149	Coding
Car8	carbonic anhydrase 8	-2.23	0.012163	Complex
Gm25175	predicted gene, 25175	-2.23	0.155615	NonCoding
Gm23660	predicted gene, 23660	-2.23	0.16284	NonCoding
Gm25648	predicted gene, 25648	-2.24	0.090449	NonCoding
Nqo1	NAD(P)H dehydrogenase, quinone 1	-2.25	0.006623	Coding
		-2.25	0.362625	NonCoding
Gpx3	glutathione peroxidase 3	-2.26	0.013808	Coding
Gm24495	predicted gene, 24495	-2.26	0.075069	NonCoding
Gm26097	predicted gene, 26097	-2.26	0.075781	NonCoding
Id2	inhibitor of DNA binding 2	-2.28	0.013723	Coding
Gm10800	predicted gene 10800	-2.28	0.021037	Coding
Mmp3	matrix metallopeptidase 3	-2.28	0.03816	Coding
Prl2c3	prolactin family 2, subfamily c, member 3	-2.32	0.020827	Coding
Gm23141	predicted gene, 23141	-2.32	0.035659	NonCoding
Kif1a	kinesin family member 1A	-2.33	0.003921	Complex
Stmn2	stathmin-like 2	-2.33	0.006715	Coding
Serping1	serine (or cysteine) peptidase inhibitor, clade G, member 1	-2.33	0.012221	Complex
Gm25314	predicted gene, 25314	-2.35	0.168775	NonCoding
Gm26467	predicted gene, 26467	-2.36	0.038759	NonCoding
Gm25087	predicted gene, 25087	-2.36	0.038759	NonCoding
Ly6a	lymphocyte antigen 6 complex, locus A	-2.37	0.012681	Complex
Gm23254	predicted gene, 23254	-2.37	0.066626	NonCoding

Gm25874	predicted gene, 25874	-2.38	0.05356	NonCoding
Gm25944	predicted gene, 25944	-2.39	0.026432	NonCoding
Rgs4	regulator of G-protein signaling 4	-2.4	0.011717	Complex
Upk1b	uroplakin 1B	-2.41	0.017945	Coding
Snord13	small nucleolar RNA, C/D box 13	-2.45	0.063447	NonCoding
Gm24088	predicted gene, 24088	-2.51	0.11467	NonCoding
Gm25120	predicted gene, 25120	-2.51	0.161612	NonCoding
Aldh1a1	aldehyde dehydrogenase family 1, subfamily A1	-2.53	0.002912	Coding
Crip2	cysteine rich protein 2	-2.55	0.009277	Coding
Serpinb9b	serine (or cysteine) peptidase inhibitor, clade B, member 9b	-2.55	0.019083	Coding
Snord13	small nucleolar RNA, C/D box 13	-2.56	0.042888	NonCoding
Gm24657	predicted gene, 24657	-2.56	0.107696	NonCoding
Gm23922	predicted gene, 23922	-2.56	0.107696	NonCoding
Gm22996	predicted gene, 22996	-2.56	0.107696	NonCoding
Gm24306	predicted gene, 24306	-2.59	0.310309	NonCoding
Gm24418	predicted gene, 24418	-2.60	0.024972	NonCoding
Gm24639	predicted gene, 24639	-2.60	0.024972	NonCoding
Gm23076	predicted gene, 23076	-2.60	0.024972	NonCoding
Gm25077	predicted gene, 25077	-2.60	0.024972	NonCoding
Aldh1a7	aldehyde dehydrogenase family 1, subfamily A7	-2.61	0.012221	Coding
Ptn	pleiotrophin	-2.65	0.387046	Complex
Prl2c2	prolactin family 2, subfamily c, member 2	-2.71	0.013723	Coding
Dcn	decorin	-2.72	0.015141	Complex
Atoh8	atonal homolog 8 (Drosophila)	-2.73	0.006415	Complex
Gm25157	predicted gene, 25157	-2.76	0.021149	NonCoding
Gm22941	predicted gene, 22941	-2.76	0.021149	NonCoding
Gm22258	predicted gene, 22258	-2.76	0.021149	NonCoding
Gm21887	predicted gene, 21887	-2.76	0.02513	Coding
Gm22510	predicted gene, 22510	-2.78	0.067236	NonCoding
Gm26390	predicted gene, 26390	-2.78	0.067236	NonCoding
Gm26336	predicted gene, 26336	-2.78	0.067236	NonCoding
Gm22348	predicted gene, 22348	-2.79	0.085678	NonCoding
Ly6c2	lymphocyte antigen 6 complex, locus C2	-2.80	0.014609	Coding
Gm25156	predicted gene, 25156	-2.85	0.040463	NonCoding
Gm23767	predicted gene, 23767	-2.86	0.022807	NonCoding
Gm26389	predicted gene, 26389	-2.86	0.029737	NonCoding
Gm23687	predicted gene, 23687	-2.86	0.029737	NonCoding
Gm22393	predicted gene, 22393	-2.86	0.029737	NonCoding
Gm24566	predicted gene, 24566	-2.86	0.029737	NonCoding
Gm22111	predicted gene, 22111	-2.86	0.029737	NonCoding
Gm22253	predicted gene, 22253	-2.87	0.013723	NonCoding
2610507I01Rik	RIKEN cDNA 2610507I01 gene	-2.93	0.005374	NonCoding

Gm22776	predicted gene, 22776	-2.93	0.014313	NonCoding
Gm25229	predicted gene, 25229	-2.95	0.02513	NonCoding
Gpr50	G-protein-coupled receptor 50	-2.96	0.012221	Complex
Gm22391	predicted gene, 22391	-2.97	0.035107	NonCoding
Gm24137	predicted gene, 24137	-2.97	0.035107	NonCoding
Upk3b	uroplakin 3B	-2.98	0.012221	Complex
Gm25474	predicted gene, 25474	-2.99	0.012221	NonCoding
Gm22047	predicted gene, 22047	-2.99	0.012221	NonCoding
Gm23619	predicted gene, 23619	-2.99	0.012221	NonCoding
Gm10801	predicted gene 10801	-2.99	0.012221	Complex
Gm24100	predicted gene, 24100	-3.02	0.036353	NonCoding
Gm26096	predicted gene, 26096	-3.06	0.006258	NonCoding
Gm26499	predicted gene, 26499	-3.06	0.006258	NonCoding
Erdr1	erythroid differentiation regulator 1	-3.12	0.017945	Complex
Nrn1	neuritin 1	-3.17	0.002912	Coding
Gm26200	predicted gene, 26200	-3.17	0.020827	NonCoding
Gm22851	predicted gene, 22851	-3.21	0.012221	NonCoding
Akr1c18	aldo-keto reductase family 1, member C18	-3.25	0.012722	Coding
Gm23953	predicted gene, 23953	-3.25	0.012722	NonCoding
Gm26332	predicted gene, 26332	-3.25	0.012722	NonCoding
Gm22863	predicted gene, 22863	-3.25	0.012722	NonCoding
Gm24618	predicted gene, 24618	-3.25	0.012722	NonCoding
Fabp7	fatty acid binding protein 7, brain	-3.26	0.025396	Coding
Gm25194	predicted gene, 25194	-3.28	0.014916	NonCoding
Gm26488	predicted gene, 26488	-3.28	0.019098	NonCoding
Gm24220	predicted gene, 24220	-3.28	0.019098	NonCoding
Gm25823	predicted gene, 25823	-3.30	0.018845	NonCoding
Gm25647	predicted gene, 25647	-3.30	0.018845	NonCoding
Gm25646	predicted gene, 25646	-3.30	0.021016	NonCoding
Gm25615	predicted gene, 25615	-3.35	0.012221	NonCoding
Gm24862	predicted gene, 24862	-3.39	0.02513	NonCoding
Gm23310	predicted gene, 23310	-3.39	0.02513	NonCoding
Gm25461	predicted gene, 25461	-3.39	0.02513	NonCoding
Gm15698	transcription elongation factor B (SIII), polypeptide 2 pseudogene	-3.42	0.003111	Complex
Gm25988	predicted gene, 25988	-3.47	0.013723	NonCoding
Gm25221	predicted gene, 25221	-3.47	0.013723	NonCoding
Gm23471	predicted gene, 23471	-3.47	0.013723	NonCoding
Gm23449	predicted gene, 23449	-3.47	0.013723	NonCoding
Gm25074	predicted gene, 25074	-3.49	0.011736	NonCoding
Gm24264	predicted gene, 24264	-3.51	0.008675	NonCoding
Gm25449	predicted gene, 25449	-3.52	0.050422	NonCoding
Tgfbi	transforming growth factor, beta induced	-3.62	0.083522	Complex
Gm22631	predicted gene, 22631	-3.71	0.012221	NonCoding
Gm22584	predicted gene, 22584	-3.72	0.021149	NonCoding
Gm22173	predicted gene, 22173	-3.76	0.012221	NonCoding
Gm24799	predicted gene, 24799	-3.79	0.011736	NonCoding

Gm26432	predicted gene, 26432	-3.85	0.02513	NonCoding
Gm22188	predicted gene, 22188	-3.88	0.0103	NonCoding
Gm23305	predicted gene, 23305	-3.88	0.027357	NonCoding
Gm25085	predicted gene, 25085	-3.88	0.027357	NonCoding
Gm26502	predicted gene, 26502	-4.18	0.012221	NonCoding
Gm23313	predicted gene, 23313	-4.18	0.012221	NonCoding
Gm23446	predicted gene, 23446	-4.18	0.012221	NonCoding
Gm23862	predicted gene, 23862	-4.21	0.013723	NonCoding
Gm22255	predicted gene, 22255	-4.23	0.024669	NonCoding
Gm24926	predicted gene, 24926	-4.24	0.021149	NonCoding
Gm22632	predicted gene, 22632	-4.24	0.021149	NonCoding
Gm26366	predicted gene, 26366	-4.27	0.022291	NonCoding
Gm23089	predicted gene, 23089	-4.29	0.014078	NonCoding
Gm24711	predicted gene, 24711	-4.29	0.014078	NonCoding
Gm26188	predicted gene, 26188	-4.29	0.014078	NonCoding
Gm25089	predicted gene, 25089	-4.30	0.029216	NonCoding
Gm26283	predicted gene, 26283	-4.47	0.02513	NonCoding
Gm23682	predicted gene, 23682	-4.47	0.02513	NonCoding
Gm24654	predicted gene, 24654	-4.47	0.02513	NonCoding
Gm25585	predicted gene, 25585	-4.47	0.02513	NonCoding
Gm25840	predicted gene, 25840	-4.47	0.02513	NonCoding
Gm24040	predicted gene, 24040	-4.47	0.02513	NonCoding
Gm22050	predicted gene, 22050	-4.47	0.02513	NonCoding
Gm23286	predicted gene, 23286	-4.47	0.02513	NonCoding
Gm24021	predicted gene, 24021	-4.47	0.02513	NonCoding
Gm22274	predicted gene, 22274	-4.47	0.02513	NonCoding
Gm24652	predicted gene, 24652	-4.47	0.02513	NonCoding
Gm23618	predicted gene, 23618	-4.47	0.02513	NonCoding
Gm23688	predicted gene, 23688	-4.47	0.02513	NonCoding
Gm24570	predicted gene, 24570	-4.47	0.02513	NonCoding
Gm22640	predicted gene, 22640	-4.47	0.02513	NonCoding
Gm24952	predicted gene, 24952	-4.47	0.02513	NonCoding
Gm23944	predicted gene, 23944	-4.47	0.02513	NonCoding
Gm22629	predicted gene, 22629	-4.47	0.02513	NonCoding
Gm26374	predicted gene, 26374	-4.47	0.02513	NonCoding
Gm26284	predicted gene, 26284	-4.47	0.02513	NonCoding
Gm25452	predicted gene, 25452	-4.47	0.02513	NonCoding
Gm25984	predicted gene, 25984	-4.47	0.02513	NonCoding
Gm25017	predicted gene, 25017	-4.47	0.02513	NonCoding
Gm22834	predicted gene, 22834	-4.57	0.024869	NonCoding
Gm24866	predicted gene, 24866	-4.59	0.021149	NonCoding
Gm25463	predicted gene, 25463	-4.59	0.021149	NonCoding
Gm24528	predicted gene, 24528	-4.59	0.021149	NonCoding
Gm23356	predicted gene, 23356	-4.59	0.021149	NonCoding
Gm24872	predicted gene, 24872	-4.59	0.021149	NonCoding
Gm24027	predicted gene, 24027	-4.59	0.021149	NonCoding
Gm22524	predicted gene, 22524	-4.59	0.021149	NonCoding
Gm22630	predicted gene, 22630	-4.59	0.021149	NonCoding
Gm25741	predicted gene, 25741	-4.59	0.021149	NonCoding
Gm26059	predicted gene, 26059	-4.59	0.021149	NonCoding
Gm22511	predicted gene, 22511	-4.59	0.021149	NonCoding
Gm25098	predicted gene, 25098	-4.59	0.021149	NonCoding
Gm24702	predicted gene, 24702	-4.59	0.021149	NonCoding

Gm25462	predicted gene, 25462	-4.59	0.021149	NonCoding
Gm25523	predicted gene, 25523	-4.59	0.021149	NonCoding
Gm22909	predicted gene, 22909	-4.59	0.021149	NonCoding
Gm26392	predicted gene, 26392	-4.59	0.021149	NonCoding
Gm24219	predicted gene, 24219	-4.59	0.021149	NonCoding
Gm25230	predicted gene, 25230	-4.59	0.021149	NonCoding
Gm22627	predicted gene, 22627	-4.59	0.021149	NonCoding
Gm24585	predicted gene, 24585	-4.59	0.021149	NonCoding
Gm24206	predicted gene, 24206	-4.59	0.021149	NonCoding
Gm25209	predicted gene, 25209	-4.59	0.021149	NonCoding
Gm26334	predicted gene, 26334	-4.59	0.021149	NonCoding
Gm25742	predicted gene, 25742	-4.59	0.021149	NonCoding
Gm25146	predicted gene, 25146	-4.59	0.021149	NonCoding
Gm24759	predicted gene, 24759	-4.59	0.021149	NonCoding
Gm23575	predicted gene, 23575	-4.59	0.021149	NonCoding
Gm22449	predicted gene, 22449	-4.59	0.021149	NonCoding
Gm22912	predicted gene, 22912	-4.59	0.021149	NonCoding
Gm25710	predicted gene, 25710	-4.59	0.021149	NonCoding
Gm26434	predicted gene, 26434	-4.59	0.021149	NonCoding
Gm23560	predicted gene, 23560	-4.59	0.021149	NonCoding
Gm22252	predicted gene, 22252	-4.72	0.017861	NonCoding
Snord116	small nucleolar RNA, C/D box 116	-4.79	0.012221	NonCoding
Snord116	small nucleolar RNA, C/D box 116	-4.79	0.012221	NonCoding
Snord116	small nucleolar RNA, C/D box 116	-4.79	0.012221	NonCoding
Snord116	small nucleolar RNA, C/D box 116	-4.79	0.012221	NonCoding
Snord116	small nucleolar RNA, C/D box 116	-4.79	0.012221	NonCoding
Snord116	small nucleolar RNA, C/D box 116	-4.79	0.012221	NonCoding
Snord116	small nucleolar RNA, C/D box 116	-4.79	0.012221	NonCoding
Snord116	small nucleolar RNA, C/D box 116	-4.79	0.012221	NonCoding
Snord116	small nucleolar RNA, C/D box 116	-4.79	0.012221	NonCoding
Snord116	small nucleolar RNA, C/D box 116	-4.79	0.012221	NonCoding
Snord116	small nucleolar RNA, C/D box 116	-4.79	0.012221	NonCoding
Snord116	small nucleolar RNA, C/D box 116	-4.79	0.012221	NonCoding
Snord116	small nucleolar RNA, C/D box 116	-4.79	0.012221	NonCoding
Snord116	small nucleolar RNA, C/D box 116	-4.79	0.012221	NonCoding
Snord116	small nucleolar RNA, C/D box 116	-4.79	0.012221	NonCoding
Snord116	small nucleolar RNA, C/D box 116	-4.79	0.012221	NonCoding

Snord116	small nucleolar RNA, C/D box 116	-4.79	0.012221	NonCoding
Snord116	small nucleolar RNA, C/D box 116	-4.79	0.012221	NonCoding
Snord116	small nucleolar RNA, C/D box 116	-4.79	0.012221	NonCoding
Gm26032	predicted gene, 26032	-4.84	0.012221	NonCoding
Gm22046	predicted gene, 22046	-4.84	0.012221	NonCoding
Gm25471	predicted gene, 25471	-4.84	0.012221	NonCoding
Gm25210	predicted gene, 25210	-4.84	0.012221	NonCoding
Snord116	small nucleolar RNA, C/D box 116	-5.04	0.012221	NonCoding
Snord116	small nucleolar RNA, C/D box 116	-5.04	0.012221	NonCoding
Snord116	small nucleolar RNA, C/D box 116	-5.04	0.012221	NonCoding
Snord116	small nucleolar RNA, C/D box 116	-5.04	0.012221	NonCoding
Snord116	small nucleolar RNA, C/D box 116	-5.04	0.012221	NonCoding
Snord116	small nucleolar RNA, C/D box 116	-5.04	0.012221	NonCoding
Snord116	small nucleolar RNA, C/D box 116	-5.04	0.012221	NonCoding
Snord116l1	small nucleolar RNA, C/D box 116-like 1	-5.04	0.012221	NonCoding
Snord116	small nucleolar RNA, C/D box 116	-5.04	0.012221	NonCoding
Snord116l2	small nucleolar RNA, C/D box 116-like 2	-5.04	0.012221	NonCoding
Snord116l1	small nucleolar RNA, C/D box 116-like 1	-5.04	0.012221	NonCoding
Klhl2	kelch-like 2, Mayven	-13.68	0.002912	Complex

APPENDIX B

GENES WITH DIFFERENTIAL EXPRESSION IN THE ABSENCE OF RAD51D IDENTIFIED BY RNA SEQ

Table B.1. Genes identified by RNA Seq with differential expression between *Rad51d*-proficient and *Rad51d*-deficient primary mouse embryonic fibroblast cell lines. Genes are listed in order of increasing fold change.

Gene	Fold Change (*Rad51d*-proficient v. *Rad51d*-deficient)	q value
Cd52	-11.56	1.51E-03
Ibsp	-10.88	1.51E-03
Bcl2a1b	-10.59	1.51E-03
Ncf4	-9.54	1.51E-03
Clec12a	-9.21	1.51E-03
Bcl2a1d	-9.18	1.51E-03
Cd48	-9.03	1.51E-03
Sash3	-8.88	1.51E-03
Rgs1	-8.84	1.51E-03
Hcst	-8.67	5.04E-03
Stap1	-8.45	1.51E-03
C1qa	-5.39	1.51E-03
Vav1	-5.38	2.72E-03
Spi1	-4.91	1.42E-02
Cyth4	-4.9	1.51E-03
Adgre1	-4.88	1.51E-03
Laptm5	-4.88	1.51E-03
Trem2	-4.87	1.51E-03
Dock2	-4.87	2.72E-03
C1qc	-4.86	1.51E-03
Cd36	-4.85	1.51E-03
C1qb	-4.84	1.51E-03
Hk3	-4.84	2.72E-03
Myo1f	-4.83	1.51E-03
Itgam	-4.76	1.51E-03
Rpl39l	-4.75	1.51E-03
C5ar1	-4.75	1.51E-03
Wdfy4	-4.74	1.51E-03
Ms4a6d	-4.74	3.95E-02
Fcrls	-4.73	1.51E-03
Lair1	-4.71	1.51E-03
Tyrobp	-4.69	1.51E-03
Lilrb4a	-4.64	2.72E-03
Ctss	-4.63	1.51E-03
Pld4	-4.61	3.86E-03
Fcer1g	-4.59	1.51E-03
Inpp5d	-4.58	1.51E-03
Fyb	-4.50	2.72E-03
Col2a1	-4.41	1.51E-03
Tlr13	-4.39	1.51E-03
P2ry6	-4.38	3.65E-02
Ncf1	-4.35	1.51E-03
Cd37	-4.32	3.20E-02

Lyz2	-4.31	1.51E-03
Mpeg1	-4.31	1.51E-03
Cd84	-4.26	3.86E-03
Clec4d	-4.22	1.51E-03
Adam8	-4.20	1.51E-03
Itgal	-4.17	1.51E-03
Msr1	-4.14	1.51E-03
Arhgap25	-4.07	1.51E-03
Ms4a6c	-4.07	4.08E-02
Myo1g	-4.05	1.42E-02
Fcgr3	-3.97	1.51E-03
Cybb	-3.96	1.51E-03
Nfam1	-3.96	2.72E-03
Lcp1	-3.89	9.82E-03
Parvg	-3.89	4.16E-02
Ms4a7	-3.75	1.51E-03
Arhgap4	-3.69	3.86E-03
Ptprc	-3.61	3.86E-03
Csf1r	-3.6	1.51E-03
Pik3ap1	-3.54	1.51E-03
Mmp12	-3.49	1.51E-03
Tph1	-3.43	1.51E-03
Arhgap30	-3.41	2.72E-03
C3ar1	-3.36	1.51E-03
Cd53	-3.22	1.51E-03
Tlr7	-3.22	2.72E-03
Was	-3.17	2.16E-02
Dpep2	-3.11	1.16E-02
Rad51d	-3.08	1.51E-03
Cd300lb	-3.08	1.51E-03
Mrc1	-2.89	1.51E-03
Lmo2	-2.82	1.33E-02
Alox5ap	-2.81	1.51E-03
Irf8	-2.81	1.51E-03
Fermt3	-2.8	1.51E-03
Zic4	-2.76	1.51E-03
Slc7a8	-2.75	1.51E-03
Nckap1l	-2.73	1.51E-03
Slc11a1	-2.59	1.51E-03
Ccl9	-2.55	1.51E-03
Ngfr	-2.54	1.51E-03
AI467606	-2.51	2.65E-02
Plac8	-2.48	1.51E-03
Ccl6	-2.48	2.78E-02
Dok2	-2.46	1.51E-03
Cd68	-2.41	1.51E-03
Hoxc8	-2.38	1.51E-03
Klhl6	-2.38	3.17E-02
Hmx1	-2.34	1.51E-03
Cdh23	-2.34	2.52E-02
Slamf9	-2.32	2.44E-02
Selplg	-2.26	1.16E-02
Gpr149	-2.25	1.51E-03

Ly9	-2.24	3.46E-02
Slfn2	-2.21	1.51E-03
Ptpn6	-2.19	1.51E-03
Plek	-2.16	1.51E-03
Hoxc12	-2.12	1.51E-03
Slc37a2	-2.12	1.51E-03
Hoxb6	-2.09	1.51E-03
Arl11	-2.09	1.51E-03
Tbx4	-2.08	1.51E-03
Tbxas1	-2.08	1.51E-03
Nrros	-2.07	1.51E-03
Zic1	-2.04	1.51E-03
Pycard	-2.04	7.00E-03
Tnmd	-2.02	1.51E-03
Hoxb8	-2.01	1.51E-03
Map3k7cl	-2.01	1.51E-03
Slfn8,Slfn9	-1.96	1.51E-03
Ush1g	-1.96	1.51E-03
Hoxb7	-1.94	1.51E-03
Hoxc9	-1.94	1.51E-03
Hoxc5	-1.94	1.51E-03
Ptpn18	-1.93	5.04E-03
Adh1	-1.93	3.20E-02
Smoc1	-1.91	1.51E-03
Ankrd1	-1.90	1.51E-03
Cfp	-1.87	1.51E-03
Hoxa3,Hoxa4,Hoxa5,Hoxa6	-1.85	1.51E-03
Hoxb2	-1.84	1.51E-03
Fmnl1	-1.84	1.51E-03
Ripk4	-1.84	1.51E-03
Apobec1	-1.83	1.51E-03
Hoxb3	-1.82	1.51E-03
Selp	-1.82	1.48E-02
Itgb2	-1.80	1.51E-03
Npy	-1.80	1.51E-03
C1qtnf3	-1.79	1.51E-03
Lor	-1.79	6.03E-03
Lpxn	-1.74	1.51E-03
Foxc2	-1.74	1.51E-03
Tfpi	-1.72	1.51E-03
Krt20	-1.71	1.51E-03
Gja3	-1.71	2.65E-02
Coro1a	-1.70	1.51E-03
Cd300a	-1.68	1.51E-03
Atp1a3	-1.68	1.51E-03
Alpl	-1.67	1.51E-03
Nsg2	-1.67	2.44E-02
Clca3a1	-1.66	1.51E-03
Dusp5	-1.64	1.51E-03
Trf	-1.64	1.51E-03
Adgrg5	-1.63	4.55E-02
Hoxc4	-1.62	1.51E-03
Huwe1,Mir3113	-1.62	1.51E-03

Neurl3	-1.62	2.72E-03
Slc1a6	-1.57	1.51E-03
Shtn1	-1.54	1.51E-03
Cd93	-1.54	1.51E-03
Ncf2	-1.53	1.51E-03
Sema4d	-1.53	1.51E-03
Lad1	-1.53	2.31E-02
Cfh	-1.52	2.72E-03
Ptpre	-1.51	1.51E-03
Krt7	-1.50	1.51E-03
Hoxb4	-1.49	1.51E-03
Hoxc6	-1.48	1.51E-03
Rbm20	-1.47	1.51E-03
Psd4	-1.46	1.51E-03
Tmem132e	-1.45	1.51E-03
Tll1	-1.43	1.51E-03
Grem2	-1.42	1.51E-03
Grap	-1.42	3.77E-02
Foxd1	-1.40	1.51E-03
Foxl1	-1.39	1.51E-03
Des	-1.38	1.51E-03
Egr2	-1.37	1.51E-03
Parvb	-1.37	1.51E-03
Ret	-1.36	1.51E-03
Clca3a2	-1.36	1.16E-02
Hoxb5	-1.35	3.90E-02
Meg3,Mir1906-1,Mir770	-1.33	1.51E-03
Cspg4	-1.33	1.51E-03
Ucp2	-1.31	1.51E-03
Ulbp1	-1.30	1.51E-03
Ankk1	-1.30	2.72E-03
Sp100	-1.30	4.79E-02
Irx1	-1.28	1.51E-03
Ifi27l2b	-1.28	7.00E-03
Fat3	-1.27	1.51E-03
Slfn3	-1.27	1.80E-02
Dmrta2	-1.26	1.51E-03
Hoxd4	-1.26	1.87E-02
Unc5b	-1.25	1.51E-03
Skap1	-1.25	1.51E-03
Irf5	-1.25	1.51E-03
Hecw1	-1.24	1.51E-03
Col11a2	-1.24	2.72E-03
Chst2	-1.23	1.51E-03
Amer2	-1.23	2.92E-02
Lrtm2	-1.23	3.60E-02
Sox13	-1.22	1.51E-03
Smim10l2a	-1.21	2.52E-02
Ctsh	-1.19	1.51E-03
Sorbs1	-1.18	1.51E-03
Glce,Mir5133	-1.18	1.51E-03
Gpsm3	-1.18	2.72E-03
Slc43a2	-1.17	1.51E-03

Jph2	-1.17	1.51E-03
Cacna1h	-1.16	1.51E-03
Kctd8	-1.16	1.55E-02
Ugt1a1,Ugt1a10,Ugt1a2,Ugt1a5,Ugt1a6a,Ugt1a6b,Ugt1a7c,Ugt1a9	-1.16	1.87E-02
Glipr1	-1.16	4.68E-02
Lims2	-1.15	1.51E-03
Il2rg	-1.15	7.00E-03
Coch	-1.14	1.51E-03
Serpine1	-1.14	1.51E-03
Podnl1	-1.14	1.51E-03
Pparg	-1.13	2.72E-03
Wnt2b	-1.12	1.51E-03
Rap1gap2	-1.10	1.51E-03
Foxs1	-1.09	1.51E-03
Abcc3	-1.09	2.72E-03
Nipal4	-1.08	1.51E-03
Egr1	-1.08	1.51E-03
Galnt18	-1.08	1.51E-03
Asb5	-1.08	7.91E-03
Tmem106a	-1.06	1.51E-03
Atoh8	-1.06	1.51E-03
Cxcr4	-1.06	6.03E-03
Adap1	-1.06	2.97E-02
Bcar3	-1.05	1.51E-03
Nrgn	-1.05	3.65E-02
Rasgrp3	-1.04	1.51E-03
Irx2	-1.03	1.51E-03
Hoxc10	-1.03	1.51E-03
Itpripl2	-1.03	1.51E-03
Rbm24	-1.02	1.73E-02
Ctgf	-1.01	1.51E-03
Zic2	-1.01	1.51E-03
Cd14	-1.01	1.51E-03
Scand1	-1.01	1.51E-03
Fgd3	-1.00	1.51E-03
Ereg	-1.00	7.00E-03
Klf5	-0.99	1.51E-03
Actg2	-0.99	1.51E-03
Satb1	-0.99	3.86E-03
Lat2	-0.99	1.24E-02
Pgf	-0.97	1.51E-03
Anpep	-0.96	1.51E-03
Dner	-0.96	1.08E-02
Fmn2	-0.95	1.51E-03
Tnfrsf11b	-0.95	1.51E-03
Adra2a	-0.95	1.51E-03
Hspb1	-0.95	1.51E-03
Epas1	-0.95	2.72E-03
Foxp2	-0.95	3.86E-03
En1	-0.94	1.51E-03
Exd2	-0.94	1.51E-03
Spry2	-0.94	1.51E-03

Phlda1	-0.93	1.51E-03
Msx2	-0.93	1.51E-03
Id1	-0.93	1.51E-03
Lfng	-0.92	1.51E-03
Dock8	-0.91	1.51E-03
Csrnp1	-0.91	1.51E-03
Socs2	-0.91	2.72E-03
Fbxo27	-0.91	2.24E-02
Krt19	-0.90	1.51E-03
Ltbp2	-0.90	1.51E-03
Ch25h	-0.90	1.51E-03
Rasgef1b	-0.90	2.72E-03
Myom1	-0.90	7.91E-03
AI661453	-0.90	3.20E-02
Csf1	-0.89	1.51E-03
Sntg1	-0.89	4.85E-02
Nog	-0.88	1.51E-03
Lrp2	-0.88	1.51E-03
Lyn	-0.88	1.51E-03
Mgll	-0.88	1.51E-03
Junb	-0.88	1.51E-03
Tmem238	-0.88	2.72E-03
Chsy3	-0.88	3.90E-02
Mmp17	-0.87	1.51E-03
Mcam	-0.87	1.51E-03
Ccdc68	-0.87	1.42E-02
Igsf9	-0.86	1.51E-03
S100a7a	-0.86	1.51E-03
Adcyap1r1	-0.86	1.51E-03
Thsd1	-0.86	8.90E-03
Rassf6	-0.86	1.48E-02
Epha4	-0.85	1.51E-03
Gas7	-0.85	1.51E-03
Cblb	-0.85	1.51E-03
Hoxa7,Mira	-0.85	1.51E-03
Rgs10	-0.85	7.91E-03
Ebf2	-0.85	1.48E-02
Rnaset2b	-0.85	3.03E-02
Siglecg	-0.84	1.51E-03
Mogat2	-0.84	1.51E-03
Zdbf2	-0.84	3.86E-03
Tnik	-0.84	6.03E-03
Smad9	-0.84	7.91E-03
Cited2	-0.83	1.51E-03
Klf2	-0.83	1.51E-03
Hlx	-0.83	2.72E-03
Slc35f1	-0.83	1.64E-02
Runx1	-0.82	1.51E-03
Plaur	-0.82	1.51E-03
Apoe	-0.82	1.51E-03
Fhl1	-0.82	1.51E-03
Lpl	-0.82	2.72E-03
Hck	-0.82	5.04E-03

Insl3,Jak3	-0.82	3.95E-02
Lmod1	-0.81	1.51E-03
Rgs16	-0.81	1.51E-03
Adam19	-0.81	1.51E-03
Itprip	-0.81	1.51E-03
Kdr	-0.81	1.51E-03
Flt1	-0.81	1.51E-03
Fbln2	-0.81	1.51E-03
Zfp771	-0.81	1.51E-03
Bmpr1b	-0.81	2.72E-03
Pax1	-0.81	1.55E-02
Kcnab1	-0.80	1.51E-03
Nipal1	-0.80	1.51E-03
Relt	-0.80	1.51E-03
Phlpp1	-0.79	1.51E-03
Fam20c	-0.79	1.51E-03
Gcnt4	-0.79	5.04E-03
Pcdh10	-0.78	1.51E-03
Ptprd	-0.78	2.72E-03
Ntn4	-0.78	3.86E-03
Tmcc3	-0.77	1.51E-03
Cotl1	-0.77	1.51E-03
Acan	-0.77	1.16E-02
C77370	-0.77	3.26E-02
Lrrc4c	-0.77	4.68E-02
Kctd11,Tmem95	-0.76	1.51E-03
Syk	-0.76	1.51E-03
Prodh	-0.76	1.24E-02
Stard8	-0.76	3.33E-02
Zfp703	-0.75	1.51E-03
Dlc1	-0.75	1.51E-03
Cdh10	-0.75	3.86E-03
Fosb	-0.75	6.03E-03
Slitrk5	-0.75	1.16E-02
Synpo2	-0.75	2.10E-02
Eya2	-0.75	4.41E-02
Fes	-0.74	9.82E-03
Tusc1	-0.74	1.48E-02
Zdhhc14	-0.74	3.03E-02
Twist2	-0.73	1.51E-03
Mboat2	-0.73	1.51E-03
Gadd45g	-0.73	1.51E-03
Cdk18	-0.73	7.00E-03
Sepp1	-0.73	8.90E-03
Fam84b	-0.73	2.85E-02
Ier5	-0.72	1.51E-03
Akap12	-0.72	1.51E-03
Arhgdib	-0.72	1.51E-03
Fgf13	-0.72	6.03E-03
Rtn4r	-0.72	2.16E-02
Cck	-0.72	2.24E-02
Brinp1	-0.72	2.72E-02
Arhgef28	-0.71	1.51E-03

Efnb1	-0.71	1.51E-03
Tsc22d2	-0.71	2.72E-03
Ptprz1	-0.71	8.90E-03
Slc6a17	-0.71	1.87E-02
Jag1	-0.70	6.03E-03
Vsig10l	-0.70	1.08E-02
Erc2	-0.70	2.92E-02
Dusp6	-0.69	1.51E-03
Mesdc1	-0.69	1.51E-03
Ngf	-0.69	3.86E-03
Acta2	-0.69	1.64E-02
Adamts14	-0.69	1.95E-02
Popdc2	-0.69	3.20E-02
Cyr61	-0.68	1.51E-03
Tm4sf1	-0.68	2.72E-03
Bcar1	-0.68	2.72E-03
Cpeb2	-0.68	7.00E-03
Il11	-0.68	2.78E-02
Epha2	-0.67	1.51E-03
Mical2	-0.67	1.51E-03
Ptk2b	-0.67	7.91E-03
Nptx2	-0.67	8.90E-03
Lpin3	-0.67	2.58E-02
Runx3	-0.67	3.03E-02
Chst7	-0.66	1.95E-02
Lhx9	-0.66	3.60E-02
Spata5l1	-0.66	3.77E-02
Cebpa	-0.66	3.90E-02
Smpdl3a	-0.66	4.41E-02
Flt4	-0.65	5.04E-03
Pdlim5	-0.65	1.16E-02
Arl4c	-0.65	1.48E-02
Plk2	-0.64	2.72E-03
Errfi1	-0.64	3.86E-03
Smad7	-0.64	5.04E-03
Smtn	-0.64	7.91E-03
Fbxl7	-0.64	1.24E-02
H2afj	-0.64	1.80E-02
Unc93b1	-0.64	2.72E-02
Mafb	-0.64	3.84E-02
Pla2g7	-0.64	3.90E-02
Amotl2	-0.63	7.91E-03
Sacs	-0.63	1.08E-02
Fgfr2	-0.63	1.08E-02
Ptgis	-0.63	1.16E-02
Gata6	-0.63	1.80E-02
Tbcc	-0.63	1.87E-02
Tgfb1i1	-0.62	3.86E-03
Plekhg3	-0.62	6.03E-03
Sdpr	-0.62	8.90E-03
Sirpa	-0.62	1.24E-02
Nnat	-0.62	1.48E-02
Tshz2	-0.62	3.46E-02

Klf6	-0.61	7.00E-03
Ptgs2	-0.61	7.91E-03
Crlf1	-0.61	9.82E-03
Plk3	-0.61	1.08E-02
Slc9a3r1	-0.61	1.24E-02
Adm	-0.61	1.24E-02
Bok	-0.61	1.33E-02
Rasa4	-0.61	1.33E-02
Tagln2	-0.61	1.80E-02
Tep1	-0.61	2.38E-02
Nppb	-0.61	3.40E-02
Pik3cd	-0.61	4.79E-02
Srf	-0.60	8.90E-03
Etv6	-0.60	9.82E-03
Fat1	-0.60	1.24E-02
Kalrn	-0.60	2.02E-02
Pim3	-0.60	2.16E-02
Trpv2	-0.60	3.20E-02
Ube2ql1	-0.60	4.22E-02
Anxa1	-0.59	1.80E-02
Flnb	-0.59	1.95E-02
Tpgs1	-0.59	2.31E-02
Sema7a	-0.59	4.22E-02
Foxp4	-0.58	1.42E-02
Rnf217	-0.58	1.87E-02
Nr2f6	-0.58	1.95E-02
Lama5	-0.58	2.16E-02
Zfp414	-0.58	2.97E-02
Igf1r	-0.57	1.42E-02
Bdnf	-0.57	1.55E-02
Sash1	-0.57	2.24E-02
Picalm	-0.57	2.31E-02
Plekha2	-0.57	2.52E-02
Il4ra	-0.57	2.58E-02
Ltbp4	-0.57	2.92E-02
Htr1b	-0.57	3.10E-02
Cds1	-0.57	3.72E-02
Map3k6	-0.57	4.75E-02
Nr4a1	-0.56	1.73E-02
Myh11	-0.56	1.95E-02
Sema3a	-0.56	2.16E-02
Unc5c	-0.56	2.31E-02
Ier5l	-0.56	3.17E-02
Lpp	-0.55	1.87E-02
Hbegf	-0.55	1.87E-02
Hic1	-0.55	2.02E-02
Slc16a3	-0.55	2.58E-02
Mapkapk3	-0.54	2.92E-02
Rnf19b	-0.54	2.97E-02
Specc1	-0.54	3.17E-02
Jund	-0.53	2.52E-02
Enc1	-0.53	2.58E-02
Itga5	-0.53	2.97E-02

Pdlim1	-0.53	2.97E-02
Rusc2	-0.53	2.97E-02
Cyba	-0.53	3.20E-02
Metrnl	-0.53	3.40E-02
Tgfb1	-0.53	3.54E-02
Fermt2	-0.52	3.26E-02
Tnk2	-0.52	3.33E-02
Sertad1	-0.52	3.77E-02
Scarf2	-0.52	3.84E-02
Adam9	-0.51	3.10E-02
Rhob	-0.51	3.77E-02
Arhgap31	-0.51	4.62E-02
Cdh2	-0.50	4.79E-02
Prrx1	0.49	4.79E-02
Postn	0.50	4.08E-02
Mt1	0.50	4.79E-02
Lss	0.52	3.40E-02
Il1rl1	0.52	3.65E-02
Dpp7	0.52	4.02E-02
Pmp22	0.53	3.20E-02
Cd276	0.53	3.60E-02
Tmem176b	0.53	3.95E-02
Pck2	0.54	3.20E-02
Mgst3	0.54	3.46E-02
Hmgcr	0.55	1.95E-02
Emilin1	0.55	2.10E-02
Srxn1	0.55	2.38E-02
Cav2	0.55	2.44E-02
Acat2	0.55	2.72E-02
Mdk	0.55	3.03E-02
Cdh13	0.55	4.22E-02
Fdps	0.56	1.48E-02
Akr1b3	0.56	1.80E-02
Sorcs2	0.56	2.52E-02
Acsl3,Utp14b	0.56	3.03E-02
Timp3	0.57	7.91E-03
Cd9	0.57	1.24E-02
Mvd	0.57	1.55E-02
Scd1	0.57	1.95E-02
Gorab	0.57	3.60E-02
Fkbp14	0.57	4.85E-02
Dkk2	0.58	2.97E-02
Crip2	0.58	3.17E-02
Cbr3	0.58	3.20E-02
Gsdmd	0.58	4.68E-02
Rab3d	0.58	4.97E-02
Cd248	0.59	1.24E-02
Htra1	0.59	1.24E-02
Col6a1	0.59	1.33E-02
Isyna1	0.59	1.48E-02
Acot13	0.59	1.87E-02
Arhgap28	0.59	2.31E-02
Fam213a	0.59	2.44E-02

Sema5a	0.59	2.92E-02
Pdpn	0.60	9.82E-03
Cxcl14	0.60	2.10E-02
Gpt2	0.60	2.10E-02
Ccl7	0.60	3.20E-02
Col6a2	0.61	6.03E-03
Myo1d	0.61	9.82E-03
Ogdhl	0.61	1.33E-02
Col1a2	0.61	1.42E-02
Usp18	0.61	2.02E-02
Ddit4	0.61	2.85E-02
Tmem176a	0.61	3.65E-02
Fmnl2	0.62	8.90E-03
Adora2b	0.62	3.10E-02
F2rl1	0.63	7.00E-03
Kif5c	0.63	9.82E-03
Rragd	0.63	1.08E-02
Atp9a	0.63	1.33E-02
Gdf11	0.63	1.95E-02
Gem	0.63	2.16E-02
Cd82	0.63	2.78E-02
Msmo1	0.64	1.51E-03
Add3	0.64	1.24E-02
Lhx6	0.64	2.31E-02
Tmem45a	0.64	2.38E-02
Cend1	0.64	2.65E-02
Sbsn	0.64	4.41E-02
Dnmt3a	0.65	1.51E-03
Nedd9	0.65	6.03E-03
Gpc3	0.65	7.00E-03
Itgb5	0.65	8.90E-03
Mgat3	0.65	1.42E-02
Ica1	0.65	1.42E-02
Ndrg2	0.65	1.55E-02
Gstt3	0.65	3.46E-02
Oaf	0.66	2.72E-03
Fam129a	0.66	5.04E-03
Lamc2	0.66	1.55E-02
Nsg1	0.66	1.64E-02
Sesn1	0.66	1.73E-02
Tob1	0.66	2.44E-02
Oplah	0.66	3.33E-02
Sat1	0.67	2.72E-03
Pde4b	0.67	6.03E-03
Xaf1	0.67	7.00E-03
Irx3	0.67	7.91E-03
Casp12	0.67	2.78E-02
Idh1	0.68	2.72E-03
Mir5114,Scd2	0.68	2.72E-03
Hspb8	0.68	2.72E-03
Prrg3	0.68	1.33E-02
Dhrs3	0.68	2.16E-02
Sim2	0.68	3.20E-02

Ubc	0.68	3.65E-02
Slc13a5	0.68	4.97E-02
Isg15	0.69	3.86E-03
Il17rd	0.69	6.03E-03
Dixdc1	0.69	3.20E-02
Adgrb2	0.69	4.92E-02
Cthrc1	0.70	1.51E-03
Igsf10	0.70	7.00E-03
Slc30a4	0.71	1.51E-03
Tubb3	0.71	1.51E-03
Tns2	0.71	2.72E-03
Nsdhl	0.71	2.72E-03
Fkbp7	0.71	1.08E-02
Nfkbie	0.71	1.33E-02
Itgb3	0.71	1.48E-02
Bdh2	0.71	3.65E-02
Net1	0.72	1.51E-03
Cdkn2b	0.72	1.51E-03
Insig1	0.72	1.51E-03
Ntn1	0.72	3.86E-03
Nnt	0.73	1.51E-03
Pdlim2	0.73	1.51E-03
Ephb3	0.73	1.51E-03
Crip1	0.73	6.03E-03
Slc2a6	0.73	1.80E-02
Sesn3	0.73	2.78E-02
Mfap4	0.74	1.51E-03
Rhoj	0.74	1.51E-03
Osmr	0.74	1.51E-03
Tnn	0.74	3.86E-03
Clmp	0.74	3.86E-03
Apol9a	0.74	1.16E-02
Sfrp1	0.75	1.51E-03
Itm2a	0.75	1.51E-03
Adamts2	0.75	2.72E-03
Ptprb	0.75	6.03E-03
Sorbs2	0.75	1.16E-02
Cth	0.75	1.87E-02
Wnt10b	0.75	2.44E-02
Alx1	0.75	3.77E-02
Mylip	0.75	4.02E-02
Sqrdl	0.76	1.51E-03
Fgf10	0.76	5.04E-03
Arhgef3	0.76	7.00E-03
Gadd45a	0.76	7.00E-03
Mtus2	0.76	7.91E-03
Crem	0.76	9.82E-03
Hsd17b7	0.77	1.51E-03
Abca1	0.77	1.51E-03
Cxcl10	0.77	1.51E-03
Il18rap	0.77	5.04E-03
Lrrn4cl	0.77	1.33E-02
Usp2	0.77	2.58E-02

Acsl6	0.77	2.85E-02
Adcy5	0.77	3.03E-02
Stat2	0.78	1.51E-03
Igfbp6	0.78	1.51E-03
Lrrc15	0.78	1.51E-03
Sulf2	0.78	1.51E-03
Il13ra1	0.78	1.51E-03
Cdo1	0.78	2.72E-03
Ifit3	0.78	7.91E-03
Ntf3	0.78	1.64E-02
Hist1h2ac	0.78	1.73E-02
Gchfr	0.78	4.41E-02
Gxylt2	0.79	1.51E-03
Cdon	0.79	1.51E-03
Ephb6	0.79	8.90E-03
Gbp3	0.79	2.97E-02
Cdkn2a	0.80	1.51E-03
Ppfibp2	0.80	1.51E-03
Mmp2	0.80	1.51E-03
Rftn2	0.80	7.00E-03
Rgs17	0.81	1.51E-03
Cyp51	0.81	1.51E-03
Slc16a2	0.81	1.51E-03
Hhip	0.81	2.72E-03
Arhgap6	0.81	5.04E-03
Scn1b	0.81	7.00E-03
Lifr	0.81	3.72E-02
Dhcr24	0.82	1.51E-03
Srpx2	0.82	1.51E-03
Ccdc106	0.82	6.03E-03
Heph	0.82	1.73E-02
Tceal5	0.82	3.95E-02
Igfbp4	0.83	1.51E-03
Apol9b	0.83	3.86E-03
Mir22,Mir22hg,Tlcd2	0.83	6.03E-03
Cped1	0.83	6.03E-03
Pdgfrl	0.83	2.72E-02
Rgs4	0.84	1.51E-03
Tbx2	0.84	1.51E-03
Tmem53	0.84	3.33E-02
Lypd6	0.84	4.36E-02
Ralgds	0.85	1.51E-03
Camk1d	0.85	1.51E-03
Bpgm	0.85	1.51E-03
Fam117a	0.85	1.48E-02
Fbxo32	0.86	1.51E-03
Col5a3	0.86	1.51E-03
Atp10d	0.86	2.58E-02
Cacna1g	0.87	1.51E-03
Mxd4	0.87	1.51E-03
Lrrn1	0.87	4.97E-02
Ackr3	0.88	1.51E-03
Serpinb2	0.88	1.51E-03

Sfrp2	0.88	1.51E-03
Pappa	0.88	1.51E-03
Abat	0.88	5.04E-03
Lgi2	0.88	3.60E-02
Rhof	0.88	4.29E-02
Ccl5	0.89	1.51E-03
Plcl2	0.89	1.51E-03
Mfap2	0.89	1.51E-03
Tuba8	0.89	1.51E-03
Stard10	0.89	1.51E-03
Arhgap18	0.89	2.72E-03
Igfbp2	0.90	1.51E-03
Lpin1	0.90	1.51E-03
Sqle	0.90	1.51E-03
Pgm5	0.90	3.86E-03
Camk4	0.90	7.91E-03
Atcay	0.90	1.24E-02
Idi1	0.91	1.51E-03
Nfatc4	0.91	1.51E-03
Pcdh17	0.91	1.51E-03
Wbscr27	0.91	7.91E-03
Dact1	0.92	1.51E-03
C1qtnf6	0.92	1.51E-03
Ociad2	0.92	1.51E-03
Mgp	0.92	1.51E-03
Homer2	0.92	1.51E-03
Htra3	0.92	2.44E-02
Gstt1	0.92	2.58E-02
Arap1	0.93	1.51E-03
Hspa1a,Hspa1b	0.94	1.51E-03
Acss2	0.94	1.51E-03
Tmsb15b1,Tmsb15b2,Tmsb15l	0.94	4.79E-02
H19,Mir675	0.95	1.51E-03
Erdr1	0.95	1.51E-03
Lama4	0.96	1.51E-03
Rgcc	0.97	3.86E-03
Wnt16	0.97	5.04E-03
Cpxm1	0.98	1.51E-03
Nkd1	0.98	2.72E-03
Sema6b	0.98	3.86E-03
Efemp1	0.99	1.51E-03
Irf1	0.99	1.51E-03
Serpina3f,Serpina3g,Serpina3h	0.99	1.51E-03
Hmgcs1	0.99	1.51E-03
Cdhr1	0.99	1.51E-03
Stmn2	0.99	1.51E-03
Car5b	0.99	1.51E-03
Zfp423	0.99	2.02E-02
Tmem26	0.99	2.10E-02
Ogn	0.99	2.65E-02
Msx1os	1.00	1.51E-03
Lmcd1	1.00	1.51E-03
Scd3	1.00	3.86E-03

Pacrg	1.00	1.80E-02
Itga4	1.01	1.51E-03
Mir5625,Slc35f6	1.01	1.51E-03
Nupr1	1.01	1.51E-03
Mt2	1.01	1.51E-03
Plcb1	1.01	1.48E-02
Rtn4rl2	1.01	2.85E-02
Hapln4	1.01	3.03E-02
Gng7	1.02	1.51E-03
Nkd2	1.02	1.51E-03
Hs3st1	1.02	1.51E-03
Sgsm1	1.02	1.51E-03
A4galt	1.02	2.78E-02
Aldh1l2	1.03	1.51E-03
Mcpt8	1.03	1.51E-03
Grem1	1.03	1.51E-03
Ppargc1a	1.03	1.51E-03
Bace2	1.03	6.03E-03
Clstn3	1.03	3.65E-02
Hmcn1	1.04	1.51E-03
Kank4	1.04	1.16E-02
Vnn1	1.04	2.16E-02
Eva1c	1.05	7.00E-03
Cst6	1.06	1.51E-03
Pde7b	1.06	9.82E-03
Map1a	1.07	1.51E-03
Sprr1a	1.07	1.51E-03
Penk	1.07	1.51E-03
Galnt16	1.07	2.72E-03
Rgs6	1.07	9.82E-03
Pax3	1.08	1.51E-03
Efs	1.08	1.51E-03
Rtp4	1.08	1.51E-03
Slc6a12	1.08	7.91E-03
Ifit1	1.09	1.51E-03
Ephx1	1.10	1.51E-03
Ccl2	1.10	1.51E-03
Oasl2	1.10	1.51E-03
Gprasp2	1.10	3.20E-02
Il1rn	1.11	1.51E-03
Sstr4	1.11	1.51E-03
Mir7025,Pdgfra	1.11	1.51E-03
Gas2	1.11	1.51E-03
Dpp4	1.11	3.86E-03
Emilin2	1.12	1.51E-03
Fam180a	1.13	1.51E-03
Slc7a3	1.13	1.51E-03
Enpp3	1.13	2.16E-02
Btn1a1	1.13	2.72E-02
Stc1	1.14	1.51E-03
Mab21l2	1.14	1.51E-03
Angpt1	1.14	2.85E-02
Gas1	1.16	1.51E-03

Card10	1.16	1.51E-03
C3	1.17	2.72E-03
Sv2c	1.17	6.03E-03
Efna1	1.18	3.86E-03
Ptgs1	1.20	1.51E-03
Plb1	1.20	1.48E-02
Igfbp3	1.21	1.51E-03
Plat	1.21	1.51E-03
Fxyd6	1.21	1.51E-03
Ppl	1.22	1.51E-03
Mgst1	1.22	1.51E-03
Tmem35	1.22	1.51E-03
Shox2	1.23	1.51E-03
Bcl3	1.23	1.51E-03
Myo16	1.23	1.51E-03
Hmx3	1.24	9.82E-03
Gria1	1.25	1.51E-03
Wnt9a	1.25	1.51E-03
C1qtnf1	1.25	1.51E-03
C1s1	1.25	1.51E-03
Crnde	1.25	3.86E-03
Fgf18	1.25	2.02E-02
Tmem179	1.25	2.85E-02
Agbl3	1.25	4.29E-02
Nrep	1.26	1.51E-03
Doc2b	1.26	2.31E-02
Spock3	1.27	1.51E-03
Col3a1	1.28	1.51E-03
Gsta4	1.28	1.51E-03
Sparcl1	1.28	4.97E-02
Tmem119	1.29	1.51E-03
Snca	1.29	1.51E-03
Kcnj2	1.30	1.51E-03
Pdlim4	1.31	1.51E-03
Tmem108	1.31	1.51E-03
C1rl	1.31	9.82E-03
Acpp	1.31	1.95E-02
Drc1	1.31	2.72E-02
Hspb7	1.31	4.55E-02
Gsc	1.34	1.51E-03
Prss12	1.34	1.51E-03
Spp1	1.35	1.51E-03
Axin2	1.36	1.51E-03
Capn6	1.36	1.51E-03
Hist1h3d	1.37	2.72E-03
Sybu	1.38	2.16E-02
Mst1r	1.38	3.03E-02
Fndc1	1.39	1.51E-03
Tenm4	1.39	1.51E-03
Nkain4	1.39	1.24E-02
Fam13c	1.39	2.72E-02
Mmp10	1.40	1.51E-03
Cygb	1.41	3.26E-02

Cxcl1	1.41	3.90E-02
Afap1l2	1.42	1.51E-03
Mmp9	1.42	1.51E-03
Prph	1.43	1.51E-03
Tgfbi	1.44	1.51E-03
Adamts8	1.44	7.00E-03
Fhod3	1.44	2.24E-02
Dnm1	1.45	1.51E-03
Ifi44	1.45	1.51E-03
C130074G19Rik	1.45	1.55E-02
Notch3	1.46	1.51E-03
Prelp	1.47	1.51E-03
Tm4sf4	1.47	1.16E-02
Prss35	1.48	1.51E-03
Fap	1.49	1.51E-03
Rasl10b	1.50	1.51E-03
Fam189a2	1.50	4.79E-02
Arsi	1.51	2.38E-02
Ahrr	1.52	1.51E-03
Rarb	1.52	1.51E-03
Glrb	1.52	1.51E-03
Il33	1.52	6.03E-03
Tbx5	1.53	1.51E-03
Lgi3	1.53	7.91E-03
Serping1	1.54	1.51E-03
Crabp2,Isg20l2	1.54	1.51E-03
Ptx3	1.55	1.51E-03
Muc1	1.55	2.72E-03
AI606473	1.56	1.51E-03
AW551984	1.58	1.51E-03
Mab21l1	1.58	2.38E-02
Igfbp5	1.61	1.51E-03
Gna14	1.61	7.00E-03
Zbp1	1.63	4.08E-02
Eln	1.64	1.51E-03
Serpinb1a	1.66	3.86E-03
Wnt10a	1.66	2.38E-02
Gfra2	1.70	1.51E-03
Ly6a	1.70	1.51E-03
Anxa8	1.71	1.51E-03
Enox1	1.71	8.90E-03
Lhx8	1.73	1.51E-03
Dcn	1.74	1.51E-03
Hopx	1.74	1.16E-02
Dkk3	1.77	1.51E-03
Cd34	1.79	1.51E-03
Gdf10	1.79	1.51E-03
Osr2	1.80	1.51E-03
LOC102636514	1.82	1.51E-03
Kcnip1	1.83	1.51E-03
Ptn	1.84	1.51E-03
Tnfsf18	1.85	1.51E-03
Itgbl1	1.85	1.51E-03

Tspan11	1.86	1.51E-03
Vat1l	1.87	1.51E-03
Ly6c2	1.90	2.72E-03
Wisp2	1.92	1.51E-03
Sod3	1.97	1.51E-03
Casp4	1.99	1.51E-03
Ptgfr	2.02	1.51E-03
Rab40b	2.02	2.44E-02
Cpxm2	2.04	1.51E-03
Eda2r	2.04	1.24E-02
Medag	2.05	1.51E-03
Icam1	2.05	1.51E-03
Barx1	2.06	1.51E-03
Pamr1	2.06	1.51E-03
Gdf5	2.06	2.72E-03
Gdf7	2.08	1.51E-03
Lgr5	2.08	2.72E-03
Ly6c1	2.12	1.51E-03
Akr1c18	2.15	1.51E-03
Mmp3	2.16	1.51E-03
Gda	2.18	1.51E-03
Dpep1	2.18	1.51E-03
Aqp5	2.19	1.51E-03
Dlx5	2.20	1.51E-03
Gpr50	2.27	1.51E-03
Aspn	2.29	1.51E-03
Podn	2.33	8.90E-03
B4galnt2	2.40	9.82E-03
Ccdc3	2.43	1.51E-03
Mrgprf	2.43	1.51E-03
Calcb	2.44	3.95E-02
Lum	2.47	1.51E-03
Gabra3	2.47	6.03E-03
Tac1	2.62	1.51E-03
Faim2	2.68	3.86E-03
Fndc5	2.69	2.24E-02
Dlx6	3.05	3.86E-03
Stra6	3.17	1.51E-03

APPENDIX C

RAD51D AND RNF138 EXPRESSION CONSTRUCTS

Table C.1. Prokaryotic expression constructs.

Construct (pUC19 vector)	Amino Acid Substitutions	Cloning Site	Resistance
RAD51D-WT	Residues 4 – 329	*Kpn*I, *Bam*HI	Ampicillin
RAD51D-K24R	Residues 4 – 329, mutant	*Kpn*I, *Bam*HI	Ampicillin
RAD51D-K26R	Residues 4 – 329, mutant	*Kpn*I, *Bam*HI	Ampicillin
RAD51D-K42R	Residues 4 – 329, mutant	*Kpn*I, *Bam*HI	Ampicillin
RAD51D-K48R	Residues 4 – 329, mutant	*Kpn*I, *Bam*HI	Ampicillin
RAD51D-K76R	Residues 4 – 329, mutant	*Kpn*I, *Bam*HI	Ampicillin
RAD51D-K91R	Residues 4 – 329, mutant	*Kpn*I, *Bam*HI	Ampicillin
RAD51D-K159R	Residues 4 – 329, mutant	*Kpn*I, *Bam*HI	Ampicillin
RAD51D-K201R	Residues 4 – 329, mutant	*Kpn*I, *Bam*HI	Ampicillin
RAD51D-K235R	Residues 4 – 329, mutant	*Kpn*I, *Bam*HI	Ampicillin
RAD51D-K261R	Residues 4 – 329, mutant	*Kpn*I, *Bam*HI	Ampicillin
RAD51D-K298R	Residues 4 – 329, mutant	*Kpn*I, *Bam*HI	Ampicillin
RAD51D-K327R	Residues 4 – 329, mutant	*Kpn*I, *Bam*HI	Ampicillin
RAD51D-K0	Residues 4 – 329, mutant	*Kpn*I, *Bam*HI	Ampicillin
RAD51D-K298	Residues 4 – 329, mutant	*Kpn*I, *Bam*HI	Ampicillin
RAD51D-K235K298 DoubleLys	Residues 4 – 329, mutant	*Kpn*I, *Bam*HI	Ampicillin
RNF138-A236G	Residues 1 – 246, mutant	*Kpn*I, *Bam*HI	Ampicillin
RNF138-S240A	Residues 1 -246, mutant	*Kpn*I, *Bam*HI	Ampicillin
RNF138-S240Q	Residues 1 – 246, mutant	*Kpn*I, *Bam*HI	Ampicillin
RNF138-Deletion	Residues 1 – 246, mutant	*Kpn*I, *Bam*HI	Ampicillin
RNF138-A236GS240A	Residues 1 – 246, mutant	*Kpn*I, *Bam*HI	Ampicillin

Table C.2. Eukaryotic expression constructs.

Construct (pcDNA3.1 vector)	Amino Acid Substitutions	Cloning Site	Resistance
Myc-RAD51D-WT	Residues 4 – 329	*Kpn*I, *Bam*HI	Ampicillin Hygromycin
Myc-RAD51D-K24R	Residues 4 – 329, mutant	*Kpn*I, *Bam*HI	Ampicillin Hygromycin
Myc-RAD51D-K26R	Residues 4 – 329, mutant	*Kpn*I, *Bam*HI	Ampicillin Hygromycin
Myc-RAD51D-K42R	Residues 4 – 329, mutant	*Kpn*I, *Bam*HI	Ampicillin Hygromycin
Myc-RAD51D-K48R	Residues 4 – 329, mutant	*Kpn*I, *Bam*HI	Ampicillin Hygromycin
Myc-RAD51D-K76R	Residues 4 – 329, mutant	*Kpn*I, *Bam*HI	Ampicillin Hygromycin
Myc-RAD51D-K91R	Residues 4 – 329, mutant	*Kpn*I, *Bam*HI	Ampicillin Hygromycin
Myc-RAD51D-K159R	Residues 4 – 329, K159R	*Kpn*I, *Bam*HI	Ampicillin Hygromycin
Myc-RAD51D-K201R	Residues 4 – 329, mutant	*Kpn*I, *Bam*HI	Ampicillin Hygromycin
Myc-RAD51D-K235R	Residues 4 – 329, mutant	*Kpn*I, *Bam*HI	Ampicillin Hygromycin
Myc-RAD51D-K261R	Residues 4 – 329, mutant	*Kpn*I, *Bam*HI	Ampicillin Hygromycin
Myc-RAD51D-K298R	Residues 4 – 329, mutant	*Kpn*I, *Bam*HI	Ampicillin Hygromycin
Myc-RAD51D-K327R	Residues 4 – 329, mutant	*Kpn*I, *Bam*HI	Ampicillin Hygromycin
Myc-RAD51D-K0	Residues 4 – 329, mutant	*Kpn*I, *Bam*HI	Ampicillin Hygromycin
Myc-RAD51D-K298	Residues 4 – 329, mutant	*Kpn*I, *Bam*HI	Ampicillin Hygromycin
HA-RAD51D-WT	Residues 4 – 329	*Kpn*I, *Bam*HI	Ampicillin Hygromycin
HA-RAD51D-K0	Residues 4 – 329, mutant	*Kpn*I, *Bam*HI	Ampicillin Hygromycin
Myc-RAD51D-Cterm	Residues 4 – 329, mutant	*Kpn*I, *Bam*HI	Ampicillin Hygromycin
Myc-RAD51D-Nterm	Residues 4 – 329, mutant	*Kpn*I, *Bam*HI	Ampicillin Hygromycin
Myc-RAD51D-K235RK298R DoubleArg	Residues 4 – 329, mutant	*Kpn*I, *Bam*HI	Ampicillin Hygromycin
Myc-RAD51D-K235K298 DoubleLys	Residues 4 – 329, mutant	*Kpn*I, *Bam*HI	Ampicillin Hygromycin

Table C.3. Yeast expression constructs.

Construct	Amino Acid Substitutions	Cloning Site	Resistance	Drop Out Supplement
pGADT7-RAD51D-K24R	Residues 4 – 329, mutant	*Eco*RI, *Bam*HI	Ampicillin	-Leu
pGADT7-RAD51D-K26R	Residues 4 – 329, mutant	*Eco*RI, *Bam*HI	Ampicillin	-Leu
pGADT7-RAD51D-K42R	Residues 4 – 329, mutant	*Eco*RI, *Bam*HI	Ampicillin	-Leu
pGADT7-RAD51D-K48R	Residues 4 – 329, mutant	*Eco*RI, *Bam*HI	Ampicillin	-Leu
pGADT7-RAD51D-K76R	Residues 4 – 329, mutant	*Eco*RI, *Bam*HI	Ampicillin	-Leu
pGADT7-RAD51D-K91R	Residues 4 – 329, mutant	*Eco*RI, *Bam*HI	Ampicillin	-Leu
pGADT7-RAD51D-K159R	Residues 4 – 329, mutant	*Eco*RI, *Bam*HI	Ampicillin	-Leu
pGADT7-RAD51D-K201R	Residues 4 – 329, mutant	*Eco*RI, *Bam*HI	Ampicillin	-Leu
pGADT7-RAD51D-K235R	Residues 4 – 329, mutant	*Eco*RI, *Bam*HI	Ampicillin	-Leu
pGADT7-RAD51D-K261R	Residues 4 – 329, mutant	*Eco*RI, *Bam*HI	Ampicillin	-Leu
pGADT7-RAD51D-K298R	Residues 4 – 329, mutant	*Eco*RI, *Bam*HI	Ampicillin	-Leu
pGADT7-RAD51D-K327R	Residues 4 – 329, mutant	*Eco*RI, *Bam*HI	Ampicillin	-Leu
pGBKT7-RAD51D-K76R	Residues 4 – 329, mutant	*Eco*RI, *Bam*HI	Kanamycin	-Trp
pGBKT7-RAD51D-K201R	Residues 4 – 329, mutant	*Eco*RI, *Bam*HI	Kanamycin	-Trp
pGBKT7-RAD51D-K235R	Residues 4 – 329, mutant	*Eco*RI, *Bam*HI	Kanamycin	-Trp
pGBKT7-RAD51D-K298R	Residues 4 – 329, mutant	*Eco*RI, *Bam*HI	Kanamycin	-Trp
pGBKT7-RAD51D-K0	Residues 4 – 329, mutant	*Eco*RI, *Bam*HI	Kanamycin	-Trp

Table C.4. Fluorescent expression constructs.

Construct (pEGFP-C1 vector)	Amino Acid Substitutions	Cloning Site	Resistance
EGFP-RAD51D-WT	Residues 4 – 329, EGFP C-terminal fusion	*Kpn*I, *Bam*HI	Kanamycin
EGFP-RAD51D-K201R	Residues 4 – 329, mutant, EGFP C-terminal fusion	*Kpn*I, *Bam*HI	Kanamycin
EGFP-RAD51D-K235R	Residues 4 – 329, mutant, EGFP C-terminal fusion	*Kpn*I, *Bam*HI	Kanamycin
EGFP-RAD51D-K298R	Residues 4 – 329, mutant, EGFP C-terminal fusion	*Kpn*I, *Bam*HI	Kanamycin
EGFP-RAD51D-K0	Residues 4 – 329, Mutant, EGFP C-terminal fusion	*Kpn*I, *Bam*HI	Kanamycin
EGFP-RAD51D-Cpep-WT	Residues 225 – 329, EGFP C-terminal fusion	*Kpn*I, *Bam*HI	Kanamycin
EGFP-RAD51D-Cpep-K235R	Residues 225 – 329, mutant, EGFP C-terminal fusion	*Kpn*I, *Bam*HI	Kanamycin
EGFP-RAD51D-Cpep-K298R	Residues 225 – 329, mutant, EGFP C-terminal fusion	*Kpn*I, *Bam*HI	Kanamycin
EGFP-RAD51D-Cpep-K0	Residues 225 – 329, mutant, EGFP C-terminal fusion	*Kpn*I, *Bam*HI	Kanamycin
EGFP-RAD51D-Cpep-K235 Only	Residues 225 – 329, mutant, EGFP C-terminal fusion	*Kpn*I, *Bam*HI	Kanamycin
EGFP-RAD51D-Cpep-K298 Only	Residues 225 – 329, mutant, EGFP C-terminal fusion	*Kpn*I, *Bam*HI	Kanamycin
EGFP-RAD51D-Cpep-DoubleLys	Residues 225 – 329, mutant, EGFP C-terminal fusion	*Kpn*I, *Bam*HI	Kanamycin

APPENDIX D

PERMISSION TO REPRINT DATA IN CHAPTER 3

APPENDIX E

PERMISSION TO REPRINT DATA IN CHAPTER 5

JOHN WILEY AND SONS LICENSE
TERMS AND CONDITIONS

Jan 26, 2018

This Agreement between University of South Carolina -- Nicole Reilly ("You") and John Wiley and Sons ("John Wiley and Sons") consists of your license details and the terms and conditions provided by John Wiley and Sons and Copyright Clearance Center.

License Number	4276590643112
License date	Jan 26, 2018
Licensed Content Publisher	John Wiley and Sons
Licensed Content Publication	Environmental and Molecular Mutagenesis
Licensed Content Title	Thiopurine-induced mitotic catastrophe in Rad51d-deficient mammalian cells
Licensed Content Author	Michael D. Wyatt,Nicole M. Reilly,Shikha Patel,Preeti Rajesh,Gary P. Schools,Phillip G. Smiraldo,Douglas L. Pittman
Licensed Content Date	Sep 25, 2017
Licensed Content Pages	11
Type of use	Dissertation/Thesis
Requestor type	Author of this Wiley article
Format	Print and electronic
Portion	Full article
Will you be translating?	No
Title of your thesis / dissertation	Mechanisms of RAD51D-Dependent Repair of DNA Damage Induced by Interstrand Crosslinking Agents and Thiopurines
Expected completion date	Jan 2018
Expected size (number of pages)	237
Requestor Location	University of South Carolina 715 Sumter Street Columbia UNIVERSITY, SC 29208 United States Attn: University of South Carolina
Publisher Tax ID	EU826007151
Total	0.00 USD
Terms and Conditions	

TERMS AND CONDITIONS

This copyrighted material is owned by or exclusively licensed to John Wiley & Sons, Inc. or one of its group companies (each a"Wiley Company") or handled on behalf of a society with which a Wiley Company has exclusive publishing rights in relation to a particular work

(collectively "WILEY"). By clicking "accept" in connection with completing this licensing transaction, you agree that the following terms and conditions apply to this transaction (along with the billing and payment terms and conditions established by the Copyright Clearance Center Inc., ("CCC's Billing and Payment terms and conditions"), at the time that you opened your RightsLink account (these are available at any time at http://myaccount.copyright.com).

Terms and Conditions

- The materials you have requested permission to reproduce or reuse (the "Wiley Materials") are protected by copyright.

- You are hereby granted a personal, non-exclusive, non-sub licensable (on a stand-alone basis), non-transferable, worldwide, limited license to reproduce the Wiley Materials for the purpose specified in the licensing process. This license, **and any CONTENT (PDF or image file) purchased as part of your order,** is for a one-time use only and limited to any maximum distribution number specified in the license. The first instance of republication or reuse granted by this license must be completed within two years of the date of the grant of this license (although copies prepared before the end date may be distributed thereafter). The Wiley Materials shall not be used in any other manner or for any other purpose, beyond what is granted in the license. Permission is granted subject to an appropriate acknowledgement given to the author, title of the material/book/journal and the publisher. You shall also duplicate the copyright notice that appears in the Wiley publication in your use of the Wiley Material. Permission is also granted on the understanding that nowhere in the text is a previously published source acknowledged for all or part of this Wiley Material. Any third party content is expressly excluded from this permission.

- With respect to the Wiley Materials, all rights are reserved. Except as expressly granted by the terms of the license, no part of the Wiley Materials may be copied, modified, adapted (except for minor reformatting required by the new Publication), translated, reproduced, transferred or distributed, in any form or by any means, and no derivative works may be made based on the Wiley Materials without the prior permission of the respective copyright owner.**For STM Signatory Publishers clearing permission under the terms of the STM Permissions Guidelines only, the terms of the license are extended to include subsequent editions and for editions in other languages, provided such editions are for the work as a whole in situ and does not involve the separate exploitation of the permitted figures or extracts,** You may not alter, remove or suppress in any manner any copyright, trademark or other notices displayed by the Wiley Materials. You may not license, rent, sell, loan, lease, pledge, offer as security, transfer or assign the Wiley Materials on a stand-alone basis, or any of the rights granted to you hereunder to any other person.

- The Wiley Materials and all of the intellectual property rights therein shall at all times remain the exclusive property of John Wiley & Sons Inc, the Wiley Companies, or their respective licensors, and your interest therein is only that of having possession of

and the right to reproduce the Wiley Materials pursuant to Section 2 herein during the continuance of this Agreement. You agree that you own no right, title or interest in or to the Wiley Materials or any of the intellectual property rights therein. You shall have no rights hereunder other than the license as provided for above in Section 2. No right, license or interest to any trademark, trade name, service mark or other branding ("Marks") of WILEY or its licensors is granted hereunder, and you agree that you shall not assert any such right, license or interest with respect thereto

- NEITHER WILEY NOR ITS LICENSORS MAKES ANY WARRANTY OR REPRESENTATION OF ANY KIND TO YOU OR ANY THIRD PARTY, EXPRESS, IMPLIED OR STATUTORY, WITH RESPECT TO THE MATERIALS OR THE ACCURACY OF ANY INFORMATION CONTAINED IN THE MATERIALS, INCLUDING, WITHOUT LIMITATION, ANY IMPLIED WARRANTY OF MERCHANTABILITY, ACCURACY, SATISFACTORY QUALITY, FITNESS FOR A PARTICULAR PURPOSE, USABILITY, INTEGRATION OR NON-INFRINGEMENT AND ALL SUCH WARRANTIES ARE HEREBY EXCLUDED BY WILEY AND ITS LICENSORS AND WAIVED BY YOU.

- WILEY shall have the right to terminate this Agreement immediately upon breach of this Agreement by you.

- You shall indemnify, defend and hold harmless WILEY, its Licensors and their respective directors, officers, agents and employees, from and against any actual or threatened claims, demands, causes of action or proceedings arising from any breach of this Agreement by you.

- IN NO EVENT SHALL WILEY OR ITS LICENSORS BE LIABLE TO YOU OR ANY OTHER PARTY OR ANY OTHER PERSON OR ENTITY FOR ANY SPECIAL, CONSEQUENTIAL, INCIDENTAL, INDIRECT, EXEMPLARY OR PUNITIVE DAMAGES, HOWEVER CAUSED, ARISING OUT OF OR IN CONNECTION WITH THE DOWNLOADING, PROVISIONING, VIEWING OR USE OF THE MATERIALS REGARDLESS OF THE FORM OF ACTION, WHETHER FOR BREACH OF CONTRACT, BREACH OF WARRANTY, TORT, NEGLIGENCE, INFRINGEMENT OR OTHERWISE (INCLUDING, WITHOUT LIMITATION, DAMAGES BASED ON LOSS OF PROFITS, DATA, FILES, USE, BUSINESS OPPORTUNITY OR CLAIMS OF THIRD PARTIES), AND WHETHER OR NOT THE PARTY HAS BEEN ADVISED OF THE POSSIBILITY OF SUCH DAMAGES. THIS LIMITATION SHALL APPLY NOTWITHSTANDING ANY FAILURE OF ESSENTIAL PURPOSE OF ANY LIMITED REMEDY PROVIDED HEREIN.

- Should any provision of this Agreement be held by a court of competent jurisdiction to be illegal, invalid, or unenforceable, that provision shall be deemed amended to achieve as nearly as possible the same economic effect as the original provision, and

the legality, validity and enforceability of the remaining provisions of this Agreement shall not be affected or impaired thereby.

- The failure of either party to enforce any term or condition of this Agreement shall not constitute a waiver of either party's right to enforce each and every term and condition of this Agreement. No breach under this agreement shall be deemed waived or excused by either party unless such waiver or consent is in writing signed by the party granting such waiver or consent. The waiver by or consent of a party to a breach of any provision of this Agreement shall not operate or be construed as a waiver of or consent to any other or subsequent breach by such other party.

- This Agreement may not be assigned (including by operation of law or otherwise) by you without WILEY's prior written consent.

- Any fee required for this permission shall be non-refundable after thirty (30) days from receipt by the CCC.

- These terms and conditions together with CCC's Billing and Payment terms and conditions (which are incorporated herein) form the entire agreement between you and WILEY concerning this licensing transaction and (in the absence of fraud) supersedes all prior agreements and representations of the parties, oral or written. This Agreement may not be amended except in writing signed by both parties. This Agreement shall be binding upon and inure to the benefit of the parties' successors, legal representatives, and authorized assigns.

- In the event of any conflict between your obligations established by these terms and conditions and those established by CCC's Billing and Payment terms and conditions, these terms and conditions shall prevail.

- WILEY expressly reserves all rights not specifically granted in the combination of (i) the license details provided by you and accepted in the course of this licensing transaction, (ii) these terms and conditions and (iii) CCC's Billing and Payment terms and conditions.

- This Agreement will be void if the Type of Use, Format, Circulation, or Requestor Type was misrepresented during the licensing process.

- This Agreement shall be governed by and construed in accordance with the laws of the State of New York, USA, without regards to such state's conflict of law rules. Any legal action, suit or proceeding arising out of or relating to these Terms and Conditions or the breach thereof shall be instituted in a court of competent jurisdiction in New York County in the State of New York in the United States of America and each party hereby consents and submits to the personal jurisdiction of such court, waives any objection to venue in such court and consents to service of process by registered or certified mail, return receipt requested, at the last known address of such party.